Cy No. 34

EARTH RESOURCES TECHNOLOGY SATELLITE
FINAL REPORT

2. ERTS SYSTEM STUDIES

PREPARED FOR

GODDARD SPACE FLIGHT CENTER
NATIONAL AERONAUTICS
AND SPACE ADMINISTRATION

UNDER CONTRACT NAS5-11260

TRW SYSTEMS GROUP

IBM FEDERAL SYSTEMS DIVISION

Itek OPTICAL SYSTEMS DIVISION

AUG 1970
RECEIVED
NASA STI FACILITY
INPUT BRANCH

Reproduced by
NATIONAL TECHNICAL
INFORMATION SERVICE
Springfield Va 22151

FACILITY FORM 602

N70-34410
(ACCESSION NUMBER)

(THRU)

281
(PAGES)

1
(CODE)

CR-109912
(NASA CR OR TMX OR AD NUMBER)

31
(CATEGORY)

EARTH RESOURCES TECHNOLOGY SATELLITE

FINAL REPORT

Volume 2. ERTS System Studies

April 17, 1970

prepared for

National Aeronautics and Space Administration
Goddard Space Flight Center

Contract NAS5-11260
item 5a

TRW Systems Group
One Space Park · Redondo Beach
Los Angeles County
California 90278

THE FOLLOWING VOLUMES CONSTITUTE TRW'S PROPOSAL FOR PHASE D OF THE ERTS PROJECT. SHADING INDICATES THE FEBRUARY SUBMITTAL WHICH IS REVISED BY THE APRIL SUBMITTAL; THE UNSHADED VOLUMES ARE EITHER NEW OR ENTIRE VOLUME REVISIONS OF THE FEBRUARY SUBMITTAL.

PART I MANAGEMENT SUMMARY	CORRESPONDING SECTION PROPOSAL INSTRUCTIONS
1 Scope of the Proposal	IIC1-3
2 Management	IIC4-7
3 Contract Work Breakdown Structure	IIC4.3
4 Summary Work Breakdown Structure	IIC8a
5 Time Schedules	IIC8c
5A PERT Printouts	IIC8c
6 Summary Hardware and Manpower Listing	IIC8b, d-k
7 Schedule of Direct Labor Hours: Codes 100-300	IIC8e (3)
7 Schedule of Direct Labor Hours: Codes 400-500	IIC8e (3)
7 Schedule of Direct Labor Hours: Code 600	IIC8e (3)
8 Schedule of Materials: Codes 100-500	IIC8e (3)
8 Schedule of Materials: Code 600	IIC8e (3)
9 Schedules of Travel and ODC: Codes 100-300	IIC8e (3)
9 Schedules of Travel and ODC: Codes 400-500	IIC8e (3)
9 Schedule of Travel and ODC: Code 600	IIC8e (3)
10 Summary Task Descriptions	IIC8l
11 Schedule of Direct Labor: Codes 100-300	IIC8e (3)
11 Schedule of Direct Labor: Codes 400-500	IIC8e (3)
11 Schedule of Direct Labor: Code 600	IIC8e (3)
PART II TECHNICAL	
1 ERTS System	IIIC1-3a-c
2 ERTS System Specifications	IIIC3d
3 ERTS System Development and Activation	IIIC3e
4 Reliability Program Plan	IIIC3e (2)
5 Quality Program Plan	IIIC3e (3)
6 Test Monitoring and Control Plan	IIIC3e
7 Configuration Management Plan	IIIC3e (4)
8 Soldering Program Plan	IIIC3e
9 Failure Reporting Plan	IIIC3e
10 Maintainability and Safety Plans	IIIC3e
11 System Interfaces and Problem Areas	IIIC3f-g
12 Observatory System	IIIC4a (1) - (6)
13 Manufacturing	IIIC4a (7), IIIC6b (2), IIIC6c (2)
14 Observatory Specifications	IIIC4a (8)
15 Observatory Subsystems: Structure, Thermal, Attitude Control, Orbit Adjustment	IIIC4b
16 Observatory Subsystems: Communications, Data Handling, Antennas, Power, Electrical Integration	IIIC4b

PART II TECHNICAL	CORRESPONDING SECTION PROPOSAL INSTRUCTIONS
17 Observatory Integration and Test, Launch and Initial Orbital Operations, and Ground Support Equipment	IIIC4c-f
18 Data Collection System	IIIC5
19 GDHS Description, Plans, and Specifications	IIIC6a (1), (3)
20 GDHS Equipment Specifications	IIIC6a (2)
21 GDHS Software Specifications	IIIC6a (2)
22 GDHS Facilities	IIIC6a (4)
22A GDHS Facilities Design Criteria	IIIC6a (4)
23 Operations Control Center	IIIC6b (1)
24 Operations Control Center: Subsystems	IIIC6b (2)
25 Operations Control Center: Installation, Integration, and Test	IIIC6b (3)
26 Operations Control Center: Operations Support	IIIC6b (4) - (5)
27 NASA Data Processing Facility	IIIC6c (1)
28 NASA Data Processing Facility: Image and Photographic Processing	IIIC6c (2)
29 NASA Data Processing Facility: Subsystems Other Than Image and Photographic Processing	IIIC6c (2)
30 NASA Data Processing Facility: Installation and Operations Support	IIIC6c (3) - (5)
31 Options	---
PART III BUSINESS AND COST/PRICE	
1 General Information and Exhibits A Through I	IVA-G
1A Award Fee Proposal	IVD2h
2 Summary Work Breakdown Structure	IVA
3 Schedule 1: Cost Analysis: Codes 100-300	IVC2a
3 Schedule 1: Cost Analysis: Codes 400-500	IVC2a
3 Schedule 1: Cost Analysis: Code 600	IVC2a
4 Schedule 2: Direct Hours: Codes 100-300	IVC2b
4 Schedule 2: Direct Hours: Codes 400-500	IVC2b
4 Schedule 2: Direct Hours: Code 600	IVC2b
5 Schedule 3: Materials: Codes 100-500	IVC2c, IVD2c
5 Schedule 3: Materials: Code 600	IVC2c, IVD2c
6 Schedules 4 and 5: Travel and ODC: Codes 100-300	IVC2c, IVD2e-f
6 Schedules 4 and 5: Travel and ODC: Codes 400-500	IVC2c, IVD2d-f
6 Schedules 4 and 5: Travel and ODC: Code 600	IVC2c, IVD2e-f
7 Options	---
8 Data Collection System: General Information and Exhibits A Through I	IVA-G
9 Data Collection System: Schedules 1-5	IVC2

ROAD MAP

REVISIONS AND ADDITIONS TO FEBRUARY SUBMITTAL

Volume 2, ERTS SYSTEM STUDIES, initially issued in February, presented the results of two study areas

- Booster vehicle choice
- Orbital analysis

As stated in the introduction and summary of that volume, the results of two additional areas

- Improving GDHS performance through observatory modifications*
- Total system accuracy

were to be presented in April.

This volume presents in detail the results of these two additional studies In addition, the introduction and summary of the previous volume has been expanded to include the new area of study Furthermore, typographical errors of the previous volume have been corrected.

---

*In that volume this study was identified as Potential for improving GDHS performance through sensor or spacecraft modifications

PRECEDING PAGE BLANK NOT FILMED

CONTENTS

		Page
1	INTRODUCTION AND SUMMARY	1-1
2	BOOSTER VEHICLE CHOICE	2-1
	2.1 Lift	2-1
	2.2 Injection Error	2-1
	2.3 Boost Environment	2-3
	2.4 Shroud Interface	2-3
	2 5 Ring-Interstage Interface	2-4
	2.6 Electrical Interface	2-4
	2 7 Launch Stand	2-5
3	ORBITAL ANALYSIS	3-1
	3 1 Basic Orbital Elements	3-1
	3 2 Effects of Perturbations	3-3
	3 3 Image Distortion Resulting From Orbit Perturbations	3-13
	3 4 Orbit Injection Errors	3-16
4	IMPROVING GDHS PERFORMANCE THROUGH OBSERVATORY MODIFICATIONS	4-1
	4 1 Introduction	4-1
	4 2 Earth Horizon Surface Model	4-4
	4 3 System Dynamic Equations	4-16
	4 4 Two-Gyro Performance Analysis	4-28
5	TOTAL SYSTEM ACCURACY	5-1
	5 1 Introduction and Summary	5-1
	5 2 MSS Error Analysis	5-2
	5 3 RBV Geometric Error Analysis	5-37
	5 4 Post Digital Processing Error Analysis	5-57
	5 5 Overall Geometric Errors	5-62
	5 6 Photometric Analysis	5-72
APPENDICES		
	A COORDINATE SYSTEMS AND TRANSFORMATIONS	A-1
	B ERTS ERROR ANALYSIS FIGURES OF MERIT	B-1

CONTENTS (Continued)

		Page
C	DERIVATION OF THE NOMINAL ROLL, PITCH, YAW DIRECTION COSINES	C-1
D	CALCULATION OF SIGNAL TO NOISE RATIOS	D-1
E	ERTS SYSTEM SPECIFICATIONS	E-1

PRECEDING PAGE BLANK NOT FILMED

1. INTRODUCTION AND SUMMARY

The results of those Phase B/C studies of the ERTS system that encompass elements of both the observatory and the ground data handling system or that can affect factors in the program beyond these two systems are reported in this volume. Four specific studies are involved

- Booster vehicle choice
- Orbital analysis
- Improving GDHS performance through observatory modifications
- Total System Accuracy

Section 2 contains a detailed examination of the relative advantages of the Thor-Delta and Thor-Agena launch vehicles It is concluded that they are both equally acceptable. Included in the analysis were weight-carrying capability, injection accuracy, vibration loads, launch facilities, and shroud Because no compatibility-associated costs arose in this analysis, vehicle costs are essentially those chargeable to any other program Thus the Thor-Delta as recommended by GSFC in the design study specification is acceptable.

Orbital analysis is the subject of Section 3. Orbital parameters for the ERTS mission have been refined to ensure a repetitive ground trace every 18 days The resultant sun-synchronous circular orbit has the following basic elements

- Semi-major axis, a = 3936 5 n mi
- Right ascension of ascending node at vernal equinox, Ω_0 = 142.5 deg
- Inclination, i = 99.0848 deg.

Analyses have been performed on the effects of luni-solar, geopotential, and atmospheric-drag perturbations on the orbit and consequently the resultant images Grouping the results of these perturbations into short periodic (equal to or less than an orbital period), long periodic, and secular, it is found that while they are appreciable, all periodic effects can be compensated A secular effect due to the gravity gradient of the

sun acting on the orbit plane is found to induce a growing inclination error and consequently deviation from sun-synchronism Approximately 17 feet per second of velocity correction is required per year to offset this effect. However, by initially biasing the inclination, a year of tolerable operation after initial correction is possible without velocity trim An additional fraction of a foot per second per year of velocity correction is required to remove the cumulative effect of atmospheric drag

Ground lighting has been calculated for a nominal launch and for one that slips one-half hour. While it was our intention at the start of the study to perform calculations for an orbit slightly off from sun-sychronism, improvements in the launch vehicle injection accuracy have been so great that it is unnecessary to be concerned with drifting from sun-synchronism as the result of booster injection errors

Computer runs have been made for orbital conditions arising from launches in the springs of 1972 and 1973 Drag models, lunar and solar attractions, and a suitable geopotential model were included in the program. The results lend credence to the analyses and affirm that all orbital requirements of the ERTS mission can be met

Section 4 is concerned with improving GDHS performance through observatory modifications. Specific subjects that have been examined during the study period are on-board light source with precisely known intensity levels that can be turned on and off by commands in order to obtain accurate photometric calibration of RBV images, projection of variable intensity periodic reseau patterns to obtain improved geometric and photometric accuracy over the opaque cross reseaus, incorporation of RBV shutter time in narrowband PCM for increased flexibility in the time line operations of the GDHS, and improved attitude determination with a two gyro system.

A synopsis of the first three study areas is given A more detailed examination of these areas is found in Volume 17 The remainder of Section 4 is concerned with attitude determination earth horizon surface model, system dynamical equations, and two gyro performance analysis.

The roll and pitch attitude of the spacecraft will be obtained from earth horizon scanners In order to achieve the 2 nautical mile accuracy

using horizon scanners, a software program to periodically update the radiance model will be required Included in Section 4 are the derivation of the equations which will form the basis for the operational software for the updating of the radiance Model

To obtain highly accurate attitude rate information using either a one or two rate gyro configuration, ground data processing of the horizon scanner, rate gyro, and reaction wheel data are required A starting point in deriving the filtering equations for processing the attitude and attitude rate information is to start with the equation of motions governing the attitude of the spacecraft Also the relationship between the observed data and the elements of the attitude state vector must be determined Developed in detail are the dynamical and measurement equations

Considered next in this volume is an analysis of the horizon scanner-two gyro system For this system the two mile objective is easily satisfied while the internal consistency error is 600 feet.

Section 5 is concerned with the total mapping accuracy and photometric performance for the selected bulk and precision processing modes - Bulk I, Bulk II, and Precision I. The mapping performance, both absolute and internal consistency, are examined separately for the RBV and MSS images because of the significance differences in their sensitivity to attitude errors and in the methods of image processing

For all image processing modes, the LBR is the first image processing black box through which both the RBV and MSS data flow. The mapping performance, as is done here, can therefore be conveniently examined in terms of pre-LBR and post-LBR

MSS pre-LBR mapping accuracy is first examined All significant error sources are identified, e g , attiude, ephemeris, sensor Given the major error sources, the sensitivity matrix of the cross track and down track errors to each of the error sources is determined numerically The sensitivity matrix is used in a covariance analysis to determine absolute location performance and internal consistency performance in which various time and spatial correlation of errors are considered

Next, the RBV pre-BR mapping accuracy is considered. Here, the analysis is accomplished in two steps. Pre-reseau and reseau estimation accuracy The pre-reseau analysis is accomplished, as in the MSS situation by the utilization of the appropriate sensitivity matrix The reseau estimation accuracy analysis determines the mapping errors due to least squares fitting a biquadratic to a 3 x 3 set of reseau points The total pre-CBR RBV error is the rss value obtained from the two analyses To obtain the post-LBR performance, the error sources and an explanation of how these errors arise for two types of LBR's are given A complete tabulation of the magnitudes of the significant sources of errors is also given. Based on these values, the mapping errors due to an LBR are then determined The LBR errors are independent of the errors previously considered in the MSS and RBV analyses The overall geometric errors is therefore easily obtained by the rss method

The section closes with a detailed MTF and photometric analysis For the MTF analysis, seven MTF are identified and evaluated This is followed by the photometric analysis. The results of the analysis was generated by utilizing a Monte Carlo computer program in which a large number of photons were generated, their paths traced through the atmosphere, reflected or observed at the surface, and the returns traced The output is the fractional photon returned

CONTENTS

		Page
2	BOOSTER VEHICLE CHOICE	2-1
2 1	Lift	2-1
2 2	Injection Error	2-1
2 3	Boost Environment	2-3
2 4	Shroud Interface	2-3
2 5	Ring-Interstage Interface	2-4
2 6	Electrical Interface	2-4
2 7	Launch Stand	2-5

2 BOOSTER VEHICLE CHOICE

Whereas in the spring of 1969 some advantage might have been ascribed to the use of a Thor-Agena, this is no longer the case. The Thor-Delta and Thor-Agena are equally acceptable technically for ERTS-A and -B Since we have found no technical reason why the Thor-Delta launch vehicle should not be used, and since the spacecraft-induced costs are approximately the same for Thor-Delta and Thor-Agena, we have made no cost comparison between Agena and Delta stages on a Thor

Three OGO's have been successfully launched by Thor-Agena, assuring the acceptability of Thor-Agena as a launch vehicle The problem of this study then was to ascertain what differences exist between Thor-Agena and Thor-Delta that could affect the ERTS. Data on vehicle performance, physical and electrical interfaces, boost environments, and launch complex have been obtained from McDonnell-Douglas and Lockheed and reviewed in the light of ERTS requirements

2 1 LIFT

A dramatic improvement has been announced in the performance of the Thor-Delta planned for 1972 launches, resulting from a new inertial guidance system and a new Delta stage engine (N_2O_4) designated DSV-3L/1D (N_2O_4) McDonnell-Douglas estimates a lifting capability of 1600 pounds into an ERTS orbit NASA/GSFC has established a more exact definition of spacecraft weight-lifting capabilities as shown below

Spacecraft Weight (pounds)	Thor-Vehicle Solid Rockets
1480	3
1900	6
2100	9

The three-solid version of the Delta is most nearly matched to the ERTS need, which is about 1400 pounds for ERTS-A and 1425 for ERTS-B

2 2 INJECTION ERROR

The Delta improvement program includes the development of a strapped-down inertial system based on inertial measurement units of the Apollo abort guidance section, providing a significant improvement in

guidance accuracy Delta engineers are confident that the improved performance will be available in the ERTS 1972 launch. The values listed below are supplied by NASA/GSFC from a McDonnell-Douglas orbital study of the ERTS mission

	99 Percent Probable	
	Minimum	Maximum
Apogee altitude deviation (n mi)	-3	11
Perigee altitude deviation (n mi)	-11	3
Orbit period deviation (min)	-0.3	0.3
Orbit eccentricity deviation	0.000	0.001
Orbit inclination deviation (deg)	-0.03	0.03

The relationship of these errors is also established in that study. Our estimate of ERTS orbit adjustment requirements based on the above is given in Section 3.4. The conclusion is that orbit error can be removed satisfactorily with a relatively simple pneumatics system (see Volume 3, Section 10).

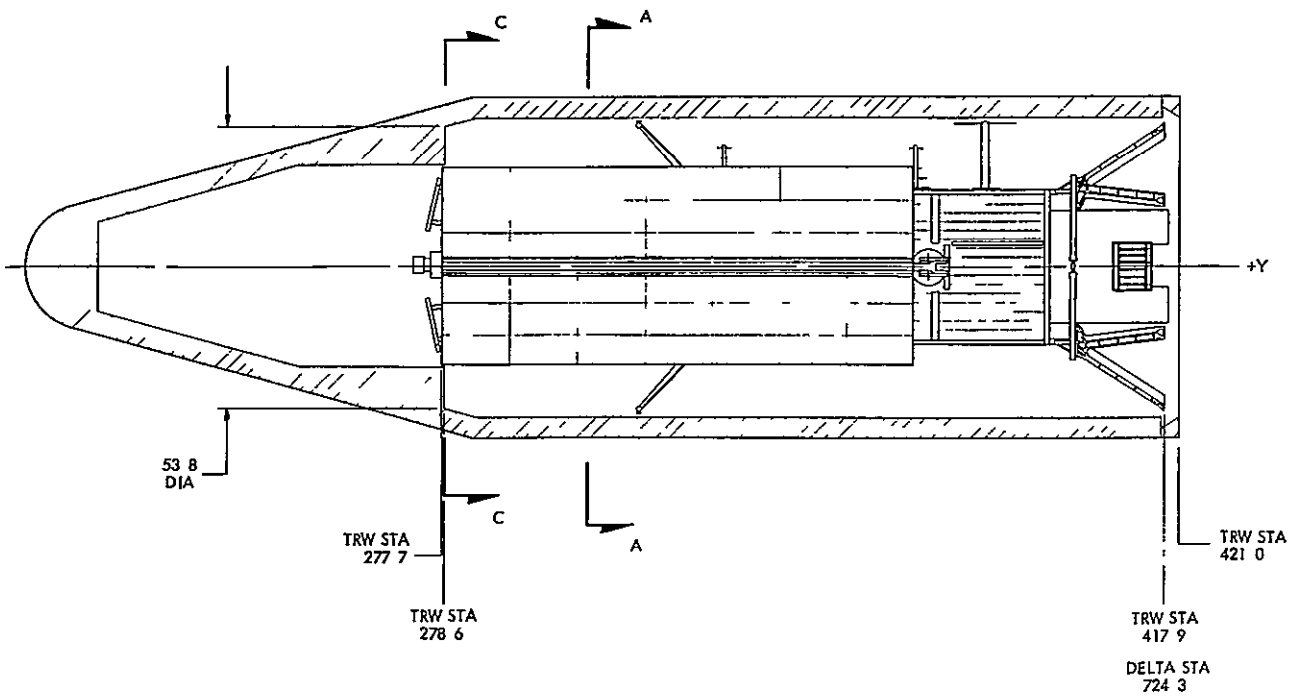

Figure 2-1
THE OBSERVATORY FITS within the

2.3 BOOST ENVIRONMENT

At the time of writing our June 1969 ERTS proposal we understood the Thor-Delta vibration environment was somewhat more severe than the Thor-Agena. In fact, as established from data from the launch of OGO 6 and other sources, the vibration environment imparted to the spacecraft is approximately the same, stemming in both cases principally from the burn of the Thor during liftoff and transonic flight Thus we can establish no sensible difference between Thor-Agena and Thor-Delta spacecraft vibration levels, and we conclude that the ERTS can survive the environment provided on both boost vehicles.

2.4 SHROUD INTERFACE

The available Thor-Delta shroud identified as Figure II of the Study Specification and also the DACS shroud are both compatible with our proposed ERTS. The specification shroud is identified by McDonnell-Douglas engineers as the Nimbus shroud, and the design has been used for OGO's 1 and 3. Figure 2-1 shows ERTS in the Thor-Delta shroud. No changes have been made in ERTS that affect shroud compatibility Array corners are unchanged from OGO. Former interference points of concern, the experiment packages on OGO, have been eliminated

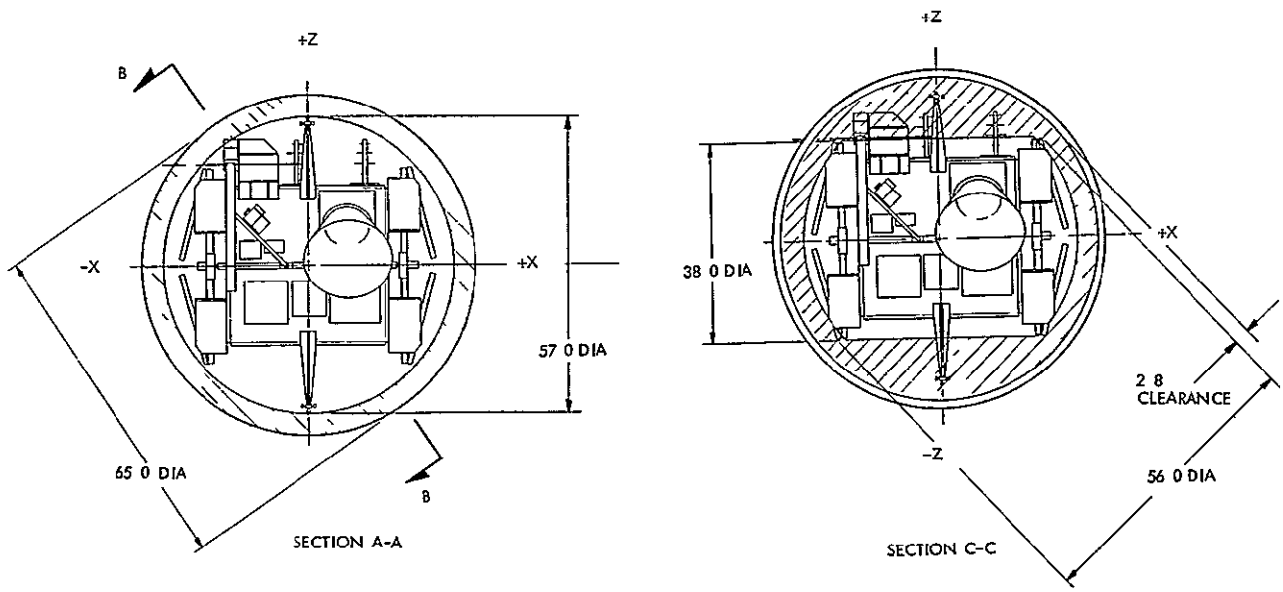

Thor-Delta shroud with adequate margins

2.5 RING-INTERSTAGE INTERFACE

The OGO-Agena interface was in the form of a two-inch-thick ring 60 inches in diameter The Delta ring defined in the Study Specification is two inches thick and 60.5 to 59.875 inches in diameter. To adapt the OGO interstage to the McDonnell-Douglas ring, all that is needed is to adjust the bolt holes slightly (Figure 2-2).

2.6 ELECTRICAL INTERFACE

The Delta umbilical disconnect is quite different from the Agena design For ERTS purposes it is superior since we have found it desirable to install equipment outside the +Y end of the spacecraft where the Agena spacecraft disconnect was located on OGO.

Delta places a 30-wire limit on the umbilical cable, which is acceptable for ERTS In addition to the umbilical, ERTS requires two coaxial cables to be brought into the spacecraft while it is on the launch stand These can be disconnected manually before stand removal McDonnell-Douglas states that these cables can be readily connected through a shroud access hole. The coaxial lines would carry PCM data and unified S-band baseband to permit tests during radio silence at Vandenberg Air Force

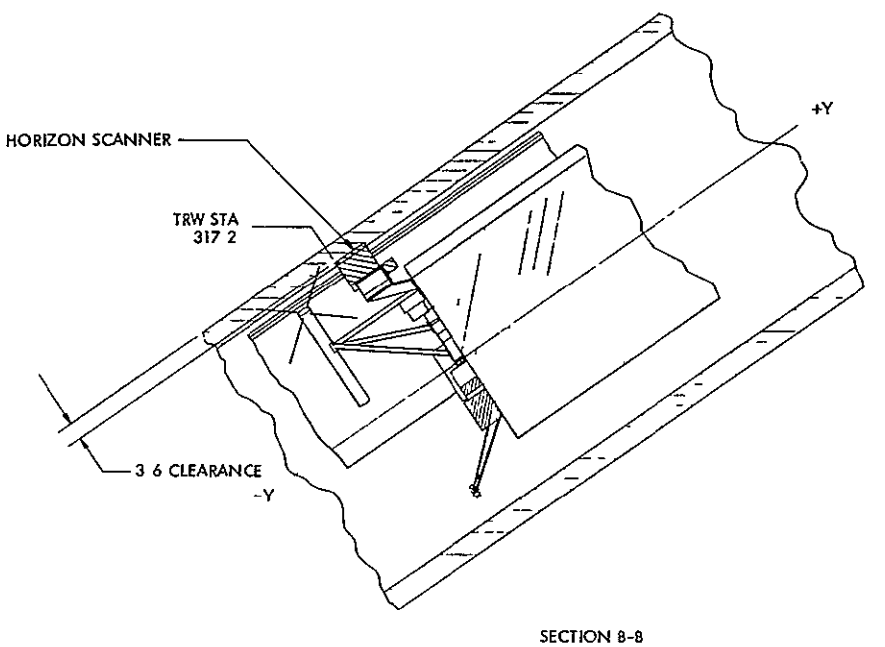

Figure 2-1 (concluded)

Base. The Agena design provides umbilical disconnect of coaxial lines, although OGO has used only one such circuit in the past. Other electrical changes in launcher, 450-foot tower, and assembly building are expected, but since these will also be needed for Agena launches they are not relevant to this comparison.

2.7 LAUNCH STAND

McDonnell-Douglas reports that launch stand SLC-2W will be used for NASA Delta launches in 1972. There is no aspect of the physical characteristic of this stand which would impede work in installing or servicing ERTS.

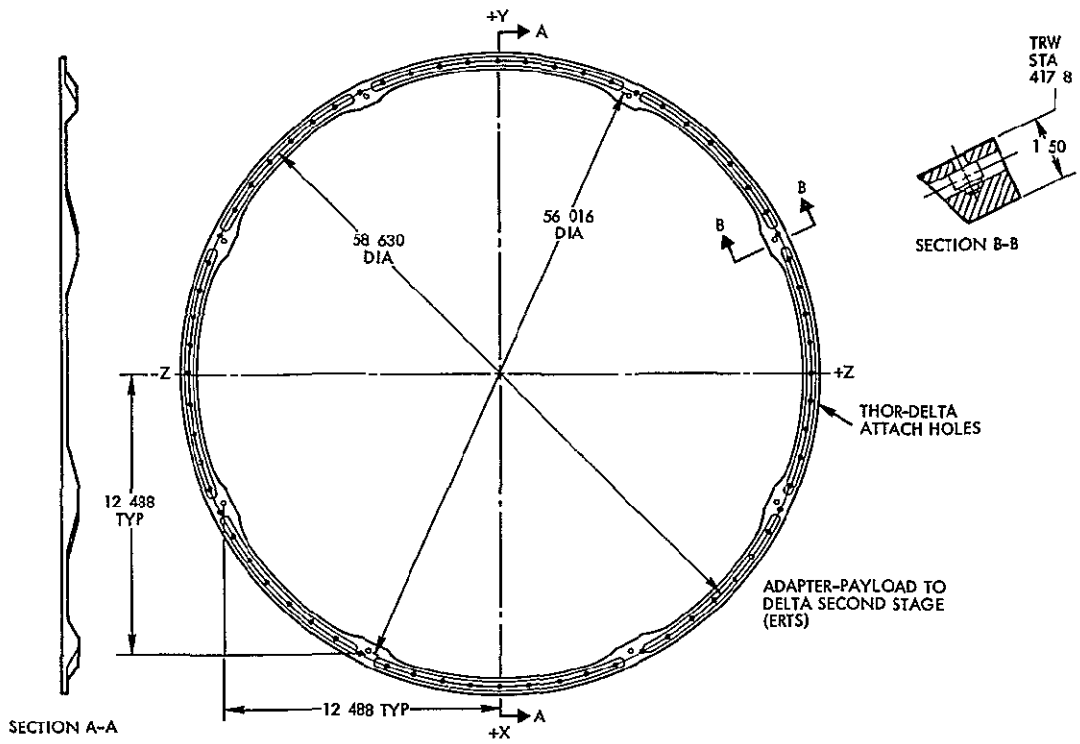

Figure 2-2

INTERSTAGE RING between Thor-Delta and ERTS is the same as that between OGO and Thor-Agena except for the location of the bolt holes

3 Orbital Analysis

CONTENTS

		Page
3	ORBITAL ANALYSIS	3-1
3.1	Basic Orbital Elements	3-1
3 2	Effects of Perturbations	3-3
3 2 1	Short Periodic Perturbations	3-3
3 2 2	Long Periodic Perturbations	3-4
3 2 3	Secular Perturbations	3-8
3 2 4	Computer Runs	3-9
3 3	Image Distortion Resulting from Orbit Perturbations	3-13
3 4	Orbit Injection Errors	3-16

3. ORBITAL ANALYSIS

The goals of the orbital analysis have been to

- Establish basic orbit elements
- Find the effects of perturbations on the nominal orbit
- Determine image distortion resulting from the orbit
- Analyze subsatellite illumination conditions
- Verify illumination angle at the satellite
- Determine orbit injection errors and define strategem for their removal
- Analyze tracking coverage.

In the Phase B/C proposal, TRW indicated the extent to which ERTS orbital studies had progressed by the spring of 1969. In that proposal some advantages of making the orbit ground trace repeat exactly on a 17- or 18-day cycle were indicated. Since the 18-day repetition is now a requirement for the ERTS program, certain parameters associated with the mission are altered and it has been necessary to repeat some earlier analyses first to obtain these new parameters and then to use them to revise the perturbation analyses, ground lighting conditions, and coverage calculations.

3.1 BASIC ORBITAL ELEMENTS

The ERTS orbit is nominally circular and sun-synchronous. Sun-synchronism exists when the right ascension of the ascending node, Ω, advances 360 degrees in one tropical year, or $\dot{\Omega} = 0.985,569,42$ deg/day. This will be true for the circular orbit when the semi-major axis, a, and the inclination, i, relate in the following way

$$\dot{\Omega} = 0.985,569 = -9.96468\ (a_e/a)^{7/2} \cos i \qquad (3\text{-}1)$$

where a_e is the earth's equatorial radius.

ERTS orbits the earth not quite 14 times a day such that after 18 days it repeats the ground trace. The rate of advance of the longitude

of the ascending node of the mean satellite, λ_N, is computed as follows*

$$\lambda_N = (M + \omega)/S_o - (\theta - \Omega) \tag{3-2}$$

where M is the mean anomaly of the orbit, ω is the argument of perigee, $S_o = 14$ is the nominal number of orbits per day, θ is the right ascension of Greenwich, and Ω is the right ascension of the ascending node.

In 18 days the observatory makes exactly 18 x 14 -1 orbits in repeating the ground trace. Thus the change $\Delta\lambda_N$ in λ_N in 18 days is

$$\Delta\lambda_N = 360 \times \left[251/S_o - 18\right] = -360/14 \text{ degrees}$$

From this,

$$\dot{\lambda}_N = \Delta\lambda_N/18 = -1.42857 \text{ deg/day}$$

λ_N was used as an input to TRW's Rapid Orbit Prediction Program (ROPP). ROPP adjusted automatically the nominal semi-major axis to yield the required λ_N value The result was

$$a = 3936.5 \text{ n mi}^{**}$$

or expressed as altitude of the circular orbit above the equator,

$$h = 492.6 \text{ n mi}^{**}$$

Using this value for a, Equation (3-1) gives

$$i = 99\ 085 \text{ degrees}$$

For a launch that does not slip, the local time of the descending node is 9 30 AM This corresponds to a right ascension of the ascending node at vernal equinox, Ω_0, of 142 5 degrees

---

*G S. Gedeon, "Tesseral Resonance Effects on Satellite Orbits," Celestial Mechanics 1, No 2, 167 (1969)

**Computed in terms of SPADATS variables

3 2 EFFECTS OF PERTURBATIONS

The orbital elements established in the previous sections are in reality only approximations to actual orbital motions. The nonsphericity of the earth, the gravitation of the sun and moon, and atmospheric drag all tend to alter the two-body orbital motion. Orbital perturbations manifest in three ways as short periodic (equal to or less than an orbital period), long periodic, and secular. The effect of these perturbations is to alter the position and velocity of the spacecraft in orbit and thus to cause size and centering shifts in both RBV and MSS images and anamorphic stretch in MSS pictures. Analysis of these perturbations follows and their effect on image quality is discussed in Section 3 4.

3 2 1 Short Periodic Perturbations

Short periodic perturbations are predominantly caused by J_2 since it is a thousand times larger than the next largest harmonic in the potential field Thus in this analysis only J_2 is used.

For circular orbits these perturbation expressions become *

$$\Delta a = (3/2)\, a\, (a_e/a)^2\, J_2 \sin^2 i \cos 2\,(M + \omega)$$

$$\Delta e = 0$$

$$\Delta i = -\,(3/4)\,(a_e/a)^2\, J_2 \sin i \cos i \cos 2\,(M + \omega)$$

$$\Delta \Omega = \frac{3}{4}\,(a_e/a)^2\, J_2 \cos i \sin 2\,(M + \omega)$$

$$\Delta \omega = \frac{3}{4}\,(a_e/a)^2\, J_2 \left[1 + (3/2) \sin^2 i\right] \sin 2\,(M + \omega)$$

$$\Delta M = -\,6\,(a_e/a)^2\, J_2 \sin^2 i \sin 2\,(M + \omega)$$

---

*G S Gedeon, "Analytic Partials," TRW memorandum 3412.4 184 (September 1968).

Substituting the values of Section 3.1,

$$\Delta a = 4.75 \cos 2 (M + \omega) \text{ n mi}$$

$$\Delta e = 0$$

$$\Delta i = -0.0055 \cos 2 (M + \omega) \text{ degrees}$$

$$\Delta \Omega = 0.0057 \sin 2 (M + \omega) \text{ degrees}$$

$$\Delta \omega = 0.086 \sin 2 (M + \omega) \text{ degrees}$$

$$\Delta M = -0.277 \sin 2 (M + \omega) \text{ degrees}$$

These short periodic perturbations (with twice the orbital frequency) due to J_2 produce a variation in the semi-major axis with an amplitude of 4.75 n mi, and an along-track oscillation resulting from the combined $\Delta\omega$ and ΔM effects with an amplitude of 0.191 degree. The semi-major axis is maximum above the equator, along-track variation is maximum at the apex of the orbit (maximum latitudes). Small amplitude across-track oscillations arise from the Δi and $\Delta\Omega$ terms.

3.2.2 Long Periodic Perturbations

The J_2 term also produces a long periodic rotation of the line of apsides. Apsidal rate is calculated from

$$\dot{\omega} = -4\ 98234 (a_e/a)^{7/2} (1 - 5 \cos^2 i)$$

When the appropriate values of a and i are substituted, $\dot{\omega}$ is found to equal 2.75 deg/day. Thus it takes 131 days to complete an apsidal cycle.

This apsidal motion interacts with an eccentricity variation introduced by the J_3 term (pear-shaped earth) to produce long periodic (131 days) variations in the eccentricity Kaula's Equation 3.77* can be put in the following form

$$\Delta e = (1/2)(J_3/J_2)(a_e/a) \sin (\omega_o + \dot{\omega} t)$$

---

*W. M Kaula, Theory of Satellite Geodesy (Blaisdell Publishing Co., Waltham, Massachusetts, 1966).

Substituting the values of a and ω gives

$$\Delta e = 0\ 001025 \sin (\omega_o + 2\ 75t)$$

Since the observatory makes almost 14 revolutions per day, it is subjected to resonance with the fourteenth-order tesseral harmonics Lagrange's planetary equations are used to evaluate the perturbations due to the tesserals The rate of change of the semi-major axis is

$$da/dt = (2/na)(\partial F/\partial M)$$

where F is the perturbing function and n = 5020 deg/day is the mean motion. It is difficult to take the partials of the potential function with respect to Kepler elements if the potential function is expressed by the standard associated Legendre polynomials. Kaula, however, made this task very simple. He rotated the reference plane from the equator to an arbitrary orbital inclination and then in this plane executed a Fourier series expansion to introduce the mean anomaly (i.e., the time). The result of this transformation is a potential function expressed by the orbital elements

$$V = \mu/r + \sum_{\ell=2}^{\infty} \sum_{m=o}^{\ell} \sum_{p=o}^{\ell} \sum_{q=\infty}^{\infty} V_{\ell mpq}$$

where

$$V_{\ell mpq} = \frac{\mu}{a}\left(\frac{a_e}{a}\right)^{\ell} F_{\ell mpq}(i)\, G_{\ell pq}(e)\, J_{\ell m}(\nu) = \begin{cases} \cos \psi & (1 - m) \text{ even} \\ \sin \psi & (1 - m) \text{ odd} \end{cases}$$

and

$$\psi = \left\{ (\ell - 2p)\,\omega + (\ell - 2p + q)\,M + m\,(\Omega - \theta - \lambda_{\ell m}) \right\}$$

In this expression $F_{\ell mpq}(i)$ is a function depending only on the inclination, and $G_{\ell pq}(e)$ is a function depending on the eccentricity alone. These functions are given by Kaula in the forms of both equations and tables

Though the above expression looks quite complicated, it has two important advantages The first is that partials needed in Lagrange's planetary equations can be immediately taken. The second is that the disturbing function $V_{\ell mpq}$ can be specified to be secular, long periodic, or short periodic by simply specifying the indices ℓ, m, p, q, e.g.,

V_{2010}	secular
V_{3021}, V_{303-1}	long periodic
V_{20pq}	(p and q $\neq$ 1, 0) short periodic

The fourteenth-order tesserals produce the following long periodic perturbing functions

$$V_{15,14,7,0}\ V_{17,14,8,0}\ V_{19,14,9,0} \cdots$$

All these can be verified by substituting the values of ℓmpq into ψ. For the sake of simplicity we restrict our analytic investigation to the $V_{15,14,7,0}$ Fourier component, for which*

$$J_{15,14} = 0.69 \times 10^{-22} \text{ and } \lambda_{15,14} = 11.3°$$

Now Lagrange's planetary equation can be integrated with $V_{\ell mpq}$ to the first order if we assume that on the right-hand side the variations are due to the dominant V_{2010} term which produces the well-known secular perturbations of the angular elements M, ω, Ω. The result is

$$a = a_o + \frac{2}{na} \frac{\ell - 2p + q}{\psi} V_{\ell mpq}$$

*R. J Anderle, "Observations of Resonance Effects on Satellite Orbits Arising from the Thirteenth and Fourteenth-Order Tesseral Gravitational Coefficients," Journal of Geophysical Research 70, 2453 (May 15, 1965)

Substituting $V_{15,14,7,0}$ and observing that $\mu = n^2 a^3$:

$$a = a_o + (2na/\psi)(a_e/a)^{15} F_{15,14,7}(i) G_{15,7,0}(e) J_{15,14} \sin\psi$$

The argument ψ can be expressed as

$$\psi = m(\lambda_N - \lambda_{\ell m}) - q\omega$$

where λ_N as defined earlier is the longitude of the ascending node of the "mean" satellite. In the case of circular orbits, $q = 0$ and $G_{\ell pq} = 1$ The inclination function for 99 085 degrees computed by a special computer program is·

$$F_{15,14,7}(99\ 085°) = 1\ 95 \times 10^{14}$$

Since $\lambda_N = -1.42857$ deg/day from the required ground trace shift,

$$\psi = m\lambda_n = -20 \text{ deg/day}$$

and the period of this perturbation is $360/\psi = 18$ days. The variation of the semi-major axis becomes $\Delta a = 22\ 5$ feet

Because of the cyclic variation of the semi-major axis there will be a periodic variation of the ground trace drift rate This can be obtained* by taking the derivative of Equation (3-2)

$$\lambda_N = (1/S_o)(M + \omega) - (\theta - \Omega)$$

The amplitude of this variation is

$$\delta\lambda_N \cong (1/S_o)\,\delta\dot{M} = -(3/2)(n/S_o)(\delta a/a)$$

For the ERTS orbit, $\delta\lambda_N = 0\ 0005$ deg/day

---

*Gedeon, op cit

The period of this variation is 18 days. Thus the amplitude of the variations of λ_N is obtained by integration as

$$\Delta\lambda_N = (P/2\pi)\ \delta\dot{\lambda}_N = 0.00145^{\circ}$$

This, then, is the amplitude of the periodic deviation from the nominal ground trace shift

Resonance also causes an along-track perturbation which can be calculated from*

$$\Delta = \frac{n}{\psi}\left[\frac{a_e}{a}\right]^{\ell} F_{\ell mp}(i)\, J_{\ell m}\left\{2(\ell+1) - 3\frac{n}{\psi}\right\}\sin\psi$$

Substituting numerical values, $\Delta = 0\ 0186\ \sin\psi$ This corresponds to a 1.28 n mi along-track oscillation, or 320-millisecond station error

3.2.3 Secular Perturbations

Secular perturbations of the line of nodes and line of apsides are represented by·

$$\Omega = -9.96468\ (a_e/a)^{7/2}\cos i$$

and

$$\omega = -4.98234\ (a_e/a)^{7/2}\ (1 - 5\cos i)$$

Secular perturbations of the semi-major axis are introduced by drag A coefficient of drag for the spacecraft was derived using free molecular flow theory and a coefficient of normal and tangential momentum exchange of 0.8 This yields $C_D = 2.4$. The frontal area of the spacecraft was taken to be A = 20 sq ft and the spacecraft weight 1400 pounds. These lead to a ballistic coefficient of

$$C_D A/W = 0.0343$$

*Gedeon, op cit

Atmospheric density is determined using the U S 1966 Standard Atmosphere and setting the solar activity index, $\overline{F}_{10.7} = 100$, for a March 1972 launch and $\overline{F}_{10.7} = 88$ for a March 1973 launch A geomagnetic planetary index of 2 0 was used for both years. Although approximate analytic results of atmospheric drag have been calculated, the complexity of the density model indicates that computer runs are more reliable Additionally, in the computer runs luni-solar perturbations can also be included.

Because the orbit is nominally sun-synchronous, a gravity gradient effect from the sun induces a change in orbital inclination and consequently a drift from sun-synchronism

3 2.4 Computer Runs

To integrate the orbit in the presence of the variety of perturbations discussed in the previous section, orbital parameters as generated in Section 3.1 were used Additionally, the eccentricity (which is nominally zero) was set at e = 0 001 to more nearly characterize launch and velocity correction residuals The initial location of perigee was at the ascending node ($\omega_o = 0$) Lunar and solar perturbations were included as were J_2, J_3, J_4, $J_{15,14}$, $J_{17,14}$, and $J_{19,14}$. The results of the computer run f 1972 and for 1973 are presented in Figures 3-1, 3-2, and 3-3.

Figures 3-1(a) and 3-1(b) show the semi-major axis and the eccentricity variations for a March 22, 1972 and a March 22, 1973 launch The semi-major axis decay is about 136 ft/year for the 1972 trajectory and 111 ft/year for the 1973 trajectory Resonance causes an oscillation with a 38-foot amplitude and 18-day period. The amplitude obtained by ROPP is higher than the analytic value, since two more harmonics were included in the ROPP run.

Eccentricity variation has an amplitude of 0 00102 and a period of 132 days, which agree very well with the analytic values presented in Section 3 2

Figure 3-2 shows the variation of the mean node in 18-day intervals. The maximum deviation is about ±3 5 n mi This graph was obtained after several corrections were made to the initial semi-major axis and to the

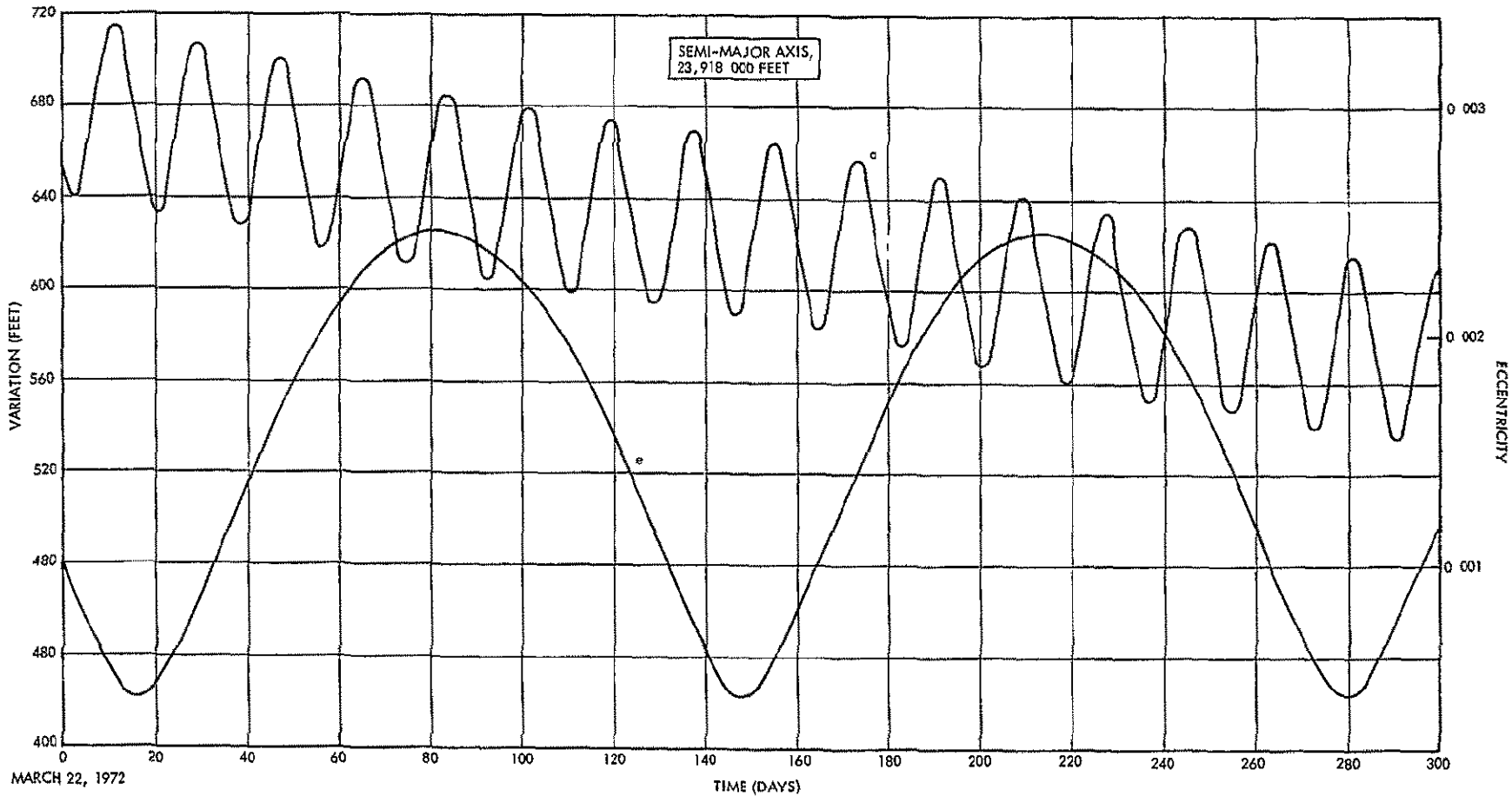

Figure 3-1(a)

SEMI-MAJOR AXIS AND ECCENTRICITY AS FUNCTIONS OF TIME,
March 22, 1972 launch

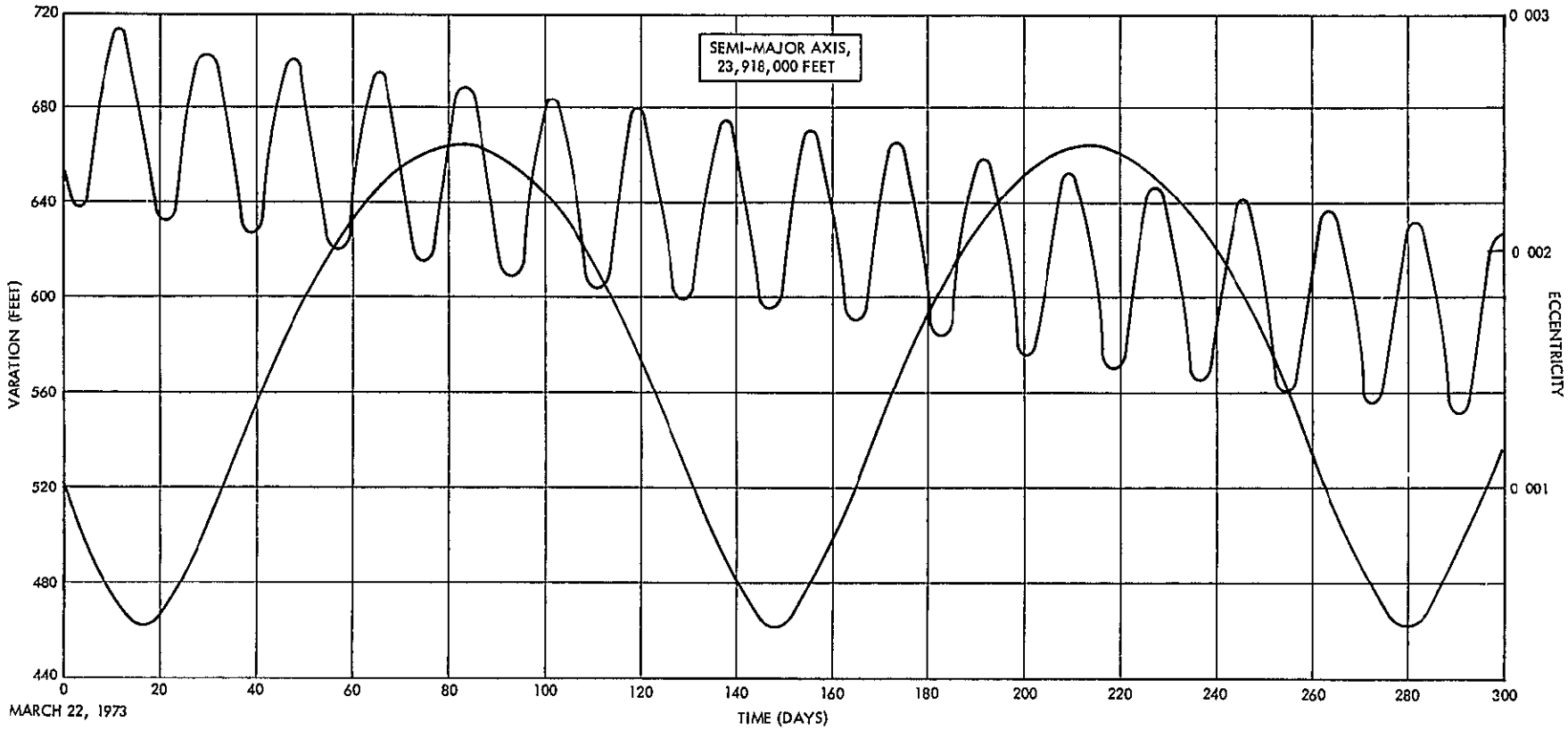

Figure 3-1(b)

SEMI-MAJOR AXIS AND ECCENTRICITY AS FUNCTIONS OF TIME,
March 22, 1973 launch

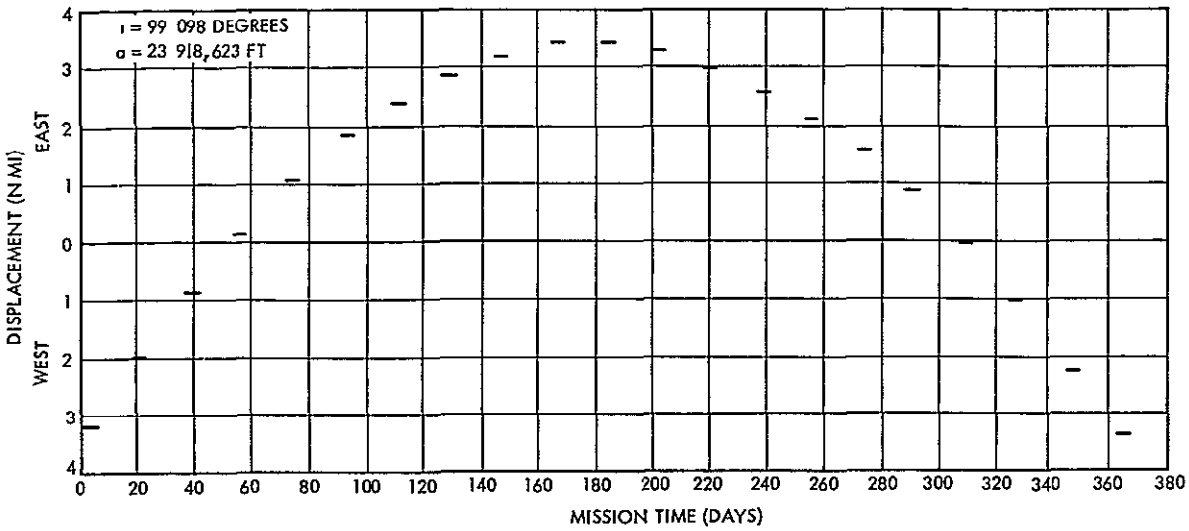

Figure 3-2
VARIATION OF THE MEAN NODE

initial inclination to offset the effect of a strong solar perturbation which affects the rate of change of the right ascension of the node, $\dot{\Omega}$

The gradient in the sun's gravity field exerts a net torque on the spacecraft about the earth's center With the inclination and right ascension of the node that prevail for ERTS, this torque can be shown to be nearly parallel to the earth's spin axis This torque causes a change in the angular momentum Since this change is northward, the orbital inclination must decrease, as shown in Figure 3-3.

Now the earth's bulge causes a precession in the line of nodes that is proportional to the cosine of the inclination. Hence as the sun reduces the inclination from the initial value, the cosine diminishes in magnitude and consequently the nodal velocity diminishes This also can be seen in Figure 3-3 (Note the "beat" which is due to the 18 period resonance and the ~15 day period lunar perturbation)

The effect of solar perturbations is to displace the line of nodes by 0.9 degree or 54 n mi after one year, in a westwardly direction Fortunately the effect of drag is to partly counteract this, since orbital decay by drag causes the nodal crossing to move eastward However, the effect is only half as large as that due to the sun The decay during one year was about 136 feet, producing an eastward shift in the equatorial

crossing (in one year) of 27 n mi Hence due to solar perturbations and drag the position error at the equatorial crossing after one year is 27 n mi (westward) This effect can be largely negated by starting the orbit at a slightly higher inclination, 0 013 degree higher than required for sun-synchronism, i e , at 99 098 degrees Then the resulting excursion in the nodal crossing is only 7 n mi Finally, by starting the orbit 3. 5 n mi westward from the nominal (at the first equatorial crossing), the maximum excursion in the equatorial crossing from a nominal one will be only ±3. 5 n mi This is shown in Figure 3-2.

3 3 IMAGE DISTORTION RESULTING FROM ORBIT PERTURBATIONS

Along- and across-track orbital perturbations result in centering shifts of images. Radial changes in orbital position as well as the earth's oblateness lead to image size errors.

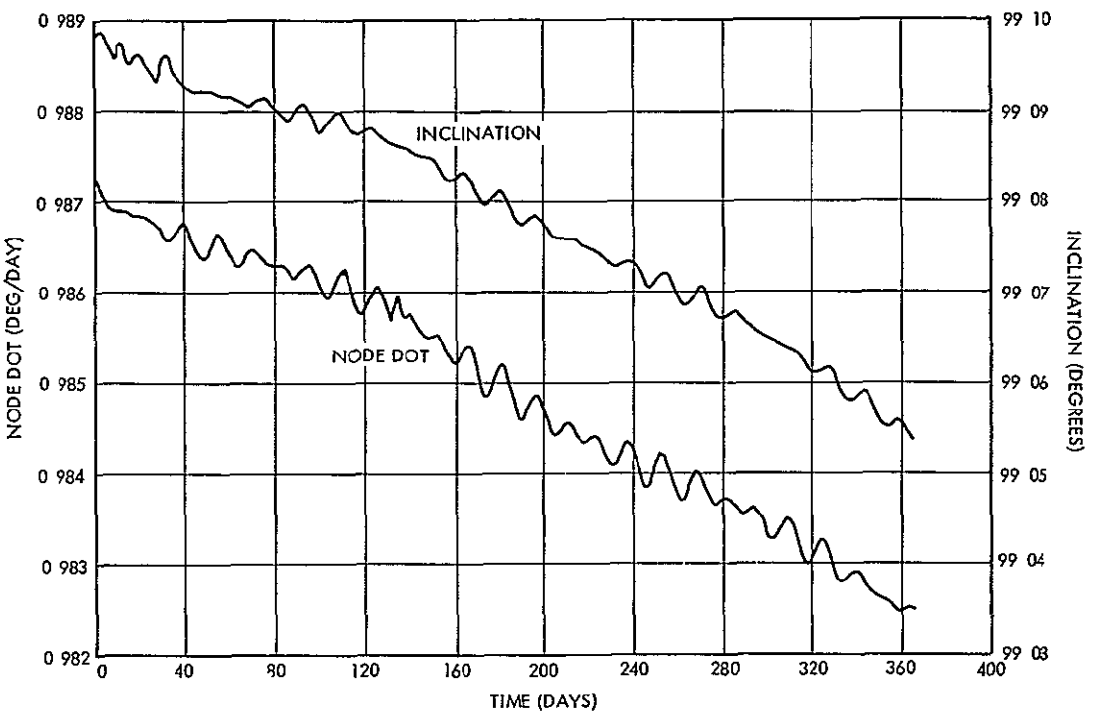

Figure 3-3

VARIATION OF THE INCLINATION AND THE RATE OF CHANGE OF THE LINE OF THE NODES

For nearly circular orbits we can write

$$r \cong a\,(1 + e \cos \nu)$$

by expanding the conic equation to the first order in e.

From Section 3.2, the semi-major axis variation due to oblateness is

$$a = a_0 + \Delta a \cos 2\,(M + \omega)$$

where $\Delta a = 4\ 75$ n mi. Substituting this in the first equation, and neglecting higher order terms, we get

$$r \cong a_0 + \Delta a \cos 2\,(M + \omega) - a_0 e \cos \nu$$

A cross section of the oblate earth which is inclined by 99 degrees to the equatorial plane can be written as·

$$R = [3444^2 \cos^2 \theta + (3444 - 11)^2 \sin^2 \theta]^{1/2}$$

where θ is a central angle measured from the equatorial plane which also equals $(M + \omega)$. Expanding R to the first power

$$R = 3438.5 + 5.5 \cos 2\theta$$

Then the geodetic height is

$$h = (a_0 - 3438\ 5) + (\Delta a - 5.5) \cos 2\theta - a_0 e \cos \nu$$

We have already seen that the J_3 harmonic causes a periodic variation of the eccentricity with

$$\Delta e = 0.001 \sin \omega$$

Then noting that $\nu = \theta - \omega$, the geodetic height with the ERTS data becomes

$$h = 498 - 0\ 75 \cos 2\theta - 3\ 94 \cos (\theta - \omega)$$

Over the ranges of θ and ω, the largest negative variations are

Equator	45° Latitude	Near the Pole
-4 7	-3 94	-3 20

Figure 3-4 shows the variation of the altitude above the reference ellipsoid and that above a sphere with radius equal to the equatorial radius of the earth. The graph was obtained by integrating an orbit with all perturbations present, but with an eccentricity of only 0.0001.

Given a side-to-side RBV field of view of 11.5 degrees, the maximum altitude variation causes a variation of 0 94 n mi in picture size The short periodic along-track oscillations due to J_2 and e cause an image slippage which can be obtained from the derivative of

$$2\ e \sin (M + \omega) - (0.191/57\ 3) \sin 2\ (M + \omega)$$

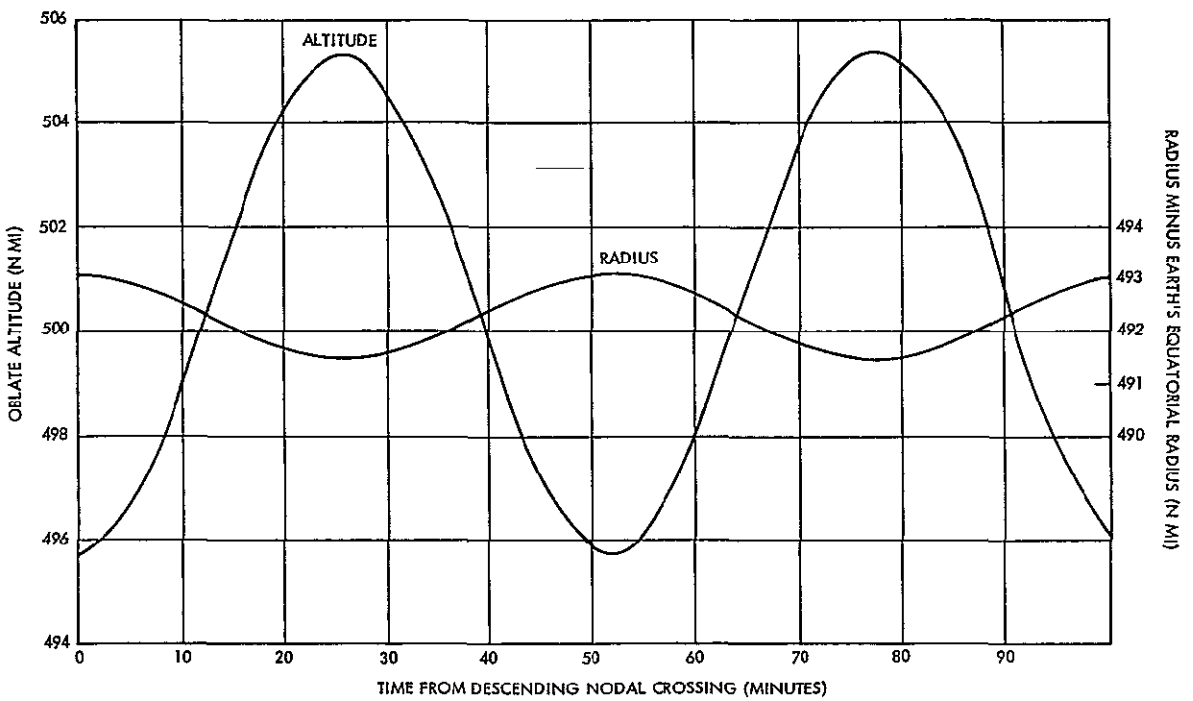

Figure 3-4
VARIATION OF ALTITUDE AND RADIUS DURING ONE ORBIT

when e = 0.002, which amounts to a maximum of 0.0000108 rad/sec. Since RBV images are snapped every 25 seconds, the slippage can amount to 0.0000108 x 25 x 3444 = 0.935 n mi. For the MSS the stretch or compression in one picture 100 miles square could be as large as 1.03 n mi.

Finally, the side overlap variation due to resonance is (0.0024/57.3) x 492.6 = 0.02 n mi.

The combined secular effect of drag and luni-solar gravity is shown in Section 3 2 to lead to a ±3.5 mile cross-track variation in the course of a year. Should it be desirable to reduce this to a smaller value or should the mission from all other considerations endure beyond a year, an out-of plane and an in-plane correction would be required to restore the orbit to its original state. The magnitude of the out-of-plane correction would be approximately 17 ft/sec per year and the magnitude of the in-plane correction would be about 0 14 ft/sec per year.

3 4 ORBIT INJECTION ERRORS

The ERTS mission requires that an orbit of very tight tolerance be established and maintained It is required that the orbit be circular as nearly as possible, with correct semi-major axis, and that orbital inclination be such as to result in sun-synchronism. The semi-major axis is determined by requiring a repeating ground trace after exactly 18 (solar) days. The sun-synchronism requirement demands a retrograde orbit with an inclination of 99.098 degrees, and the repeating ground trace requirement then demands that the mean semi-major axis be 3936 5 n mi. The eccentricity is established by requiring a "minimum altitude variation orbit." The mean eccentricity is therefore small, but is not quite zero because of the asphericity of the earth

Orbital tolerances are determined by the desire to obtain complete photographic coverage without any gaps between adjacent picture frames This requires that the eccentricity be less than 0.003 and that the semi-major axis be correct within 20 feet in order that the track after one year comes within 10 n mi of the first track of day zero.

The tight orbital tolerances cannot be established at injection with any of the guidance systems considered, and it is therefore necessary to

perform a series of orbital correction maneuvers by the spacecraft Until quite recently two different guidance systems were in principal contention The first, with relatively large injection errors, is the Western Electric Company guidance system (WECO) This is an open-loop radio command system The second contender (and that adopted for this study) is the Delta Inertial Guidance System (DIGS) As the name implies, it is a closed-loop, on-board inertial system, with errors considerably below the WECO system

Although the DIGS system will be used on ERTS, previous analyses of the WECO system are also reviewed here Upon analyzing the latest WECO covariance matrix it was found that in approximately 33 percent of the cases the total velocity required for removing all the significant injection errors (i. e , errors in apogee, perigee, and inclination) exceeded a nominal velocity correction capability of 100 ft/sec. Therefore, in about 33 percent of the cases the desired orbit could not be established In such cases it was assumed that the least critical of the ERTS requirements was the sun-synchronism Consequently, where all the errors could not be removed, a residual error in the inclination was allowed However, in such cases the targeted value or the semi-major axis must be slightly changed or a repeating ground trace is not obtained To illustrate, with a spacecraft velocity correction capability of 100 ft/sec the expected value in the (absolute) residual inclination error using the WECO system is about 0 03 degree. This transfers into an error in the nodal velocity of 0 003 degree per day If the orbit were targeted to the nominal semi-major axis, the error in the nodal crossing after 100 days would be 0 3 degree, or about 18 n mi, an intolerable error. To prevent this, the orbital period would have to be changed by 0. 05 second. The required change in the semi-major axis is 130 feet, and the required velocity necessary to change by this amount is 0. 06 ft/sec, an insignificant amount from the standpoint of total velocity correction requirements Notice that with this scheme the ground tract would remain periodic (repeating) but the period of coverage cycles would change by 1 2 minutes, i e , would be 18 days ±1 2 minutes The orbit would therefore deviate from sun-synchronism by this amount every 18 days or 24 3 minutes per year

The critical orbital parameters for the ERTS mission are a, e, and i Instead of a and e, however, a more fruitful way of looking at the problem is to say that we must target for specified values of i, R_a, and R_p The last two terms denote the radius at apogee and perigee, respectively For a given set of injection conditions the purpose of the correction maneuver is to remove the errors in i, R_a, and R_p To establish the minimum velocity correction required for the removal of these errors is a difficult problem since a nonplanar transfer must be considered In general the minimum required correction velocity depends not only on Δi, ΔR_a, and ΔR_p (the errors in i, R_a, and R_p), but also on the argument of perigee. However, for the ERTS mission other constraints enter in, to rule out certain types of transfers. Thus the desire to exclude complicated attitude maneuvers has led to the decision to use separate thrusters for the in-plane and out-of-plane corrections Effectively, this means that the in-plane and out-of-plane corrections decouple, and the total velocity correction requirement is the sum of the two Of course a velocity correction penalty must be paid which in some instances is as high as 50 percent over the velocity requirements if a coordinated maneuver were made.

The optimum in-plane transfer is given by Hohmann's bi-tangential ellipse The required total in-plane transfer velocity is given by

$$\Delta V_1 = (V/4a)\,(\Delta R_a + \Delta R_p)$$

where a is the semi-major axis and $V = (\mu/a)^{1/2}$ is the constant orbital speed (since the orbit is circular). The subscript 1 in ΔV_1 does not refer to the first of the two in-plane impulses, but to the sum of the two impulses If we denote by ΔV_2 the velocity necessary to correct the inclination alone, then $\Delta V_2 = V\,\Delta i$ The total required velocity, denoted by ΔV_3, is the sum of the two

$$\Delta V_3 = \Delta V_1 + \Delta V_2$$

The small thrust provided by each thruster, about 0 05 pound, prevents the velocity correction from being completed in one orbit It

Table 3-1. Injection Covariance Matrix

	Velocity	Path Angle	Altitude	Azimuth	Latitude	Longitude
Velocity (ft/sec)	0.3568×10^{3}	-0.5994×10^{-1}	-0.5206×10^{6}	0.1084×10^{0}	0.2643×10^{1}	0.5708×10^{0}
Path angle (deg)		0.2393×10^{-3}	0.9349×10^{2}	0.6893×10^{-5}	0.3750×10^{-3}	0.8129×10^{-4}
Altitude (ft)			0.7598×10^{9}	-0.1594×10^{3}	-0.3835×10^{4}	-0.8281×10^{3}
Azimuth (deg)				0.2348×10^{-3}	0.9078×10^{-3}	0.1887×10^{-3}
Latitude (deg)		Symmetrix matrix			0.2251×10^{-1}	0.4861×10^{-2}
Longitude (deg)						0.1050×10^{-2}

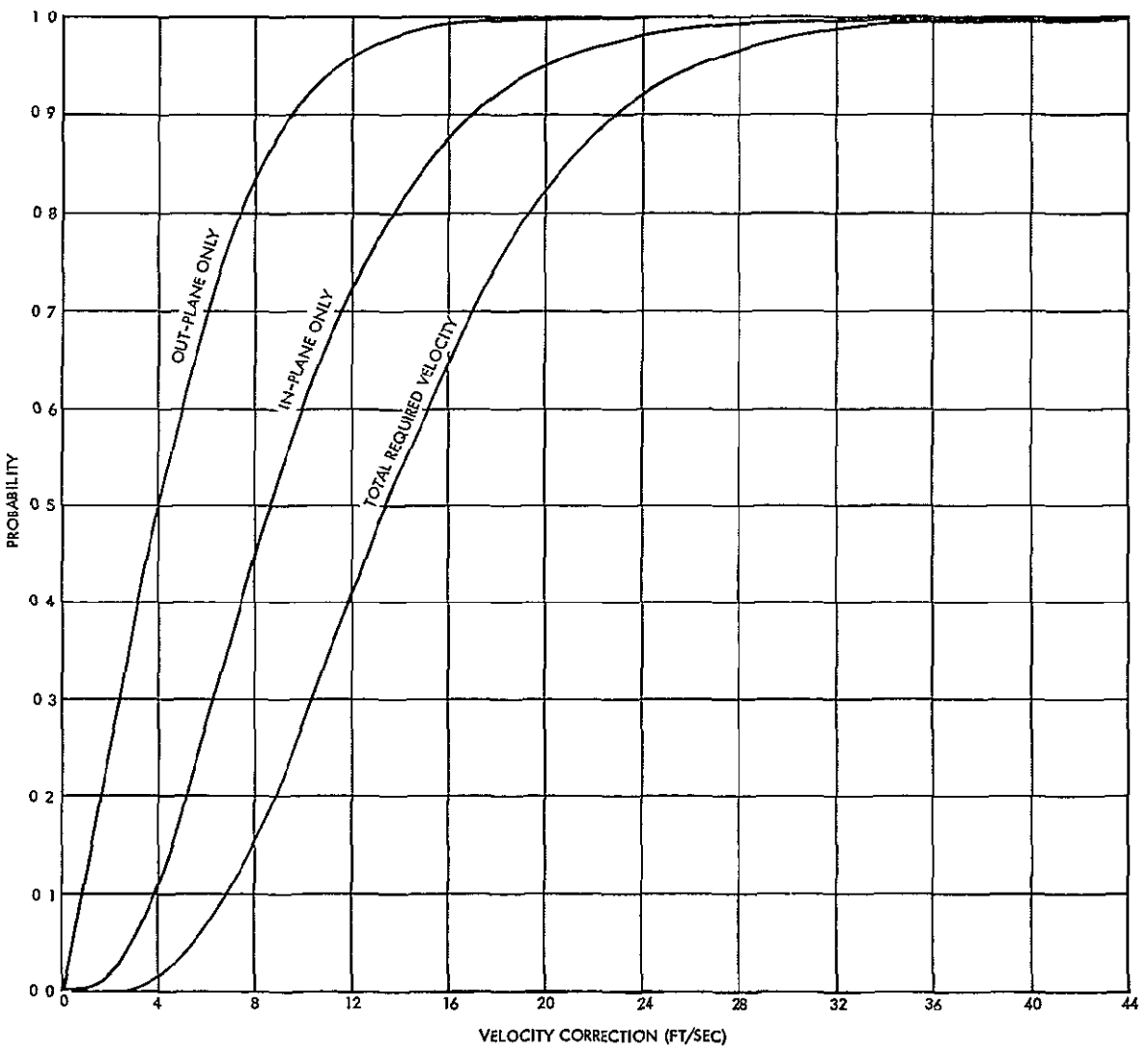

Figure 3-5

VELOCITY REQUIREMENTS

is necessary to perform the correction in bursts over several orbits, each burst contributing about 0.58 ft/sec. In some cases 20 or more orbits, i.e., up to two days, are required to complete the in-plane correction alone. If it is assumed that the in-plane correction is completed before the out-of-plane correction is made (although there is no particular reason for doing this), then the total maneuver may require four days or more.

The covariance matrix for the Delta inertial guidance system used in establishing the orbit correction requirements is shown in Table 3-1

Table 3-2. Injection Statistics of Selected Parameters

Parameter	Mean	Standard Deviation	Parameter	Mean	Standard Deviation
Apogee radius error (n mi)	1 88	3 56	Out-of-plane correction velocity (ΔV_2 ft/sec)	4 6	3 5
Perigee radius error (n mi)	-1 78	3 41	Total correction velocity (ΔV_3 ft/sec)	14 3	6 4
Inclination (deg)	0 0	0 013	Uncorrectable inclination error (deg)	0 0	0 0
In-plane correction velocity (ΔV_1 ft/sec)	9 7	5 4			

3σ = high apogee error = 12 56 n mi
3σ = low perigee error = -12 01 n mi

Although listed for completeness, the variance and covariances of the longitude error were not used in the analysis since longitude errors do not affect any of the critical parameters Table 3-2 shows how this covariance matrix translates into other parameters of interest The cumulative distribution functions for the in-plane (ΔV_1), out-of-plane (ΔV_2), and total (ΔV_3) velocity requirements are shown in Figure 3-5. The 99.8 percent confidence-of-not-exceeding the in-plane and out-of-plane velocity requirements (3σ on a normal distribution) are 17 ft/sec and 31 ft/sec, respectively. The corresponding figure for the combined requirements is 39 ft/sec or about 9 ft/sec less than the sum of the two components

4 Improving GDHS Performance Through Observatory Modification

CONTENTS

		Page
4	IMPROVING GDHS PERFORMANCE THROUGH OBSERVATORY MODIFICATIONS	4-1
4 1	Introduction	4-1
4 2	Earth Horizon Surface Model	4-4
4 2 1	Introduction	4-4
4 2 2	Analysis	4-4
4 2 3	Accuracy of Mathematical Model	4-11
4 3	System Dynamic Equations	4-16
4 3 1	Introduction	4-16
4. 3 2	Dynamical Equations	4-16
4 3 3	Measurement Equations	4-24
4 4	Two-Gyro Performance Analysis	4-28
4 4 1	Introduction	4-28
4 4 2	Development of the Two-Gyro Error Model	4-28
4 4 3	Covariance Analysis of Error Model	4-42

4. IMPROVING GDHS PERFORMANCE THROUGH OBSERVATORY MODIFICATIONS

4.1 INTRODUCTION

The major portion of the ERTS study effort has been directed toward the design of a spacecraft system and a ground data handling system which meets the mission specifications Studies have also been undertaken to ensure that the interface between the two leads to the desired mission performance with a minimum overall burden to the system This section summarizes certain studies related to the spacecraft and payload which could improve GDHS performance.

The effort with the biggest impact has been attitude determination. The remaining parts of this section deal with that subject. Other tasks were also performed and are covered in detail in other volumes of this report. Those results are summarized here.

An important source of information that can be obtained from the RBV's is the multispectral imagery For this imagery to have its greates value, a degree of color fidelity is required This ensures that identical phenomena always appear the same from image to image An evaluation of the basic fidelity of the system without calibration indicates that a 10 to 15 percent photometric accuracy can be held over a year As calibration could improve this accuracy, the GDHS implementation and the performance improvement of having RBV calibration signals have been investigated Although preflight calibration data can be used, its accuracy will degrade over a period of time. To overcome this degradation it has been suggested that the RBV's carry a light source with accurately known descrete intensity levels. The resulting light source generated RBV image would be processed on the ground system to determine the photometric response of the RBV camera in terms of picture element location and light intensity. The updated calibration curves would then be used in recording the imagery A discussion of the implementation and use of RBV calibration data is contained in Section 5, Volume 17

Going from a received video signal to a deliverable photograph requires several off-line functions essential but not directly associate

with the image reproduction. These include the generation of annotation tapes and the reduction of attitude data. Improved image processing efficiency results from carrying out these off-line functions ahead of receiving the video tapes. If the required information exists in the narrow band telemetry data which can be forwarded over data lines from Alaska and Corpus Christi, the prior preparation can take place before the arrival of the shipped video tapes. Key to all information processing is the time of RBV shuttering. From this time, spacecraft position, spacecraft attitude, sun angle, etc., are all established. Thus provision has been made for the RBV shutter time to be inserted in the narrowband telemetry main frame.

Reseau points are used to determine the RBV geometric image distortions The reseau array format proposed for the ERTS sensors is shown in Figure 5.15. At the GDHS, the 9 x 9 reseau grid is subdivided into 16 squares with three reseau points to a side for a total of nine points each. A two-dimensional quadratic polynomial is then fitted to the distortions at the nine points of each subregion Each reseau point, however, occupies some space on the photograph and since the reseau point is completely opaque, all photographic information beneath the reseau points is lost and can only be partly restored by interpolation. The number of reseau points and their arrangement is also fixed.

TRW has investigated an alternate reseau approach where the low-density, high contrast pattern normally used would be substituted with a high density low contrast pattern such as a finely gridded checkerboard of very low contrast. The thought behind this is that no picture information would be completely destroyed and, after geometric correction, the barely visible checkerboard would be completely removed by an inverse process.

Reseau extraction would be accomplished using a correlation technique similar to that mechanized in the Itek PPR where the reference image would be an undistorted reseau pattern. Such a system could handle quite high order distortions depending on reseau contrast employed.

It was visualized that a reseau pattern of this type would be projected onto the RBV faceplate through an auxiliary optical system. Using a variable intensity projection lamp the reseau could be removed at any time,

altered to match scene contrast, and used for photometric calibration Details of the tradeoffs between required contrast ratio, correlation region, and mesh dimensions is covered in Volume 17, Section 2.

Three study areas comprise the attitude determination tasks filling the balance of this section For ERTS, the absolute pitch and roll attitude of the spacecraft are obtained from the earth horizon scanners. Volume 4, Section 6 discusses the use of these measurements and states the necessity to periodically update the radiance model to achieve the required two mile absolute location accuracy. The radiance model is rather slowly varying and hence calibration is entirely feasible Details of the horizon model calibration and updating are described in Section 4 2.

The use of Kalman filtering to establish precise relative attitude data is also discussed in Volume 4, Section 6 6 Here the discussion of attitude determination is completed by going into the mechanization of the ground processing required. The general approach is to smooth the observation data by equations of motion. Section 4.3 discusses the dynamical system of equations governing the attitude of the spacecraft. The relationship between the observations and the state variables of the system equations are also given.

The complexity of the dynamic modeling required to give accurate attitude data, coupled with the discovery of a mechanically and electrically interchangeable gyrocompass rate gyro of lower drift rate, stimulated further analysis of a multi gyro attitude determination system A two-gyro system (one additional gyro) appeared most attractive. The second gyro whose input axis lies along the roll axis permits a direct measurement of the angular-momentum unbalance of tape recorders, thus easing a difficult modeling problem It also permits a more accurate measurement of absolute yaw through the ability to separate cross-coupled roll noise. The two-gyro attitude determination system is discussed in Section 4 4. The section gives a complete analysis of the two-gyro configuration - one gyro along the negative roll axis and the second one along the negative yaw axis The performance of the configuration is determined by the covariance equations of the Kalman filter.

4 2 EARTH HORIZON SURFACE MODEL

4 2 1 Introduction

In order to obtain accurate roll and pitch data from the earth horizon trackers, an accurate model of the Earth's horizon surface profile must be known. This section presents the formulation of a mathematical model which may be used to accurately define the horizon surface profile The formulation is based on the fact that from a known spacecraft position and a well defined horizon model only two orthogonal horizon measurements are required to establish body pitch and roll The measurements of the remaining two scanners provide redundant information and will completely define the parameters of an ellipsoid which is assumed to characterize the horizon model. Because of horizon-scanner noise, correlation over many measurements is performed in establishing parameters for use in characterizing the horizon model This correlation approach permits an inclusion of important variations in the horizon profile due to the Earth's oblateness and the seasonal effect of the atmospheric radiance

The horizon model is assumed to be an ellipsoid with azimuthal symmetry A number of ellipsoids are used to curve-fit the measured data, each assigned to a specific band of latitudes— Mathematically speaking, the size of the major and minor axes for each ellipsoid is determined as a function of the latitude band.

4 2.2 Analysis

In this section the semi-major axis, a, and the semi-minor axis, b, of the earth horizon profile ellipsoid will be determined. The data available for determining these parameters are the pitch plane central angle and roll plane central angle that the ellipsoid subtends from the spacecraft orbit position. This is illustrated in Figure 4-1 The central angles are obtained from the horizon scanner data which are telemetered to the ground station The problem of determining the ellipsoid can be conveniently solved by expressing the ellipsoid in a coordinate system centered at the spacecraft.

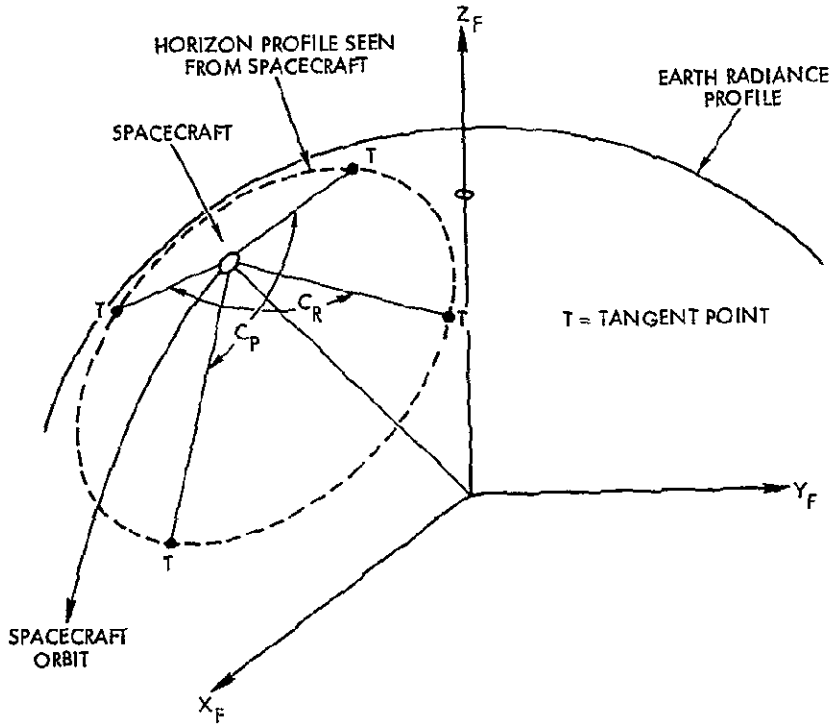

Figure 4-1
GEOMETRY OF THE CENTRAL ANGLES AND THE ELLIPSOID

4.2.2 1 Equation of Ellipsoid

In the analysis to follow, the definitions of three coordinate systems are needed Earth center inertial (ECI), Earth center fixed (ECF), and orbital reference (OR). The definitions of these coordinate systems are given in Appendix A

An ellipsoid to represent the earth horizon profile model can be expressed in ECF coordinates as

$$\frac{x_F^2 + y_F^2}{a^2} + \frac{z_F^2}{b^2} = 1, \text{ or } x_F^2 + y_F^2 - a^2 + \frac{a^2}{b^2} z_F^2 = 0 \qquad (4\text{-}1)$$

Using the transformation from ECF to ECI, Equation (4-1) can be rewritten in ECI

$$X_I^2 + Y_I^2 - a^2 + \frac{a^2}{b^2} Z_I^2 = 0 \tag{4-2}$$

Where the identity of the forms of (4-1) and (4-2) is easily explained from the symmetry of the ellipsoid about the polar axis

Next write the equation of the ellipsoid in OR coordinates through transformation T_2 given by Equation (A-4), Appendix A (Note ascending node Ω is arbitary) Using the components of $T_2(i, j)$ with indicating column and j the row

$$\left[T_2(1,1)X_R + T_2(2,1)Y_R + T_2(3,1)\,(Z_R - R)\right]^2$$
$$+ \left[T_2(1,2)X_R + T_2(2,2)Y_R + T_2(3,2)\,(Z_R - R)\right]^2 - a^2$$
$$+ \frac{a^2}{b^2}\left[T_2(1,3)X_R + T_2(2,3)Y_R + T_2(3,3)\,(Z_R - R)\right]^2 = 0 \tag{4-3}$$

To solve the problem at hand we want to find the angle, β, between an arbitrary ray from the spacecraft just tangent to the ellipsoid and the nadir line (see Figure 4-2) The angle α defines the orientation of the plane P in which the ray and the nadir axis lie When $\alpha = 0$ or $180°$, the ray is in the pitch plane and when $\alpha = \pm 90°$, it is in the roll plane We begin more generally by allowing the ray to intersect the ellipsoid at a distance ρ from the nadir axis

This ray can be written in the OR system as

$$\begin{aligned} x_R &= \rho \sin\beta \cos\alpha \\ y_R &= \rho \sin\beta \sin\alpha \\ z_R &= \rho \cos\beta \end{aligned} \tag{4-4}$$

Substituting these into (4-3) gives

$$(\lambda_1\rho + \mu_1 R)^2 + (\lambda_2\rho + \mu_2 R)^2 - a^2 + \frac{a^2}{b^2}(\lambda_3\rho + \mu_3 R)^2 = 0 \tag{4-5}$$

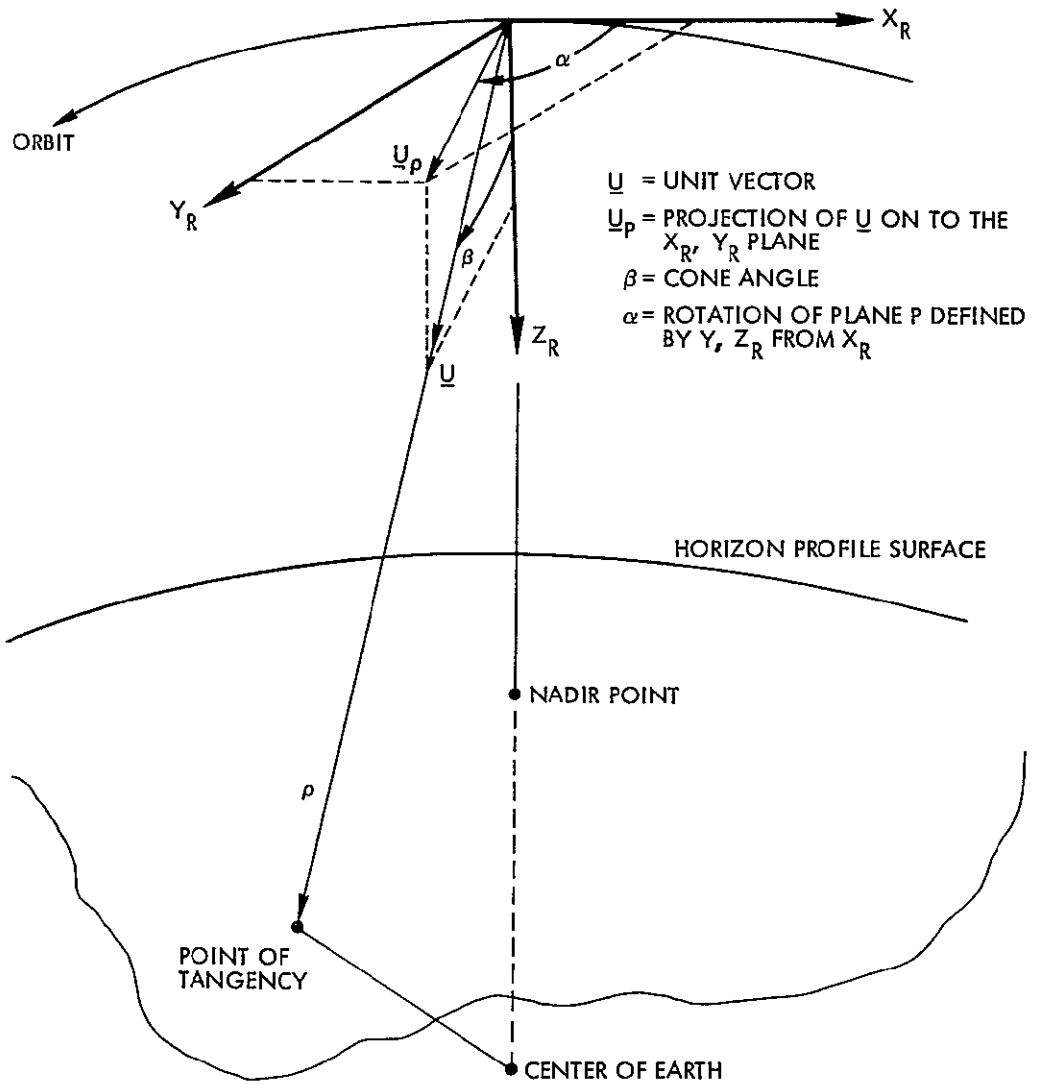

Figure 4-2

ORIENTATION OF RAY IN THE ORBITAL REFERENCE SYSTEM

where

$$\lambda_1 = T_2(1,1)\sin\beta\cos\alpha + T_2(2,1)\sin\beta\sin\alpha + T_2(3,1)\cos\beta$$

$$\lambda_2 = T_2(1,2)\sin\beta\cos\alpha + T_2(2,2)\sin\beta\sin\alpha + T_2(3,2)\cos\beta$$

$$\lambda_3 = T_2(1,3)\sin\beta\cos\alpha + T_2(2,3)\sin\beta\sin\alpha + T_2(3,3)\cos\beta \tag{4-6}$$

$$\mu_1 = -T_2(3,1)$$

$$\mu_2 = -T_2(3,2)$$

$$\mu_3 = -T_2(3,3)$$

Multiplying out (4-5) and collecting coefficients of powers of ρ gives·

$$\rho^2\left(\lambda_1^2 + \lambda_2^2 + \frac{a^2}{b^2}\lambda_3^2\right) + 2\rho R\left(\lambda_1\mu_1 + \lambda_2\mu_2 + \frac{a^2}{b^2}\lambda_3\mu_3\right)$$

$$+ R^2\left(\mu_1^2 + \mu_2^2 + \frac{a^2}{b^2}\mu_3^2\right) - a^2 = 0 \tag{4-7}$$

This can be solved for ρ to give

$$\frac{R\left(\lambda_1\mu_1 + \lambda_2\mu_2 + \frac{a^2}{b^2}\lambda_3\mu_3\right) \pm R\sqrt{\left(\lambda_1\mu_1 + \lambda_2\mu_2 + \frac{a^2}{b^2}\lambda_3\mu_3\right)^2 - \left(\lambda_1^2 + \lambda_2^2 + \frac{a^2}{b^2}\lambda_3^2\right)\left(\mu_1^2 + \mu_2^2 + \frac{a^2}{b^2}\mu_3^2 - \frac{a^2}{R^2}\right)}}{\left(\lambda_1^2 + \lambda_2^2 + \frac{a^2}{b^2}\lambda_3^2\right)} \tag{4-8}$$

From (4-8) two real roots are obtained This may be physically interpreted as the distances between the two points of intersection and the nadir axis If the line of sight is tangent to the horizon surface, the two points of intersection degenerate into a single point and mathematically speaking, the quadratic equation can have only one real root Therefore, the condition for line of sight to be tangent to the surface is represented by a zero discriminant of the quadratic equation

Hence, from Equation (4-8), we have

$$\left(\lambda_1\mu_2 - \lambda_2\mu_1\right)^2 + \frac{a^2}{b^2}\left[\left(\lambda_2\mu_3 - \lambda_3\mu_2\right)^2 + \left(\lambda_1\mu_3 - \lambda_3\mu_1\right)^2\right]$$

$$- \frac{a^2}{R^2}\left(\lambda_1^2 + \lambda_2^2 + \frac{a^2}{b^2}\lambda_3^2\right) = 0 \qquad (4\text{-}9)$$

The above equation provides the geometric relations necessary for the determination of the horizon surface profile The equation is completely general and can be used for any orientations of the orbital plane and the tracker's line of sight It is noted from Equation (4-6) that the equation of tangency is a function of ι, ν, α, β, a, b, and R

The angles ι and ν and the radial coordinate R specify the position of the satellites and are inputs from the spacecraft ephemeris program

4 2 2 2 Method of Solution

Using Equation (4-9) we can now solve for the angle β in terms of a, b, α and the orbital parameters

The form of Equation (4-9) expressed in powers of tan β is

$$A \tan^2 \beta - 2B \tan \beta + C = 0 \qquad (4\text{-}10)$$

where A, B, and C are functions of ι, ν, α, a, and b

The solution of this equation is

$$\tan \beta_{1,2} = \frac{\sqrt{B^2 - AC} \pm B}{A} \qquad (4\text{-}11)$$

where the sign of one of the roots has been reversed to yield both values of β positive The two solutions now correspond to the opposite horizon scanners in the same plane

The sum of the two roots corresponds to the sum of the readings (θ_1 and θ_2) of the corresponding horizon scanners independent of the actual body orientation

Thus

$$\tan(\theta_1 + \theta_2) = \tan(\beta_1 + \beta_2) = \pm\left|\frac{2\sqrt{B^2 - AC}}{A + C}\right| \qquad (4\text{-}12)$$

where positive sign is implied for $(\theta_1 + \theta_2) < 90°$ and negative sign is implied for $(\theta_1 + \theta_2) > 90°$

Now considering the measurements in both the roll and pitch planes two equations like (4-12) can be generated. From these the values of a and b are found

Since some variations of a and b with the spacecraft latitude position are expected, the values of a and b are determined as functions of the latitude position If the variations are small, a single ellipsoid with appropriately averaged a and b may be used If the variations are large, a number of judiciously selected ellipsoids with locally averaged a and b may be used Since values of a and b in the pitch plane differ from those in the roll plane, two sets of ellipsoids, one for pitch and the other for roll, should be used

Once the values of a and b are determined with sufficient accuracy from the foregoing correlation equation, these values may be substituted back into Equation (4-11) to determine the two angles β_1 and β_2 Now the angle between the geocentric axis and the bisector can be determined by

$$\delta = \frac{|\beta_1 - \beta_2|}{2} \qquad (4\text{-}13)$$

Figure 4-3 is the geometric description of measured and computed angles defining the directions of the geocentric axis, the null axis, and the bisector In Appendix A the angle δ is used to specify the nominal orientation, NO, coordinate system

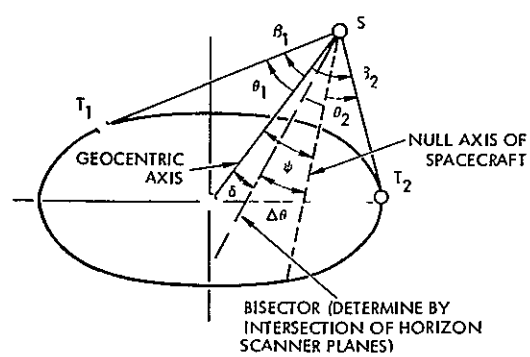

Figure 4-3
ATTITUDE ERROR determination

4 2 2 3 Simplifying Assumptions

It has been shown in the foregoing analysis that the Earth horizon model can be determined by correlation of the mathematical model with the measured data from the Earth horizon trackers A number of simplifying assumptions have been introduced in the formulation of the model The first assumption was made when the horizon surface profile was assumed to be an ellipsoid This assumption facilitates the use of an analytical solution and is also considered reasonable since the mean sea level surface may be approximated by an oblate spheroid. The second assumption is that of the azimuthal symmetry This assumption is regarded as a reasonable one as evidenced by the Tiros' flight measurements of the Earth's radiance The third assumption was introduced when the effects of the pitch and the roll attitude errors were uncoupled This was done when the pitch and the roll planes were assumed to be coplaner with the x_R, z_R and the y_R, z_R planes, respectively If the attitude errors in pitch and roll are sufficiently small, then the coupling effects are negligible In the case of large errors, an iterative scheme is suggested First, the attitude errors are determined by assuming an uncoupled effect Then, by transformations of coordinates using the computed values of pitch and roll attitude errors, the new attitude errors may be determined For each iteration, the angle α is determined from the aforementioned transformations

4 2 3 Accuracy of Mathematical Model

4 2 3 1 Introduction

In Section 4 2 2, the formulation of a mathematical model for the earth's horizon surface profile has been presented The horizon model consists of a number of ellipsoids each of which represents the local horizon surface Presented in this section is an investigation of the accuracy of the proposed mathematical model For the basis of comparison, a realistic horizon model has been constructed by using the horizon data presented in Figure (6-6) of the final report, Volume 4 The mathematical model based on ellipsoidal surfaces is then compared with the foregoing realistic horizon model

4.2 3 2 Analysis

The latitude variations of horizon profile for the months of August and January were added to the mean sea level surface profile to obtain a realistic horizon model The August curve and the January curve were used respectively for Northern and Southern hemispheres by assuming a summer season in the Northern hemisphere and a winter season in the Southern hemisphere The Hayford International Ellipsoid, a = 6378 388 (KM), (b/a) = (296/297), has been assumed for the mean sea level surface The resulting horizon model is shown in Figure 4-4 (solid curve) This curve is assumed to represent the three sigma Earth horizon surface

The foregoing horizon model is approximated by a number of ellipsoidal surfaces The least squares fit technique is used to determine the mean values of the major and the minor axes.

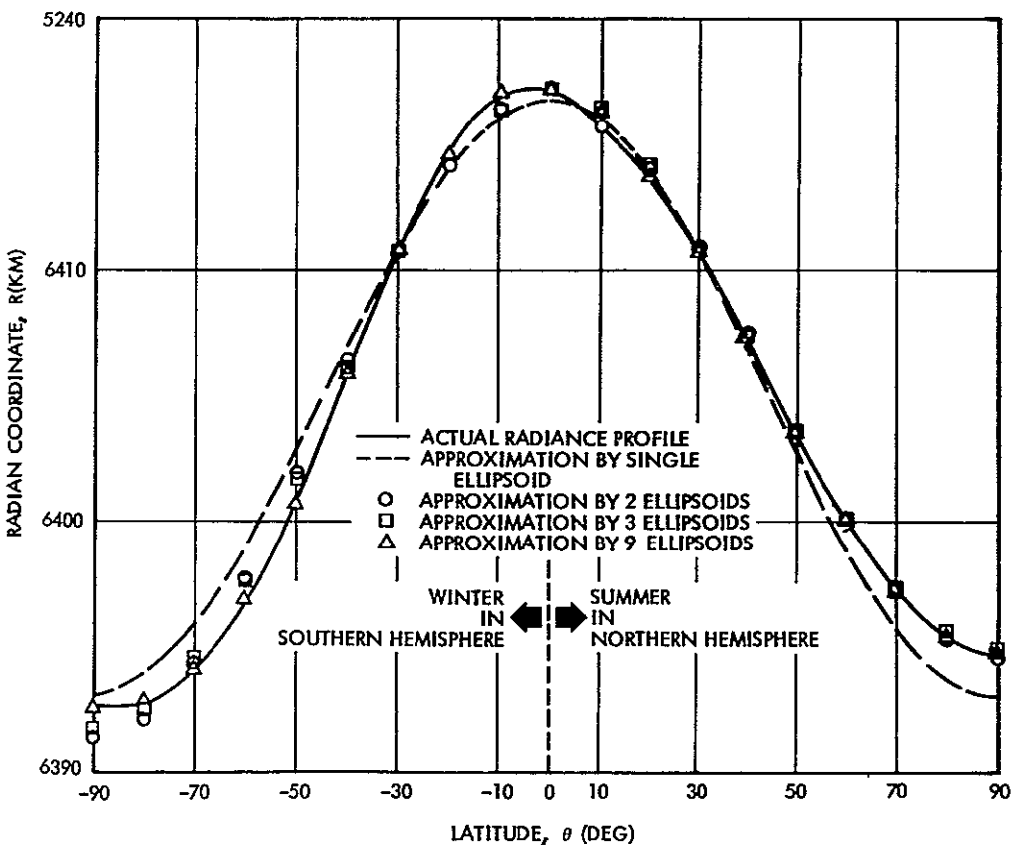

Figure 4-4
RADIAL COORDINATE OF EARTH RADIANCE PROFILE

First, using the radial coordinate $R(\phi_i)$ of the horizon model, the x and z components are determined

$$x_i = R(\phi_i) \cos \phi_i \tag{4-14}$$

$$z_i = R(\phi_i) \sin \phi_i \tag{4-15}$$

where ϕ_i is latitude angle Then, the equation of ellipse may be written as

$$Ax_i^2 + Bz_i^2 - 1 = 0 \tag{4-16}$$

where

$A = 1/\langle a \rangle^2$

$B = 1/\langle b \rangle^2$

$\langle a \rangle$ is a mean of the semi-major axis

$\langle b \rangle$ is a mean of the semi-minor axis

According to the least squares method, the following quantity is minimized by setting its first derivatives with respect to A and B equal to zero

$$Q = \sum_{i=1}^{M} \left(Ax_i^2 + Bz_i^2 - 1 \right)^2 \tag{4-17}$$

where M is total number of data points to be used for the curve-fit

then,

$$\frac{\partial Q}{\partial A} = 2\sum_{i}^{M} \left(Ax_i^2 + Bz_i^2 - 1 \right) x_i^2 = 0 \tag{4-18}$$

$$\frac{\partial Q}{\partial B} = 2\sum_{i}^{M} \left(Ax_i^2 + Bz_i^2 - 1 \right) z_i^2 = 0 \tag{4-19}$$

Solving the above equations for $\langle a \rangle$ and $\langle b \rangle$, we get

$$\langle a \rangle = \left[\frac{\left(\Sigma x_1^4\right)\left(\Sigma z_1^4\right) - \left(\Sigma x_1^2 z_1^2\right)^2}{\left(\Sigma x_1^2\right)\left(\Sigma z^4\right) - \left(\Sigma x_1^2 z_1^2\right)\left(\Sigma z_1^2\right)} \right]^{1/2} \tag{4-20}$$

$$\langle b \rangle = \left[\frac{\left(\Sigma x_1^4\right)\left(\Sigma z_1^4\right) - \left(\Sigma x_1^2 z_1^2\right)^2}{\left(\Sigma x_1^4\right)\left(\Sigma z_1^2\right) - \left(\Sigma x_1^2 z_1^2\right)\left(\Sigma x_1^2\right)} \right]^{1/2} \tag{4-21}$$

Thus, using the above equations, the ellipsoidal surfaces representing the horizon model have been determined

4 2 3 3 Results

A number of ellipsoids were used to fit the three-sigma earth horizon model One, two, three, and nine ellipsoids with the following ranges of latitude were selected

a) One ellipsoid $\theta = (-90 \sim +90)$

b) Two ellipsoids $\theta = (-90 \sim 0)$
$\theta = (0 \sim +90)$

c) Three ellipsoids $\theta = (-90 \sim -30)$
$\theta = (-30 \sim +30)$
$\theta = (+30 \sim +90)$

d) Nine ellipsoids $\theta = (-90 \sim -70)$
$\theta = (-70 \sim -50)$
$\theta = (-50 \sim -30)$
$\theta = (-30 \sim -10)$
$\theta = (-10 \sim +10)$
$\theta = (+10 \sim +30)$
$\theta = (+30 \sim +50)$
$\theta = (+50 \sim +70)$
$\theta = (+70 \sim +90)$

No attempt was made to match the value nor the slope of the radial coordinate at the boundary points However, the maximum deviations are observed to be 0 014 percent in value and 13 percent in slope The values of radial coordinate based on these ellipsoids are shown in Figure 4-4 The correlation with the three-sigma horizon model is observed to improve with the number of ellipsoids Figure 4-5 shows the variation of RMS deviation in radial coordinate with the selected number of ellipsoids It is observed that a single ellipsoid approximates the horizon model to ±1 18 (KM)

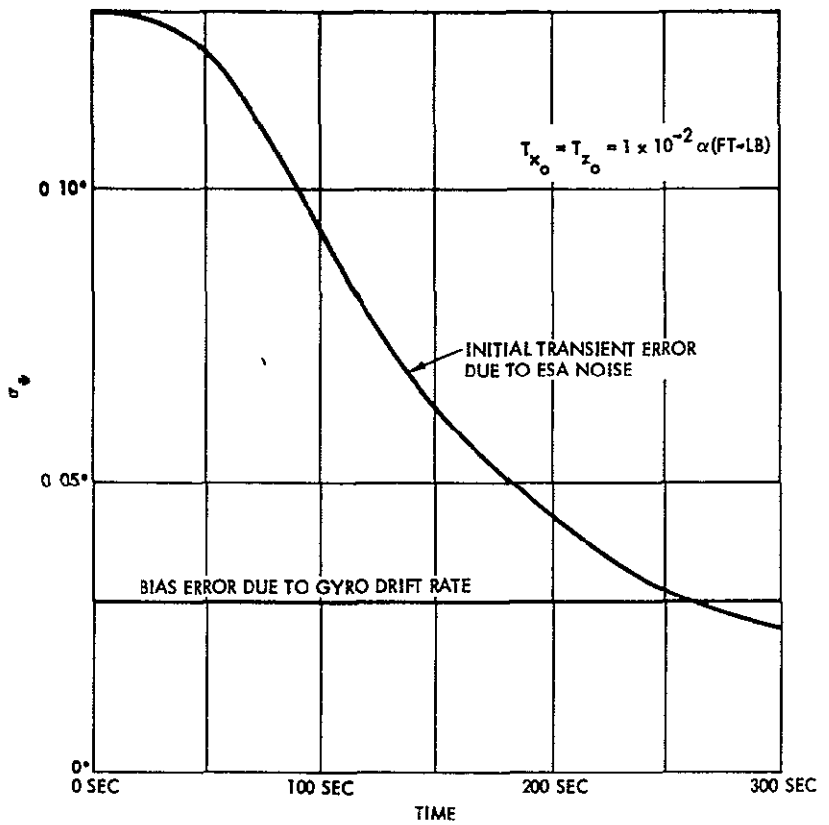

Figure 4-5
RMS DEVIATION OF ELLIPSOIDAL MODEL
from earth radiance profile

4 3 SYSTEM DYNAMIC EQUATIONS

4 3. 1 Introduction

In section 6 of Volume 4 a discussion of an attitude determination technique is presented which makes use of horizon scanner, rate gyro, and reaction wheel position data to establish time histories of both absolute and relative attitudes of the spacecraft for use in assuring accurate image reconstruction and annotation As an aid in carrying out ground processing of the spacecraft signals, evaluate total performance and suggest areas of improvement, a set dynamic system equations have been developed The various coordinate systems and transformations between them necessary for the development are given in Appendix A

4 3 2 Dynamical Equations

4 3 2 1 Euler Angle Equation

The attitude of the spacecraft is expressed in terms of Euler angles defined between the true body (TB) coordinate system and the nominal orientation (NO) coordinate system The dynamical equations are now derived for both the spacecraft and the reaction wheels The equation of motion for the wheel is conveniently expressed in terms of the TB system

Inertial Body Rate Equation

The angular momentum $\underline{H}$ of the spacecraft in body coordinates is given as,

$$\underline{H} = I\underline{\omega}_B + I_s\mathring{\underline{\Omega}}_s + \sum_{i=1}^{3}\underline{\eta}_i I_i \mathring{\Omega}_i + \sum_j \underline{H}_{T,j} \qquad (4\text{-}22)$$

where, in body coordinates,

I = Total spacecraft moment of inertia tensor including the instantaneous static inertia of the solar array, all wheels, tape recorders, etc

ω_B = Inertial angular velocity vector of spacecraft = $(\omega_x, \omega_y, \omega_z)$ expressed in body coordinates.

I_s = Solar panel moment of inertia expressed in the body coordinate system

$\underline{\mathring{\Omega}}_s$ = Angular velocity vector of solar panels relative to spacecraft

$\underline{\eta}_i$ = Unit vector defining ith wheel axis with respect to the body axes

I_i = Scalar moment of inertia of ith wheel about wheel spin axis

$\mathring{\Omega}_i$ = Scalar angular velocity if the ith wheel relative to the spacecraft

$\underline{H}_{T,j}$ = Angular momentum vector of the jth tape recorder relative to the body

In the remainder of the system equation development let $\underline{\mathring{\Omega}}_s = 0$ since, during picture taking, the solar array is not driven It will be assumed that the tape recorders angular momentum are adequately compensated for, and hence will be neglected If later information indicates this is not so, the procedure similar to deriving the reaction wheel equations can be used for developing the recorder equations. We will therefore proceed to develop the system equations based on the angular momentum equation

$$H = I\underline{\omega}_B + \sum \underline{\eta}_i I_i \mathring{\Omega}_i \tag{4-23}$$

where I is a known function of the solar array orientation with respect to the body

Now the external torque $\underline{T}$ applied to the spacecraft equals the rate of change of angular momentum.

$$\underline{T} = \frac{d\underline{H}}{dt} = (\mathring{\underline{H}}) + \underline{\omega}_B \times \underline{H} \tag{4-24}$$

where,

$\frac{d(\ )}{dt} = (\dot{\ }) =$ total inertial time derivative of ( )

$(\mathring{\ }) =$ time derivative of ( ) in body coordinates.

Since $\underline{\omega}_B \times \underline{\omega}_B = 0$, it follows that

$$\dot{\underline{\omega}}_B = \frac{d\underline{\omega}_B}{dt} = \mathring{\underline{\omega}}_B + \underline{\omega}_B \times \underline{\omega}_B = \mathring{\underline{\omega}}_B \tag{4-25}$$

and since $\underline{\eta}_1$ is constant in body coordinates

$$(\mathring{\underline{\eta}}_1) = 0 \tag{4-26}$$

so that equation 4-24 can be written as

$$\underline{T} = I\mathring{\underline{\omega}}_B + \sum_{i=1}^{3} \underline{\eta}_i I_i \mathring{\mathring{\Omega}}_i + C(\underline{\omega}_B)\left\{ I\underline{\omega}_B + \sum_{i=1}^{3} \underline{\eta}_i I_i \mathring{\Omega}_i \right\} \tag{4-27}$$

where all vectors are in body coordinates and $C(\underline{\omega}_B)$ is the cross product operator in matrix form.

$$C(\underline{\omega}_B) = \underline{\omega}_B \times = \begin{bmatrix} 0 & -\omega_z & \omega_y \\ \omega_z & 0 & -\omega_x \\ -\omega_y & \omega_z & 0 \end{bmatrix} \tag{4-28}$$

Rearranging yields the body rate equation,

$$\dot{\underline{\omega}}_B = \mathring{\underline{\omega}}_B = I^{-1}\left\{ \underline{T} - \sum_{i=1}^{3} \underline{\eta}_i I_i \mathring{\mathring{\Omega}}_i - C(\underline{\omega}_B)\left[I\underline{\omega}_B + \sum_{i=1}^{3} \underline{\eta}_i I_i \mathring{\Omega}_i \right] \right\} \tag{4-29}$$

Using $\dot{\underline{\omega}}_B$ we can derive the Euler acceleration of the spacecraft with respect to the NO system. The inertial rate of spacecraft can be thought of as the sum of the two components, one due to rate of the body with respect to the NO system and the other due to the rotation rate of the NO system with respect to ECI

Let $\underline{\omega}_{o,I}$ = total rotation rate of the NO system relative to the ECI system expressed in ECI coordinates. It can be assumed that Ω (ascending node) and ι (inclination) change slowly with respect to ν (true anomaly) (see Section 3 of this Volume). It can also be tentatively assumed that the angular rate of the NO coordinate with respect to the OR coordinates is negligible

Now express $\omega_{o,I}$ in the OR system by equation (A-4),

$$\underline{\omega}_o = T_2\underline{\omega}_{o,I} = (0, \dot{\nu}, 0)^T \tag{4-30}$$

Transformation T_3 takes $\underline{\omega}_o$ into NO coordinates, and S_1 takes it into body coordinates Thus the body rate relative to the NO system expressed in TB coordinates is,

$$\underline{\omega}_B - S_1T_3\underline{\omega}_o \tag{4-31}$$

In addition, applying transformation S_2 from equation (A-17) gives Euler rates.

$$\underline{e} = S_2\left[\underline{\omega}_B - S_1T_3\underline{\omega}_o\right] \tag{4-32}$$

where the Euler angle rate vector is defined as,

$$\underline{e} = (\phi, \theta, \dot{\psi})^T \tag{4-33}$$

where nominally,

$$\begin{aligned} \phi &= \text{roll} \\ \theta &= \text{pitch} \\ \psi &= \text{yaw} \end{aligned} \tag{4-34}$$

Taking the derivative of (4-32) yields,

$$\underline{e} = S_2\underline{\omega}_B + S_2\underline{\omega}_B - S_3T_3\underline{\omega}_o \tag{4-35}$$

where,

$$S_3 = S_2S_1 \tag{4-36}$$

Note that equation (4-35) can be integrated twice using equation (4-29) directly, or equations (4-29) and (4-32) can be simultaneously integrated to give Euler angles. The latter method avoids some matrix differentiations given in Appendix A. The choice of integration method depends on a study of numerial integration accuracy and speed.

From (4-32), note that,

$$\underline{\omega}_B = S_2^{-1}\underline{e} + S_1 T_3 \underline{\omega}_o \tag{4-37}$$

Equation (4-35) is the desired system equation for the body To integrate (4-35) requires knowing the external torques and the reaction wheel equations. The external torques are considered first

4 3.2.2 External Torques

Some tentative estimates of ERTS external torque magnitudes are as follows

Source	Max. Value (lb-ft)
Residual magnetic moment	2.6×10^{-5}
Gravity gradient	1.4×10^{-5}
Solar pressure	2.0×10^{-6}
Aerodynamic pressure	-

The last source is considered to be negligible, the first two are easily modeled and comprise over 95 percent of the external torque. Solar pressure effects appear too small to warrant the complicated model required to describe them. Thus the external torque $\underline{T}$ is modeled as

$$\underline{T} = \underline{T}_{GG} + \underline{T}_{RM} \tag{4-38}$$

$$\underline{T}_{RM} = \underline{m} \times \underline{B}_b \tag{4-39}$$

$$\underline{T}_{GG} = \frac{3\mu}{R^3}\hat{\underline{r}} \times I\hat{\underline{r}} \tag{4-40}$$

where, in TB coordinates,

$\underline{m}$ = residual magnetic moment vector (ft lb/gauss)

$\underline{B}_b$ = Earth magnetic field flux density model (gauss)

μ = Earth gravitational constant (1.4082×10^{16} ft^3/sec^3)

R = distance from the Earth's center to the spacecraft (ft)

$\hat{\underline{r}}$ = unit vector along the OR z axis (ft)

I = spacecraft moment of inertia matrix (lb ft sec^2)

Other torques can be considered as state noise.

Let $\underline{B}_b$, the magnetic field flux density of the spacecraft position, be expressed in the radial, tangential unit vector directions $\underline{e}_r$ and $\underline{e}_t$ respectively, as shown in Figure 4-6. It is given by

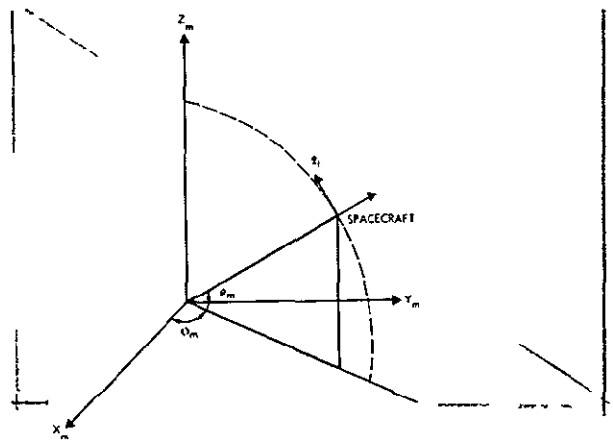

Figure 4-6
MAGNETIC COORDINATE
unit vectors

$$\underline{B}_b = -B_o\left[\left(2 \sin \theta_m\right) \underline{e}_r - \left(\cos \theta_m\right)\underline{e}_t\right] \tag{4-41}$$

where

$$\sin \theta_m = \frac{z_m}{\left(x_m^2 + y_m^2 + z_m^2\right)^{1/2}} \tag{4-42}$$

$$\cos \theta_m = \left(1 - \sin^2 \theta_m\right)^{1/2} \tag{4-43}$$

$$\sin \phi_m = \frac{x_m}{\left(x_m^2 + y_m^2\right)^{1/2}} \tag{4-44}$$

$$\cos \phi_m = \frac{y_m}{\left(x_m^2 + y_m^2\right)^{1/2}} \tag{4-45}$$

$$\underline{e}_r = \begin{bmatrix} \cos\theta_m & \cos\phi_m \\ \cos\theta_m & \sin\phi_m \\ & \sin\theta_m \end{bmatrix} \tag{4-46}$$

$$\underline{e}_t = \begin{bmatrix} -|\sin\theta_m| & \cos\phi_m \\ -|\sin\theta_m| & \sin\phi_m \\ & \cos\theta_m \end{bmatrix} \tag{4-47}$$

Based on the transformations defined in Appendix A the magnetic in the TB system is given by the sequence of matrix operations

$$\underline{B}_b = S_1 T_3 T_2 T_1 T_4 \underline{B} \tag{4-48}$$

4.3.2.3 Wheel Rate Equation

For one wheel, define a cartesian coordinate system fixed relative to the spacecraft with one axis along the spin axis of the wheel. The angular momentum vector of the wheel $\underline{H}_w$ is then given as

$$\underline{H}_w = \Lambda \underline{\omega}_w \tag{4-49}$$

where

Λ = wheel moment of inertia tensor

$\underline{\omega}_w$ = inertial angular wheel rate in wheel coordinates

The total torque on the wheel T_w is given as

$$\underline{T}_w = \underline{T}_M + \underline{T}_B - K\left[\underline{\omega}_w - \left(\underline{\omega}_B^T \underline{\eta}_w\right)\underline{\eta}_w\right] \tag{4-50}$$

where, in wheel coordinates

$\underline{T}_M$ = motor torque

$\underline{T}_B$ = bearing torque

K = dynamic friction coefficient

$\underline{\omega}_B$ = body inertial rotation rate

$\underline{\eta}_w$ = unit vector in direction of wheel axis

since,

$$\underline{T}_w = \frac{d\underline{H}_w}{dt} = \mathring{\underline{H}}_w + \underline{\omega}_B \times \underline{H}_w \tag{4-51}$$

$$\underline{T}_M + \underline{T}_B - K\left[\underline{\omega}_w - \left(\underline{\omega}_B{}^T\underline{\eta}_w\right)\underline{\eta}_w\right] = \left(\mathring{\Lambda\underline{\omega}_w}\right) + \underline{\omega}_B \times \Lambda\underline{\omega}_w \tag{4-52}$$

Take the dot product of this equation with the wheel axis unit vector

$$T_M - K\left[\omega_w - \underline{\omega}_B{}^T\underline{\eta}_w\right] = I\omega_w - \underline{\eta}_\omega{}^T\left(\underline{\omega}_B \times \Lambda\underline{\omega}_w\right) \tag{4-53}$$

Note

$$\underline{\omega}_w = \omega_w\underline{\eta}_w \tag{4-54}$$

and that the dot product

$$\underline{\eta}_w \quad \underline{T}_B = 0 \tag{4-55}$$

based on the assumption, quite valid, that the bearing torque is perpendicular to the spin axis

Also by symmetry of the wheel, $\underline{\eta}_w$ is a principal axis of Λ, i e ,

$$\Lambda\underline{\eta}_w = I\underline{\eta}_w \tag{4-56}$$

where I = moment of inertia of the wheel with respect to the spin axis

By a vector identity and (4-54) and 4-55) we will show that last term of (4-53) is zero. By vector identity, we have

$$\underline{\eta}_w^T\left(\underline{\omega}_B \times \Lambda\underline{\omega}_w\right) = \underline{\omega}_B^T\left(\Lambda\underline{\omega}_w \times \underline{\eta}_w\right)$$

By utilizing (4-54) and (4-55) we obtain,

$$\underline{\omega}_B^T \left(\Lambda\underline{\omega}_w \times \underline{\eta}_w\right) = I\omega_w\underline{\omega}_B^T\left(\underline{\eta}_w \times \underline{\eta}_w\right) = 0 \tag{4-57}$$

which was to be shown. Thus (4-53) becomes

$$T_M - K\left[\omega_w - \left(\underline{\omega}_B^T\underline{\eta}_w\right)\right] = I\,\dot{\underline{\omega}}_w \tag{4-58}$$

Using (4-58) we wish now to obtain equation for $\ddot{\Omega}$, the relative angular acceleration of the body with respect to the body. The reason for this is that the wheel data is relative to body.

Now recall,

$\dot{\Omega}$ = Angular rate of wheel relative to body

$$\dot{\Omega} = \omega_w - \left(\underline{\eta}_w^T\underline{\omega}_B\right) \tag{4-59}$$

Differentiation gives,

$$\omega_w = \ddot{\Omega} - \underline{\eta}^T\underline{\omega}_B \tag{4-60}$$

Thus,

$$T_M - K\dot{\Omega} = I\left(\ddot{\Omega} - \underline{\eta}_w^T\dot{\underline{\omega}}_B\right) \tag{4-61}$$

Now add subscript i to denote the ith wheel and note.

$$\underline{\eta}_w^T\underline{\omega}_B = \underline{\eta}_i^T\underline{\omega}_B \tag{4-62}$$

where $\underline{\eta}_i$ and $\dot{\omega}_B$ are in body coordinates. This gives the ith wheel equation.

$$\ddot{\Omega}_i = -\frac{K_i}{I_i}\dot{\Omega}_i + \frac{T_{Mi}}{I_i} - \underline{\eta}_i^T\underline{\omega}_B \tag{4-63}$$

With the wheel equation now derived we can summarize the complete dynamical system of equation

From (4-35)

$$\dot{e} = S_2 \underline{\omega}_B + \dot{S}_2 \underline{\omega}_B - \dot{S}_3 T_3 \underline{\omega}_o \tag{4-64}$$

and

$$\ddot{\Omega} = -\frac{K_1}{I_1}\Omega_1 + \frac{T_{M1}}{I_1} - \underline{\eta}_\iota^T \underline{\omega}_B \tag{4-65}$$

where

Terms	Given by Equation
S_2	A-17
S_2	A-22
S_3	A-23
$\dot{\underline{\omega}}_B$	(4-29)
$\underline{\omega}_B$	(4-37)
$\underline{\omega}_o$	(4-30)

4 3 3 Measurement Equations

4 3 3 1 Introduction

From various data telemetered down from the spacecraft very precise estimates are to be made of Euler angles and rates These Euler angles combined with the orbit coordinate axis directions and ephemeris data, provide sufficient information to determine the center and corner coordinates of the image frame

Telemetered attitude data which needs to be related to the Euler angles and Euler rates are

- Horizon sensor angles A, B, C, D
- Rate gyro readings $\left(\omega_{IA_1}, \omega_{IA_2}\right)$

For angles A, B, C, D see Figure A-1

The reaction wheel position data are also available. The relationship between it and the corresponding wheel i of (4-60) is obvious.

4.3 3.2 Horizon Scanner Measurement

The angles A and C are related to roll, and B and D are related to pitch — the precise relationships to be derived — the horizon sensor angle differences are shown in Figure 4-7 If the spacecraft Euler angles are all zero, the Z_b body axis aligns with the orbit coordinate Z_o axis For nonzero Euler angles, the difference in horizon head angle measurements $\Delta\theta_1$, $\Delta\theta_2$ can be related to any shift of Z_b from the Z_o direction

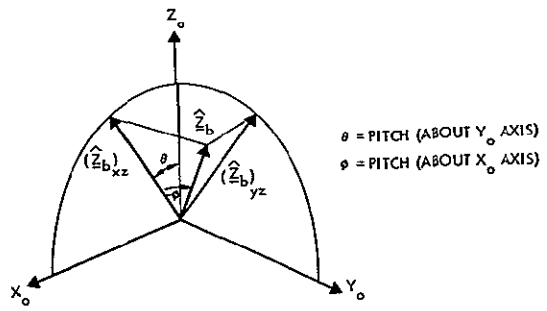

$$\Delta\theta_1 = \frac{A - C}{2} \qquad (4\text{-}66)$$

$$\Delta\theta_2 = \frac{B - D}{2} \qquad (4\text{-}67)$$

Figure 4-7
Z BODY AXIS
and sensor angle differences

The effect of yaw does not change the A, B, C, D readings by any significant degree. Thus, Δ_1, Δ_2 can be related directly to roll (ϕ) and pitch (θ) as is clear from Figures 4-7 and 4-8. From Figure 4-8 note,

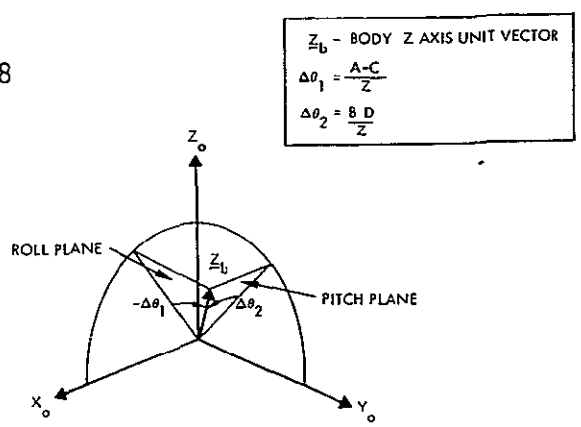

$$\sin\theta = \frac{\left|(\hat{Z}_b)_x\right|}{\left|(\hat{Z}_b)_{xy}\right|} = \frac{\sin(\Delta\theta_2)}{\cos(\Delta\theta_1)} \qquad (4\text{-}68)$$

$$\phi = \Delta\theta_1 \qquad (4\text{-}69)$$

Figure 4-8
Z BODY AXIS
and euler angles

Thus the horizon measurements in terms of Euler angles are,

$$\frac{A - C}{2} = \Delta\theta_1 = \phi \qquad (4\text{-}70)$$

$$\frac{B - D}{2} = \Delta\theta_2 = \sin^{-1}(\sin\theta\cos\phi) \qquad (4\text{-}71)$$

4.3 3 3 Rate Gyro Measurements

In Figure 4-9 two rate gyro measurements are shown in the x, z plane If the rate gyros have a direction unit vectors $\underline{\eta}_{Gx}$ and $\underline{\eta}_{Gz}$ respectively then,

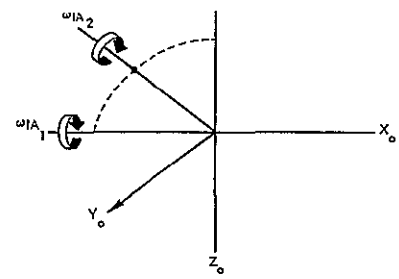

$$\begin{bmatrix} \omega_{IA_1} \\ \\ \omega_{IA_2} \end{bmatrix} = \begin{bmatrix} \underline{\eta}_{G_1}^T \\ \\ \underline{\eta}_{G_2}^T \end{bmatrix} \begin{bmatrix} \omega_x \\ \omega_y \\ \omega_z \end{bmatrix} \tag{4-72}$$

Figure 4-9
RATE GYRO measurements

where $(\omega_x, \omega_y, \omega_z)$ are the inertial body rate components

$$\underline{\omega}_B = (\omega_x, \omega_y, \omega_z)^T \tag{4-73}$$

Recall from Equation (4-37),

$$\underline{\omega}_B = S_2^{-1} \dot{\underline{e}} + S_1 T_3 \underline{\omega}_o \tag{4-74}$$

Substituting above,

$$\begin{bmatrix} \omega_{IA_1} \\ \omega_{IA_2} \end{bmatrix} = \left[\eta_G\right] \left[S_2^{-1} \dot{\underline{e}} + S_1 T_3 \underline{\omega}_o\right. \tag{4-75}$$

where

$$\left[\eta_G\right] \triangleq \begin{bmatrix} \underline{\eta}_{G_1}^T \\ \underline{\eta}_{G_2}^T \end{bmatrix} \tag{4-76}$$

4 4 TWO-GYRO PERFORMANCE ANALYSIS

4 4 1 Introduction

This section presents an analysis of an attitude determination system with two horizon scanners and two rate gyros, henceforth referred to as the two-gyro system, with respect to mapping accuracy. First, a quantitative summary of the effect of the two-gyro system attitude errors on the mapping accuracy of the RBV and MSS is given Next, a detailed explanation of the source of the errors is presented A simplified error model is derived from the exact equations of motion for the spacecraft The effect of all assumptions made in obtaining the error model are stated A covariance analysis of the Kalman filter mechanization employing the model is performed Finally, a summary is given tabulating the effect of both the assumptions used in deriving the error model and the errors from the Kalman filter convariance analysis

4 4 2 Development of the Two-Gyro Error Model

The following paragraphs derive an attitude error model for the two-gyro system mechanization The model is derived from the basic equations of motion and the Euler angle rate equations. Expressions for the Kalman filter measurements are also presented The effect on attitude accuracy of all assumptions and approximations is given

4 4 2 1 Equations of Motion

The equations of motion derived in Section 4.3 are repeated below in slightly modified form

$$\dot{\omega}_B = I_B^{-1}\left[T - I_S\mathring{\Omega}_S - A_\theta I_1\mathring{\Omega}_1 - \dot{H}_T - C\left(I_B\omega_B + I_S\Omega_S + A_\theta I_1\Omega_1 - H_T\right)\right] \tag{4-77}$$

$$\mathring{\Omega}_1 = I_1^{-1}\left[T_m - K_1\Omega_1\right] - A_\theta^{-1}\,\dot{\omega}_B \tag{4-78}$$

where

ω_B = inertial angular rate of S/C in S/C reference coordinates — 3 x 1 vector

Ω_1 = angular rate of reaction wheels about their spin axes relative to the S/C — 3 x 1 vector

Ω_S = angular rate of solar panels about their spin axis relative to the S/C — 3 x 1 vector

T = external S/C disturbance torques in S/C coordinates — 3 x 1 vector

T_m = reaction wheel motor torques — 3 x 1 vector

H_T = tape recorders total momentum in S/C coordinates — 3 x 1 vector

I_B = inertia tensor of S/C in S/C coordinates — 3 x 3 matrix

I_1 = diagonal matrix giving inertias of reaction wheels about their spin axes — 3 x 3 matrix

I_S = inertia tensor of solar panels in S/C coordinates — 3 x 1 vector

K_1 = diagonal matrix giving damping coefficient of reaction wheels about their spin axes — 3 x 3 matrix

A_θ = non-orthogonal reaction wheel spin axes misalignment matrix — 3 x 3 matrix

and

$$C \triangleq \begin{bmatrix} 0 & -\omega_z & \omega_y \\ \omega_z & 0 & -\omega_x \\ -\omega_y & \omega_x & 0 \end{bmatrix}$$

The reaction wheel misalignment matrix is defined as

$$A_\theta \triangleq \begin{bmatrix} 1 & \theta_{xy} & \theta_{xz} \\ \theta_{yx} & 1 & \theta_{yz} \\ \theta_{zx} & \theta_{zy} & 1 \end{bmatrix}$$

where

θ_{ij} = misalignment of i — reaction wheel spin axis into the j axis of the S/C coordinate system

It has been decided from an operational viewpoint to stop the motion of the solar panels relative to the spacecraft body during the time pictures are taken Therefore,

$$\Omega_S = \mathring{\Omega}_S = 0$$

From the relation

$$\begin{bmatrix} T_1 \\ T_2 \\ T_3 \end{bmatrix} \triangleq I_B \dot{\omega}_B$$

one can obtain the torque components from (4-77)

$$\begin{aligned} T_1 = {} & T_x - I_{x_w} \mathring{\Omega}_x - \theta_{xy} I_{y_w} \mathring{\Omega}_y - \theta_{xz} I_{z_w} \Omega_{z_w} - \mathring{H}_{x_T} \\ & + \omega_z \left(I_{y_B} \omega_y + I_{yx} \omega_x + I_{yz} \omega_z \right) \\ & + \omega_z \left(I_{y_w} \Omega_y + \theta_{yx} I_{x_w} \Omega_x + \theta_{yz} I_{z_w} \Omega_z \right) + \omega_z \left(H_{y_T} \right) \\ & - \omega_y \left(I_{z_B} \omega_z + I_{zx} \omega_x + I_{zy} \omega_y \right) \\ & - \omega_y \left(I_{z_w} \Omega_z + \theta_{zx} I_{x_w} \Omega_x + \theta_{zy} I_{y_w} \Omega_y \right) - \omega_y \left(H_{z_T} \right) \end{aligned} \qquad (4\text{-}79)$$

$$
\begin{aligned}
T_2 = T_y &- I_{y_w}\mathring{\Omega}_y - \theta_{yx} I_{x_w}\mathring{\Omega}_x - \theta_{yz} I_{z_w}\mathring{\Omega}_z - \mathring{H}_{y_T} \\
&+ \omega_x\left(I_{z_B}\omega_z + I_{zx}\omega_x + I_{zy}\omega_y\right) \\
&+ \omega_x\left(I_{z_w}\Omega_z + \theta_{zx} I_{x_w}\Omega_x + \theta_{zy} I_{y_w}\Omega_y\right) + \omega_x\left(H_{z_T}\right) \\
&- \omega_z\left(I_{z_B}\omega_x + I_{xy}\omega_y + I_{xz}\omega_z\right) \\
&- \omega_z\left(I_{x_w}\Omega_x + \theta_{xy} I_{y_w}\Omega_y + \theta_{xz} I_{z_w}\Omega_z\right) - \omega_z\left(H_{x_T}\right) \qquad (4\text{-}80)
\end{aligned}
$$

The equation for T_3 involves approximately the same relative magnitudes as that for T_1 so it will not be presented here Whatever simplified form is derived for T_1 will be used for T_3 The following paragraphs will examine the magnitude of various terms in (4-79) and (4-80) in order to arrive at a simplified though accurate approximation of (4-77)

The known parameters are

$$I_{x_B} = 210 \text{ slug ft}^2$$

$$I_{y_B} = 250 \text{ slug ft}^2$$

$$I_{z_B} = 390 \text{ slug ft}^2$$

$$I_{x_w} = 3\ 05 \times 10^{-3} \text{ slug ft}^2$$

$$I_{y_w} = 3\ 05 \times 10^{-3} \text{ slug ft}^2$$

$$I_{z_w} = 12\ 20 \times 10^{-3} \text{ slug ft}^2$$

Approximate RMS values for the other parameters are

$$\omega_x \cong \omega_z \cong 6 \times 10^{-5} \text{ rad/sec}$$

$$\omega_y \cong 1 \times 10^{-3} \text{ rad/sec}$$

$$\Omega_x \cong \Omega_y \cong \Omega_z \cong 65 \text{ rad/sec (1/2 saturation speed)}$$

$$T_x \cong T_y \cong T_z \cong 1 \times 10^{-5} \text{ ft lb}$$

$$\theta_{ij} \cong 4 \times 10^{-4} \text{ rad (4 arc min } 3\sigma)$$

$$I_{ij} \cong 4 \text{ slug ft}^2$$

The tape recorders are aligned so that their total momentum vector lies normal to the S/C y axis to within 1×10^{-3} rad This results in

$$H_{x_T} \cong H_{z_T} \cong 0\ 007 \text{ ft lb sec}$$

$$H_{y_T} \cong 7 \times 10^{-6} \text{ ft lb sec}$$

The term $I_i \mathring{\Omega}_i$ consists of two separate torques as indicated in equation (4-78) The first torque is due to the reaction wheel motors The motors are turned on and off by the ACS and produce the following torques

$$T_{x_m} = T_{y_m} = 21 \times 10^{-3} \text{ ft lb}$$

$$T_{z_m} = 52 \times 10^{-3} \text{ ft lb}$$

The second torque is due to motor windage At 1/2 saturation speed the torque values are

$$K_x\Omega_x = K_y\Omega_y = 0\ 54 \times 10^{-3} \text{ ft lb}$$

$$K_z\Omega_z = 2\ 82 \times 10^{-3} \text{ ft lb}$$

Using the above parameter values, equation (4-79) can be rearranged as

$$T_1 = \left(-I_{x_w}\mathring{\Omega}_x - \mathring{H}_{x_T}\right) - \omega_y I_{z_w}\Omega_z$$

$$+ \left[T_x - \omega_z\omega_y\left(I_{z_B} - I_{y_B}\right) + \omega_z I_{y_w}\Omega_y - \omega_y H_{z_T}\right]$$

$$+ \left[\text{other torques}\right] \qquad (4\text{-}81)$$

where the right-hand side of the equation has been grouped into terms with expected values of

1st term $\leq 1 \times 10^{-2}$ ft lb

2nd term $\cong 0\ 8 \times 10^{-3}$ ft lb

3rd term $\cong 1 \times 10^{-5}$ ft lb

4th term $< 1 \times 10^{-5}$ ft lb

Similarly, equation (4-80) can be rearranged as

$$T_2 = \left(-I_{y_w}\Omega_y - \mathring{H}_{y_T}\right) - \left(\omega_z I_{x_w}\Omega_x - \omega_x I_{z_w}\Omega_z\right)$$

$$+ T_y + (\text{other terms}) \qquad (4\text{-}82)$$

where the right-hand side of the equation has been grouped into terms with expected values of

1st term $\leq 1 \times 10^{-2}$ ft lb

2nd term $\cong 5 \times 10^{-5}$ ft lb

3rd term $\cong 1 \times 10^{-5}$ ft lb

4th term $< 1 \times 10^{-5}$ ft lb

As noted above, T_3 involves approximately the same magnitudes as T_1 so it will not be presented here

It should be pointed out that the short term effect of the $I_1 \mathring{\Omega}_1$ torques is to produce the spacecraft limit cycle From the ACS analysis it is known that the limit cycle worst case magnitude is 0 18° peak Since the motion is very random, assume an RMS of 0 10° The torque terms involving the misalignment of the reaction wheels will couple the limit cycle motion of another axis into the axis being considered Since the misalignment angles are about four arc minutes (3σ), the attitude error due to misaligned wheels is about 4×10^{-5} degrees Therefore, this term was included in the category of "other torques "

The same limit cycle consideration is applicable when the above torque expressions are substituted into equation (4-77) The substitution gives

$$\dot{\omega}_x = I_{x_B}^{-1} T_1 + \left(I_{xy}^{-1} T_2 + I_{xz}^{-1} T_3 \right)$$

$$\dot{\omega}_y = I_{y_B}^{-1} T_2 + \left(I_{yx}^{-1} T_1 + I_{yz}^{-1} T_3 \right) \qquad (4\text{-}83)$$

$$\dot{\omega}_z = I_{z_B}^{-1} T_3 + \left(I_{zx}^{-1} T_1 + I_{zy}^{-1} T_2 \right)$$

The products of inertia are in the neighborhood of 2 percent of the moments of inertia for the spacecraft If their effect is neglected, they will introduce an attitude error due to gross axis limit cycles of 0 002° This

error is considered negligible for spacecraft attitude determination in view of the larger magnitude of other uncorrectable errors in the overall system With this approximation, the above equations reduce to:

$$\dot{\omega}_x \cong I_{x_B}^{-1} T_1$$

$$\dot{\omega}_y \cong I_{y_B}^{-1} T_2$$

$$\dot{\omega}_z \cong I_{z_B}^{-1} T_3$$

The two-gyro system mechanization uses a rate gyro along both the x and z spacecraft axes to measure relative attitude motion No information concerning the reaction wheel torques in these axes is used Therefore, the approximation is made that

$$T_1 \cong -I_{x_w} \Omega_x - \mathring{H}_{w_T}$$

$$T_3 \cong -I_{z_w} \Omega_z - \mathring{H}_{z_T}$$

For purposes of a covariance analysis, the assumption is made that T_1 and T_3 are correlated random error torques with a standard deviation of 1×10^{-2} ft lb Their correlation time is short enough to preclude their being estimated to any effective extent. That is

$$\dot{\omega}_x \cong \frac{T_{x_o}}{I_{x_B}}, \qquad \dot{\omega}_z \cong \frac{T_{z_o}}{I_{z_B}} \tag{4-84}$$

where

$$E\left[T_{x_o}^{\ 2}\right] = E\left[T_{z_o}^{\ 2}\right] = (1 \times 10^{-2} \text{ ft lb})^2$$

The attitude determination system uses reaction wheel revolution data to measure the relative pitch attitude motion of the spacecraft, i.e., it implicitly determines the angular acceleration $\mathring{\Omega}_y$ and solves for $\mathring{\omega}_y$ using the equation

$$\mathring{\omega}_y = \frac{I_{y_w}}{I_{y_B}} \mathring{\Omega}_y$$

A 2 percent error in the knowledge of the ratio of inertias will result in a scale factor error of 2 percent in estimating the limit cycle of the spacecraft in pitch attitude This produces the same magnitude of error as was introduced by the products of inertia, i e , 0 002°

In addition to using pitch reaction wheel data to determine pitch relative attitude, the mechanization also uses roll and yaw wheel data to estimate the roll and yaw wheel momentum Since roll and yaw body rates are measured directly by the rate gyros, it is assumed that the second term of the right-hand side of equation (4-82) can be neglected Therefore, the approximation is made that

$$T_2 \cong -I_y \mathring{\Omega}_y - \mathring{H}_{y_T} + T_y$$

For purposes of a covariance analysis, the assumption is made that T_y is a correlated random error torque with a standard deviation of 1×10^{-5} ft lb The correlation time is short enough to prevent the torque from being estimated That is

$$\dot{\omega}_y \cong \frac{-I_{y_w} \mathring{\Omega}_y - \mathring{H}_{y_T} + T_{y_o}}{I_{y_B}} \tag{4-85}$$

where

$$E\left[T_{y_o}^{\ 2}\right] = (1 \times 10^{-5} \text{ ft lb})^2$$

In summary, equation (4-77) has been reduced to the following equations

$$\dot{\omega}_x \cong \frac{T_{x_o}}{I_{x_B}}$$

$$\dot{\omega}_y \cong \frac{-I_{y_w}\mathring{\Omega}_y - \mathring{H}_{y_T} + T_{y_o}}{I_{y_B}} \tag{4-86}$$

$$\dot{\omega}_z \cong \frac{T_{z_o}}{I_{z_B}}$$

where

$$E\left[T_{x_o}^{\ 2}\right] = E\left[T_{z_o}^{\ 2}\right] = (1 \times 10^{-2} \text{ ft lb})^2$$

$$E\left[T_{y_o}^{\ 2}\right] = (1 \times 10^{-5} \text{ ft lb})^2$$

The assumptions made were

1) The solar panels were not moved during attitude estimation.

2) $\mathring{H}_{x_T}$, $\mathring{H}_{z_T}$ $< 10^{-2}$ ft lb.

3) Gyroscopic torques in the y axis due to x and z axis wheel momentum can be estimated better than 1×10^{-5} ft lb.

The approximations made were

1) Misalignment of the reaction wheels was not corrected. This resulted in an attitude error of 4×10^{-5} degrees in all three axes.

2) Products of inertia of the spacecraft were neglected. This resulted in an attitude error of 0.002° in all three axes.

3) The ratio of wheel to body inertia in the pitch axis was known to within 2 percent. This resulted in an attitude error in pitch of 0.002°

4.4.2.2 Euler Angle Rate Equations

The Euler angle rate equation derived in Section 4.3 is repeated below.

$$\omega_B = S_2^{-1}\dot{e} + S_1\omega_o \tag{4-87}$$

where

e = Euler angles (yaw, pitch, roll, in order) describing the attitude of S/C reference axes relative to rotating orbital axes.

ω_o = inertial angular rate of orbital axes in orbital axes coordinates.

S_1 = direction cosine matrix describing attitude of S/C reference axes relative to rotating orbital axes.

and

$$S_2^{-1} \triangleq \begin{bmatrix} 1 & \cos\theta & -\sin\theta \\ 0 & \cos\theta & \cos\theta\sin\phi \\ 0 & -\sin\theta & \cos\theta\cos\phi \end{bmatrix}$$

The orbital coordinate system is defined as follows 1) the origin is at the center of the S/C reference axes, 2) the z axis points to the center of the Earth, 3) the y axis is normal to the orbit plane and in the approximate direction of the orbit rate vector, and 4) $\underline{x} \times \underline{y} = \underline{z}$.

The inertial rate of the orbital coordinates consists of two components 1) the orbit rate of approximately 210°/hr due to rotation about the Earth, and the orbit plane precession rate of approximately 0.04°/hr due to the sun synchronous orbit. Although an attitude determination system can account for its presence, the assumption is made here that it can be omitted from the performance analysis without affecting the predicted results. Therefore, in orbit coordinates

$$\omega_o = \begin{bmatrix} 0 \\ \omega_o \\ 0 \end{bmatrix}$$

The largest Euler angle expected is 0.4° and all Euler angle rates are expected to be in the same order of magnitude. Therefore, the following small angle approximations are made for all three Euler angles.

$$\cos e_i \cong 1$$

$$\sin e_i \cong d_i \qquad i = 1, 2, 3 \quad e_1 = \phi,\ e_2 = \theta,\ e_3 = \psi$$

$$e_i \gg e_i \dot{e}_i$$

Using this approximation, Equation (4-87) becomes

$$\begin{aligned} \omega_x &\cong \dot{\phi} + \psi\omega_o \\ \omega_y &\cong \dot{\theta} + \omega_o \\ \omega_z &\cong \dot{\psi} - \phi\omega_o \end{aligned} \tag{4-88}$$

In summary, Equation (4-87) was reduced to Equation (4-88) using the following assumptions

1) Small angle approximations are valid.

2) Omission of orbit precession rate does not affect the performance analysis accuracy.

4.4 2.3 Measurement Equations

Now that the simplified dynamical equations have been derived, measurement equations, are needed before the covariance analysis can be performed. Referring to Figure 4-10, it is observed that a perfect Earth sensor in a perfect attitude control loop will not point the spacecraft z axis at the center of the Earth. Instead, its attitude will lie somewhere between geocentric and geodetic if the equipotential radiance surface tracked by Earth sensors is an ellipsoid fairly close to the Earth For reference, the maximum difference between geocentric and geodetic latitude on the Earth (at 45° latitude) is about 0 2°.

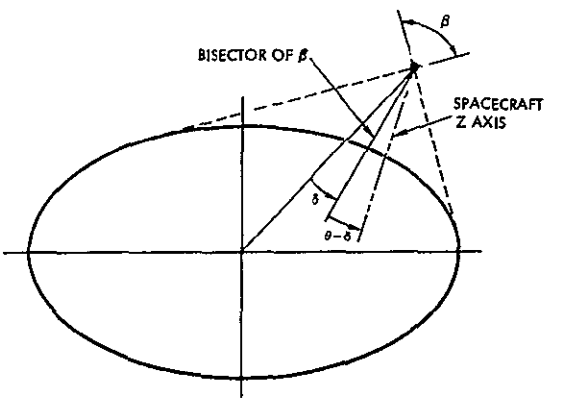

Figure 4-10
GEOMETRIC DEFINITION of earth sensor measurement in polar plane

In view of the fact that the maximum δ shown in Figure 5.1 will be less than 0 2° and that small angle approximations have been assumed valid for the Euler angles, then the Earth sensor pitch and roll signals are assumed to be

$$\theta_{ESA} = \theta - \delta_\theta + \theta'_B + \theta_n$$

$$\phi_{ESA} = \phi - \delta_\phi + \phi'_B + \phi_n$$

where

θ'_B, ϕ'_B = Earth sensor bias errors, excluding misalignment.

θ_n, ϕ_n = Earth sensor high frequency noise (f_o > 1 cps).

$\delta_\theta, \delta_\phi$ = error in prediction of the pitch and roll components of δ.

Misalignment errors are not included for either Earth sensor since it is assumed an initial calibration of attitude sensor plus camera misalignments will be made using pictures with ground truth points along with attitude estimate data.

The error in predicting δ is 0.022° (1σ). The ESA bias is 0.028° (1σ) and the noise is 0.04° (1σ). Assuming that δ is subtracted from the measured signal, the ESA signals are redefined as

$$\theta_{ESA} = \theta + \theta_B + \theta_n$$

$$\phi_{ESA} = \phi + \phi_B + \phi_n$$

where

$$E\left[\theta_B{}^2\right] = E\left[\phi_B{}^2\right] = (0.036°)^2$$

$$E\left[\theta_n{}^2\right] = E\left[\phi_n{}^2\right] = (0\ 04°)^2$$

The roll and yaw gyros measure roll and yaw inertial rates plus errors For the same reason as stated above, misalignment angles are not considered. The gyros have a bias error of 0 06°/hr (1σ) and a high frequency noise of 0.1°/hr (1σ). Their outputs are

$$\omega_\phi = \omega_x + \epsilon_\phi + n_\phi$$

$$\omega_x = \omega_z + \epsilon_x + n_x$$

where

$$E\left[\epsilon_\phi{}^2\right] = E\left[\epsilon_\psi{}^2\right] = (0.06°/hr)^2$$

$$E\left[n_\phi{}^2\right] = E\left[n_\psi{}^2\right] = (0.1°/hr)^2$$

At every 45° of the pitch reaction wheel revolution, a pulse is provided and recorded and hence a quantization error of 45° is introduced. It is easily shown that error has a uniform probability density function

with zero mean and a standard deviation of 13°. Therefore, the reaction wheel signal, η_{RW}, is

$$\eta_{RW} = \eta_{\theta} + n_{RW}$$

where

$$E\left[\eta_{RW}^2\right] = (13^{\circ})^2$$

In summary, the equation for the measured attitude sensor signals are

$$\theta_{ESA} = \theta + \theta_B + \theta_n$$

$$\phi_{ESA} = \phi + \phi_B + \phi_n$$

$$\omega_{\phi} = \omega_x + \epsilon_{\phi} + n_{\phi}$$

$$\omega_{\psi} = \omega_z + \epsilon_{\psi} + n_{\psi}$$

$$\eta_{RW} = \eta_{\theta} + n_{RW}$$

where

$$E\left[\theta_B^2\right] = E\left[\phi_B^2\right] = (0.036^{\circ})^2$$

$$E\left[\theta_n^2\right] = E\left[\phi_n^2\right] = (0.04^{\circ})^2$$

$$E\left[\epsilon_{\phi}^2\right] = E\left[\epsilon_{\psi}^2\right] = (0\ 06^{\circ}/hr)^2$$

$$E\left[n_{\phi}^2\right] = E\left[n_{\psi}^2\right] = (0.1^{\circ}/hr)^2$$

$$E\left[n_{RW}^2\right] = (13^{\circ})^2$$

The assumption used in deriving the above equations is that the small angle approximations apply to both the Euler angles and δ.

4.4.2.4 Error Model

Equation (4-86), (4-88), and (4-89) are expressed in block diagram form in Figure 4-11. This error model will be used in the covariance analysis

4.4.3 Covariance Analysis of Error Model

The previous paragraphs developed a simplified error model and a set of measurement equations which made noisy observations of various states in the model. This section will determine the variance of the error in trying to estimate the three attitude angles in the model by processing the measurement data. In addition to estimating absolute

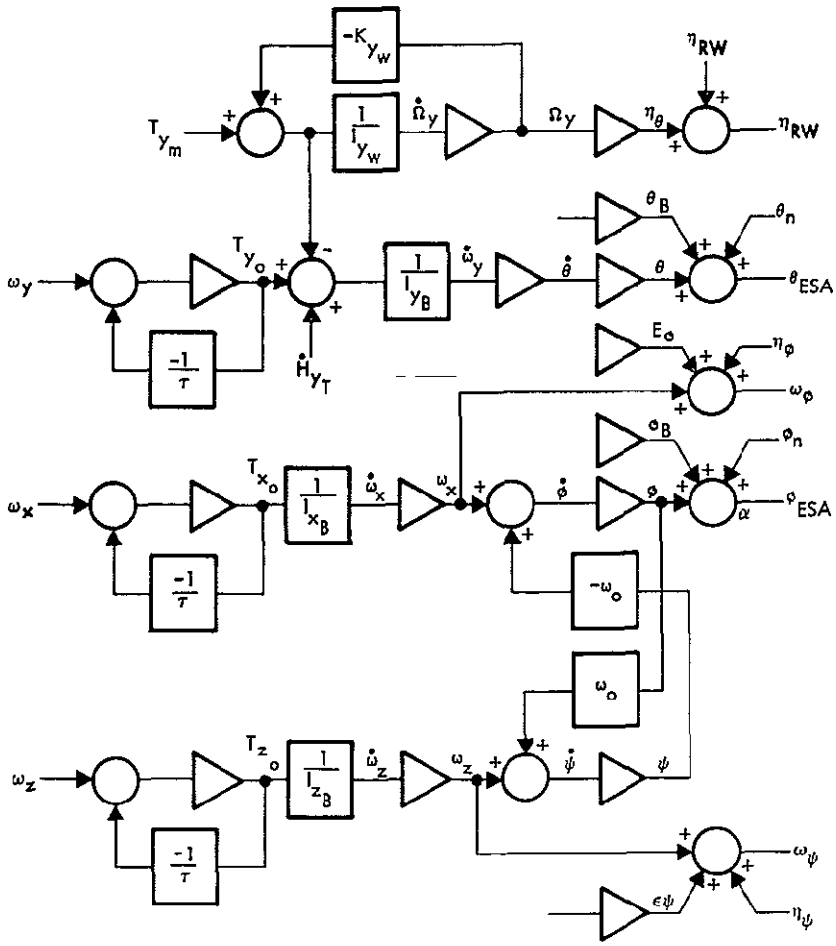

Figure 4-11
ERROR BLOCK DIAGRAM FOR COVARIANCE ANALYSIS

pitch, roll, and yaw, an estimate of the relative change in pitch and roll during a 28 second period will also be made.

In determining the estimation error, a Kalman filter mechanization was employed The Kalman filter was used to indicate the best results achievable without the necessity of a Monte Carlo analysis.

4 4.3.1 Relative Pitch Attitude

An error model for relative pitch attitude estimation is shown in Figure 4-12. This model is the same as Figure 4-11 except for omission of the pitch bias error The bias will not affect the relative attitude estimation as long as the assumption that it is a constant during the estimation period is valid. Figure 4-12 also shows the tape recorder momentum as a step rate input instead of a torque. This simulates the effect of turning on or off the tape recorders.

A Kalman filter mechanization using the error model in Figure 4-12 was programmed on a digital computer and the covariance of the estimation error was recorded as a function of time for various error magnitudes and initial conditions.

The first effect noted was that the estimation of relative pitch attitude was mostly unaffected by reaction wheel motor torques. The reason for this is that the motor torques produce a wheel motion identical to the body motion except for a scale factor equal to the ratio of wheel and body

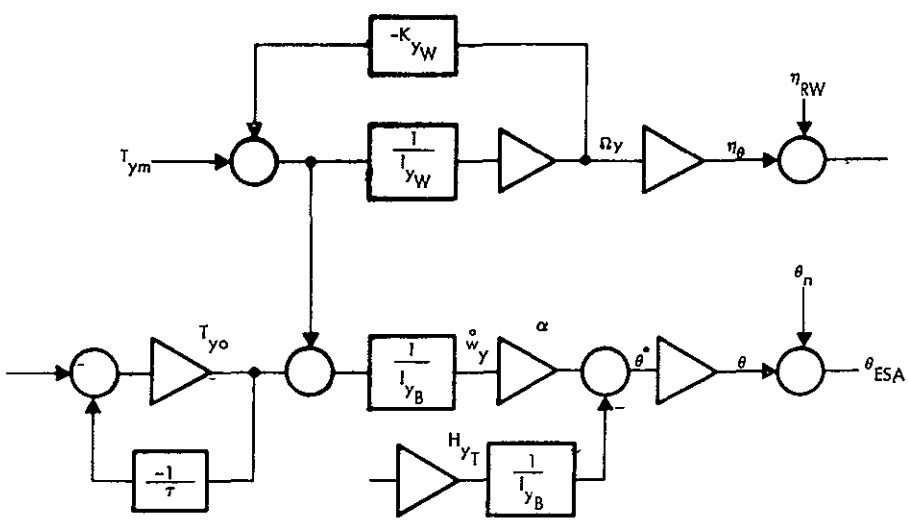

Figure 4-12
PITCH ATTITUDE ERROR MODEL

inertias. The uncertainty in wheel position because of the quantized data is insignificant compared to the error due to other spacecraft disturbance torques. In starting the filter, initial spacecraft and wheel rates of 0.003°/sec and 58 rad/sec were assumed. With a one second sampling rate, the filter converged on a steady state wheel rate estimate within 20 seconds. Converging on a steady state body rate estimate produced the predominate time constant in the estimation process. The steady state values for body rate and attitude are a function of the magnitude of disturbance torque, T_{y_o}, assumed. It was found that variations in the disturbance torque time constant, τ, produced little effect on attitude estimation for values below 100 seconds. In view of the many factors producing the disturbance torque, T_{y_o}, the assumption of a longer time constant was questionable. Figure 4-13 shows the effect of the magnitude of T_{y_o} on the standard deviation of the error in estimating θ.

The maximum tape recorder momentum is 0.007 ft lb sec. The tape recorders are aligned so that their total momentum vector is normal to the pitch axis within 1 milliradian. Therefore, turning the tape recorders on or off will result in a momentum change in the pitch axis

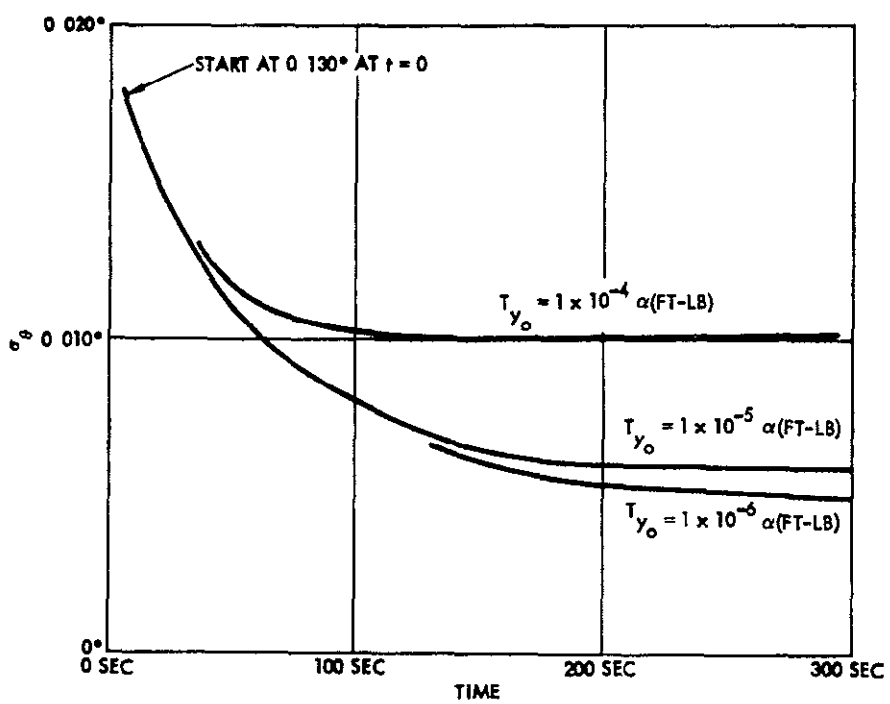

Figure 4-13
PITCH RELATIVE ACCURACY VERSUS DISTURBING TORQUES

of 7×10^{-6} ft lb sec. In turn, this will produce a body rate of 1.6×10^{-6} deg/sec. It was determined that this step change in rate did not significantly affect the estimation of pitch attitude.

From the derivation of the error model it was found that a reasonable value for the magnitude of T_{y_o} was 1×10^{-5} ft lb. Referring to Figure 4-13, this will produce a relative pitch attitude accuracy of 0.006° in 150 seconds from the time that the Kalman filter starts processing data.

4.4.3.2 Absolute Pitch Attitude

The error model for absolute pitch attitude estimation is the complete pitch channel shown in Figure 4-11. As pointed out previously, the only difference between the absolute and relative error models is the bias θ_B. The bias arises from radiance model and Earth sensor errors and has a magnitude of 0.036° (1σ).

A digital computer analysis was performed using the absolute pitch error model in a Kalman filter mechanization. Within seconds the pitch attitude error leveled out at approximately 0.036° This result was predictable since the bias is uncorrelated with the relative attitude error and their net effect on absolute pitch attitude is the RSS of the two errors.

4.4.3.3 Relative Roll Attitude

The error model for relative roll attitude estimation is exactly as shown in Figure 4-11 except that the roll Earth sensor bias is omitted. The bias was omitted for the same reasons explained in the paragraphs on relative pitch estimation.

A Kalman filter mechanization using this error model was programmed on a digital computer and the covariance of the estimation error was recorded as a function of time for various error magnitudes and initial conditions.

Figure 4-14 shows the transient response of the error in the estimation of roll attitude. As would be expected, the rate gyro on the roll axis immediately estimates the initial roll rate of the spacecraft down to the neighborhood of the gyro noise. However, the filter must still esti-

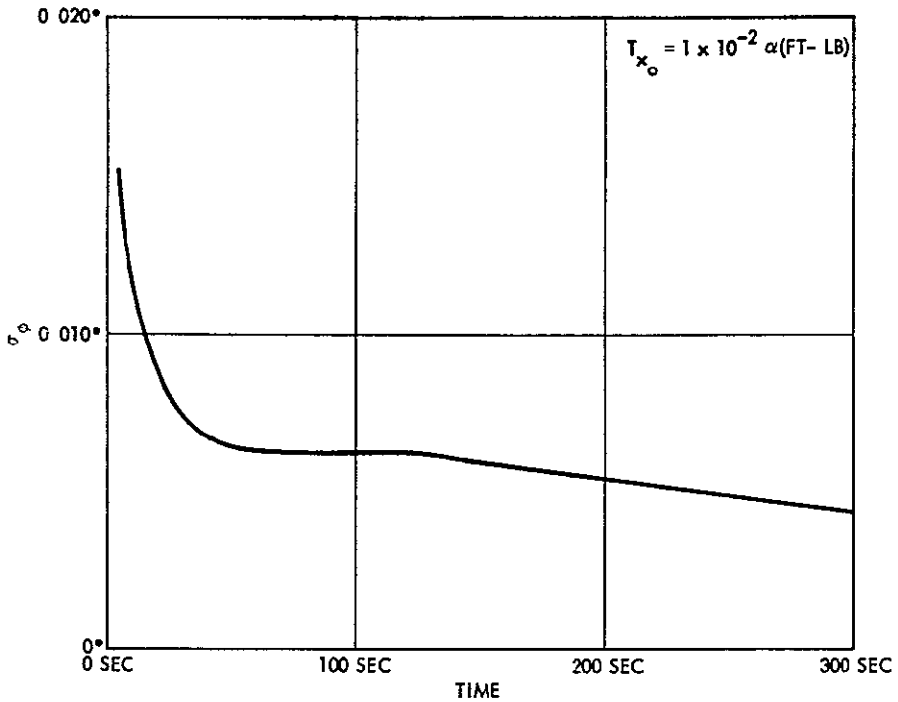

Figure 4-14
ROLL RELATIVE ACCURACY

mate the rate introduced in roll by an initial yaw misalignment. This is the reason the error remains relatively constant from 50 seconds to 100 seconds. After 100 seconds the error gradually decreases mostly due to the fact that the yaw estimate is also improving.

Referring to Figure 4-14, after a time period of 300 seconds, the error has a value of 0.005° (1σ). Three hundred seconds is chosen because the Kalman filter requires this long to reduce the error in the yaw estimate to an acceptable level.

4.4.3.4 Absolute Roll Attitude

This error model for absolute roll attitude estimation is the complete roll and yaw channels shown in Figure 4-11. As pointed out previously, the only difference between the absolute and relative error models is the bias ϕ_B. The bias arises from radiance model and Earth sensor errors and has a magnitude of 0.036° (1σ).

A digital computer analysis was performed using the absolute roll error model in a Kalman filter mechanization The result was the same as found for the absolute pitch case, i.e., the resultant error was the RSS of the bias and the relative roll error, approximately 0 036° (1σ).

4.4 3.5 Absolute Yaw Attitude

The error model for absolute yaw attitude determination consists of the complete yaw and roll channels shown in Figure 4-11.

An examination of the error model indicates that yaw is estimated not only by processing the gyro signals, ω_ϕ and ω_ψ, but also by observing the roll Earth sensor signal. Use of the roll signal is not readily apparent in the ACS mechanization since the signal is not used in the yaw attitude control electronics. The premise for the yaw control loop, however, is that roll will be maintained at approximately zero. For example, if the body coordinates and the orbit coordinates are both rotating about their y-axis at orbit rate, ω_o, but are initially misaligned by a yaw angle, then as time progresses the roll angle will increase. To counter this increase, the roll control channel will command a counter rate about the body roll axis. This counter rate will be equal to the yaw misalignment times orbit rate. The ACS gyro, which has a component of its input axis along the body roll axis, will measure this rate and correct the yaw misalignment.

The above example also illustrates the basic time constant in the transient response of either the ACS or ADS yaw channel. Correction or estimation of the yaw misalignment depended on both detecting the roll-misalignment, which is proportional to ω_o, in the presence of roll ESA noise and detecting the commanded roll rate, also proportional to ω_o, in the presence of gyro noise. Therefore, with an optimum estimation scheme, the transient response becomes a function of both orbit rate and sensor noise levels.

Figure 4-15 illustrates the result of a covariance analysis of the yaw and roll channels. The errors are broken up into two components in order to illustrate the transient response of the estimation error without the roll gyro bias included. At t = 300 seconds the total yaw error is approximately the RSS of the transient response and the error due to the gyro drift rate, namely 0.038° (1σ).

4.5 SUMMARY OF TOTAL ADS ERRORS

Section 4.4 2 derived an error model from the basic equations describing spacecraft attitude by making assumptions and approximations concerning

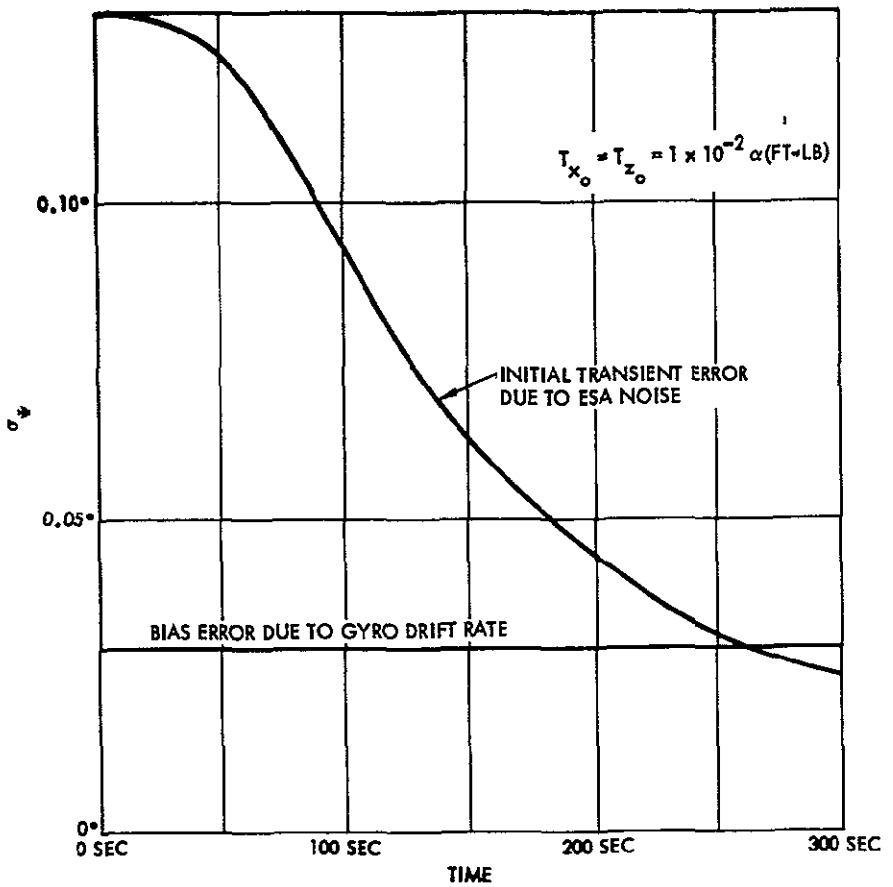

Figure 4-15
YAW ABSOLUTE ACCURACY

1) Solar panel motion

2) Tape recorder torques

3) Correction of gyroscopic torques from reaction wheel momentum

4) Misalignment of reaction wheels

5) Spacecraft products of inertia

6) Accuracy of spacecraft moments of inertia

7) Small angle approximations

8) Omission of orbit precession in analysis

Section 4.4.3 used the error model in a Kalman filter mechanization and presented the covariance of the error in estimating the three spacecraft

attitude angles, both absolute and relative. Additional assumptions were required concerning:

1) The time invariance of the gyro and Earth sensor bias.

2) The autocorrelation function of the disturbance torques modeled.

3) The statistical independence of one second samples of the gyro and Earth sensor high frequency noise terms.

Table 4-1 presents a summary of the attitude errors resulting from both the approximations of Section 4.2 and the covariance errors predicted in Section 4.3.

The roll, pitch, and yaw bias errors were increased to 0.05° (1σ) in subsequent analyses of the volume, for the two gyro systems, for the purpose of conservative error analyses.

Table 4-1 Summary of ADS Attitude Errors

Criteria/Error Sources	Error Source Magnitude	Attitude Error
Absolute Attitude Determination		
Pitch		
Radiance model	1.4 km (1σ)	0.022 (1σ)
ESA bias	0.028 (1σ)	0.028 (1σ)
Limit cycle (see below)	—	0.007 (1σ)
		RMS = 0.036 (1σ)
Roll		
Radiance model	1.4 km (1σ)	0.022 (1σ)
ESA bias	0.028 (1σ)	0.028 (1σ)
Limit cycle (see below)	—	0.005 (1σ)
		RMS = 0.036 (1σ)
Yaw		
Gyro drift rate bias	0.06 /hr (1σ)	0.029 (1σ)
Gyro noise	0.10 /hr (1σ)	0.000 (1σ)
ESA noise (transient error at 300 sec)	0.04 (1σ)	0.025 (1σ)
		RMS = 0.038 (1σ)
Relative Attitude Determination		
Pitch limit cycle		
Reaction wheel quantization	8 pul/rev	0.000 (1σ)
Ratio of inertias	2%	0.002 (1σ)
Reaction wheel misalignment	4 arc min max	0.000 (1σ)
S/C disturbance torques	1×10^{-5} ft lb	0.006 (1σ)
Tape recorder momentum change	0.007 ft lb sec	0.000 (1σ)
S/C products of inertia	4 slug ft^2	0.002 (1σ)
		RMS = 0.007 (1σ)
Roll limit cycle		
ESA noise (transient error at 300 sec)	0.04 (1σ)	0.005 (1σ)
Gyro noise	0.10 /hr (1σ)	0.000 (1σ)
		0.005 (1σ)

CONTENTS

			Page
5	TOTAL SYSTEM ACCURACY		5-1
	5 1	Introduction and Summary	5-1
	5 2	MSS Error Analysis	5-2
		5 2 1 Summary	5-2
		5 2 2 Computation of Sensitivity Matrix for the MSS Imagery	5-6
		5 2 3 Mathematical Description of Internal Consistency Errors in the MSS Imagery	5-13
		5 2 4 Error Analysis Results	5-18
		5 2 5 Pseudo-Reseau Correction	5-31
	5 3	RBV Geometric Error Analysis	5-37
		5 3 1 Pre-reseau Errors	5-37
		5 3 2 Reseau Distortion Estimation Analysis	5-39
		5. 3 3 Ground Truth Incorporation Analysis	5-52
	5 4	Post Digital Processing Error Analysis	5-57
		5 4 1 Precision Photo-Restitutor Geometric Error Analysis	5-57
		5. 4 2 Laser-Beam Recorder Geometric Error Analysis	5-59
	5 5	Overall Geometric Errors	5-62
	5 6	Photometric Analysis	5-72
		5. 6 1 MTF Analysis	5-72
		5 6 2 Radiometric Error Analysis	5-90

5. TOTAL SYSTEM ACCURACY

5 1 INTRODUCTION AND SUMMARY

This section documents the results of the overall ERTS system geometric and photometric error analysis investigations Only the error analyses of the selected data processing configuration are presented here Tradeoff studies supporting the final configuration selection are documented in Volume 17. A complete description of the selected data processing configuration is given in Volume 14 The data processing is divided into the following four modes

Bulk I

No geometric correction for MSS or RBV, hard copy imagery produced on the LBR with photometric adjustments for gain, gamma and shading.

Bulk II

Digital RBV reseau measurements used to geometrically correct RBV image in PPR (precision photo restitutor), attitude determination data used to geometrically correct MSS image in PPR

Precision I

Similar to bulk II but all geometric corrections in MSS and RBV performed digitally, also attitude data may be improved by ground truth measurements

Precision II

A "special request" mode, can include image enhancement, cosmetic corrections, etc

Error analyses were performed to obtain overall system mapping and photometric accuracies for both the MSS and RBV payloads. The chief results of the geometric analysis are given in Table 5-1 The photometric analysis results are summarized in the MTF curves and the radiometric analysis of Section 5-6 Tradeoff studies which supported the final data processing configuration selection are presented separately in Volume 17 Only the error analyses of the selected configuration are presented here

Table 5-1 Geometric Error Analysis Summary

Processing Mode	Picturing Centering Error Due to Attitude Determination		Internal Consistency Error		Total Error	
	MSS	RBV	MSS	RBV	MSS	RBV
Bulk I (No geometric correction)	11 000 ft (3σ)	8 000 ft (3σ)	9 000 ft (3σ)	12 000 ft (3σ)	11 000 ft (3σ)	14 000 ft (3σ)
Bulk II (In PPR correct RBV using digital reseau measurements and MSS using attitude data from the spacecraft)	9 000 ft (3σ)	8 000 ft (3σ)	1 900 ft (3σ) {2 700 ft (3σ) one gyro case}	880 ft (3σ) {880 ft (3σ) one gyro case}	9 000 ft (3σ)	8 000 ft (3σ)
Precision 1* (Digitally correct RBV using digital reseau measurements digitally correct MSS using attitude data (a) ground truth (b) PPR correlation of RBV with MSS to improve estimate of yaw bias or (c) both	I* II		(a) 1 500 ft to 1 900 ft (3σ) depends on ground truth location accuracy (b) 1 500 ft (3σ) (c) 1 110 ft to 1 400 ft (3σ)	320 ft (3σ)	(a) 1 500 ft to 1 900 ft (3σ) depends on ground truth location accuracy (b) 8 000 ft (3σ) (c) 1 500 ft to 1,900 ft (3σ)	8 000 ft (3σ) 930 ft (3σ) using ground truth
Precision 2 Special request mode						

*The accuracy numbers are errors in the digital tape output and do not include LBR or film processing errors

5 2 MSS ERROR ANALYSIS

5 2 1 Summary

In digital processing of the MSS picture, satellite attitude and ephemeris data is used to correct for geometric distortions of the picture. The MSS scans out, on an angle versus time basis, the full 100 nmi X 100 nmi picture To understand the relationship between the scanner image and scanner attitude see Figure 5-1 The vehicle moves along the orbital path as shown during the first scan Δt During this time period a corresponding series of terrain points are swept out by the scanner, these points correspond to the intersection of the instantaneous scan vector $\underline{\beta}$ with the earth's surface. In digital data processing this is done by a knowledge of vehicle attitude and satellite motion during the scan The latitude-longitude is computed by the intersection of $\underline{\beta}$, originating from the satellite location, with an "adjusted" geoidal surface representing the mean altitude of the terrain within one MSS picture. Because of attitude and ephemeris errors the wrong terrain

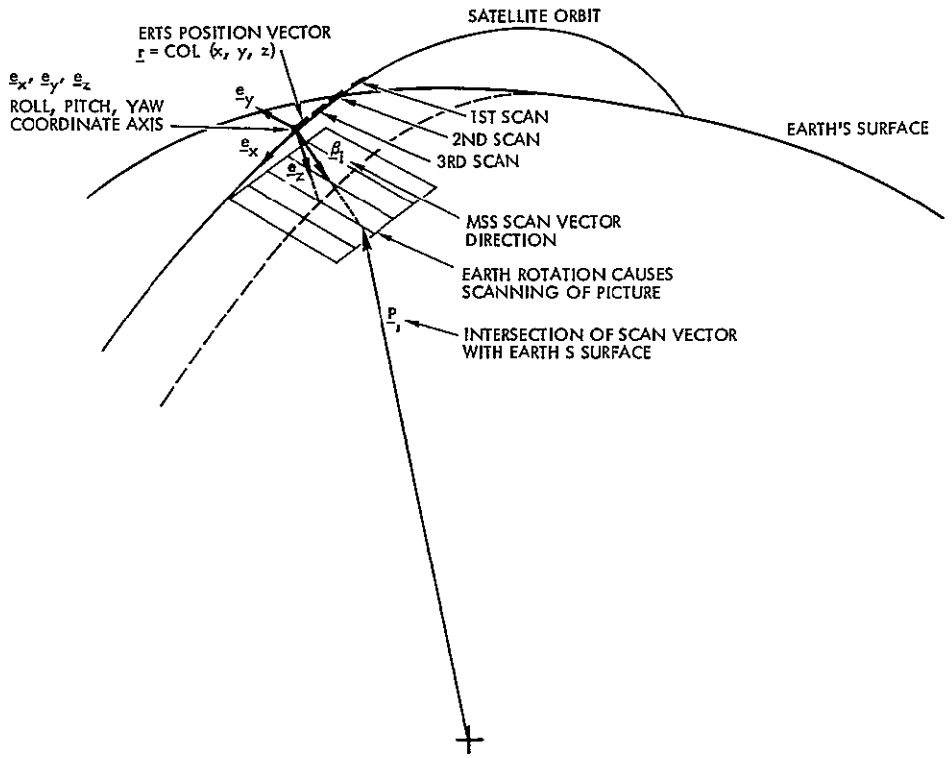

Figure 5-1
MSS PICTURE Geometry During Scanning

points will be computed Obviously earth rotation must be considered in order to accurately reconstruct longitude from the data

Volume 17 contains a discussion of the picture distortions produced by various error sources The principal effects, however, are pitch and roll bias (producing a MSS picture centering error), yaw bias (producing a skewing of the picture), and vehicle attitude time variations that produce internal consistency errors within the picture Due to computing time involved, the precision ground point is not computed for each of the 11 million picture elements, instead, only some 25 reference points are computed within the picture, the rest are computed by a "pseudo-reseau" technique similar to that used in the RBV data processing

Equations have been derived for the absolute position error sensitivities These equations give the sensitivity of picture errors to geometric and sensor error sources A computer program for MSS error analysis has been developed using these sensitivities in a covariance

analysis of both absolute mapping and internal consistency errors. Internal consistency errors are of more importance than absolute position errors since, if the internal consistency is good, one ground truth point can establish the absolute position of all other points in the 100 nmi X 100 nmi picture. Let Δx, Δy represent the cross-scan and along-scan absolute position errors, respectively, and let $e_1, \ldots, e_n$ represent error sources 1 through n. Then

$$\begin{pmatrix} \Delta x \\ \\ \Delta y \end{pmatrix} = \begin{pmatrix} \frac{\partial \Delta x}{\partial e_1} & \cdots & \frac{\partial \Delta x}{\partial e_n} \\ \\ \frac{\partial \Delta y}{\partial e_1} & \cdots & \frac{\partial \Delta y}{\partial e_n} \end{pmatrix} \begin{pmatrix} e_1 \\ \cdot \\ \cdot \\ e_n \end{pmatrix} \tag{5-1}$$

or, in matrix form

$$\underline{\xi}_i = M_i \underline{e}_i \tag{5-2}$$

$\underline{\xi}_i$ is the vector absolute position error at time t_i, $\underline{e}_i$ is the error source vector at time t_i, and M_i is the sensitivity matrix

Internal consistency is defined as the accuracy with which one ground point can be located relative to another. Thus, the internal consistency, or relative position error, can be found by differencing the absolute errors at two different points t_i and t_j in the MSS picture (taking into account the error-correlation between the two points). One of the two points, the reference point, is normally taken to be at the center of the picture Thus, if $\underline{\Delta\xi}$ represents the internal consistency error vector

$$\underline{\Delta\xi} = \underline{\xi}_i - \underline{\xi}_j = M_i \underline{e}_i - M_j \underline{e}_j \tag{5-3}$$

a covariance analysis of (5-2) gives, for the absolute error

$$C_{\xi_i} = M_i C_{e_i} M_i^T \tag{5-4}$$

where for the relative error, a covariance analysis gives

$$C_{\Delta\xi} = C_{\xi_i} + C_{\xi_j} - M_i \langle \underline{e}_i \underline{e}_j^T \rangle M_j^T - M_j \langle \underline{e}_j \underline{e}_i^T \rangle M_i^T \qquad (5\text{-}5)$$

From (5-5) it should be noted that with the exception of uncorrelated noise, the internal consistency errors go to zero as $t_i \rightarrow t_j$ (that is, the two points approach each other within one scan line) It should also be noted from (5-5) that the buildup of internal consistency errors with time separation $t_j - t_i$ depends critically on the time as well as the spatial correlation of the error sources $\langle \underline{e}_i \underline{e}_j^T \rangle$. It is expected that the attitude determination errors will be exponentially correlated in time as well as being cross-correlated in roll and yaw. Terrain variations will be exponentially correlated in terms of their spatial separation (distance) in the picture. MSS alignment errors will be constant in time with zero ensemble average. Sensor quantization will be assumed as white noise (uncorrelated from one point to the next)

Thus it can be seen that the internal consistency error analysis is critically dependent upon the assumed error-correlation model The final MSS error analysis results are shown in Table 5-2, where the relative errors are given as measured from picture point No 13 (center of the picture) or picture point No 25 (corner of the picture) As can be seen from the totals, the 3-sigma absolute error is on the order of 1.5 mile while the 3-sigma internal consistency errors are 2700 feet as measured from one corner to the diagonally opposite corner Table 5-2 also shows that ground truth data reduces the absolute errors to the order of the relative errors (about 1500 feet 3-sigma for ground truth data on the order of 200 feet 1-sigma)

The results given in this table apply to the precision digitally processed "pseudo reseau" points which can then be used in conjunction with a quadratic distortion interpolation function to remove the picture distortions caused by spacecraft motion and attitude limit cycling.

Table 5-2 MSS Error Analysis Summary

Summary (Errors at #1)		1-Sigma North (Cross-scan) (feet)	1-Sigma East (Along-scan) (feet)
Attitude Determination* (No ground truth)	Absolute	2680	2738
	Relative (#13)	493	284
	Relative (#25)	880	385
Attitude Determination (With ground truth) of 200 ft 1σ	Absolute	381	356
	Relative (#13)	316	282
	Relative (#25)		
Terrain Variations σ_h = 200 ft $1/\beta_h$ < 25 miles	Absolute	33	230
	Relative (#13)	33	230
	Relative (#25	51	324
Quantization Only (230 ft maximum)	Absolute	66	66
	Relative (#13)	94	94
	Relative (#25)	94	94
Sensor & Alignment + Quantization	Absolute	200	365
	Relative (#13)	126	385
	Relative (#25)	136	449
Totals* (no ground truth)	Absolute	2682	2756
	Relative (#13)	505	485
	Relative (#25)	890	592

*Numbers are for the 1-gyro configuration. For the 2-gyro configuration the 1-sigma total errors are reduced to 2690 ft. absolute and 653 ft relative (as measured from picture point #25)

5 2. 2 Computation of Sensitivity Matrix for the MSS Imagery

5 2. 2. 1 Summary

The equations for the absolute position error sensitivities are presented. These equations give the sensitivities as a function of satellite position and scan location at a particular time or interest t_1 These equations in addition to those of Section 5 2 2 3 and the orbit prediction equations were programmed on the time shared computer for use in conducting MSS systems error analysis The computer program will

evaluate both absolute and relative (internal consistency) position errors Appendix B contains a derivation of these equations

5 2.2 2 Satellite Reference Coordinate Axes

Compute the altitude vector (measured up from subsatellite point to ERTS position along normal to geoid)

$$\underline{h} = \frac{Kx}{1+K}\underline{i} + \frac{Ky}{1+K}\underline{j} + \frac{a^2/b^2\, Kz}{1 + a^2/b^2\, K}\underline{k} \tag{5-6}$$

Where $\underline{i}$, $\underline{j}$, $\underline{k}$ are inertial coordinates with $\underline{k}$ along the polar axis and $\underline{i}$ in the equatorial plane along the vernal equinox direction, x, y, z are the ERTS position vector components in Earth fixed axes, a is the equatorial radius and b the polar radius of the geoid, and K is determined by iteration of the following equations

$$K_{n+1} = K_n + \Delta K_n, \quad K_0 = \frac{\sqrt{x^2 + y^2 + z^2} - a}{a}$$

$$\Delta K_n = - \frac{S_n}{\frac{d\, S_n}{d\, K_n}} \tag{5-7}$$

where

$$S_n = \frac{x^2 + y^2}{(1 + K_n)^2} + \frac{b^2}{a^2} \frac{z^2}{(b^2/a^2 + K_n)^2} - a^2$$

$$\frac{d\, S_n}{d\, K_n} = - \frac{2(x^2 + y^2)}{(1 + K_n)^3} - \frac{2b^2}{a^2} \frac{z^2}{(b^2/a^2 + K_n)^3}$$

The iteration proceeds until $\Delta K \leq 10^{-7}$, this corresponds to an error in $\underline{h}$ less than 10 feet. The satellite reference coordinate axes (which represent the gyrocompass attitude of ERTS with zero limit cycle angles) are given by equation sets (5-8), (5-9), and (5-10) for $\underline{e}_z$, $\underline{e}_x$, $\underline{e}_y$ respectively.

for the $\underline{e}_z$ yaw axis vector

$$\underline{e}_z = (Z_x, Z_y, Z_z) \tag{5-8}$$

$$Z_x = -\frac{x}{A}, \; Z_y = -\frac{y}{A}, \; Z_z = -\frac{q}{A}$$

where

$$q = \frac{(1+K)}{(b^2/a^2 + K)} z$$

$$A^2 = x^2 + y^2 + q^2$$

For the $\underline{e}_x$ roll axis vector

$$\underline{e}_x = (X_x, X_y, X_z)$$

$$X_x = -\frac{Z_x}{B}, \; X_y = -\frac{Z_y}{B}, \; X_z = -\frac{Z_z}{B} \tag{5-9}$$

where

$$A = \frac{1}{A}(x\,x + y\,y + q\,q)$$

$$q = \frac{(b^2/a^2 - 1)z\,K}{(b^2/a^2 + K)^2} + \frac{1+K}{(b^2/a^2 + K)} z$$

$$B^2 = Z_x^2 + Z_y^2 + Z_z^2$$

$$Z_x = \frac{x\,A}{A^2} - \frac{\dot{x}}{A}\,,\quad Z_y = \frac{y\,A}{A^2} - \frac{y}{A}\,,\quad Z_z = \frac{q\,A}{A^2} - \frac{q}{A} \tag{5-10}$$

For the $\underline{e}_y$ pitch axis vector

$$\begin{aligned} Y_x &= Z_y X_z - Z_z X_y \\ Y_y &= Z_z X_x - Z_x X_z \\ Y_z &= Z_x X_y - Z_y X_x \end{aligned} \tag{5-11}$$

5.2.2.3 Scan Vector Computation

The MSS scan vector $\underline{\beta}_1$ in satellite roll, pitch, yaw coordinates is

$$\underline{\beta}_1 = \mathrm{Col}\,(0,\ \sin\beta_1,\ \cos\beta_1) \tag{5-12}$$

The scan angle β_1 is given by

$$\beta_1 = -\beta + \frac{2\beta}{\Delta t}\,(t_1 - t_s) \tag{5-13}$$

Where β is the maximum excursion of the scan line, t_s is the time of the start of the current scan line, Δt is the scan time (for one line) The start of the current scan is

$$t_s = n_1\,\Delta t + t_o$$

$$n_1 = \mathrm{Int}\left[\frac{t_1 - t_o}{\Delta t}\right]$$

Where

n_1 = number of current scan line

t_o = start of scan

Δt = scan time

The scan vector is then transformed to Earth fixed coordinates to give the LOS vector $\underline{u}_1$

$$\underline{u}_1 = [\tau]\,[E]\,[L]\,\underline{\beta}_1 \tag{5-14}$$

where the coordinate transformation matrices $[\tau]$, $[E]$, $[L]$ are

$$[\tau] = \begin{bmatrix} \cos wt_1 & \sin wt_1 & 0 \\ -\sin wt_1 & \cos wt_1 & 0 \\ 0 & 0 & 1 \end{bmatrix} \text{(Earth rotation)} \tag{5-15}$$

where time t_1 is measured from zero when the Greenwich meridian pass through the vernal equinox line, and w is the Earth's rotation rate

The $[E]$ matrix transforms from satellite (normal to surface) reference axes to inertial coordinates

$$[E] = \begin{bmatrix} X_x & Y_x & Z_x \\ X_y & Y_y & Z_y \\ X_z & Y_z & Z_z \end{bmatrix} \tag{5-16}$$

The roll, pitch, yaw limit cycle matrix is (Small angle approximation)

$$[L] = \begin{bmatrix} 1 & -\alpha_z & \alpha_y \\ \alpha_z & 1 & -\alpha_x \\ -\alpha_y & \alpha_x & 1 \end{bmatrix} \tag{5-17}$$

5.2 2 4 Ground Point Computation

The vector point on the surface of the Earth, where the LOS vector $\underline{u}_1$ from the satellite intersects the geoid, is the vector sum of the satellite position $\underline{r}_1$ plus $\rho\underline{u}_1$ or

$$\underline{P}_1 = \rho\underline{u}_1 + \underline{r} \tag{5-18}$$

The equation of the geoid is, in terms of ground point position $\underline{P}_1 = \text{col}\,(P_x, P_y, P_z)$

$$P_x^2 + P_y^2 + \frac{a^2}{b^2} P_z^2 - a^2 = 0 \tag{5-19}$$

or, substituting (5-18) into (5-19)

$$(\rho\, u_x + x)^2 + (\rho\, u_y + y)^2 + \frac{a^2}{b^2} (\rho\, u_z + z)^2 = 0 \tag{5-20}$$

Equation (5-20) constitutes a quadratic in the satellite-ground point range ρ that can be solved to give

$$\rho = \frac{-C_2 - \sqrt{C_2^2 - 4\, C_1\, C_3}}{2C_1} \tag{5-21}$$

Where

$$C_1 = u_x^2 + u_y^2 + \frac{a^2}{b^2} u_z^2$$

$$C_2 = 2(xu_x + y\, u_y + \frac{a^2}{b^2} z\, u_z)$$

$$C_3 = x^2 + y^2 + \frac{a^2}{b^2} z^2 - a^2$$

Equation (5-21) and (5-18) give the ground point position $\underline{P}_i$ corresponding to time point t_i on the scan.

5.2.2 5 Computation of Sensitivity Matrix

The sensitivity matrix M is computed numerically by introducing unit error sources into $\underline{u}_i$, the satellite ephemeris $\underline{r}_i$, or geoid parameters a and b (corresponding to terrain variations) Thus, each error source $e_1, \ldots, e_n$ has associated with it an erroneous ground point $\underline{P}_{1i}$, , $\underline{P}_{ni}$

The position error vector is (for unit error sources Δe_1, . , Δe_n)

$$\begin{aligned} \underline{\Delta P}_{1i} &= \underline{P}_{1i} - \underline{P}_i \quad \text{for } \Delta e_1 \\ &\vdots \\ \underline{\Delta P}_{ni} &= \underline{P}_{ni} - \underline{P}_i \quad \text{for } \Delta e_n \end{aligned} \tag{5-22}$$

The cross scan Δx_1 and along scan Δy_1 components of the absolute position error are

$$\left.\begin{aligned} \Delta x_{11} &= \underline{\Delta P}_{11} \cdot \underline{e}_x \\ \Delta y_{11} &= \underline{\Delta P}_{11} \cdot \underline{e}_y \end{aligned}\right\} \text{ for } \Delta e_1$$

$$\vdots \qquad \vdots \tag{5-23}$$

$$\left.\begin{aligned} \Delta x_{n1} &= \underline{\Delta P}_{n1} \quad \underline{e}_x \\ \Delta y_{n1} &= \underline{\Delta P}_{n1} \cdot \underline{e}_y \end{aligned}\right\} \text{ for } \Delta e_n$$

The numerical sensitivities are then

$$M = \begin{pmatrix} \frac{\Delta x_{11}}{\Delta e_1} & \cdot & \cdot \frac{\Delta x_{n1}}{\Delta e_n} \\ \\ \frac{\Delta y_{11}}{\Delta e_1} \cdot & \cdot & \frac{\Delta y_{n1}}{\Delta e_n} \end{pmatrix} \tag{5-24}$$

5.2.3 Mathematical Description of Internal Consistency Errors in the MSS Imagery

5 2 3 1 Summary

Mathematical expressions giving the internal consistency errors in the MSS imagery are derived for various models of the error source correlation Both time and spatial correlations are considered and will be included in the ERTS error analysis program The assumed time correlation critically effects the growth of the internal consistency position errors in that the various time correlation models result in internal consistency errors ranging from zero to greater than the absolute position error. Section 5.2.4 shows an assignment of error models and error sources for use in the internal consistency analysis

5.2 3.2 Effect of Correlated Noise on ERTS Internal Consistency Errors

Let Δx, Δy represent the cross-scan and along-scan absolute position errors, respectively. Let $e_1, \ldots, e_n$ represent error sources 1 through n Then

$$\begin{pmatrix} \Delta x \\ \\ \Delta y \end{pmatrix} = \begin{pmatrix} \frac{\partial \Delta x}{\partial e_1} & \frac{\partial \Delta x}{\partial e_n} \\ \\ \frac{\partial \Delta y}{\partial e_1} \cdot & \frac{\partial \Delta y}{\partial e_n} \end{pmatrix} \begin{pmatrix} e_1 \\ \cdot \\ \cdot \\ \cdot \\ e_n \end{pmatrix} \tag{5-25}$$

or

$$\underline{\xi}_i = M_i \underline{e}_i \tag{5-26}$$

where

$$\underline{\xi}_i = \text{col}\,(\Delta x(t_i), \Delta y(t_i))$$

$$\underline{e}_i = \text{col}\,(e_1, \ldots, e_n) \text{ @ } t = t_i$$

$$M_i = \frac{\partial \underline{\xi}_i}{\partial \underline{e}_i} \text{ (matrix of sensitivities)}$$

Internal consistency is defined as the accuracy with which one ground point can be located relative to another ground point Thus, the internal consistency, or relative position error, can be found by differencing the absolute errors at two different time points t_i and t_j in the MSS picture (taking into account the error-correlation between the two points) One of the two points, the reference point, is normally taken to be at the center of the picture Thus, if $\underline{\Delta\xi}$ represents the internal consistency error vector.

$$\underline{\Delta\xi} = \underline{\xi}_i - \underline{\xi}_j = M_i \underline{e}_i - M_j \underline{e}_j \tag{5-27}$$

The mean and covariance of the absolute error $\underline{\xi}_i$ are

$$\begin{aligned} <\underline{\xi}_i> &= M_i <\underline{e}_i> \\ C_{\xi_i} &= M_i C_{e_i} M_i^T \end{aligned} \tag{5-28}$$

where

C_{ξ_i} = 2 x 2 covariance of absolute error

C_{e_i} = n x n error source covariance

Equation (5-28) does not depend on the time-behavior of $\underline{e}_i$ in any sense. The mean and covariance of the internal consistency errors are (from equation (5-27)).

$$\begin{aligned} <\underline{\Delta\xi}> &= M_i <\underline{e}_i> - M_j <\underline{e}_j> \\ <\underline{\Delta\xi}> &= <\underline{\xi}_i> - <\underline{\xi}_j> \end{aligned} \tag{5-29}$$

The covariance is (assuming the $\underline{e}_i$ have zero mean values)

$$\begin{aligned} C_{\Delta\xi} = {} & M_i <\underline{e}_i \underline{e}_i^T> M_i^T + M_j <\underline{e}_j \underline{e}_j^T> M_j^T - M_i <\underline{e}_i \underline{e}_j^T> M_j^T - \\ & M_j <\underline{e}_j \underline{e}_i^T> M_i^T \end{aligned} \tag{5-30}$$

or

$$C_{\Delta\xi} = C_{\xi_i} + C_{\xi_j} - M_i <\underline{e}_i \underline{e}_j^T> M_j^T - M_j <\underline{e}_j \underline{e}_i^T> M_i^T \tag{5-31}$$

From equations (5-29) and (5-31), note that the internal consistency errors go to zero as $t_i \rightarrow t_j$ (that is, the two points approach each other within one scan line)

$$\left.\begin{aligned} \langle \underline{\Delta\xi} \rangle &= 0 \\ C_{\Delta\xi} &= 0 \end{aligned}\right\} \text{ for } t_i = t_j \qquad (5\text{-}32)$$

Equation (5-32) applies for all error sources with the exception of the sensor resolution. Thus, it is obvious that internal consistency errors are critically dependent on the time-correlation of the error sources

5.2.3 3 Effects of Three Types of Correlated Noise

First, consider errors that are constant over the whole picture but have zero ensemble average

$$\begin{aligned} C_{\Delta\xi} &= \langle (M_i \underline{e}_i - M_j \underline{e}_j)(M_i \underline{e}_i - M_j \underline{e}_j)^T \rangle \\ &= (M_i - M_j) \langle \underline{e}_i \underline{e}_i^T \rangle (M_i - M_j)^T \text{ for all } t_i,\ t_j \end{aligned} \qquad (5\text{-}33)$$

Second, consider errors that are constant within one scan line and uncorrelated from one scan line to the next.

$$\begin{aligned} C_{\Delta\xi} &= (M_i - M_j) \langle \underline{e}_i\, e_i^T \rangle (M_i - M_j)^T \\ &\text{for Int}\left[\frac{t_i - t_o}{\Delta t}\right] = \text{Int}\left[\frac{t_j - t_o}{\Delta t}\right] \end{aligned} \qquad (5\text{-}34)$$

and

$$\begin{aligned} C_{\Delta\xi} &= M_i \langle \underline{e}_i \underline{e}_i^T \rangle M_i^T + M_j \langle \underline{e}_j \underline{e}_j^T \rangle M_j^T \\ &\text{for Int}\left[\frac{t_i - t_o}{\Delta t}\right] \neq \text{Int}\left[\frac{t_j - t_o}{\Delta t}\right] \end{aligned}$$

Third, consider white noise

$$C_{\Delta\xi} = M_i <\underline{e}_i \underline{e}_i^T> M_i^T + M_j <\underline{e}_j \underline{e}_j^T> M_j^T \text{ for all } t_i,\ t_j \qquad (5\text{-}35)$$

In the first case, equation (5-33), internal consistency errors are proportional to the change in the sensitivities from t_i to t_j, and go to zero as t_i approaches t_j. In the third case, equation (5-35), internal consistency errors are the statistical sum of the absolute error covariance matrices for t_i and t_j.

5.2.3 4 Exponentially Correlated Noise Model

Consider a single error source e_i, then equation (5-27) becomes

$$\underline{\Delta\xi} = M_i e_i - M_j e_j \qquad (5\text{-}36)$$

Where M_i is now a 2 x 1 sensitivity vector Then, if e_i is exponentially correlated noise*

$$<e_i e_j> = \sigma_e^2 e^{-\beta|t_j - t_i|} \qquad (5\text{-}37)$$

From (5-37) note that as the time separation of the ground points increases, their error source cross correlation decreases exponentially The covariance of the internal consistency error is

$$C_{\Delta\xi} = M_i <e_i^2> M_i^T + M_j <e_j^2> M_j^T - M_i <e_i e_j> M_j^T - M_j <e_j e_i> M_i^T \qquad (5\text{-}38)$$

* Exponentially correlated noise can be thought of as white noise passed through a first order filter.

or, substituting equation (5-37) into (5-38)

$$C_{\Delta\xi} = \sigma_e^2 \left[M_i M_i^T + M_j M_j^T - e^{-\beta|t_j - t_i|} (M_i M_j^T + M_j M_i^T) \right] \quad (5\text{-}39)$$

Note that for $t_j = t_i$, equation (5-39) gives a zero covariance of internal consistency errors. If the time difference is long compared to the correlation time (white noise case)

$$C_{\Delta\xi} = \sigma_e^2 \left[M_i M_i^T + M_j M_j^T \right] \text{ for } |t_j - t_i| \gg \frac{1}{\beta} \quad (5\text{-}40)$$

Equation (5-40) is simply the sum of the absolute error covariance matrices C_{ξ_1} and C_{ξ_2}

Another limiting case of interest is for $t_j - t_i$ small compared to the correlation time

$$C_{\Delta\xi} = \sigma_e^2 \left[(M_i - M_j)(M_i - M_j)^T + \beta |t_j - t_i| (M_i M_j^T + M_j M_i^T) \right]$$

$$\text{for } \beta |t_j - t_i| \ll 1 \quad (5\text{-}41)$$

Equation (5-41) gives a square root of time increase of internal consistency error if the sensitivities are locally constant $M_i = M_j$

$$C_{\Delta\xi} = 2\sigma_e^2 \left\{ \beta |t_j - t_i| M_i M_i^T \right\} \quad (5\text{-}42)$$

5 2.4 Error Analysis Results

The MSS error analysis program was run for the noise model in Table 5-3 as a function of the 25 picture locations of Table 5-4. The simulation program computes the absolute and relative error covariance matrices as a function of picture location The 1-sigma North and East position error variances are given in Figures 5-2 through 5-10 for various error sources and reference point locations

Table 5-3 Noise Models for Error Analysis*

Error Sources	Numerical Value 1-Sigma	Description
Attitude Determination Bias Error (Radiance Mod & Gyro Drift)	Roll = Pitch = 0.05° Yaw = 0.05° + 0.707 roll	Constant error source with zero ensemble average Roll and pitch uncorrelated but roll and yaw correlated
Attitude Determination Time Varying	Roll = Pitch = Yaw = 0 006°	Time-Exponentially correlated with time constant = 30 sec.
Alignment	0 01° max	Constant-Uncorrelated
Resolution	0 00146°	$\Delta\beta$ Random within one scan-line
Scan Rate Variation	2 μsec (3σ)	ΔT Constant within one scan-random from one scan to the next
Dwell Time Variation	3%	$\Delta\beta$ White noise
Sync Variation	40 ft max	$\Delta\beta$ Constant over one scan, random from one scan to next
Scan Nonlinearities	0 2% (3σ)	$\Delta\beta$ Random in one scan
Terrain Variation from Geoid	σ_n = 2000 ft. $1/\beta_n$ = 12,000 ft.	Spatially-Exponentially correlated (in terms of distance)
Ephemeris Errors	Negligible immediately after a state vector update	Time and spatially correlated

Figure 5-2 gives the absolute and relative 1-sigma errors for attitude determination error sources only with no ground truth data for 25 picture points For example at point No 1 the 1-sigma North and East absolute errors are 2680 feet and 2738 feet respectively, and the 1-sigma North and East relative errors (with respect to the center of the picture) are 493 feet and 284 feet respectively At picture point No 13, as can be seen from Figure 5-2, the relative errors are zero (see equation 5-32). The relative error at picture point No 3 is 280 feet x 280 feet,

1-gyro error model

Table 5-4. Location of Picture Points for MSS Error Analysis

Picture Point	Latitude	Longitude
1	45° 44' 56.0"	-99° 46" 35 0"
2	45° 41' 9 1"	-100° 22' 35 7"
3	45° 37' 12.3"	-100° 58' 19.2"
4	45° 33' 4.5"	-101° 33' 58.3"
5	45° 28' 44.0"	-102° 9' 45.9"
6	45° 19' 57 5"	-99° 43' 22 2"
7	45° 16' 12.2"	-100° 19' 7 0"
8	45° 12' 17.1"	-100° 45' 34 8"
9	45° 8' 11 1"	-101° 29' 58 5"
10	45° 3' 52.7"	-102° 5' 30 7"
11	44° 54' 58.8"	-99° 40' 13.4"
12	44° 51' 14.9"	-100° 15' 42.7"
13	44° 47' 21 5"	-100° 50' 55 2"
14	44° 43' 17 4"	-101° 26' 3 7"
15	44° 39' 0 9"	-102° 1' 20 7"
16	44° 29' 59.7"	-99° 37' 8.6"
17	44° 26' 17.3"	-100° 12' 22 7"
18	44° 22' 25.6"	-100° 45' 20.1"
19	44° 18' 23.2"	-101° 22' 13.7"
20	44° 14' 8.6"	-101° 57' 15 9"
21	44° 5' 0 3"	-99° 34' 7.5"
22	44° 1' 19 4"	-100° 9' 6.7"
23	43° 57' 29.2"	-100° 43' 49 5"
24	43° 53' 28.6"	-101° 18' 28 4"
25	43° 49' 15 9"	-101° 53' 16.1"

NO 5 2742,2679 498,285	NO 4 2702,2671 348,280	NO 3 2678,2678 280,280	NO 2 2671,2700 344,280	NO 1 2680,2738 493,284
NO 10 2741,2679 409,45	NO 9 2701,2670 203,20	NO 8 2677,2677 0,0	NO 7 2670,2699 203,20	NO 6 2680,2737 403,44
NO 15 2740,2678 409,45	NO 14 2700,2670 203,20	NO 13 2677,2676 0,0	NO 12 2670,2698 203,20	NO 11 2679,2736 403,44
NO 20 2738,2677 451,204	NO 19 2699,2669 290,210	NO 18 2676,2676 209,210	NO 17 2669,2697 292,209	NO 16 2678,2735 459,214
NO 25 2737,2677 491,283	NO 24 2698,2668 343,280	NO 23 2675,2675 280,280	NO 22 2668,2697 347,280	NO 21 2678,2734 496,284

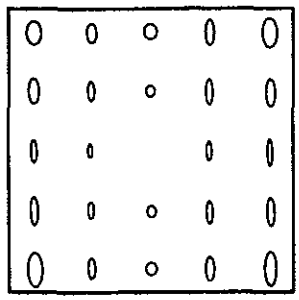

Figure 5-2
MSS Absolute and Relative Errors for Attitude Determination Error Sources Only No Ground Truth Errors with Respect to Picture Point No 13

NO 5	NO 4	NO 3	NO 2	NO 1
381,357	359,353	351,351	359,353	381,356
316,282	289,280	279,279	289,280	316,282
NO 10	NO 9	NO 8	NO 7	NO 6
381,356	359,353	351,351	359,353	381,356
255,211	221,209	209,209	222,210	256,212
NO 15	NO 14	NO 13	NO 12	NO 11
381,356	359,352	351,351	359,353	381,256
147,29	74,15	0,0	74,15	148,26
NO 20	NO 19	NO 18	NO 17	NO 16
381,356	359,352	351,351	359,352	381,356
256,212	222,210	209,209	221,209	255,211
NO 25	NO 24	NO 23	NO 22	NO 21
381,356	359,352	351,351	359,352	381,356
316,282	289,280	279,279	289,280	315,382

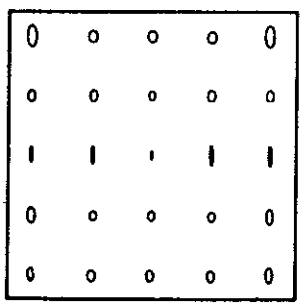

Figure 5-3
MSS Absolute and Relative Errors for Attitude Determination Errors Only with Two Ground Truth Points on Opposite Sides of Map Relative Errors with Respect to Picture Point No 13

NO 5	NO 4	NO 3	NO 2	NO 1
2742, 2679	2702, 2671	2678, 2678	2671, 2700	2680, 2738
358, 360	408, 359	536, 363	700, 370	880, 385
NO 10	NO 9	NO 8	NO 7	NO 6
2741, 2679	2701, 2670	2677, 2677	2670, 2699	2680, 2737
326, 328	382, 328	517, 332	686, 340	870, 356
NO 15	NO 14	NO 13	NO 12	NO 11
2740, 2678	2700, 2670	2677, 2676	2670, 2698	2679, 2736
281, 283	345, 283	492, 288	667, 297	855, 315
NO 20	NO 19	NO 18	NO 17	NO 16
2738, 2677	2699, 2669	2676, 2676	2669, 2697	2678, 2735
210, 211	292, 213	457, 220	643, 232	836, 253
NO 25	NO 24	NO 23	NO 22	NO 21
2737, 2677	2698, 2668	2675, 2675	2668, 2697	2678, 2734
0, 0	205, 35	408, 66	609, 99	811, 140

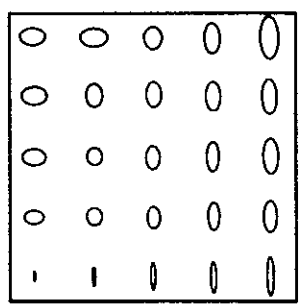

Figure 5-4
MSS Absolute and Relative Errors for Attitude Determination Errors Only. Relative Errors with Respect to Picture Point No 25

NO 5 39,229	NO 4 19,114	NO 3 0,0	NO 2 17,114	NO 1 33,230
NO 10 39,229	NO 9 19 114	NO 8 0,0	NO 7 17,114	NO 6 33,230
NO 15 39,229	NO 14 19,114	NO 13 0,0	NO 12 17,114	NO 11 33,230
NO 20 39,229	NO 19 19,114	NO 18 0,0	NO 17 17,114	NO 16 33,230
NO 25 39,229	NO 24 19,114	NO 23 0,0	NO 22 17,114	NO 21 33,230

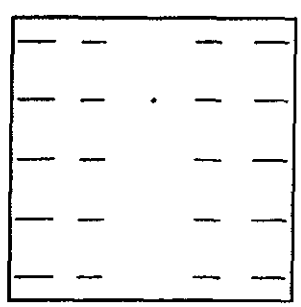

Figure 5-5
MSS North, East Absolute (Relative) Errors for Terrain Error Only, σ_h = 2000 ft, Errors With Respect to Picture Point No 13

NO 5 40,229 55,323	NO 4 19,114 43,256	NO 3 0,0 38,229	NO 2 17,114 42,256	NO 1 33,230 51,324
NO 10 39,229 55,323	NO 9 19,114 43,256	NO 8 0,0 38,229	NO 7 17,114 42,256	NO 6 33,230 50,324
NO 15 39,229 55,323	NO 14 19,114 43,256	NO 13 0,0 38,229	NO 12 17,114 42,256	NO 11 32,230 50,324
NO 20 39,229 54,323	NO 19 18,114 43,256	NO 18 0,0 38,229	NO 17 17,114 42,256	NO 16 32,230 50,324
NO 25 38,229 0,0	NO 24 18,114 43,256	NO 23 0,0 38,229	NO 22 17,114 42,256	NO 21 32,230 50,324

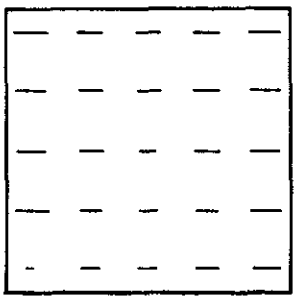

Figure 5-6
MSS Absolute and Relative Errors for Terrain Error Sources Only. Relative Errors with Respect to Picture Point No 25.

NO 5 203,364 130,384	NO 4 198,303 123,328	NO 3 197,280 121,307	NO 2 198,304 122,328	NO 1 200,265 126,385
NO 10 202,364 130,384	NO 9 198,303 123,328	NO 8 197,280 121,307	NO 7 198,304 122,328	NO 6 200,385 126,285
NO 15 202,364 129,383	NO 14 198,303 123,326	NO 13 197,280 121,305	NO 12 197,303 122,328	NO 11 200,365 126,385
NO 20 202,364 129,384	NO 19 198,303 123,328	NO 18 197,280 121,307	NO 17 197,303 122,328	NO 16 200,365 126,385
NO 25 202,364 129,384	NO 24 198,303 123,328	NO 23 196,280 121,307	NO 22 197,303 122,328	NO 21 200,365 126,385

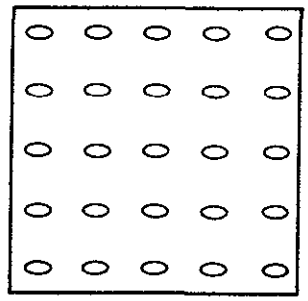

Figure 5-7
MSS Absolute and Relative Errors for Sensor and Alignment Error Sources Only Relative Errors with Respect to Picture Point No. 13

NO 5	NO 4	NO 3	NO 2	NO 1
203,364	198,303	197,280	198,304	200,365
135,448	130,401	129,384	132,401	136,449
NO 10	NO 9	NO 8	NO 7	NO 6
202,364	198,303	197,280	198,304	200,365
135,448	130,401	129,384	131,401	136,449
NO 15	NO 14	NO 13	NO 12	NO 11
202,364	198,303	197,280	197,303	200,365
135,448	130,401	129,384	131,401	136,449
NO 20	NO 19	NO 18	NO 17	NO 16
202,364	198,303	197,280	197,303	200,365
135,448	130,401	129,384	131,401	136,449
NO 25	NO 24	NO 23	NO 22	NO 21
202,364	198,303	196,280	197,303	200,365
134,447	130,400	129,383	131,400	136,448

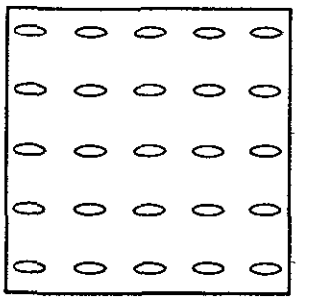

Figure 5-8
MSS Absolute and Relative Errors for Sensor and Alignment Error Sources Only Relative Errors with Respect to Picture Point No 25

NO 5 2743,2698 515,481	NO 4 2703,2682 369,433	NO 3 2680,2687 305,415	NO 2 2673,2711 364,415	NO 1 2682,2756 505,485
NO 10 2742,2697 478,443	NO 9 2702,2682 317,390	NO 8 2679,2686 241,371	NO 7 2672,2711 314,391	NO 6 2681,2755 471,447
NO 15 2741,2697 428,389	NO 14 2701,2681 237,328	NO 13 2678,2685 121,305	NO 12 2671,2710 236,329	NO 11 2681,2754 423,394
NO 20 2740,2696 475,443	NO 19 2700,2680 315,390	NO 18 2677,2684 241,371	NO 17 2670,2709 316,391	NO 16 2680,2753 473,447
NO 25 2739,2695 508,480	NO 24 2699,2679 365,432	NO 23 2676,2684 304,415	NO 22 2670,2708 367,433	NO 21 2679,2752 409,484

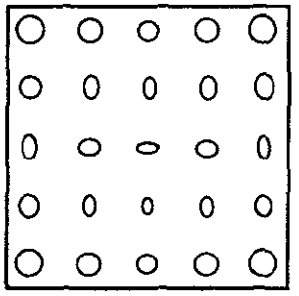

Figure 5-9
MSS Absolute and Relative Errors for All Error Sources. Relative Errors with Respect to Picture Point No 13

NO 5	NO 4	NO 3	NO 2	NO 1
2743,2698	2703,2682	2680,2687	2673,2711	2682,2756
383,575	428,539	551,528	712,546	890,592
NO 10	NO 9	NO 8	NO 7	NO 6
2742,2697	2702,2682	2679,2686	2672,2711	2681,2755
353,556	403,518	533,508	598,526	880,573
NO 15	NO 14	NO 13	NO 12	NO 11
2741,2697	2701,2681	2678,2685	2671,2710	2681,2754
312,530	369,491	508,480	680,499	865,548
NO 20	NO 19	NO 18	NO 17	NO 16
2740,2696	2700,2680	2677,2684	2670,2709	2680,2753
250,486	320,454	474,443	655,463	847,515
NO 25	NO 24	NO 23	NO 22	NO 21
2739,2695	2699,2679	2676,2684	2670,2708	2679,2752
123,309	243,401	427,388	623,412	822,469

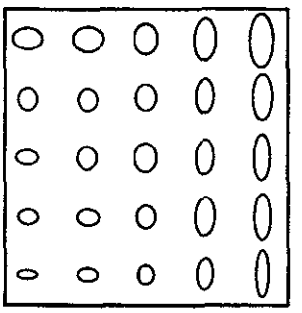

Figure 5-10
MSS Absolute and Relative Errors for All Error Sources. Relative Errors with Respect to Picture Point No 25

since this point is directly below the spacecraft the error is primarily due to time varying pitch and roll errors Note that the errors at points No 3, 8, 18 and 23 vary as the square root of the time difference from point No. 13 (this was demonstrated by equation (5-42) The north component of internal consistency error at the corners is primarily due to the yaw bias error (because the sensitivity to yaw is maximum at the corners and zero at the center of the picture) A pictorial representation of the relative position error ellipse is also shown in Figure 5-2

Figure 5-3 shows the absolute and relative errors for attitude determination error sources only, assuming that the yaw, pitch, and roll error biases are calibrated by means of two ground truth points (1-sigma = 200 feet) at opposite ends of a scan line The first thing to be noted from Figure 5-3 is that ground truth data makes the absolute and relative errors of comparable size (instead of the order of magnitude difference in Figure 5-2). It should be noticed, however, that internal consistency error is not much reduced over Figure 5-2 (without ground truth).

Figure 5-4 gives the effects of attitude determination error without ground truth, with the internal consistency errors referred to picture point No 25 The maximum relative error is now increased to 1-sigma 880 feet north, 385 feet east at the corner of the picture (point No 1)

Figure 5-5 gives the absolute error and relative error with respect to picture point No 13 for spatial-exponentially correlated terrain variations of 2000 feet 1-sigma Since the center of the picture was taken as the reference point, the absolute and relative errors are equal (the sensitivity to terrain variations being zero at this point) The error ellipse, in this case, is degenerate with the error being along the scan line only. Also, it should be noted that with point No. 13 as reference the spatial correlation has no effect on the relative errors

Figure 5-6 gives the effects of terrain variation with point No 25 (the corner of the picture) as reference. In this case the correlation distance does effect the internal consistency However, as long as the correlation distance is less than the distance between picture points, the error behaves essentially as white noise This accounts for the fact that relative error is $\sqrt{2}$ times the absolute error at the edges of the picture

Figures 5-7 and 5-8 give the effects of sensor and alignment error sources only. A picture quantization of 230 feet (equal to the resolution) is included in the sensor error sources, this is why the relative error does not go to zero at the reference point

Figures 5-9 and 5-10 give the total of all error sources in Table 5-3 (without ground truth data) The 3-sigma absolute error is on the order of 1 5 nmi which easily meets the 2 nmi requirement.

All the data given here are for the 1-gyro configuration If the 2-gyro configuration is used, the 1-sigma internal consistency error is reduced to 653 ft (from 890 ft in Figure 5-9)

5 2 5 Pseudo-Reseau Correction

In MSS Bulk I, no geometric corrections are made, and the picture is represented in the scan angle (β_i) versus time (t_i) plane MSS precision processing involves finding the mapping from the (β_i, t_i) plane into the (θ_i, ϕ_i) latitude-longitude plane by means of a knowledge of a small number of reference points To do this, θ_i and ϕ_i are represented by the polynomials

$$\theta_i = \theta(\beta_j, t_j) + \left[\beta_i - \beta_j, t_i - t_j, (\beta_i - \beta_j)(t_j - t_i), (\beta_i - \beta_j)^2, (t_i - t_j)^2 \right] \begin{pmatrix} a_1 \\ a_2 \\ a_3 \\ a_4 \\ a_5 \end{pmatrix} \quad (5\text{-}43)$$

$$\phi_i = \phi(\beta_j, t_j) + \left[\beta_i - \beta_j, t_i - t_j, (\beta_i - \beta_j)(t_j - t_i), (\beta_i - \beta_j)^2, (t_i - t_j)^2 \right] \begin{pmatrix} b_1 \\ b_2 \\ b_3 \\ b_4 \\ b_5 \end{pmatrix} \quad (5\text{-}43)$$

The distortion vectors $\underline{a}$ and $\underline{b}$ can then be computed from (5-43) by a knowledge of the precision ground points of six picture elements (obtained from attitude and ephemeris data).* The latitude and longitude components of picture distortion are the differences between the interpolated values (5-43) and the precision computed values. If the six points are chosen as in Figures 5-11 through 5-14, namely points (1), (3), (5), (11), (21) and (25), the modeling errors go to zero at these points and reach a maximum between pseudo-reseau points. Figures 5-11 and 5-12 give the latitude-longitude distortion errors in radians versus picture location and were obtained via computer simulation The errors reach a maximum of 7 74x10^{-6} rad latitude at point No 22 and a maximum longitude error of -3 936 x 10^{-5} rad at point No 17.

Translated into distance errors this is 162 ft North and 582 ft East. Figures 5-11 and 5-12 also apply for the case of constant attitude errors and rates (that is to say that the quadratic distortion polynomial accurately models the effects of these errors) Figures 5-13 and 5-14 give the modeling errors for a maximum limit cycle of 0.01°/sec at 0.1 cps The maximum distortion is in Figure 5-14 at picture point No. 19, and is 1690 ft**

*Volume 17 contains a more detailed discussion of the MSS distortion correction algorithms and associated throughput

**More complicated algorithms have been developed that give even smaller distortions The important thing is that the distortions be small compared to the interval consistency of the reference points.

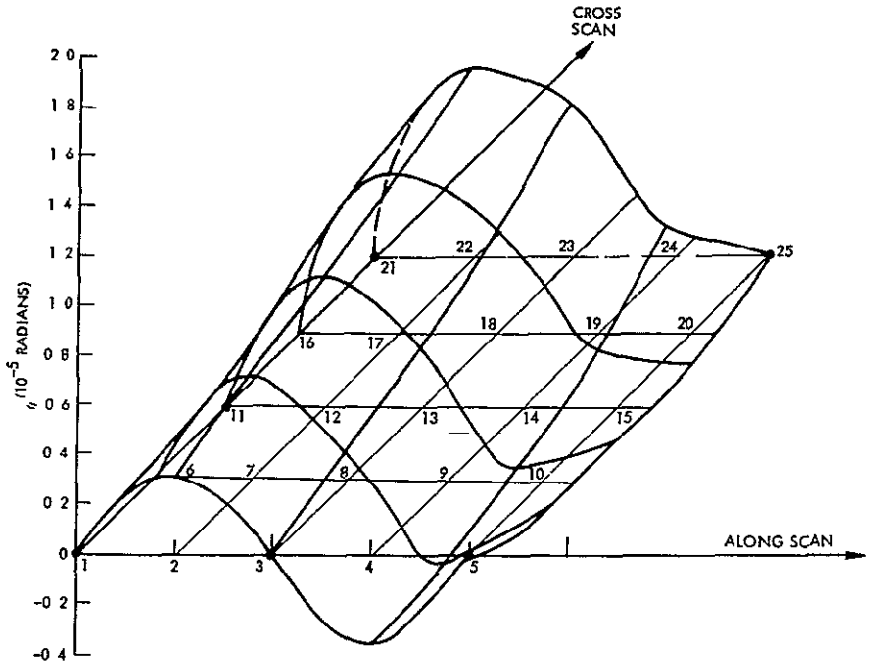

Figure 5-11

MSS LATITUDE Distortion vs Picture Location
Limit Cycle = 0

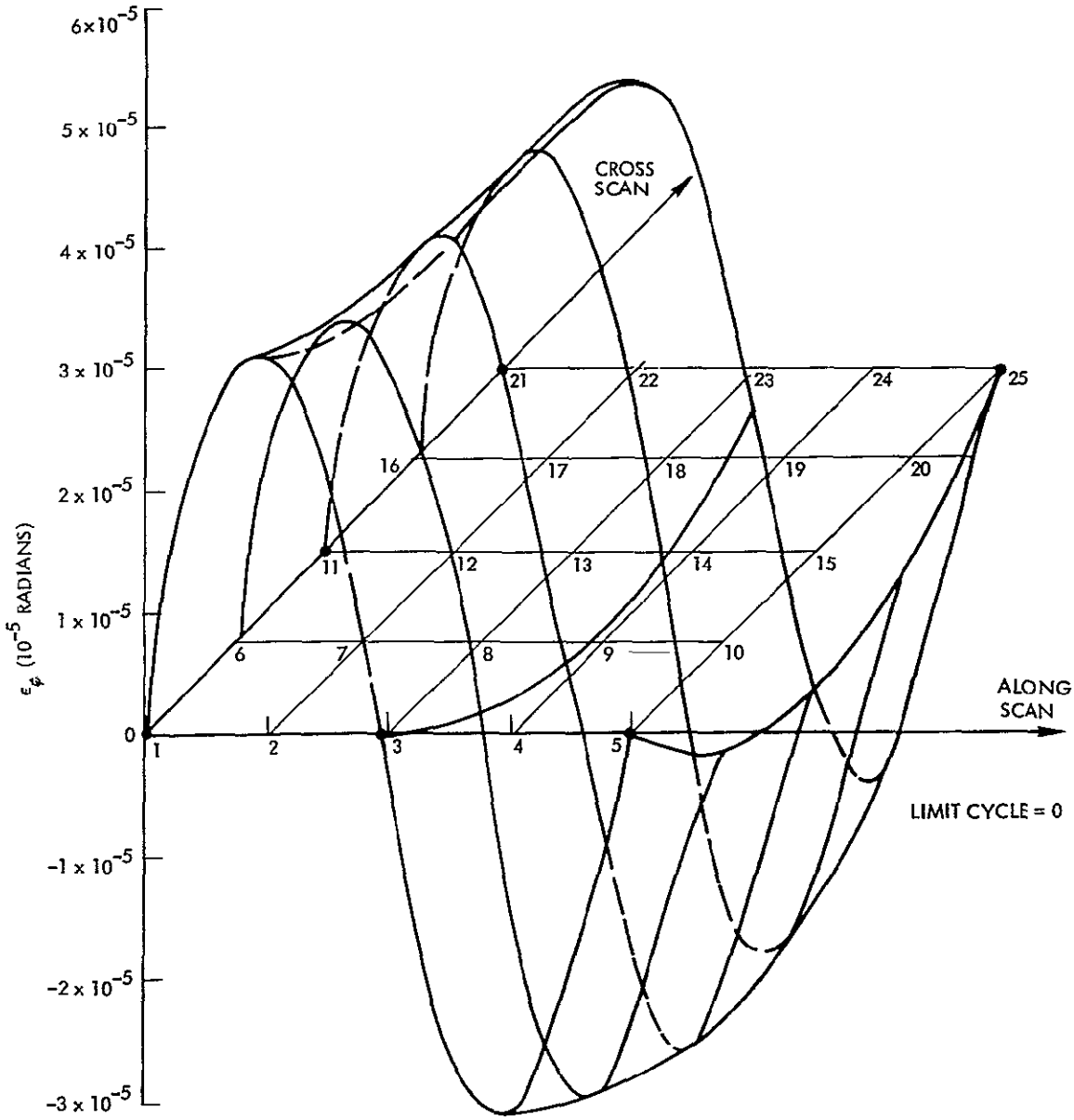

Figure 5-12

MSS LONGITUDE Distortion vs Picture Location
Limit Cycle = 0

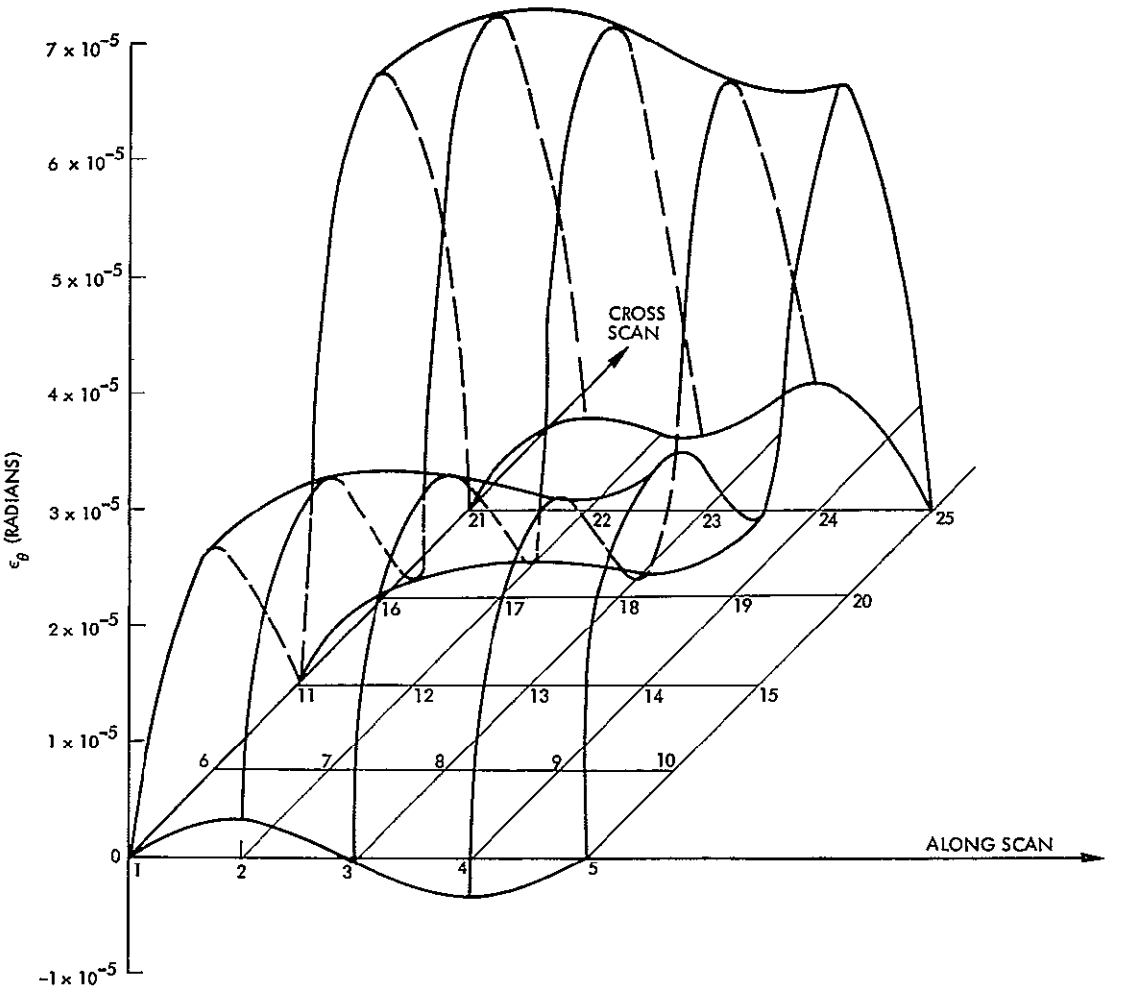

Figure 5-13

MSS LATITUDE Distortion vs Picture Location
Limit Cycle is 0 01°/sec, 10 sec period

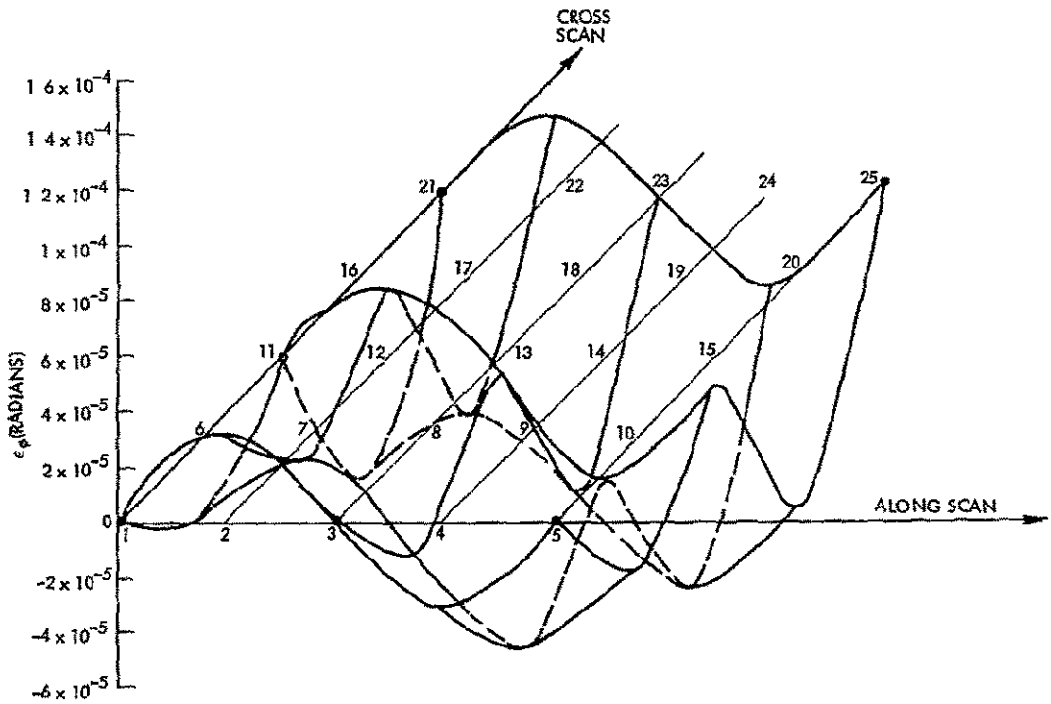

Figure 5-14

MSS LONGITUDE Distortion vs Picture Location
Limit Cycle is 0.01°/sec, 10 sec period.

5 3 RBV GEOMETRIC ERROR ANALYSIS

The ERTS RBV camera system consists of three RCA return beam vidicon cameras which simultaneously photograph the same image in three corresponding spectral bands A pattern of fiducial marks, or reseau, is interposed between each camera and the scene to provide a reference for estimation of the RBV camera distortion The images taken by the three cameras are read out sequentially and transmitted to the ground data handling system, where each of the reseau points positions are determined Based on these positions, the camera distortion is determined and the image subsequently corrected, either digitally or via analog (Precision Photo-Restitutor). This section will determine the image geometric distortion correction accuracy as a function of the various system error sources This will include determination of the error sources, modeling of the error sources and processing algorithms, and evaluation of the algorithm performance

The RBV system geometric errors can be divided into three distinct groups pre-reseau errors, or errors which are caused by spacecraft attitude and ephemeris, camera alignment, and terrain irregularities, and are thus undetected by the reseau measurement, post-reseau/pre-processing errors, which include the camera distortion and data link/tape recorder errors, and can be estimated through the reseau image distortion by the digital processing, and post-digital processing errors, including the geometric distortion correction errors and the image recording and processing errors The image distortions caused by each of the three groups of errors are independent and thus may be evaluated separately The post-digital processing errors are discussed in Section 5 4 and the post-reseau/preprocessing errors are discussed in Section 5.3 2

5 3 1 Pre-reseau Errors

Image distortions due to spacecraft attitude and ephemeris errors for the RBV differ from those for the MSS in that the attitude error rates do not affect the geometric distortions of the RBV, other than through smear, due to the fact that the entire RBV image is exposed at one time Keystoning and distortions related to the earths curvature and spacecraft

attitude, however, must be considered. To correct for these distortions, a linear transformation from spacecraft attitude and ephemeris to geometric image distortion is determined as a function of position in the image Assuming small-angle approximations for roll θ_R, pitch θ_p, and yaw θ_y, and independence of their effects on image distortions, it can easily be shown that apparent x and y distortions δ_x, δ_y, respectively, are given by

$$\begin{bmatrix} \delta_x \\ \delta_y \end{bmatrix} = \frac{1}{H} \begin{bmatrix} xy & (H^2 + x^2) & -yH & x \\ (H^2 + y^2) & xy & xH & y \end{bmatrix} \begin{bmatrix} \theta_R \\ \theta_p \\ \theta_y \\ \delta H \end{bmatrix} + \begin{bmatrix} \delta x_o \\ \delta y_o \end{bmatrix}$$

where δH is spacecraft altitude error, and δx_o, δy_o are ephemeris errors The errors of interest here are internal consistency errors, those which will change distances between points in the image These can be expressed as

$$\begin{bmatrix} \delta x \\ \delta y \end{bmatrix} = \frac{1}{H} \begin{bmatrix} xy & x^2 & x \\ y^2 & xy & y \end{bmatrix} \begin{bmatrix} \theta_R \\ \theta_p \\ \delta H \end{bmatrix}$$

The knowledge of θ_R, θ_p and δH is corrupted by uncorrelated noise with variances σ_R^2, σ_p^2 and σ_H^2, respectively The estimation accuracies of x and y are then

$$\sigma_x^2 = \frac{1}{H^2} \left[x^4 \sigma_p^2 + x^2 y^2 \sigma_R^2 + x^2 \sigma_H^2 \right]$$

$$\sigma_y^2 = \frac{1}{H^2}\left[y^4 \sigma_R^2 + x^2 y^2 \sigma_p^2 + y^2 \sigma_H^2\right]$$

For $\sigma_p = 05° = \sigma_R$ and $\sigma_H = 200$ ft , the specifications on the attitude determination system and ephemeris data, the maximum error is

$$(3\sigma_y) = (3\sigma_x)_{max} = 141 \text{ ft}$$

with a correlation coefficient of one, giving $(3\sigma)_{max} = 200$ ft

This is a maximum deviation, occurring only at the picture corners and diminishing greatly at the interior of the image For example, at the picture edge, halfway between two adjacent corners, the 3σ deviation is only 141 ft Implementation of this transformation is easily accomplished in conjunction with the camera distortion correction algorithm, as discussed in the following section

5 3 2 Reseau Distortion Estimation Analysis

The images generated by the RBV cameras will contain geometric distortions which are primarily a result of imperfect scanning by the electron beam of the RBV Data link and tape recorder geometric errors will be negligible with respect to the camera errors In the camera, an optical system focuses an image on a faceplate, which is scanned by an electron beam and converted to a voltage train to be transmitted to and demodulated on the ground Image distortion may arise through nonlinearities in the scanning beam path or scan rates To obtain an estimate of this distortion, a known reseau grid (Figure 5-15) consisting of 81 evenly spaced fiducials in a 9x9 array is placed in front of the camera focal plane By measuring the apparent reseau distortion, the camera distortion parameters may be estimated

A comprehensive trade-off study was performed to select the best algorithms for estimating the distortion parameters Selection was based on a computer study of functional and statistical estimation errors

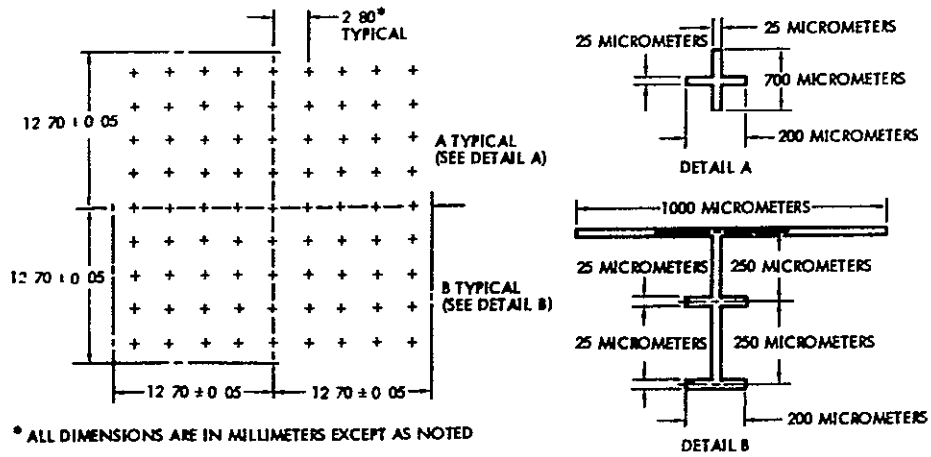

Figure 5-15
RESEAU ARRAY Format for RBV

and on computer timing requirements for each algorithm The results of this study are discussed in Section 2. 5 3, Volume 17 Only the error analysis results for the recommended system are presented here

Typical sources of distortion may be modeled as follows First, a coordinate system is defined, centered at the image plane center and with coordinate axes x and y. Position displacements at a point (x, y) due to distortion are given by $\delta x(x, y)$ and $\delta y(x, y)$

An image centering shift can result from incorrect deflection voltage bias or misalignment and causes distortion terms of the form

$$\delta x = a_0 \ , \ \delta y = b_0$$

The specifications call for a maximum centering error of 1 percent full scale.

Image size error can result from incorrect deflection gain and cause distortion terms of the form

$$\delta x = a_1 x \ , \quad \delta y = b_1 y$$

The specifications require these terms to be less than 1 percent full scale.

Skew distortions can arise from sources such as misaligned deflection coils and may be represented by terms of the form

$$\delta x = a_2 y \ , \quad \delta y = b_2 x$$

According to specifications, these terms should be less than 5 percent full scale

Pincushion distortion can arise from magnetic field imperfections and gives terms of the form

$$\delta x = x\left[a_3(x^2 + y^2) + a_4(x^2 + y^2)^2 + \quad \right]$$

$$\delta y = y\left[b_3(x^2 + y^2) + b_4(x^2 + y^2)^2 + \quad \right]$$

Symmetric tangential distortion can be caused by the combined effect of unwanted radial electric fields and the axial focusing magnetic field and gives terms of the form

$$\delta x = y\left[a_5(x^2 + y^2) + a_6(x^2 + y^2)^2 + \quad . \right]$$

$$\delta y = x\left[b_5(x^2 + y^2) + b_6(x^2 + y^2)^2 + \quad \right]$$

Specifications call for the maximum "image distortion" to be less than 1 percent full scale Since specifications for skew, size, and centering are quoted separately, an "image distortion" is assumed referring to all other distortions including pincushion and tangential distortion

The total effect of all of these sources of distortion becomes

$$\delta x = a_0 + a_1 x + a_2 y + a_3 x (x^2 + y^2) + a_4 x (x^2 + y^2)^2$$

$$+ a_5 y (x^2 + y^2) + a_6 y (x^2 + y^2)^2$$

$$\delta y = b_0 + b_1 y + b_2 x + b_3 y (x^2 + y^2) + b_4 y (x^2 + y^2)^2$$

$$+ b_5 x (x^2 + y^2) + b_6 x (x^2 + y^2)^2$$

where only the first two terms in pincushion and tangential have been included. No specifications could be found which give the stability of the distortions from picture to picture This list of distortion terms is not exhaustive, possibly other sources of distortions will be found in the RBV Because these terms are not uncommon, they can serve as a specific test of proposed distortion correction schemes It can be assumed that the distortions are of the form·

$$x + \delta x = f(x, y) + v$$

where f is a smoothly varying function and v is random spatial noise A similar equation exists for y distortion The function f, which will be called the functional distortion, contains terms arising from all smooth distortion sources, such as those listed above The spatial noise terms

can arise from sources such as sync-jitter, beam jitter, and high frequency distortions It is assumed that the noise is spatially uncorrelated so that

$$E(v_i v_j) = \delta_{ij} \sigma_N^2$$

at points i and j The values of δx_i for the reseau points are given as

$$\delta x_i = f(x_i, y_i) + v_i + m_i, \quad i = 1, 2, \quad , N_R$$

where m_i represents the measurement error for the ith reseau point It is assumed that

$$E(m_i m_j) = \delta_{ij} \sigma_m^2 \text{ and } E(v_i m_i) = 0$$

The reseau displacements are fit by an interpolation algorithm to determine the distortion elsewhere

The 9x9 reseau grid is subdivided into 16 squares with three reseau points to a side and a total of nine points each A two-dimensional quadratic polynomial is then fitted to the distortions at the nine points of each subregion The form of the biquadratic model for x (or y) distortion is

$$\delta\tilde{x} = \sum_{i=1}^{2} \sum_{j=1}^{2} a_{ij} x^i y^j$$

where the a_{ij} are parameters to be determined In matrix format, this becomes

$$\delta\tilde{x} = A(x, y) \underline{a}_M$$

where

$$A(x, y) = \left[1 \mid x \mid y \mid xy \mid x^2 \mid y^2 \mid xy^2 \mid x^2y \mid x^2y^2 \right]$$

$$\underline{a}_M = \left[a_{oo}, a_{1o}, a_{o1}, a_{11}, a_{2o}, a_{o2}, a_{12}, a_{21}, a_{22} \right]^T$$

The actual distortion δx also contains other terms such as first-order pincushion $x(x^2 + y^2)\, a_{3o}$ and spatially uncorrelated noise v as discussed above Thus,

$$\delta x(x, y) = \left[A(x, y) \mid N(x, y) \right] \begin{bmatrix} \underline{a}_M \\ \underline{a}_N \end{bmatrix} + v(x, y)$$

where $\delta x(x, y)$ is x-distortion at (x, y), $\underline{a}_N$ are the unmodeled distortion parameters, and N(x, y) are the coefficients of $\underline{a}_N$ in the distortion The distortion can be measured at each of the nine reseau points in each subregion and arranged as follows

$$\underline{\delta x} = \left[\underline{A} \;\; \underline{N} \right] \begin{bmatrix} \underline{a}_M \\ \underline{a}_N \end{bmatrix} + \underline{v}$$

where

$$\underline{\delta x} = \begin{bmatrix} \delta x(x_1, y_1) \\ \delta x(x_2, y_2) \\ \\ \delta x(x_N, y_N) \end{bmatrix}, \quad \underline{A} = \begin{bmatrix} A(x_1, y_1) \\ A(x_2, y_2) \\ \\ A(x_N, y_N) \end{bmatrix}, \quad \underline{N} = \begin{bmatrix} N(x_1, y_1) \\ N(x_2, y_2) \\ \cdot \\ N(x_N, y_N) \end{bmatrix}, \quad \underline{v} = \begin{bmatrix} v(x_1, y_1) + m_1 \\ v(x_2, y_2) + m_2 \\ \\ v(x_N, y_N) + m_N \end{bmatrix}$$

where for biquadratic model, N = 9.

The distortion estimation equation, based on the biquadratic model, is given by

$$\delta\hat{x}(x, y) = A(x, y)\, \hat{\underline{a}}_M = A(x, y)\, \underline{A}^{-1} \underline{\delta x}$$

which leaves a distortion estimation error $\epsilon(x, y)$

$$\epsilon(x, y) = \epsilon_E(x, y) + \epsilon_M(x, y)$$

where $\epsilon_E(x, y)$ is the statistical error caused by the noise $v(x, y)$

$$\epsilon_E(x, y) = A(x, y)\, \underline{A}^{-1} \underline{v} - v(x, y)$$

and $\epsilon_M(x, y)$ is the functional error caused by neglecting the terms $\underline{a}_N$ in the distortion estimation

$$\epsilon_M(x, y) = K(x, y)\, \underline{a}_N$$

where

$$K(x, y) = A(x, y)\, \underline{A}^{-1} \underline{N} - N(x, y)$$

The term $\underline{v}$ in $\underline{\epsilon}_E(x, y)$ includes reseau point measurement errors which are small with respect to the term $v(x, y)$ and can be root-sum-squared

A computer study was made of the performance of this algorithm with respect to the variance of the spatially-uncorrelated distortions and reseau measurement errors

$$E\left[v(x_j, y_j)^2\right] = \sigma_R^2, \text{ all reseau points } (x_j, y_j)$$

The results of this study are shown in Figures 5-16 and 5-17 Figure 5-16 presents the ratio of the standard deviation of the statistical error due to reseau point distortion to σ_R The grid represents one quadrant of the image plane, the center of the image appearing in the upper left corner Entries appear twice per reseau point spacing in the horizontal direction and four times per reseau point spacing in the vertical The entries corresponding to reseau locations are encircled It can be seen that the statistical error in the far corner of the image has uncertainty of 5 219 times the uncertainty of the reseau location due to measurement and random camera distortion The sensitivity of the residual distortion estimation error to unmodeled distortions is shown in Figure 5-17. The format of the grids in this figure is the same as that

Statistical (σ/σ_R)

1 000	848	1 000	848	1 000	848	1 000	848	1 000	2 284
794	673	794	673	794	673	794	673	794	1 814
848	719	848	719	848	719	848	719	848	1 937
955	810	955	810	955	810	955	810	955	2 182
1 000	848	1 000	848	1 000	848	1 000	848	1 000	2 284
955	810	955	810	955	810	955	810	955	2 182
848	719	848	719	848	719	848	719	848	1 937
794	673	794	673	794	673	794	673	794	1 814
1 000	848	1 000	848	1 000	848	1 000	848	1 000	2 284
794	673	794	673	794	673	794	673	794	1 814
848	719	848	719	848	719	848	719	848	1 937
955	810	955	810	955	810	955	810	955	2 182
1 000	848	1 000	848	1 000	848	1 000	848	1 000	2 284
955	810	955	810	955	810	955	810	955	2 182
848	719	848	719	848	719	848	719	848	1 937
794	673	794	673	794	673	794	673	794	1 814
1 000	848	1 000	848	1 000	848	1 000	848	1 000	2 284
1 523	1 291	1 523	1 291	1 523	1 291	1 523	1 291	1 523	3 478
2 284	1 937	2 284	1 937	2 284	1 937	2 284	1 937	2 284	5 219

Figure 5-16
BIQUADRATIC INTERPOLATION

Modeling Biquadratic Interpolation

(First-Order Pincushion)

000	-000	-000	-000	-000	-000	-000	-000	-000	-000
-180	-180	-180	-180	-180	-180	-180	-180	-180	-180
-206	-206	-206	-206	-206	-206	-206	-206	-206	-206
-129	-129	-129	-129	-129	-129	-129	-129	-129	-129
-000	-000	-000	-000	-000	-000	-000	-000	-000	-000
129	129	129	129	129	129	129	129	129	129
206	206	206	206	206	206	206	206	206	206
180	180	180	180	180	180	180	180	180	180
-000	-000	-000	-000	-002	-003	-003	-004	-005	-005
-180	-180	-180	-180	-183	-183	-184	-184	-185	-186
-206	-206	-206	-206	-209	-209	-210	-211	-211	-212
-129	-129	-129	-129	-132	-132	-134	-134	-135	-136
-000	-000	-000	-000	-003	-004	-005	-006	-007	-008
129	129	129	129	125	124	123	122	121	120
206	206	206	206	202	201	200	199	198	197
180	180	180	180	176	175	174	173	172	170
-000	-000	-000	-000	-004	-005	-007	-008	-009	-011
-386	-386	-386	-386	-391	-392	-393	-394	-396	-397
-1 029	-1 029	-1 029	-1 029	-1 034	-1 035	-1 036	-1 038	-1 039	-1 041

(Second-Order Pincushion)

000	-000	-000	-000	-000	-000	-000	-000	-000	-000
-035	-041	-044	-049	-070	-105	-115	-128	-177	-301
-044	-056	-055	-056	-085	-137	-136	-137	-207	-422
-031	-046	-038	-028	-057	-115	-088	-061	-133	-417
-000	-018	-000	023	-000	-058	-000	063	-000	-343
039	018	045	082	064	006	096	196	141	-261
070	046	080	127	110	046	161	290	232	-239
068	039	077	128	104	021	148	288	210	-352
-000	-036	-000	046	-001	-119	-002	124	-003	-689
-357	-399	-366	-326	-394	-546	-439	-326	-503	-1 313
-425	-472	-436	-391	-468	-637	-520	-394	-592	-1 493
-277	-328	-284	-229	-305	-480	-337	-184	-383	-1 354
-000	-053	-000	069	-002	-178	-003	-187	-004	-1 034
301	245	307	390	324	148	355	581	398	-690
502	442	512	605	540	358	590	844	659	-499
457	393	466	563	490	290	533	799	594	-655
-000	-071	-000	091	-003	-237	-004	249	-006	-1 379
-1 060	-1 141	-1 079	-1 006	-1 140	-1 431	-1 236	-1 029	-1 371	-2 911
-2 940	-3 033	-2 991	-2 952	-3 147	-3 525	-3 402	-3 283	-3 760	-5 520

Figure 5-17
BIQUADRATIC INTERPOLATION

in Figure 5-16 The entries in the first grid represent the sensitivity to the low-order effects of pincushion-type (second-order) distortions and those in the second grid the sensitivity to higher-order effects Thus, if 1 percent full scale first-order pincushion is present in the image, 1 04 percent of this distortion or 01 percent full scale will remain in the image corner Similarly, 5 52 percent of second-order pincushion distortion will remain in the same corner

If a (small) number of reseau points cannot be detected, their positions are estimated in a similar manner In this event, the matrix A(x, y) is given by

$$A(x, y) = \left[1 \mid x \mid y \mid xy \mid x^2 \mid y^2 \mid xy^2 \mid x^2y \mid x^3 \mid y^3 \right]$$

and the parameter $\underline{a}_M$ is determined for the entire image using all 81 reseau points in a least squares algorithm The appropriate estimation equation is thus

$$\delta\hat{x}\,(x_j, y_j) = A(x, y)\,(\underline{A}^T\underline{A})^{-1}\underline{A}^T\underline{\delta x}$$

where $\underline{\delta x}$ and $\underline{A}$ contain all the available reseau distortion measurements and coefficients. Here the matrix $\underline{A}$ is a 81 x 9 The corresponding error is $\epsilon(x, y)$ as before, with

$$\epsilon_E(x, y) = A(x, y)\,(\underline{A}^T\underline{A})^{-1}\,\underline{A}^T\,\underline{v} - v(x, y)$$

$$\epsilon_M = (A(x, y)\,(\underline{A}^T\underline{A})^{-1}\underline{A}^T\underline{N} - N(x, y))\,\underline{a}_N$$

Again, these errors were evaluated over a quadrant of the image plane and the results are shown in Figure 5-18 The format of these grids is the same as in the previous figures The sensitivity of ϵ_M to first-order pincushion is identically zero since first-order pincushion is included in the model The errors of interest in this figure are the reseau point

Statistical (σ/σ_R)

211	217	231	247	259	265	272	303	387	542
212	218	232	248	260	265	273	304	388	543
217	222	236	251	262	267	274	305	389	544
223	228	241	255	265	269	276	307	391	547
231	236	247	260	269	272	278	309	394	550
239	243	254	265	273	275	280	311	397	554
247	.251	260	270	276	277	282	313	400	559
254	257	265	274	278	278	283	315	404	565
259	262	269	276	279	278	283	317	409	573
262	265	271	277	279	277	283	320	415	582
265	267	272	277	278	277	284	324	424	595
267	269	274	278	279	278	288	332	436	611
272	274	278	282	283	284	297	346	455	632
283	285	289	292	294	298	316	370	481	661
303	305	309	313	317	324	346	404	518	699
337	339	.343	348	354	365	392	454	568	748
387	389	394	400	409	424	455	518	633	811
455	457	462	470	462	500	535	600	713	888
542	544	550	559	573	595	632	699	811	982

Figure 5-18 Global 3rd-Order Polynomial

errors The standard deviation of the statistical reseau location estimation error is a maximum of $633\sigma_R$ at the outermost reseau point, where the modeling error reaches a maximum of 5 91 percent of the maximum second-order pincushion in the image The maximum errors are summarized in Table 5-5 together with a typical conversion to picture element (pixel) magnitudes It can be seen that errors are much greater in the image region outside the reseau pattern, indicating the advisability of extending the reseau pattern as close to the image edge as possible

It should be stressed that these are worst case numbers which apply when only one image frame is available If the functional distortion is fairly constant over subsequent frames, then an average of the coefficients

Modeling Error (Second-Order Pincushion)

000	-1 757	-3 182	-3 994	-4 015	-3 218	-1 778	- 127	1 001	315
000	-1 740	-3 150	-3 949	-3 961	-3 160	-1 722	- 081	1 028	513
000	-1 690	-3 054	-3 815	-3 800	-2 987	-1 557	055	1 107	504
000	-1 608	-2 896	-3 595	-3 536	-2 704	-1 287	273	1 229	479
000	-1 496	-2 680	-3 293	-3 175	-2 319	- 923	562	1 382	425
000	-1 355	-2 410	-2 916	-2 726	-1 844	- 478	908	1 549	321
000	-1 1[illegible]	-2 091	-2 473	-2 200	-1 291	031	1 290	1 706	141
000	-1 000	-1 731	-1 974	-1 612	- 680	583	1 684	1 825	145
000	- 7[illegible]4	-1 338	-1 432	- 978	- 030	1 153	2 060	1 875	- 576
000	- 575	- 921	- 860	- 316	634	1 713	2 386	1 815	- 1 193
000	- 54[illegible]	- 491	- 276	350	1 287	2 230	2 623	1 604	- 2 046
000	- 119	- 060	304	998	1 896	2 668	2 730	1 192	- 3 189
000	104	353	858	1 600	2 430	2 988	2 660	527	- 4 682
000	316	749	1 365	2 128	2 852	3 144	2 361	- 449	- 6 591
000	507	1 096	1 801	2 550	3 121	3 091	1 778	- 1 801	- 8 986
000	666	1 384	2 140	2 830	3 196	2 775	851	- 3 597	-11 946
000	793	1 593	2 355	2 934	3 030	2 142	- 484	- 5 911	-15 553
000	870	1 704	2 417	2 820	2 573	1 134	-2 297	- 8 820	-19 895
000	888	1 696	2 293	2 447	1 774	- 314	-4 660	-12 410	-25 067

Figure 5-19
GLOBAL THIRD-ORDER Polynomial

obtained for past frames will lower the statistical uncertainty by $\sqrt{n}$, where n is the number of frames averaged If severe beam-pulling is an important factor in reseau position determination, coefficient averaging will greatly diminish this source of error After enough frames are averaged, the functional error will dominate and thus be the determining factor in accuracy calculations

The pre-reseau distortion correction algorithm discussed in Section 5 3.1 is incorporated into the camera distortion correction algorithm with negligible increase in processing time as follows The parameters $\underline{a}_M$ in the biquadratic interpolation algorithm are augmented by the following vector

$$\underline{b}_x = \left[H\,\theta_p \,\middle|\, \frac{1}{H}\,\delta H \,\middle|\, -\theta_y \,\middle|\, \frac{1}{H}\theta_R \,\middle|\, \frac{1}{H}\,\theta_p \,\middle|\, 0 \,\middle|\, 0 \,\middle|\, 0 \right]^T$$

Table 5 5 Maximum Error Magnitudes for RBV Processing

	Biquadratic Interpolation (Entire Image)	Biquadratic Interpolation (Interior to Reseau)	Reseau Location Estimation
Statistical $\frac{\sigma}{\sigma_R}$	5 219	1 000	633
Sensitivity to 1st Order Pincushion	1%	2%	0
Sensitivity to 2nd Order Pincushion	5 5%	85%	5 9%
RSS*	1 ± 8 pixels	2 ± 1 5 pixels	5 ± 1 pixel

Assuming 1 % max 1st order pincushion
2% max 2nd order pincushion
1/2 pixel (0125%) random distortion (1σ)
1/2 pixel (0125%) reseau location error (1σ)

for x distortion and

$$\underline{b}_y = \left[H\,\theta_R \;\vdots\; \theta_y \;\vdots\; \frac{1}{H}\,\delta H \;\vdots\; \frac{1}{H}\,\theta_p \;\vdots\; 0 \;\vdots\; \frac{1}{H}\,\theta_R \;\vdots\; 0 \;\vdots\; 0 \right]^T$$

for y distortion The modified estimation algorithm is then

$$\delta\hat{x}_T(x, y) = A(x, y)\,\hat{\underline{a}}_M = A(z, y)\,(\underline{A}^{-1}\,\underline{\delta x} - \underline{b}_x)$$

Here, as before, $\hat{\underline{a}}_M = (\underline{A}^{-1}\,\underline{\delta x} - \underline{b}_x)$ must be calculated only once per interpolation subregion, thus increasing the computational load negligibly with respect to that for calculating $\delta\hat{x}\,(x, y)$ at each of the 17 million image points (x, y) The pre-reseau and camera distortion errors are

independent and may thus be root-sum-squared, giving a total internal consistency error within the reseau grid of 360 ft (3σ) under the assumptions of Table 5-5

5 3 3 Ground Truth Incorporation Analysis

An important performance parameter of the RBV (and MSS) system is the residual absolute and relative image errors when image UTM coordinates (ground truth) are known for a number of image points and are used to reduce the effects of attitude and ephemeris uncertainties of the spacecraft This section will detail a computer analysis of the accuracy of the RBV ground truth incorporation algorithm

It is pointed out in Section 5 3 1 of this volume that the image error at a point (x, y) in the image due to spacecraft attitude/ephemeris deviations can be expressed by.

$$\begin{bmatrix} \delta x \\ \delta y \end{bmatrix} = \frac{1}{H} \begin{bmatrix} H & 0 & xy & (H^2+x^2) & -yH & x \\ 0 & H & (H^2+y^2) & xy & xH & y \end{bmatrix} \begin{bmatrix} \delta x_o \\ \delta y_o \\ \theta_R \\ \theta_p \\ \theta_y \\ \delta H \end{bmatrix}$$

or

$$\delta = M(x, y)\, \underline{a}$$

where x and y are along-and across-track distances from image center, H is nominal altitude, δx_o, δy_o, and δH are ephemeris deviations, and θ_R, θ_p and θ_y are roll, pitch, and yaw deviations The parameters $\underline{a}$ are measured by the attitude determination and ephemeris systems as $\underline{a}^*$ with specified random errors $\underline{w}$

$$\underline{a}^* = \underline{a} + \underline{w}$$

where $\underline{w}$ is zero mean with covariance W Thus, based on these systems alone, the attitude/ephemeris pre-reseau errors are given by ϵ_δ

$$\epsilon_\delta = M(x, y)\, \underline{w}$$

as shown in Section 5 3 1

However, if N ground truth measurements δ_i^* at (x_i, y_i) $i = 1,$, N, are available, the estimate of $\underline{a}$ can be improved through the following least-squares approach Define

$$\underline{\delta} = \begin{bmatrix} \delta_1 \\ \\ \\ \delta_N \end{bmatrix}, \quad \underline{M} = \begin{bmatrix} M(x_1, y_1) \\ \\ \\ M(x_N, y_N) \end{bmatrix}, \quad \underline{\delta}^* = \begin{bmatrix} \delta_1^* \\ \\ \\ \delta_N^* \end{bmatrix}$$

Then

$$\underline{\delta} = \underline{M}\, \underline{a}$$

The measurements δ_i^* are corrupted by residual internal consistency image processing errors, geodetic ground control point errors, and image reading errors, which are essentially uncorrelated between widely-spaced ground-truth points If these errors are given by v_i, with mean zero and variance σ_v^2, or

$$\underline{v} = \left[v_1, \cdots, v_N\right]^T, \quad E\left[\underline{v}\, \underline{v}^T\right] = \sigma_V^2 I$$

Then

$$\underline{\delta}^* = \underline{M}\, \underline{a} + \underline{v}$$

The least squares estimate of $\underline{a}$ has an error covariance J_a

$$J_a = (\underline{M}^T \underline{M} \frac{1}{\sigma_V^2} + W^{-1})^{-1}$$

giving a distortion error covariance at (x, y) of

$$J_\delta = M(x, y)\ J_a M^T(x, y)$$

The least squares estimate is given by

$$\hat{\delta}(x, y) = M(x, y)\ J_a\ \underline{M}^T \frac{1}{\sigma_V^2} (\underline{\delta}^* - \underline{M}\ \underline{a}^*)$$

The equations for the pre-reseau distortion estimation error covariance J_δ were solved via digital computer for several system configurations; one- and two-gyro attitude determination with digital and PPR-distortion correction The appropriate specifications are seen in Table 5-6

Table 5-6 Pre-Reseau Error Source Magnitudes

Ephemeris	σ_{xo}, σ_{yo}, $\sigma_{\delta H}$	=	200' (1σ)
Attitude	σ_{ROLL}, σ_{PITCH}	=	05° (1σ)
	σ_{Yaw}	=	05° dual gyro (1σ)
			073° single gyro (1σ)
Roll-yaw correlation	=	0 dual gyro	
		47 single gyro	
Ground Truth δ_{GT}	=	312' (digital correction)	
		350' (PPR correction)	

The ground truth error standard deviations are obtained by root-sum-squaring the geodetic map position error, the residual relative distortions in the corrected photographs, and the image point location measurement errors

Tables 5-7 and 5-8 present the residual pre-reseau errors both without ground truth and with one to three ground truth points The case of one ground truth point assumes the point at image center, that of two points at opposite image corners, and that of three points at image corners The residual errors are shown at the image center and the far image corner, thus giving the minimum and maximum of the random errors These errors are then summarized with the remaining system errors in Table 5-14 It is noted for the single gyro case that roll and yaw are correlated Errors in y caused by these angles will add in one-half the picture and subtract in the other The tables contain an average of the y error in the four corners

Table 5-7 Digital Processing Ground Truth Incorporation Errors

		Absolute Errors*						Relative Errors		
		Picture Center			Picture Corner			Picture Corner		
No of Ground Truth Points		x	y	correl	x	y	correl	x	y	correl
Single Gyro	0	2674	2674	0	2730	2730	- 07	43	43	-1
	1	310	310	0	463	463	52	21	21	-1
	2	218	218	- 02	262	262	25	20	20	-1
	3	182	182	03	246	246	42	20	20	-1
Dual Gyro	0	2674	2674	0	2714	2714	- 01	43	43	-1
	1	310	310	0	412	412	41	21	21	-1
	2	218	218	- 02	259	259	24	20	20	-1
	3	182	182	04	241	241	41	20	20	-1

*All numbers are 1σ values in feet

Table 5-8 PPR Processing Ground Truth Incorporation Errors

	No of Ground Truth Points	Absolute Errors*						Relative Errors		
		Picture Center			Picture Corner			Picture Corner		
		x	y	correl	x	y	correl	x	y	correl
Single Gyro	0	2674	2674	0	2730	2730	- 06	43	43	-1
	1	347	347	0	489	489	45	21	21	-1
	2	244	244	- 02	292	292	24	20	20	-1
	3	200	200	- 01	256	256	34	20	20	-1
Dual Gyro	0	2674	2674	0	2713	2713	- 01	43	43	-1
	1	347	347	0	441	441	35	21	21	-1
	2	244	244	- 02	287	287	23	20	20	-1
	3	204	204	03	267	267	40	20	20	-1

*All numbers are 1σ values in feet.

5 4 POST DIGITAL PROCESSING ERROR ANALYSIS

After the distortion parameters for the RBV have been estimated by the digital computer in the bulk II processing, the parameters are used off-line with a precision photo-restitutor (PPR) to generate an image corrected for this distortion In precision mode I, the RBV and MSS corrections are applied digitally within the computer and then reproduced via a laser beam recorder (LBR) and processed photographically The digital distortion correction procedure will contribute less than one pixel error, thus indicating the LBR and photo processing as the limiting functions in image accuracy This section will provide an error analysis of the PPR and the LBR Geometric errors due to photographic processing and film shrinkage is estimated at 182 ft (1-sigma) and is independent of the remaining errors

5 4 1 Precision Photo-Restitutor Geometric Error Analysis

The PPR is used in two distinct modes In the bulk II processing, digital computer distortion correction data for each image is input to the PPR, which generates an image corrected for geometric distortion In the precision I mode, the red RBV channel is used as a control photo to which the red channel of the MSS is correlated and registered The amount of correction necessary to register the images is used to further estimate the yaw bias of the spacecraft attitude and thus decrease the MSS error substantially The operation of the PPR is covered in detail elsewhere in this report, it is the intent of this section to investigate geometric image distortions left by the device

The PPR system must be controlled online from a computer All transformation can be pre-programmed and is available for each frame to be procured, but the position of the input and control images are not known accurately until they are measured at the PPR Minor adjustment to the control equations must be made after frame fiducial marks are measured To reduce the online data rates, it may be convenient to drive the PPR through a computer interface buffer which is loaded with data for one printing strip The PPR will be operated automatically after all film rolls are loaded

Two primary computer requirements exist for the PPR in its operation on RBV data The first set of calculations is needed prior to the insertion of the photograph into the PPR, so its results must be available from online storage The second set of calculations is the rotation, translation, and scale change of the first set of data to the coordinate system on the film actually in the PPR at that time This set of data is determined from three LBR points measured in the PPR in combination with the output of the first calculations. The new data is returned to drive the PPR The PPR will read the three LBR points, pause for computation, and begin to expose the nine strips of the photograph Each strip begins at a known center position (x, y), known scale (M), and known rotation (χ) Increments of the strip are exposed by moving the PPR slit with differential incremental values (dx, dy, dM, dα) stored in a 4 by 147 buffer The computer can proceed strip by strip, calculating values at the beginning, inserting these values in the buffer, and calculating again at the beginning of the new strip. If all data is known, the computer can initially calculate for the entire nine-strip photograph

The residual errors are based on the relative and absolute errors that exist after error is removed by reseau calibration, lens calibration, and satellite attitude from ground truth using 1 25,000 map geodetic positions and are also based on the internal characteristics of the PPR Since the bulk II images and the master RBV for MSS processing are always accomplished on the PPR, the figures for errors will be those given in Table 5-9 If the maximum excursion of the satellite is 0 8 degree and the Earth rotation effect is 20,000 feet in one-half picture, a size of maximum excursion on Δx, Δy, scale, and rotation was obtained The maximum distortion per column is 3 degrees, 54 minutes rotation, 12 6 percent increase in scale, and a maximum x or y displacement of 39,361 feet In a single element of the column (9 x 147) the maximum rotation is 23 minutes, scale change is 1 4 percent, and Δx incremental change is 229 minutes, Δy incremental changes are not significant for sizing the PPR True scale is increased to 105 7 percent as seen in the first increment in a column and this decreased to 93 1 percent at the bottom Appropriate limits have been included in the

Table 5-9 Geometric Residual Errors

Output of Master Copy

	Geographic Residual Error, Feet		Relative Residual Error, Feet	
PPR performance (0 8- or 0 4-inch slit)	206	150	206	150

design of the PPR The residual errors are a function of the extreme excursions of the PPR error removal capability

Dynamic errors are those that occur during exposure time with resultant loss of restitutor resolution The dynamic error allowance is budgeted equally in the main servos to result in an error allowance of 20 micrometers per servo This error is added (rms) to the error that results from averaging from top to bottom of the 0 5- by 0 8-inch slit to obtain the table for the worst condition of distortion (Table 5-10) These resolution losses are cut down for the 0 4-inch-wide slit

The residual errors are the rms sum of relative errors, absolute (geographic) errors, LBR errors, film shrinkage errors, and PPR induced errors If the RBV master is produced in the PPR and if all error removing capabilities are used, the figures given in Table 5-10 result The errors indicated as PPR errors in Table 5-11 are the registration errors in the multispectral image registration

5 4 2 Laser-Beam Recorder Geometric Error Analysis

An accurate error analysis requires a sufficiently detailed physical description and configuration of the device being investigated Because LBR technology is still relatively new and undergoing changes, the information available from manufacturers (especially those that relate to

Table 5-10 Overall Dynamic Errors

	Servo	Dynamic	Total 0 05 by 0 8	Total 0 05 by 4
K rotator, ft	112	70	132	118
Z motion (scale) ft	100	78	127	108
x and y input, ft	100	70	122	106
x and y motion, ft	---	35	35	18

Table 5-11 Comparison of Errors in Master RBV and Control Images

	PPR Slit	
	0 8 by 0 05 inch	0 04 by 0 05 inch
Correlation error	±60 microns	±30 microns
Setting error		
Δx, Δy	±30	±30
$\theta \pm 0$ 1 degree	±34	±17
M ± 0 3 percent	±30	±15
Linear interpolation and blur	±20	±10
RSS	±83 microns	±49 microns
	±276 ft	±163 ft

error sources and their valuation) is meager and quite often sketchy For this reason the following assumptions and restrictions are placed upon the analysis

- The error estimates presented are based on published information currently available from the manufacturer and as a result of visits and telephone calls
- Where error data was not forthcoming, estimates were made on the basis of experience and analysis of the relevant error source
- The list of error sources presented in the body of the text does not attempt to present a comprehensive compilation Instead the list shows the most significant error sources on the basis of our current understanding of the physical system

- For the purpose of this analysis, the output image from the LBR is defined to be the exposed film prior to its processing This suggests that the error analysis does not include any photometric and geometric changes in the output image (such as film shrinkage, film gamma variations) due to photoprocessing

- The LBR error analysis assumes the same device will be used for all three types of input - RBV and MSS type image data as well as the precision processed data coming from the NDPF computers

The recorder analysis task selected LBR as the technology most suitable to the ERTS requirements at the present time While specifications will be prepared for an LBR film recorder in this phase of the ERTS program the selection of a unit by a particular manufacturer is left for Phase D In the absence of a specific unit, the approach in the error analysis has been to categorize the LBR units or models currently available in the field and from these categories determine the errors to be expected from their component functions and then arrive at composite error estimates

- Swept Beam Scan Type

  This type of LBR generates its scanning motion by sweeping its laser beam through reflection off a rotating mirror or prism The RCA and Ampex LBR's and the CBS Lab LBR use this kind of scanning motion Two variations are shown, where in one case the spot forming function is performed before and in the other case after the scanning mechanism The movement of the beam in the longitudinal direction is provided by a film transport

- Swept Film Scan Type

  This type of LBR generates its scanning motion by the use of film wrapped around a rotating drum over which a fixed orientation laser beam is projected Translation of the beam longitudinally is provided by a transport mechanism which moves the laser modulator and spot forming system parallel to the scanning drum.

The error analysis presented investigates each of the two types and uses the results to determine a composite LBR error estimation In the absence of a selection of a particular LBR, the results really indicate what is currently realizable in LBR performance in the field without its being identified with a particular unit

Each functional block of the LBR has been analyzed in Table 5-12 listing the error sources with the estimates of their magnitudes given in Table 5-13 The error sources are listed which cause spatial distortions

in the output image and therefore affect the accuracy of locating areas of interest on the ground and their relative distances and orientations They are divided into two groups

1) Scan Coordinate Error (S) - These relate to errors along the direction of the scan as it is generated on the output image

2) Longitudinal Errors (L) - These errors relate to the error sources in a direction perpendicular to the scan motion

The error estimates prepared in Table 5-12 are indicated in Table 5-13 in summary fashion for every one of the LBR functional blocks This manner of presentation permits comparison of the error estimates for both basic types of LBR - the swept beams scan type and the swept film scan type It is evident from the tables that the differences are minor so that it is reasonable to characterize both types of LBR by a single set of error estimates This is precisely the intent of the use of a so-called "composite" LBR model for error analysis It should be noted that for the sake of being conservative, whenever there was a choice among estimates, the higher values were used

Errors for all the LBR functional blocks are combined in rms fashion when they are unrelated errors or otherwise by direct addition to arrive at the overall combined errors for each LBR type. These two sets of estimates are in turn combined to obtain an overall LBR set of error estimates They are as follows

- Longitudinal error 0 05 percent
- Scan coordinate error 0 02 percent

The geometric error is the resultant of the errors in the two coordinates

5 5 OVERALL GEOMETRIC ERRORS

The overall geometric distortion errors for the RBV and MSS imagery are shown for bulk I, bulk II and precision I processing in Tables 5-14 and 5-15 Precision processing absolute errors are shown with and without ground truth data Applicable uncertainty values are shown in the Table All entries are 3 sigma values Precision processing also includes digital tape output accuracy, i e , accuracy before LBR and photo processing distortion

Table 5-12 List of Geometric Error Sources

Item No			
1 0	1	Laser	
1 1		1	Variation in beam position due to vibration in laser mounting - geometric effect on image
1 2		2	Temp changes may cause beam variations due to the large heat input probably associated with a laser
2 0	2	Modulator	
2 1		1	Variation in beam position due to mechanical vibration of the modulator
2 2		2	Temperature changes may cause variations in beam position since a modulator is inherently inefficient in converting input energy
3 0	3	Spot Forming System	
		This is the optical system which operates to form the spot It may consist of several lenses and reflectors, but for this block it excludes any scanning optics if used	
3 1		1	Variation is spot position on the film due to vibration of the spot forming system and/or temperature changes
4 0	4	Swept Beam-Scan Mechanism	
		This functional block includes the scanning motor	
4 1		1	Longitudinal errors
		a	Spacing - optical error due to variations in prism or mirror surface causing a variation in line spacing
		b	Pairing error, if multiple beams are used
		c	Sequential skew error due to axial misalignment of mirror axis with motor rotational axis

Table 5-12 List of Geometric Error Sources (Cont)

Item No		
4 2	2	Scan coordinate error
		a Jitter along scan - caused by motor hunting
		b Shift of the scan line along the scan This error is caused by the optical error between mirror faces - i e , azimuth alignment errors
		c Fixed skew error due to multiple input beams departing from a common plane
		d Scan non-linearity
		(1) Scan velocity error, in contrast to jitter, is a longer term error It is also caused by variations in motor speed (see sketch below)
		(2) Non-uniform film distance to the rotational axis will cause deviations in spot velocity at the film (see sketch below) This may be due to rotational axis motion

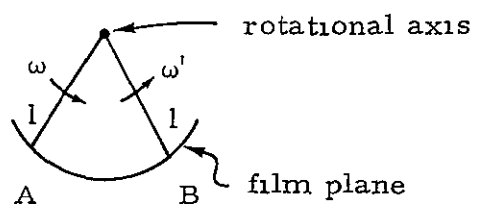

Scan velocity error is due to ω changing with l = l'

Film distance error is due to l changing with ω = ω'

5 0	5	Film Transport
5 1		1 Table speed deviations from desired values result in longitudinal error This is a rate error, and depending on whether it is open or closed loop would determine its characteristics

Table 5-12 List of Geometric Error Sources (Cont)

Item No			
5 2		2	Transport banding error due to the same cause as 1 The error is manifested as a bunching or separation of lines and is expressed as a percentage of the line to line dimension
5 3		3	Longitudinal jitter - due to drive motor random hunting or drive mechanism high speed variations The error may be a function of the operating speed
5 4		4	The errors shown in the above sketch may also be due to transport misalignment having similar effects
6 0	6	Film	
		Only exposure of film considered, not its photo processing	
6 1		1	Non-uniform film thickness or tension causing slip may result in non-uniform film speed resulting in 1) longitudinal error and 2) scan coordinate error
6 2		2	Wave-like distortions (buckling, etc) of film may result in non-linearities in both coordinates
7 0	Swept Film Scan Mechanism (Scanning Drum)		
7 1		1	Longitudinal error
		a	Scan jitter caused by axial end-play of the drum, improper alignment of the axis Temperature changes can also produce this effect
7 2		2	Scan coordinate error
		a	Jitter along scan - caused by motor hunting
		b	Shift of the scan line - due to the timing error between the start of the scan and drum position

Table 5-12 List of Geometric Error Sources (Cont)

Item No			
		c	Scan non-linearity due to surface speed variations of the drum caused by rotational speed changes and out-of-roundness of the drum
8 0	Beam Translation (Laser beam, spot forming transport)		
8 1		1	Transport errors due to speed variations This can cause striations in the output image
8 2		2	Non-uniform drum surface distance to beam caused by variations in the movement of the beam transport
8 3		3	Misalignment of the beam transport axis with the drum axis causing a shift of the scan line along the scan giving a biased skew to the output

Table 5-13 LBR Error Estimates

Item No	Error Source	Error Estimates (N = negligible)
1 0	Laser	
1 1	Vibration	N
1 2	Temperature Changes	N
2 0	Modulator	
2 1	Vibration	N
2 2	Temperature Changes	N
3 0	Spot Forming System	
3 1	Geometric Variations	N
4 0	Swept Beam Scan	Ampex - 0 1%
4 1	Longitudinal Errors	RCA - 0 05%
		CBS - 0 01%
4 2	Scan Coordinate Errors	Ampex - 0 02%
		RCA - 0 02%
		CBS - 0 01%
5 0	Film Transport	
5 1	Table Speed Variations	Included with 4 0
5 2	Transport Banding Error	< 0 01%
5 3	Longitudinal Jitter	Included with 4 0
5 4	Misalignment	Included with 4 0
6 0	Film	
6 1	Thickness or Slip	N
6 2	Wave-like Distortions	N
7 0	Swept Film Scan	
7 1	Longitudinal Errors	0 001%
7 2	Scan Coordinate Errors	0 001%
8 0	Beam Translation	
8 1	Geometric Error	< 0 1% overall

Table 5-14 RBV Total Errors

Bulk I	Internal Consistency (3σ)	Absolute (3σ)
• Attitude (6000 ft altitude, 0 35° pitch, roll, 0 7° yaw errors)	960 ft	8000 ft
• Camera distortion (2% max)	12000 ft	12000 ft
• LBR distortion	328 ft	328 ft
• Photo processing distortion	540 ft	540 ft
Total	12000 ft	14000 ft
Bulk II		
• Attitude (600 ft altitude, 0 15° pitch, roll, 0 21° yaw 3 sigma uncertainty)	200 ft	8000 ft
• Camera distortion estimation (internal to reseau)	230 ft	230 ft
• PPR correction accuracy (0 8 x 0 5" slit)	618 ft	618 ft
• Photo processing distortion	540 ft	540 ft
Total (RSS)	880 ft	8000 ft

Precision I		With Ground Truth	Without Ground Truth
• Attitude (See Bulk II)	200 ft	630 ft	8000 ft
• Camera distortion estimation (See Bulk II)	230 ft	230 ft	230 ft

Table 5-14 RBV Total Errors (Cont)

	Internal Consistency (3σ)	With Ground** Truth	Without Ground Truth
• Digital distortion correction accuracy	100 ft	100 ft	100 ft
• LBR distortion	328 ft	328 ft	328 ft
• Photo processing distortion*	540 ft	540 ft	540 ft
Total (RSS)	710 ft	928 ft	8000 ft
*Tape only (not including terms asterisked)	320 ft	680 ft	8000 ft

**Ground truth location 600 ft (3σ), 2 data points

Table 5-15 MSS Total Errors

Bulk I	Internal Consistency (3σ)	Absolute (3σ)
• Attitude/sensor errors (6000 ft alt, 0 35° pitch, roll, 0 7° yaw)	9000 ft	11000 ft
• LBR distortion	328 ft	328 ft
• Photo processing distortion	540 ft	540 ft
Total (RSS)	9000 ft	11000 ft
Bulk II		
• Attitude/sensor errors (600 ft alt, 0 15° pitch, roll, 0 21° yaw)	1900 ft (2700 ft)**	9000 ft
• PPR correction accuracy (0 8 x 0 05" slit)	618 ft	618 ft
• Photo processing distortion	540 ft	540 ft
Total (RSS)	2100 ft (2700 ft)	9000 ft

Precision I		With Ground Truth	Without Ground Truth
• Attitude/sensor errors (yaw bias determined by PPR correlation of MSS and RBV)	1500 ft	1500 ft	8000 ft
• Digital distortion correction accuracy	600 ft	600 ft	600 ft
• LBR distortion*	328 ft	328 ft	328 ft

Table 5-15 MSS Total Errors (Cont)

	Internal Consistency (3σ)	With Ground** Truth	Without Ground Truth
• Photo processing distortion*	540 ft	540 ft	540 ft
Total (RSS)	1700 ft	1700 ft	8000 ft
*Tape only (not including terms asterisked)	1600 ft	1600 ft	8000 ft

**Ground truth location 600 ft (3 sigma), 2 data points

***Numbers in parentheses are for the one gyro configuration If there are no numbers in parentheses, they are the same for the one gyro configuration as for the two gyro configuration

5 6 PHOTOMETRIC ANALYSIS

5 6 1 MTF Analysis

5 6 1 1 Summary

The payload of the first earth resources technology satellite will be three return beam vidicon (RBV) cameras and a multispectral scanner (MSS) These sensors provide pictures of the earth in various optical bands for identifying and cataloging features of interest It is important to determine the expected radiometric performance of the system, in order to properly identify and size its operations

This section computes the S/N ratios and the modulation transfer functions of the return beam vidicon cameras and the multispectral scanner These sensors are then characterized by their S/N ratios viewing a 200 foot bar pattern and by their limiting resolutions Table Table 5-16 lists the analysis steps The specifications of the two sensors, listed in Tables 5-17 and 5-18, are taken from the "Design Study Specifications for the Earth Resources Technology Satellite ERTS A and B," as outlined in Attachments I and II of that document Table 5-19 summarizes important system parameters The assumed target is the one listed in Section 3 3.1 5 of Attachment II Its properties are extrapolated for use in the RBV analysis as shown in Table 5-20 Granted the above assumptions, the "DC" S/N ratio may be computed and used to normalize the zero frequency of the modulation transfer function curves From these curves, Figures 5-20 through 5-27, signal to noise ratios for various targets may be found. Table 5-21 lists the system SPP/NRMS for extended targets Table 5-22 summarizes the sensor performance relating to the hypothetical target

A somewhat separate question concerns the information degradation of the data link It need not be configured for the high contrast target considered above, as very few such targets exist in nature Instead, a data link S/N ratio of 33 dB is probably satisfactory. Table 5-23 characterizes such a data link Finally, Table 5-24 summarizes over-all system performance, for viewing targets of moderately high contrast.

Table 5-16. Design Approach

RBV		MSS	
Highlight/lowlight radiance		Highlight/lowlight radiance	
Exposure time		Detector area	
Vidicon sensitivity		Detector responsivity	
Highlight/lowlight current		Highlight/lowlight current	
Assume noise-in-signal limit		Assume noise-in-signal limit	
S_{PP}/N_{RMS} low spatial frequency		S_{PP}/N_{RMS} low spatial frequency	
Cross Track MTF (Along Scan)	Along Track MTF (Cross Scan)	Cross Track MTF (Along Scan)	Along Track MTF (Cross Scan)
1 Atmospheric Turbulence	Atmospheric Turbulence*	Atmospheric Turbulence*	Atmospheric Turbulence
2 Optics Resolution	Optics Resolution	Optics Resolution	Optics Resolution
3 Vidicon Beam	Vidicon Beam	NA	NA
4 Video Amplifier	NA	Video Amplifier	NA
5 S/C Limit Cycle Oscillation	S/C Limit Cycle Oscillation	S/C Limit Cycle* Oscillation	S/C Limit Cycle Oscillation
6 NA	Uncompensated Image Motion	NA	Uncompensated Image Motion
7 NA	Raster Line Spacing	Sampling Aperture	Sampling Aperture
Limiting Resolution S/N @ 200 feet	Same	Same	Same

*Negligible

Table 5-17 Return Beam Vidicon Camera Specifications

	Camera 1	Camera 2	Camera 3
Resolution (at maximum scene highlight contrast)			3400 TVL
Edge resolution (percent of center)	80	80	80
Signal-to-noise ratio (at 10 TVL)	33dB	33dB	25dB
Dynamic range	50 1	50 1	30 1
Grey scale ($\sqrt{2}$ transmission steps)	10	10	8
Shading (maximum vertical and horizontal)	15%	15%	15%
Residual image (maximum)	3%	3%	3%
Horizontal scan rate (lines/sec)	1250	1250	1250
Number of scan lines	4200	4200	4200
Read out time (seconds)	3 5	3 5	3 5
Video bandwidth (MHz)	3 5	3 5	3 5
Time between picture sets (Sec)	25	25	25
Exposure time (milliseconds)	12 ± 5%	12 ± 5%	12 ± 5%
Exposure control (milliseconds)	8, 12, 16	8, 12, 16	8, 12, 16
Image distortion (maximum)	1%	1%	1%
Deflection skew (maximum)	±0 5°	±0 5°	±0 5°
Size and centering shift (maximum)	±2%	±2%	±2%
Spectral bandwidth (nanometers)	475 - 575	580 - 680	690 - 830

Table 5-18 Multispectral Scanner Specifications

Sensitivity and Signal/Noise Ratio - The sensitivity of the MSS shall be adequate to provide high signal/noise (S/N) ratios (peak to peak signal/rms noise) for typical scene reflectances The following S/N voltage ratio shall be provided for radiance values corresponding to a 230 ft equivalent target

	Bands			
	1	2	3	4
High radiance (high contrast) watts cm^{-2} $ster^{-1}$	$(25)(10)^{-4}$	$(23)(10)^{-4}$	$(13)(10)^{-4}$	$(15)(10)^{-4}$
Signal/noise	156	120	60	71
Low radiance (high contrast) watts cm^{-2} $ster^{-1}$	$2\ 5 \times 10^{4}$	$2\ 3 \times 10^{-4}$	$1\ 3 \times 10^{-4}$	$1\ 5 \times 10^{-4}$
Signal/noise	47	36	18	21

Band 5 shall provide 1°C noise equivalent temperature difference (NEΔT) for a scene temperature of 300°K under normal operating conditions

Modulation Transfer Function - The MTF for the MSS shall be adequate to provide a 35% response at a spatial frequency corresponding to 200 feet in Bands 1, 2, 3, and 4 A 35% response at a spatial frequency corresponding to 600 feet shall be provided in Band 5

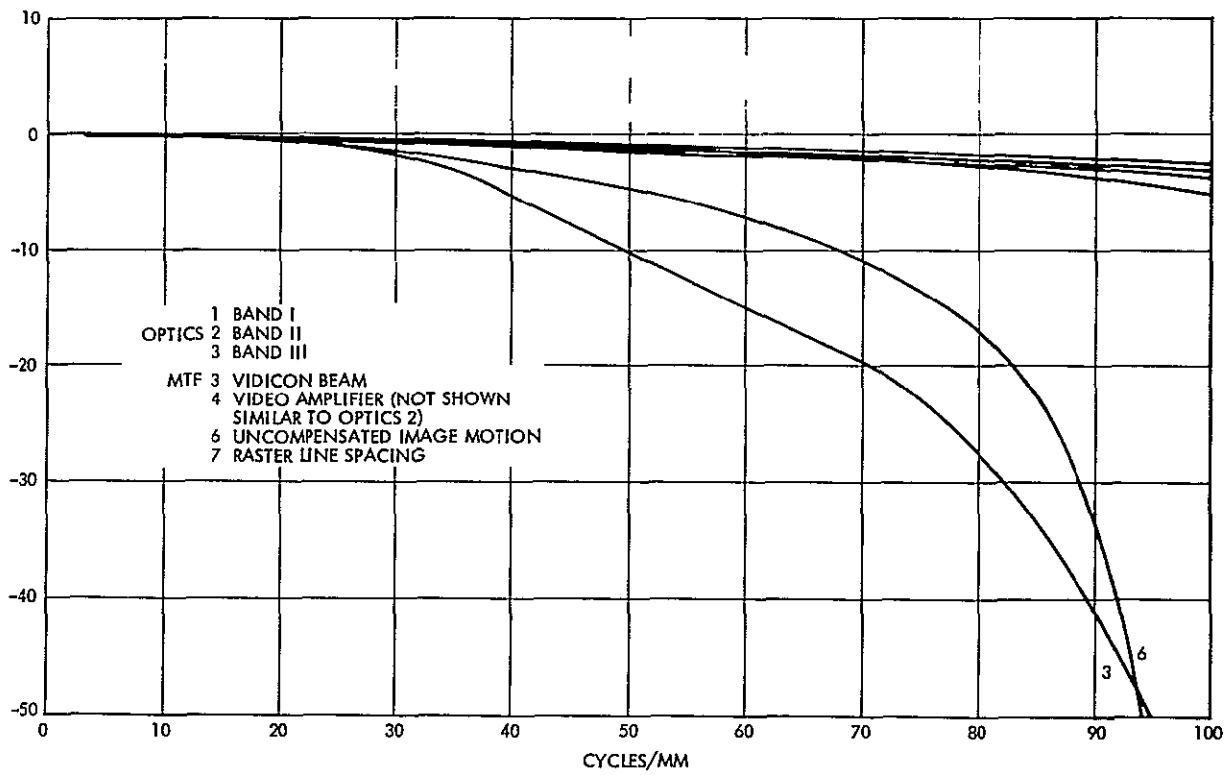

Figure 5-20
RBV CONTRIBUTORY MTF's

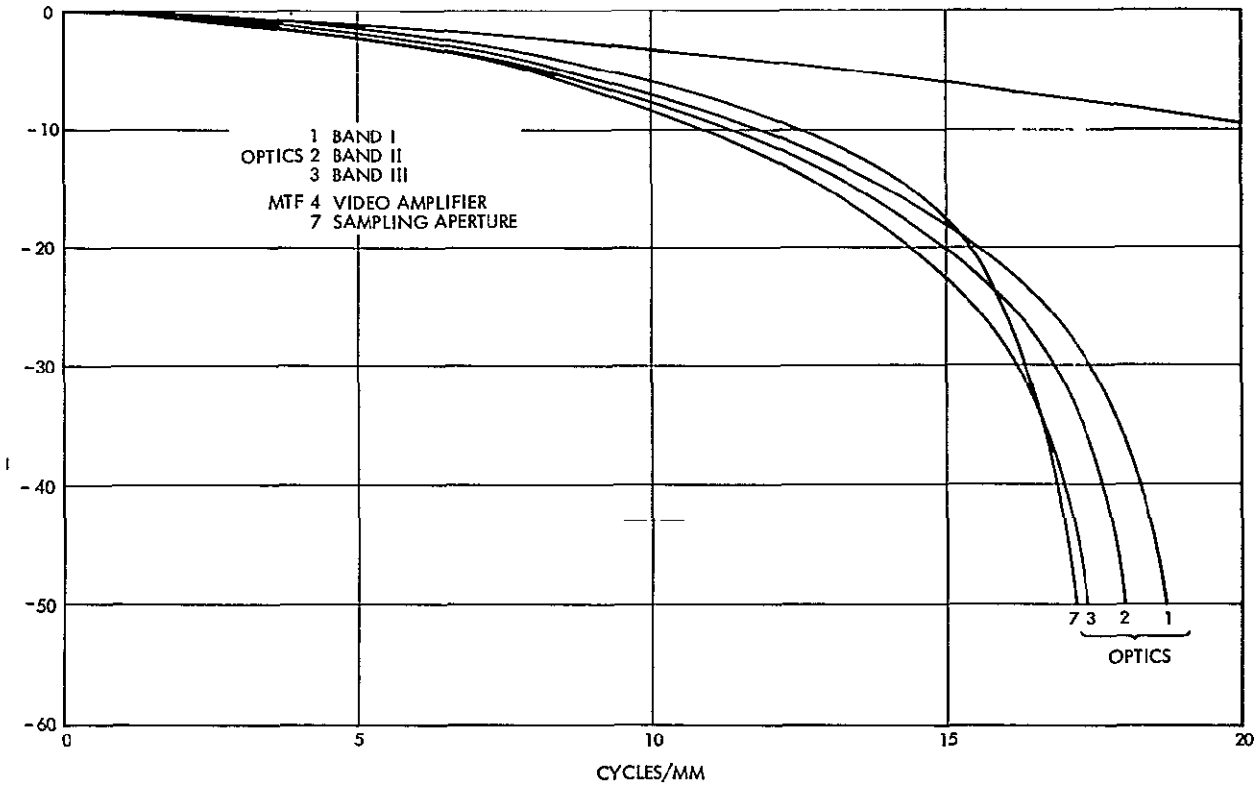

Figure 5-21
MSS CONTRIBUTORY MTF's

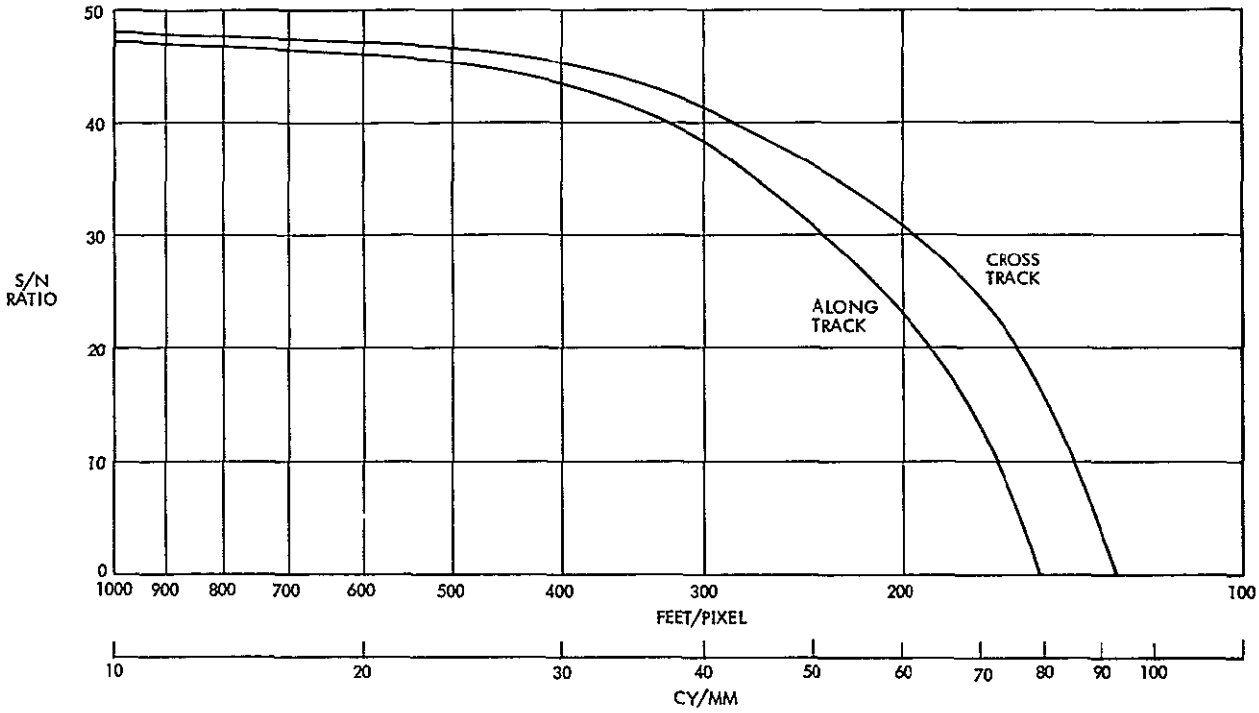

Figure 5-22
SYSTEM S/N Performance, RBV Band I, High Contrast Bar Targets

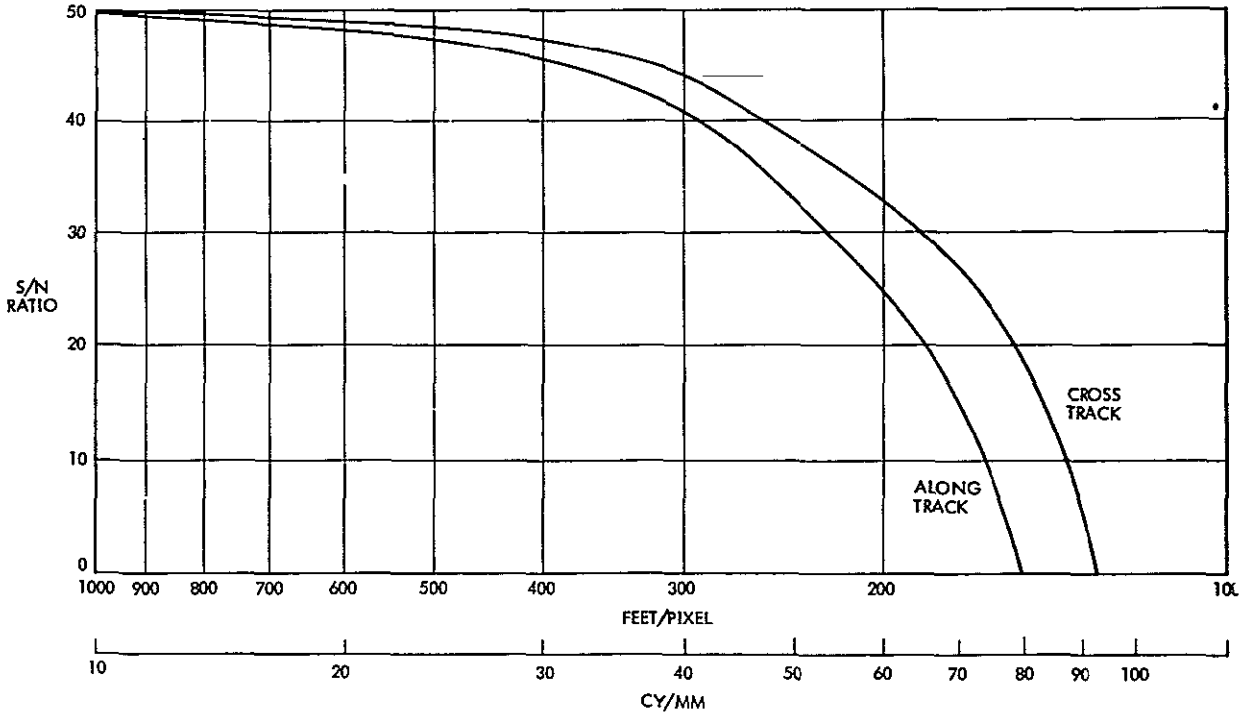

Figure 5-23
SYSTEM S/N Performance, RBV Band II, High Contrast Bar Targets

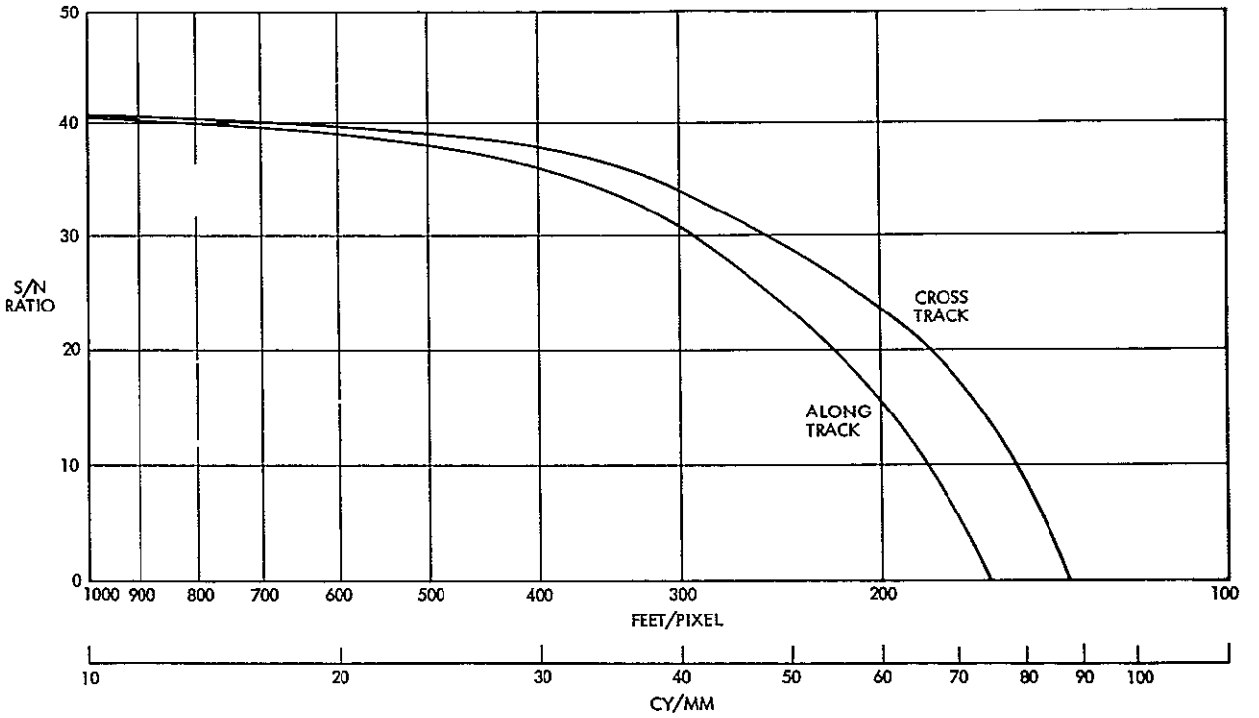

Figure 5-24
SYSTEM S/N Performance, RBV Band III, High Contrast Bar Targets

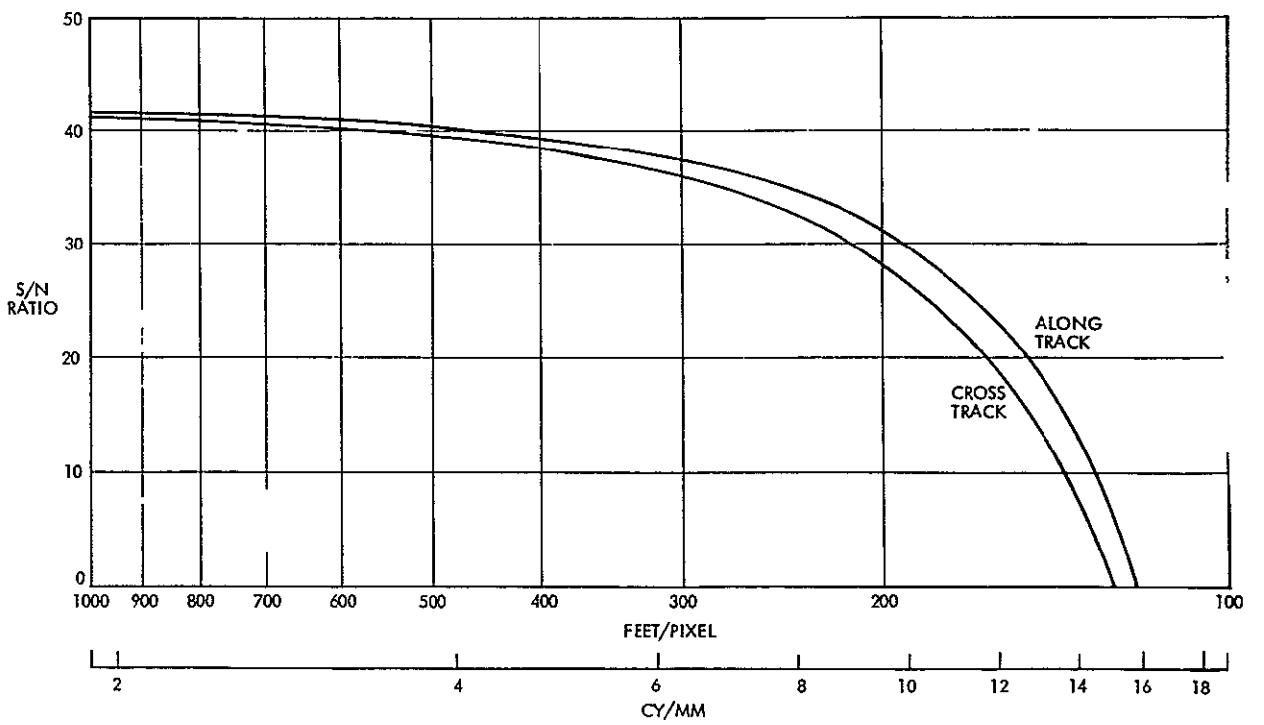

Figure 5-25
SYSTEM S/N Performance, MSS Band I, High Contrast Bar Targets

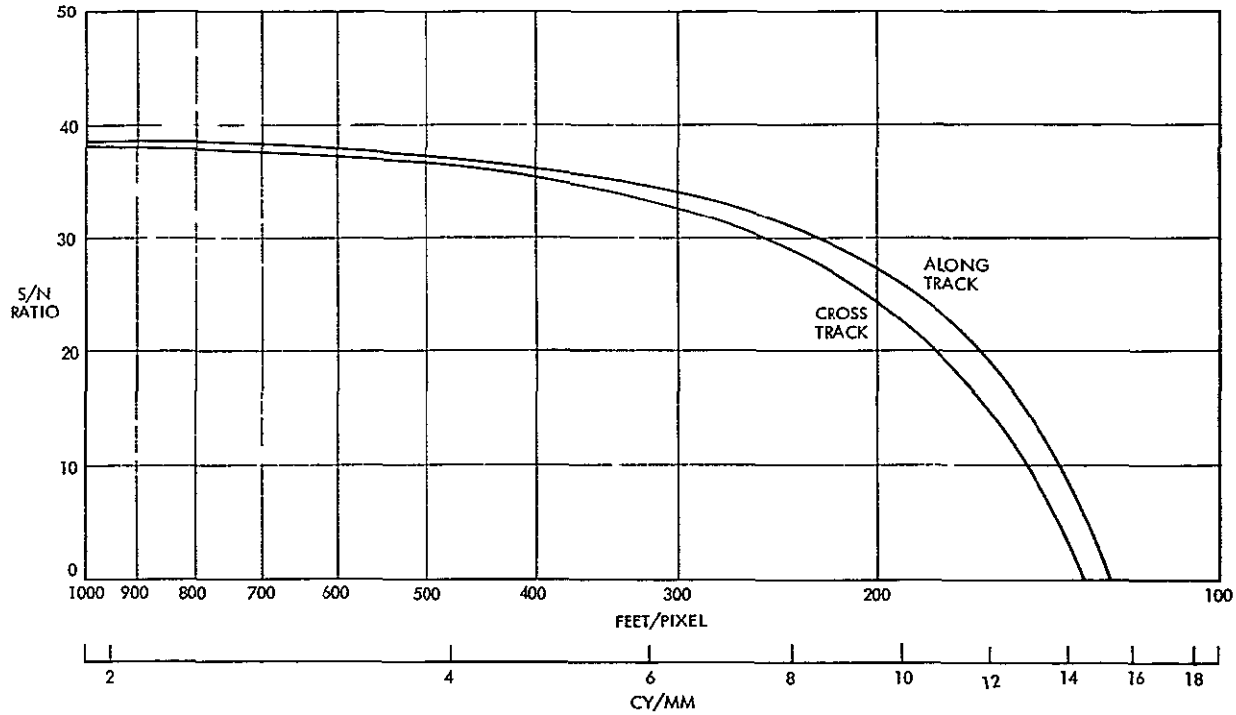

Figure 5-26
SYSTEM S/N Performance, MSS Band II, High Contrast Bar Targets

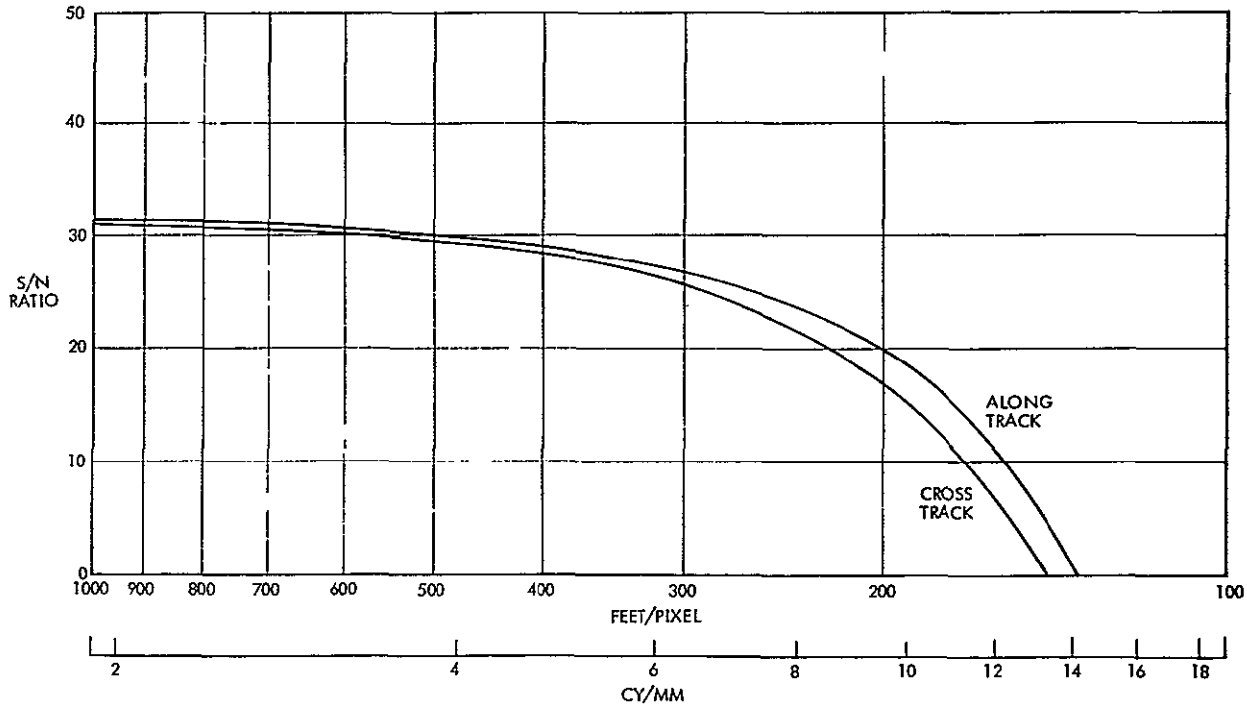

Figure 5-27
SYSTEM S/N Performance, MSS Band III, High Contrast Bar Targets

5 6 1 2 Analysis DC S/N

The standard equation relating irradiance in the focal plane to radiance of the target is

$$H_\lambda = \frac{\pi T N_\lambda}{4(F/\#)^2}$$

H_λ = spectral irradiance in the focal plane

N_λ = apparent spectral radiance of the target

T = optics transmission

$F/\#$ = optics focal ratio

The resultant signal current for the RBV is

$$I_S = \tau S H_\lambda$$

and for the MSS is

$$I_S = A_d R H_\lambda$$

where

S = vidicon photocathode sensitivity ($A/J/cm^2$)

τ = vidicon exposure time (sec)

R = photomultiplier photocathode responsivity (A/W)

A_d = area of resolution cell of MSS (cm^2)

So, we may define a variable K such that

$$I_S = K H_\lambda$$

$$K = \tau S \text{ for RBV}$$

$$K = A_d R \text{ for MSS}$$

If the dominant noise is shot noise (which is a good approximation for photomultiplier tubes and for vidicons operated in the ruturn beam mode), the noise current is

$$I_N = \sqrt{2 e I_S \Delta f}$$

I_N = Noise current

e = Electron charge (coulombs)

Δf = Noise bandwidth (Hz)

As our target is a square wave pattern of radiance, the signal to noise ratio is

$$S/\overline{N} = (I_2 - I_1)/N$$

S/N = Peak-to-peak signal to root mean square noise ratio

I_2 = Highlight current

I_1 = Lowlight current

$\overline{N}$ = Average noise current

$$= \sqrt{2e\Delta f \ \frac{1}{2}(I_1 + I_2)}$$

Hence,

$$S/N = \frac{1}{\sqrt{e\Delta f}} \ \frac{I_2 - I_1}{\sqrt{I_2 + I_1}}$$

$$S/N = \alpha \frac{N_{\lambda_2} - N_{\lambda_1}}{\sqrt{N_{\lambda_2} + N_{\lambda_1}}}$$

where

$$\alpha = \sqrt{\frac{K\pi T}{4e\Delta f(F/\#)^2}}$$

These system parameters are listed in Table 5-19 Target parameters of apparent radiance and approximate reflectance are listed in Table 5-20

The results of these calculations are the signal/noise ratios of both sensing systems in their different spectral bands when viewing a large high contrast target

5 6 1 3 Analysis MTF

The overall MTF is the product of the MTF functions of each degradation process These are summarized in Table 5-16 and will be considered in that order

Table 5-19 System Parameters

Parameter		Band 1	Band 2	Band 3
λ	RBV	0 475→0 575μ	0 58→0 68μ	0 69→ 0 83μ
	MSS	0 5→ 0 6μ	0 6→ 0 7μ	0 7→ 0 8μ
$\bar{\lambda}$	RBV	0 525μ	0 63μ	0.76μ
	MSS	0 55μ	0 65μ	0 75μ
S	RBV	20 mA/J/cm^2	36 mA/J/cm^2	7 5 mA/J/cm^2
R	MSS	43 5 mA/w	22 mA/w	6 mA/w
τ	RBV	12 msec		
A_d	MSS	(5 84 x 10^{-3} cm)^2		
Δf	RBV	3 5 MHz		
	MSS	43 1 KHz		
F/#	RBV	2 66		
	MSS	3 52		
T	RBV	69% (Spectral)		
	MSS	70% (Spectral) 90% (Obscuration)		
α	RBV	5 77 x 10^3	7 74 x 10^3	3 53 x 10^3
	MSS	2 94 x 10^3	2 10 x 10^3	1 22 x 10^3
		cm w$^{-1/2}$	cm w$^{-1/2}$	cm w$^{-1/2}$

1 Atmospheric Turbulence

The MTF defining the effect of turbulence within the atmosphere in the spatial frequency response of the cameras is defined by the following equation [1]

$$T_1(k) = \exp(-2\pi^2 f^2 \sigma^2 k^2)$$

$T_1(k)$ = MTF function

k = corner frequency (cycles/mm)

f = focal length

σ = seeing strength (radians)

[1] Hufnagel, R E , "Random Wavefront Effects," Perkin-Elmer Symposium on Modulation Transfer Functions, March 6, 1963

Table 5-20 Target Characteristics

In Band Radiance*	0 5→0 6μ	0 6→0 7μ	0 7→0. 8μ	0 8→1 1μ
Hilite	2 5	2 3	1 3	1 5
Lolite	0 25	0 23	0 13	0 15

*mwatts cm^{-2} $ster^{-1}$

MSS target radiance (from NASA-GFSC Specification)

Spectral Reflectivity	0 55	0 65	0 75	0 95
Hi Clear	91%	94%	66%	
Hi Haze	92%	97%	70%	
Lo Clear	5%	5%	6%	
Lo Haze	0%	1%	4%	

Target reflectance (for 60° Solar Zenith Angle)

In Band Radiance	0 475→0 575μ	0 58→0 68μ	0 69→0 83μ
Hilite	2 65	2 3	1 75
Lolite	0 26	0 23	0 17

*m watts cm^{-2} $ster^{-1}$

RBV target reflectance (for similar reflectivity)

Table 5-21 Peak-to-Peak Signal/Root Mean Square Noise

Sensor	Band 1	Band 2	Band 3
RBV	257 48 dB	318 50 dB	117 41 dB
MSS	126 42 dB	87 39 dB	38 32 dB

$= 0.30/\text{altitude in feet}$

$= 10^{-4}$ radians

The effect of atmospheric turbulence is negligible as the MTF is 1 00 for spatial frequencies up to 1000 cycles/mm

2 Optics Resolution

The optics of the two systems are quite different An MTF for the MSS optics is supplied so it will be used [2] The RBV cameras utilize refractive optics which may be characterized as follows [3]

$$T_2(k) = \frac{2}{\pi} \left\{ \cos^{-1}\left(\frac{k}{k_L}\right) - \left(\frac{k}{k_L}\right)\left(1 - \frac{k^2}{k_L^2}\right)^{1/2} \right\}$$

$T_2(k)$ = MTF function

k = spatial frequency (cycles/mm)

k_L = diffraction limit spatial frequency

$= (\lambda F/\#)^{-1}$

This function of course assumes diffraction limited optics

3 Vidicon Beam Resolution

This MTF applies only to the RBV cameras It is supplied by the manufacturer [4]

4 Video Amplifier

This MTF is applied only in the direction of scan The two systems have considerably different bandwidths and only the MSS bandpass characteristic is specified, a two pole RC filter [5] For convenience a similar filter will be assumed for the RBV

---

[2] "System Design Study, Multi-Spectral Scanner (MSS)," Hughes Aircraft Company, Santa Barbara Research Center, August 26, 1969

[2] O'Neill, E L , Introduction to Statistical Optics, Addison-Wesley Publishing Company, Inc , Reading, Mass , 1963

[4] "Vidicon-2" Diameter Return-Beam Camera Tube, RCA Developmental Type Number C23061A," RCA Preliminary Technical Data Sheet, January 1968

[5] Ibid 2

$$T_4(k) = \frac{1}{1 + k^2/k_o^2}$$

$T_4(k)$ = MTF function

k = spatial frequency (cycles/mm)

k_o = corner frequency (cycles/mm)

For the RBV we have

$$k_o = 164 \text{ cycles/mm}$$

For the MSS we have

$$k_o = 15 \text{ cycles/mm}$$

5 Spacecraft Limits Cycle Oscillation

The MTF defining the effect of spacecraft limit cycle motion on the spatial frequency response of the cameras is

$$T_5(k) = \text{sinc}(\pi\, a_5 k)$$

$T_5(k)$ = MTF function

k = spatial frequency (cycles/mm)

a_5 = image motion during exposure (mm)

$$a_5 = F\,\theta\,\tau$$

F = objective focal length

θ = angular rate (radians/sec)

τ = exposure time

The anticipated angular rate of the ERTS satellite is 1 4 x 10^{-4} radians/sec per axis The nominal exposure time of the RBV cameras is 12 msec For the RBV,

$$a_5 = 0\ 212 \times 10^{-3} \text{ mm}$$

The nominal exposure time of the MSS is microseconds Hence this term is significant only for the RBV cameras

6 Uncompensated Image Motion

This MTF is applied in the direction of flight The MTF function of UMC is

$$T_6(k) = \text{sinc}(\pi\, a_6 k)$$

$T_6(k)$ = MTF function

k = spatial frequency (cycles/mm)

a_6 = image motion during exposure (mm)

$$a_6 = \frac{F}{A} v \tau$$

F = focal length

A = satellite altitude

v = satellite subpoint velocity

τ = exposure time

For the RBV

$$a_6 = 1\ 09 \times 10^{-2} \text{ mm}$$

As before, the MSS exposure time is so short that its MTF is unaffected

7 Sampling Aperture

Raster line spacing and aperture size represent the same phenomenon, although raster MTF is applied only in the cross scan direction The MTF for both is

$$T_7 = \sin(\pi a_7 k)$$

$T_7(k)$ = MTF function

k = spatial frequency (cycles/mm)

a_7 = aperture size (mm)

For the RBV

$$a_7 = 5\ 443 \times 10^{-3} \text{ mm}$$

For the MSS

$$a_7 = 5\ 84 \times 10^{-2} \text{ mm}$$

This list represents all the MTF's believed to affect sensor resolution up to the data down link Aperture correction is believed to be undesirable for this application [6]

The MTF of each sensor is

$$MTF(k) = \Pi T_i(k)$$

where the product is taken over the appropriate i Table 5-16 lists the appropriate i. The individual MTF's for each sensor are shown in Figures 5-20 and 5-21 The appropriate products are shown in Figures 5-22 through 5-27 Table 5-22 lists the S/N ratio for viewing 200' bars and the limiting resolution These values apply to the information output from the sensor Further calculations are necessary to determine the S/N ratio of the data used to reconstruct the images

[6] Laverty, N P , "Resolution of Film Records of Video Data from ERTS Return-Beam Vidicon Cameras," IOC 7244. 3-23, TRW Systems 28 Aug 69

Table 5-22. Sensor System Performance

		Band 1		Band 2		Band 3	
		RBV	MSS	RBV	MSS	RBV	MSS
S/N 200' bar target	Along Track	23 dB	31 dB	25 dB	28 dB	16 dB	20 dB
	Cross Track	31 dB	28 dB	33 dB	25 dB	24 dB	17 dB
Bar size S/N=0 dB	Along Track	150'	120'	150'	125'	160'	135'
	Cross Track	130'	125'	130'	130'	140'	145'

5 6 1.4 Data Link

The S/N ratio and the MTF from the two camera systems will be degraded by the spacecraft video tape recorder, the RF link and the ground based recorder The degradation can be computed by the following equation

$$S/N = \frac{\frac{S_1}{N_1} \times \frac{S_2}{N_2}}{\sqrt{\left(\frac{S_1}{N_1}\right)^2 + \left(\frac{S_2}{N_2}\right)^2}}$$

Table 5-23 lists the S/N ratios of the various items of the data link and the total degradation The S/N ratio for viewing 200' bars and the limiting resolution may be calculated and are presented in Table 5-24 The MTF's of the various items in the data link are believed flat in the frequency region of interest The photo reproducer similarly will not degrade the MTF (as it is down 3 dB @ 9000 TVL) The S/N ratio of the finished prints is not well defined and is not generally a useful parameter Radiometric quantities must be measured from the tapes

Table 5-23. Data Link S/N Degradation

	Band 1		Band 2		Band 3	
	RBV	MSS	RBV	MSS	RBV	MSS
Sensor S/N	257	126	318	87	117	38
SC recorder	126	225	126	225	126	225
RF link	153		153		153	
Ground recorder	40	10^{-4} error rate	40	10^{-4} error rate	40	10^{-4} error rate
Output S/N	38	93	38	73	36	37
	32 dB	39 dB	32 dB	37 dB	31 dB	31 dB
Degradation	16 dB	3 dB	18 dB	2 dB	10 dB	1 dB

Table 5-24 System Performance

		Band 1		Band 2		Band 3	
		RBV	MSS	RBV	MSS	RBV	MSS
S/N ratio 200' bar target	Along Track	7 dB	28 dB	6 dB	25 dB	5 dB	19 dB
	Cross Track	15 dB	25 dB	14 dB	22 dB	13 dB	16 dB
Bar size S/N-0 dB	Along Track	180'	125'	180'	125'	185'	135'
	Cross Track	150'	130'	150'	135'	155'	145'

5 6 2 Radiometric Error Analysis

5 6 2 1 Basic Considerations

The transfer of information through an imaging system, whether a photographic, television, or direct viewing optical system, is accompanied by degradation of the information content by the inherent characteristics of the system Generally, such systems are designed to display an image for direct viewing by a human observer Therefore, the observer must be considered as a component of the system

The system may be designed to compensate in part for the degradation of information caused by the characteristics of the observer's eye and brain Image enhancement techniques are used to increase or change those characteristics of the input information, as required, to ease the task of the photointerpreter in detecting, recognizing, and identifying objects from their images in the output display

The return beam vidicon (RBV) three-camera system and the multispectral spot scanner (MSS), used in the Earth Resources Technology Satellite (ERTS), depend on energy derived from the Sun and reflected by objects on the surface of the Earth or within the Earth's atmosphere The variations in reflectivity, as recorded at the output of the ground station, provide clues to the nature of the object The division of the intensity of reflectivity into spectral bands affords further information about the scene to be analyzed

In most imaging systems, the quality criterion is that the imagery be pleasing to the observer Those qualities that present a pleasing appearance are determined by the characteristics of tonal reproduction, sharpness (as contrasted with resolution), and, in color reproduction systems, the color balance or fidelity both in hue and purity In general, it may be said that a pleasing reproduction of a scene is one that the observer feels is a reasonable likeness of the original

For scientific work, the criterion is more stringent The data received from the imaging system must be capable of interpretation with precision and repeatability with regard to position within the image field (geometry), intensity of the reflected radiance with regard to object characteristics, both spectral and intensity, and the characteristics of the radiating source, modified by the characteristics of the transmission path (atmosphere, radiometry) It is also necessary that the edges of objects seen in the image be sharply defined (MTF)

Error models of each of these aspects of the RBV and the MSS system to be flown aboard ERTS have been constructed Fixed systematic errors may be compensated for either in the satellite system or during processing of the imagery at the data processing stations

A second form of systematic errors is one in which the errors are variable but predictable, based on Sun angle, satellite orientation, and similar criteria If these variables are known, corrections can be applied to the imagery or in the interpretation of the imagery to reduce the errors to within close tolerances

A third form of errors is one in which the errors are random, and generally cannot be predicted or corrected Knowledge of the nature of these errors permits the calculation of possible deviation from prescribed tolerances

The reflective characteristics of objects on the Earth's surface may range from completely diffuse to completely specular Generally, the characteristics will lie somewhere between these extremes A completely diffuse (Lambertian) surface reflects energy as a function of the cosine of the angle between the normal to the surface and line of interest Since the projected area of the object as viewed along the line of sight varies inversely as a function of the cosine, the radiance of the Lambertian surface is independent of the angle at which it is viewed Diffuse surfaces appear equally bright in all directions

Specular surfaces obey the law of reflection for mirrors All energy is reflected at an angle equal to the angle of incidence. Unless the line of sight lies along this line, little energy will be received by the sensor Energy reflected specularly and viewed by the sensor along the angle of reflection will be very intense and may cause overload of the sensor or the video transmission channel

The sensor measures the intensity of the reflected light from the scene by exploring an image formed optically on the photosensitive surface, point by point The accuracy of the measurement relative to the actual intensity of the target depends on the quality and spectral characteristics of the illumination, the attenuation by the atmosphere, and the flare light caused by the radiance of the atmosphere and in the optical system Atmospheric haze varies with locality as well as weather, and its attenuation of information bearing light is a variable

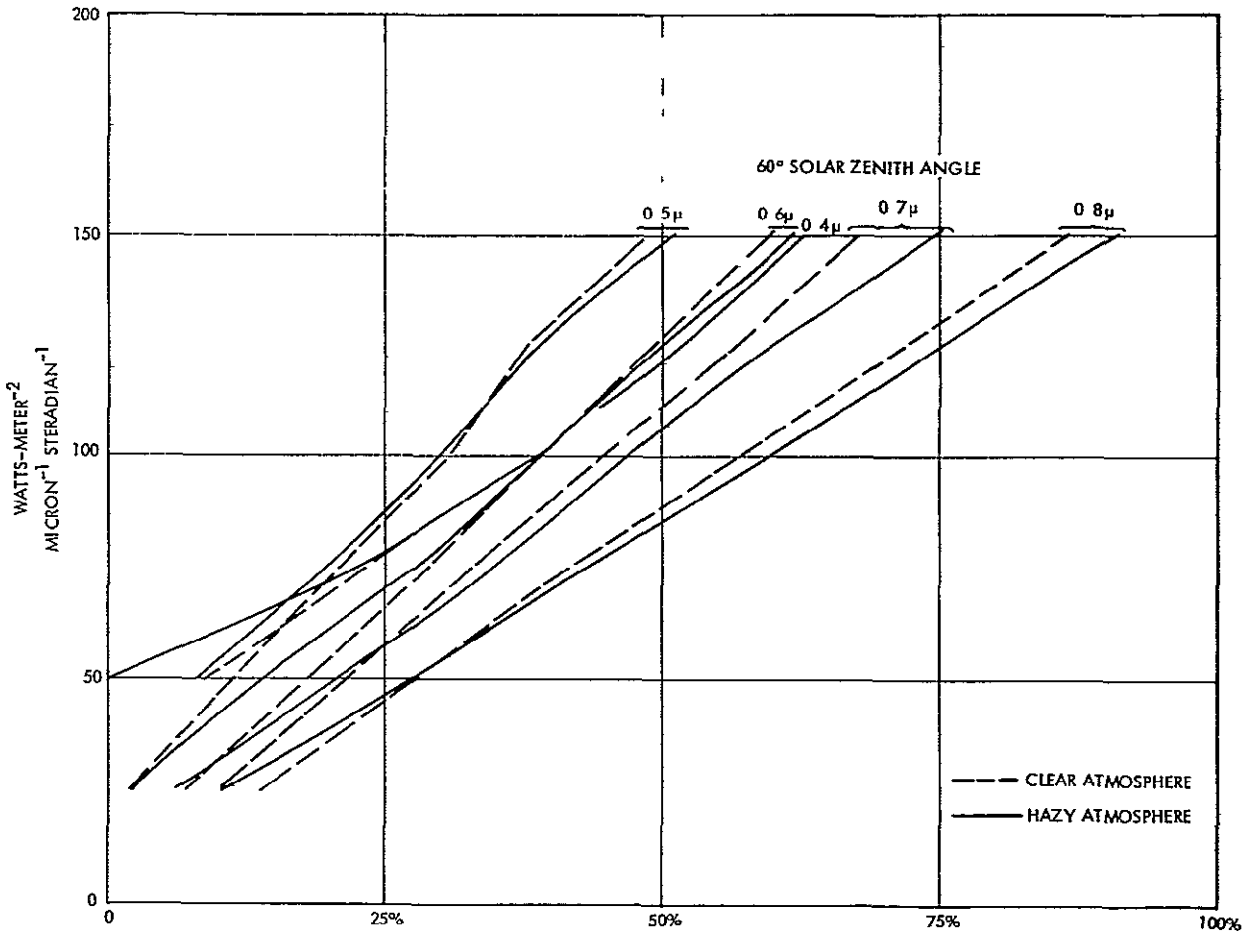

Figure 5-28
60° SOLAR Zenith Angle

Rayleigh scattering of radiance caused by molecular characteristics of air in the atmosphere varies inversely as the fourth power of the wavelength Blue light is scattered more than red Larger atmospheric particles on the order of 10 times the wavelength of light, such as smoke, dust, water, fog, and other particles, also cause a scattering, which is not spectrally variable, known as Mie scattering

On a clear day, the scattering is predominantly Rayleigh and is evidenced by the clear blue sky In hazy weather, Mie scattering is predominant with a neutral gray overcast or white clouds that reflect radiant energy uniformly throughout the spectrum

Scattered light reduces the modulation of the target, causing a reduction in contrast in the reproduction Compensation for this reduction of contrast may be applied by increasing the gamma of the reproduction In a linear system, a value of luminance may be subtracted from the video signal (clipping), increasing contrast of objects that are of greater radiance than the flare light It is difficult to bring out details of objects that are of lesser radiance than the radiance of flare light since the noise (random fluctuations) which is always additive, cannot be removed

An analysis utilizing a Monte Carlo computer program, developed by TRW illustrates atmospheric effects A large number of (numerical) photons are generated, their paths are followed down through the atmosphere, reflected or absorbed at the surface, and the returns counted The output which is the fractional photon return, is normalized by the solar constant and plotted in these terms

The first analysis considers a large uniformly reflecting target and both hazy and clear atmospheres No distinction is made between target/signal photons and atmosphere/noise photons If one chooses a given albedo and wavelength, the radiance at orbital altitude is readily obtained from Figure 5-28

The second analysis contains several refinements The first analysis considers a large uniform target Actually, any target has small structure and here we consider a small target of variable albedo surrounded by a larger area of constant (20 percent) albedo Further, we may now define a target return which includes the radiance reflected

off the target and an atmospheric return which includes everything else The target return contains the functional dependence on albedo which interests us, the atmospheric return is an additive noise-type term which degrades resolution The radiance at orbital altitude is the sum of the two It is important to note that the atmospheric return can vary greatly and the results obtained apply only to a particular case Figure 5-29 shows these results Note that the two analyses are consistent only to about 30 percent as certain assumptions differ

The results of these analyses, particularly the second, indicate that atmospheric radiance is a serious problem when one wishes to determine spectral signatures Further work is necessary to model these effects and determine the accuracy with which they may be removed

5 6. 2. 2 In-Flight Sensor Calibration

Absolute in-flight radiometric calibration of the signal transfer function of the RBV and the MSS system will depend on the availability of an absolute radiometric source of energy, modulated by known step values If the step values are measured at the output of the system when they are plotted against the absolute input values the transfer function can be determined

It is proposed that the input energy source be obtained from the erase lights, normally used in the preparation of the photoconductor surface before exposure Several levels of intensity may be used, each exposing the RBV surface uniformly and being read before the next value is used If the method of prelaunch calibration is used, the input values are known, and the signal transfer function can, in principle, be obtained, as previously described

Aging effects of incandescent lamps can be compensated for by using a second set of lamps as a primary calibration standard The limited use of these lamps will prevent serious error that results from again effects over the life of the onboard systems

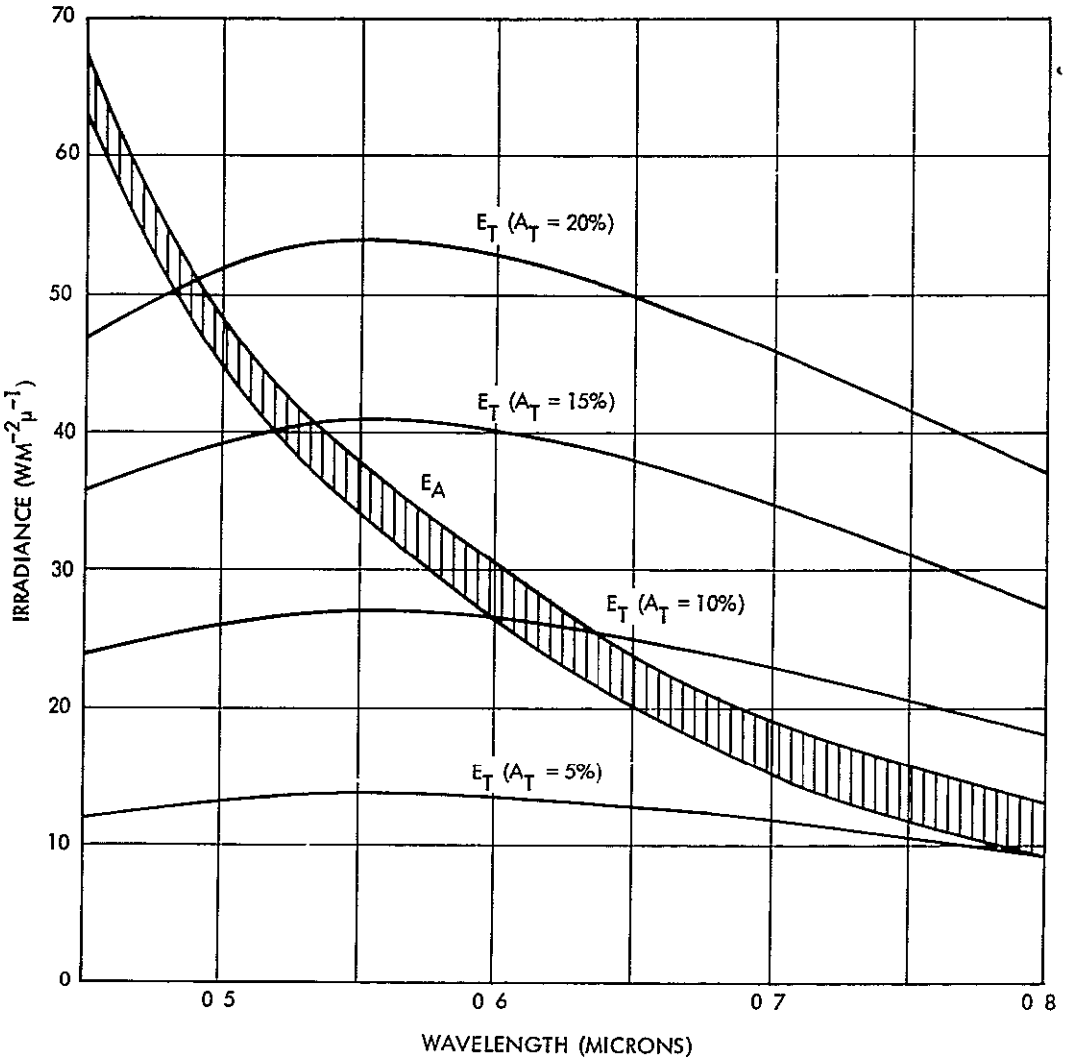

Figure 5-29
NADIR SPECTRAL Return Radiance
E_A = Atmospheric Return (For Average Terrain Reflectance of 20%)
E_T = Target Return (For Target Reflectances 5% 20%)
(50° Solar Zenith Angle)

This concept is similar to that used in conventional photographic sensitometry The lamp, used as the exposure source in daily work with the sensitometer, is compared on a more or less regular schedule with a second lamp which is reserved as a primary standard and used only for calibration purposes Adjustments in the voltage and current of the everyday lamp are made as the result of each calibration to reduce the errors caused by aging effects When the lamp fails, the primary standard lamp is used to calibrate its replacement so that no discontinutity in the calibration need exist

Sources of error in calibration will be caused by the aging of the primary standard lamp, variations in lamp voltage (lamp output variations in lamp voltage (lamp output varies as V^4), and changes in color temperature Changes in the transmission of the optics will not be corrected or detected, unless the exposure is made through the total system

A more basic approach to the problem of calibration in flight is to use the Sun, which, since the system is operating above the atmosphere with all its variables, represents an ultimate in stability both in irradiance and spectral content An integrating sphere can be mounted at a convenient position on the spacecraft Fiber optics conduct the energy to a photocell, placed so that the erase lights can be compared to the sun by chopping or alternating the light from one source to the other, and adjusting the intensity of the Sun-derived energy automatically to produce a null Readout of the amount of attenuation required for balance will calibrate the system

A better system of in-flight radiometric calibration is using the sunlight to provide the exposure source However, since this may present severe engineering problems it may be impractical

Basically, the best system of in-flight calibration is one which requires the least dependence on preflight calibration The use of several exposure cycles, each illuminating the total surface of the vidicon to a different intensity (as proposed by RCA) is dependent on preflight calibration, and will not necessarily detect variations that result from aging or other causes A single exposure of several gray-scale step tablets, placed at strategic points over the surface of the

photoconductor, would produce more reliable information for the dynamic signal transfer function than the proposed single intensity step method

It should be noted that at least a two-level signal is always required because, unless the system is capable of transmitting dc levels accurately, a knowledge of the output intensity relative to input is indeterminate Normally, the two-level signal contains what is termed a black level reference This portion of the signal waveform represents zero radiance input This knowledge of intensity value is used to restore dc levels at the output end of the system

5. 6. 2. 3 Sensor Differential Shading

Shading variations that are acceptable in a black and white reproduction may not be acceptable in a three-color system Differences in the responses of the three RBV tubes as a function of position on the photoconductor when exposed to a uniform spectrally neutral field may cause noticeable departures from neutrality in the reproduction when printed onto color material Variations noticeable as color shading of reproduction of a gray field will indicate the need for further shading correction beyond the correction that is inserted in each RBV camera systems

5. 6. 2. 4 Gray-Scale Tracking

In all three-color systems, a certain ratio of energy inputs to the three sensors is specified as neutral or gray As the intensity of the input energy is increased while the specified ratio is maintained, the luminance of the reproduction increases (lighter grays) toward white A change in the ratio will produce color

Adjustments of the three RBV camera systems to maintain gray-scale tracking over the range from black to white is critical if spectral signatures are to be reproducible in the false color hard copy output of the system

Differences in nonlinearity of each camera and associated video amplifier and differences in black level setting affect the tracking capability of a three-color vidicon camera system If the system is adjusted for correct tracking of large area gray steps, errors in small area gray steps at the black end may still exist because of flare light

addition Since the photoconductor of the vidicon may exhibit increased transparency toward the red end of the spectrum, this flare increases for the red as compared with the blue-green Before flight, the RBV system should be calibrated for black level shifts in small area blacks as a function of the average irradiation reaching each sensor Some correction can be made in the image recorder by resetting the black level of the recorder for each spectral band

5. 6 2. 5 Gamma Correction

The term gamma, originating in photography, denotes the maximum slope or gradient of a characteristic (D-log E) curve plotted on log-log paper Also, for signal changes of a small percentage, the value of gradient or gamma is the ratio of relative output to relative input For example, when a gradient of 2 0 is specified for a given point in the characteristic curve, it means that a 2 percent change in input will cause a 4 percent change in output If the characteristic curve that describes the dynamic transfer function of log radiance input to log radiance output were a straight line, the gamma would be a constant at all points This does not occur in practical systems, so that gamma refers only to the maximum slope of the curve The term gradient should be applied to describe the derivative of the curve at all points other than the maximum

Thus, the measure of gamma is a measure of the enhancement or reduction of contrast of a reproduction relative to the original If the gamma is greater than unity, contrast differences in the object are increased in the reproduction If gamma is lower than 1, contrast is reduced When gamma is unity, the reproduction system is linear at the point of maximum gradient

The characteristic curve of practically all image reproduction systems has an S-shaped characteristic, so that the gradient in the low light or toe and the high light or shoulder of the curve is considerably less than the maximum gradient or gamma that is measured in the middle of the curve This lowering of gradient causes a compression of gray step values at these points Generally, this is considered beneficial since it permits fitting a relatively large input dynamic range into a somewhat more restricted dynamic range of the reproducing system

Photographic systems using negative films that are printed onto positive materials for final reproduction have a minus gamma for each step, negative and positive The system gamma is the product of the two minus gammas, which results in a positive gamma This is important in electronic video systems, since simple polarity inversion of the video signal is sometimes used to produce a direct positive recording with the result that tonal values are greatly distorted in the reproduction A nonlinear amplifier whose output is inversely proportional to the input is required to correct the video signal for direct positive film recording

This discussion is based on the plot of the characteristic curve in log-log coordinates This is significant when the human observer is part of the system because, as described by the Weber-Fechner law, the observer's response to a change in stimulus is proportional to the existing stimulus In other words, the eye's response is logarithmic, to a best approximation, so that equal increments along the abscissa of the log-log plot represent equal increases in the gray-scale step value For example, the range from 0 1 to 1 foot-lambert has as many perceptible steps of gray as the range from 10 to 100 foot-lamberts Also, in a dynamic range of 30 1, there are as many gray-scale values between 3 3 and 18 percent as there are between 18 and 100 percent

The RBV light signal transfer function has a maximum gradient (gamma) of 0 65 This is a function of the photoconductor surface This value is complementary to the maximum gradient of cathode-ray display tubes, which is about 2 0 The product gamma of a vidicon and the cathode-ray tube is somewhat higher than 1 0, which produces good tone reproduction

The laser beam recorder (LBR) is a highly nonlinear device, because of the modulator characteristics The modulator nonlinearity is corrected by means of a circuit whose sighted function is the inverse of the LBR modulator This circuit can be adjusted to provide a linear transfer function over a dynamic range greater than 100 1, or to provide a further change of gamma to compensate for nonlinearities elsewhere in the system

If no gamma correction is used in the satellite RBV camera subsystem and the vidicon has a gamma of 0 65, gamma correction can be provided as part of the LBR system The amount of correction to be used will be based on the gamma of the photographic process (film, chemical processing, and reproduction)

The RBV noise is caused by shot noise inherent in the scanning beam The noise varies as the square root of the beam current Since the beam modulation is negative, i e , maximum return beam occurs for darker areas and minimum beam for bright areas, the RBV noise becomes greater in the darker areas of the image as compared to the brighter areas

An increase in gamma increases the signal increments in the white end of the transfer function and decreases it in the dark end The perceptibility of noise for the RBV will be lessened by this approach

When the video signal is applied to the image recorder, two adjustments are required The gain or amplitude of the video signal must be set, thereby setting the exposure range for the film record Also, a dc voltage or bias must be added to the video to position the exposure at the optimum point on the modulator-film characteristic

In a linear system, these two operations are straightforward and each operates independently without affecting the other, if the video signal reference level is a black level reference and is clamped to the inserted bias The dc bias then sets the value of exposure for the darkest part of the video, while the gain adjustment sets the maximum exposure

5 6. 2 6 Tone Reproduction of ERTS Imagery

A multispectral acquisition system provides a means of enhancing differences in recorded imagery by breaking the spectrum of an object into several component bands This allows increased information discrimination Tonal differences that may exist in narrow spectral bands are often masked when integrated over a broad spectral range For a multispectral band acquisition system, the system should be balanced to acquire the maximum amount of information discrimination

in each individual band Tests have indicated that this condition is satisfied when the dynamic range of each band is on the order of 10 1 and when the individual bands are of equal dynamic range

The ERTS system will utilize tonal change detection to enhance our ability to detect and recognize Earth resources information Since multispectral change detection is the main goal, the system should be precalibrated for maximum information acquisition for nominal image acquisition conditions Once these conditions have been established they should be fixed, and at least in bulk mode reproduction should reflect the same system parameters In this way, any tonal or color changes in the final output imagery will reflect only changes in the appearance of the imagery as seen by the satellite and will not reflect changes in either the satellite telemetry or reproduction systems In special cases, such as in the precision mode, it would be advantageous to deviate from this fixed tone reproduction standard

Because of atmospheric attenuation and scattering, one would expect the dynamic range of the multiband records to be different Atmospheric scattering, often referred to as haze or atmospheric radiance, is basically a wavelength dependent function and varies from being completely selective to being almost totally nonselective depending on the types and concentrations of particles in the atmosphere For pure Rayleigh atmosphere, the scattering goes inversely as the fourth power of wavelength For a hazy atmosphere with large concentrations of water vapor and smoke, the scattering is almost wavelength dependent Some authorities have stated that a typical atmosphere combining both Rayleigh and Mie scattering goes approximately as a function inverse to the 1 6 power of wavelength In any case, the nominal conditions for scattering are predominantly in the ultraviolet and blue region of the spectrum and fall off significantly as one goes to the red and infrared regions of the spectrum For the ERTS case, one would expect the apparent contrast in the red band to be higher than that in the green, and that in the infrared to be higher than that in the red

5 6 2 7 Tonal Balancing of Records

Test results at Itek have indicated that optimum results are obtained when the density range of the individual spectrum records are approximately equal If the density of the records are equivalent, the printing and color balancing of the resultant additive color records are simplified A nominal dynamic range on the order of about 10 1 (equivalent to a density range of 1 0) has been found to be ideal for making additive color records Most color reproduction materials have a fairly high gamma with a relatively narrow exposure latitude Too high a contrast on the separation records can result in a loss of information because the color reproduction material is not able to record the entire tonal range of the input imagery The density range should also be kept down because it makes exposure and color balancing easier in the additive color process

The individual separation records can be dynamically balanced to some extent either in the satellite or in the ground handling equipment Some correction may be possible in the satellite by adjusting the gain control on the individual RBV cameras Thus, it may be possible to telemeter equivalent signal ranges for each RBV This will have the effect of altering the apparent scene contrast range in one or more of the records to produce a near balance This would be done in a calibrated fashion so that the actual apparent object radiance could be reconstructed if desired Once this calibration is set, the RBV responses would not be changed during the life of the system Uncontrollable system changes that result from aging and temperature variations would be determined by calibrated reference standards within the satellite

The input dynamic range can also be altered in the initial printout state Here the taped input data for each channel can be computer analyzed and a corrected signal can be fed to the LBR In this manner, the dynamic range for each record can be either raised or lowered to a prescribed level to produce a nominal standard equivalency Again, once this condition has been established for the bulk mode, it should remain constant

For the precision mode, one might want to deliberately deviate from this standard For example, there might be three possible atmospheric conditions, heavy haze, moderate haze, and clear Specific precalibrated correction functions could be stored in the computer for these three cases The computer would input these specific input specifications to the LBR to balance the dynamic ranges of the individual records for each specific condition

A third possible way to correct the contrasts of the multispectral black and white records is by processing each individually to different gammas However, this is not recommended, since the control and repeatability of such a process would be a complex process with a high potential error The major tone reproduction corrections should be made in the computer and LBR stages of the reproduction process

Itek's experience has shown that, in subsequent duplication stages, a near ideal tone reproduction produces best results This occurs at a process gamma of 1 0 at which there is 1 1 correspondence between log exposure range and density range Once the film type and processing conditions have been established to achieve the optimum nominal condition, they are held constant to ensure repeatable results in all future reproductions

If a calibrated reference step wedge is generated in the LBR, the best process control and color balancing of the imagery is obtained This step wedge can be used as a process control standard for subsequent production stages By monitoring the densities reproduced on the wedge, proper exposure and photographic processing control can be assessed The three integrated calibrated step wedges on the RBV records should produce a neutral black and white tone Deviation from a neutral tone would indicate an improper balancing of one or more of the multispectral print channels used to produce the additive color record

Neutral tone balancing has been used as a standard in color printing for many years In spectral cases, balancing to a neutral tone for certain types of images may not produce optimum results In the precision mode, the balance may be altered to produce ac records that meet the optimum needs of a user However, this would be a special process

5 6 2 8 Radiometric Accuracy of a Photographic Process

Since the ERTS imagery will extract radiometric data from the ground scene, it is necessary to carefully consider the accuracy of photographic materials used as quantitative radiation sensors A well controlled photographic process can produce remarkably accurate and repeatable radiometric and photometric data

Several types of errors can occur when film is used as a radiometer The first error is caused by the nonuniformity of sensitivity in the typical photographic material Any nonuniformity in sensitivity across the film web will produce errors in the developed imagery However, the uniformity of the quality films made today is exceptionally good, and sensitivity variations are less than 5 percent as a result of manufacturing tolerances As long as the film is stored in a suitable environment, uniform sensitivity is maintained until the film is used The absolute sensitivity of photographic materials can vary with each batch However, batch variations can be determined in a quality controlled sensitometric operation Batch variations in sensitivity might vary as much as 10 to 15 percent in a normal photographic material

The largest radiometric error generally occurs in film processing To achieve good radiometric results, the uniformity of the processing must be well controlled Each part of the film must receive the same chemical treatment This requires uniform agitation and uniform temperature as well as constancy of developing solutions Processing uniformity on the order of 5 percent can be achieved in precise sensitometric processing However, in a normal well controlled production processing operation, variations might run as high as 10 percent This variation would be the total variation across the format and not the point to point variation between adjacent detail The relative radiometric accuracy will be significantly higher

The size of the object or objects being evaluated influences radiometric accuracy Photographic film is composed of small grains of silver These grains represent the noise in the photographic process When a large area is being evaluated, we are well above the noise level of the system and the radiometric accuracy will be very good However,

as we begin to evaluate smaller objects, we begin to get into the grain noise of the system and density fluctuations as a function of this grain noise begin to appear We begin to lose accuracy as the signal to noise level increases The film that has been selected for ERTS duplication, EK-2430, has the lowest granularity (18) of currently available production duplicating materials and it will have a minimal effect on the radiometric accuracy of the system

Exposure effects could also affect photographic materials used as quantitative radiation sensors The uniformity of the exposure on the film will affect results Most quality printing devices can be made to accuracies of within a few percent

The possible reciprocity effect that results from large exposure variations could cause error However, we do not anticipate this problem in the ERTS system because it will be basically fixed and extraordinarily large ranges are not anticipated

Latent image decay is another potential source of radiometric error There will be an essentially constant time in all photographic operations so that significant time variations between exposure and processing are not anticipated

After considering these factors, it would appear that a well-controlled photographic process involving good sensitometric calibration and control procedures could maintain a radometric accuracy on the order of 95 percent for objects whose images are in the size range of a millimeter and larger The objects whose images approach the grain noise limit of the film will have larger errors

PRECEDING PAGE BLANK NOT FILMED

APPENDIX A

COORDINATE SYSTEMS AND TRANSFORMATIONS

In order to facilitate the discussion of Sections 4.2 and 4 3 the right handed orthogonal coordinate systems used in those two sections are defined in this appendix Also the required transformations among the various coordinate systems are given.

1 COORDINATE SYSTEMS

1 1 Earth Centered Inertia (ECI)

The earth centered inertia system, $\underline{x}_I = (x_I, y_I, z_I)^T$, has it origin at the center of the earth, x and y axes lying in the equatorial plan with the positive x axis directed toward vernal equinox

1 2 Earth Centered Fixed (ECF)

The earth centered fixed system, $\underline{x}_F = (x_F, y_F, z_F)^T$, has its origin at the center of the earth, x and y axes lying in the equatorial plane with the positive x axis directed toward the prime meridian

1.3 Orbital Reference (OR)

The orbital reference system, $\underline{x}_R = (x_R, y_R, z_R)^T$ is centered at the spacecraft position in orbit and oriented such that the positive z axis points down to the center of the earth. The positive x axis lies in the orbit plane and has a negative dot product with the spacecraft velocity vector, and the y axis completes the right hand set.

1 4 True Body (TB)

The true body coordinates, $\underline{x}_B = (x_B, y_B, z_B)^T$, are fixed in the spacecraft body and are defined with respect to the horizon scanner planes where it is assumed that the horizon scanner planes are orthogonal to each other The positive z axis points downward along the intersection of the A, C, and B, D scanner planes The position x and y directions are as described in Figure A-1.

1 5 Nominal Orientation (NO)

The nominal orientation coordinate system, $\underline{x}_O = (x_O, y_O, z_O)^T$, is centered at the spacecraft position in orbit and oriented such that with

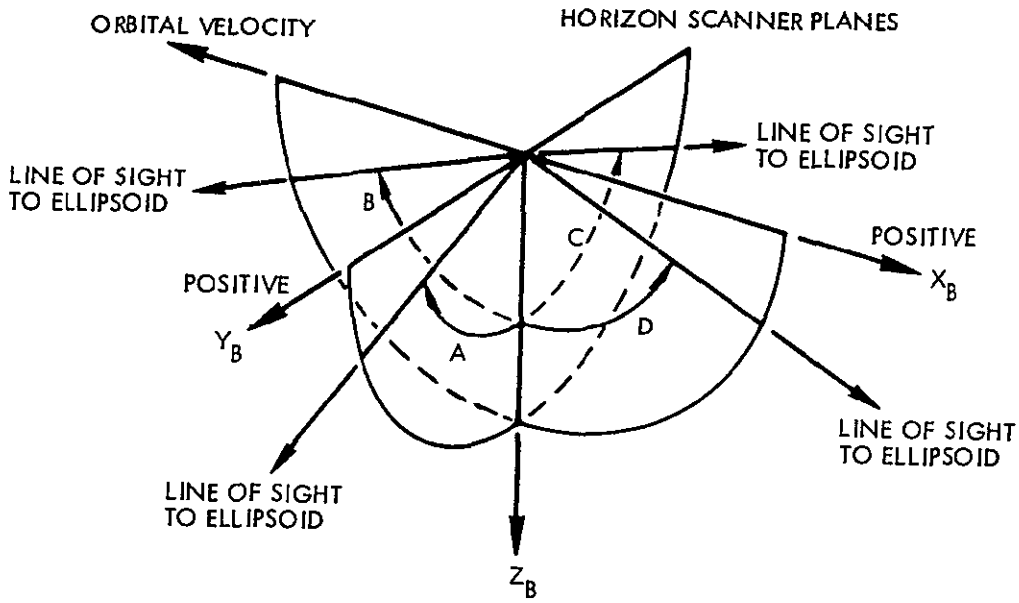

Figure A-1 Body Coordinates Defined Based on the Horizon Scanner

the horizon sensors tracking the horizon profile $\beta_A = \beta_C$ and $\beta_B = \beta_D$ where β_i is the angle the ith sensor makes with the +z axis With the positive direction of the z axis so defined, the positive x axis lies in the orbital plane and has a negative dot product with the spacecraft velocity vector The y axis completes the right hand set

2 MAGNETIC COORDINATE SYSTEM (MC)

The magnetic coordinate system $\underline{x}_M = (x_M, y_M, z_M)^T$ has its positive x axis at longitude -150° and latitude -11° with respect to the EFC system The y axis lies in the equatorial plane and z completes the right hand coordinate system

2 1 Transformation

The transformation from the ECF system to the ECI system is

$$\underline{x}_I = T_I \underline{x}_F \tag{A-1}$$

where

$$T_1 = \begin{bmatrix} \cos \omega_1 t & -\sin \omega_1 t & 0 \\ \sin \omega_1 t & \cos \omega_1 t & 0 \\ 0 & 0 & 1 \end{bmatrix} \tag{A-2}$$

where

ω_1 = earth's rotation rate

t = time of passage of the prime meridian past vernal equinox

The transformation from OR system to the ECI system is

$$\underline{x}_R = T_2 \, \underline{x}_I + \underline{R} \tag{A-3}$$

where

$$T_2 = \begin{bmatrix} \cos\Omega \sin v + \sin\Omega \cos \iota \cos v & -\cos\Omega \cos \iota \cos v + \sin\Omega \sin v & -\sin \iota \cos v \\ \sin\Omega \sin \iota & -\cos\Omega \sin \iota & \cos \iota \\ -\cos\Omega \cos v + \sin\Omega \cos \iota \sin v & -\sin\Omega \cos v - \cos\Omega \cos \iota \sin v & -\sin \iota \sin v \end{bmatrix} \tag{A-4}$$

and where for the spacecraft orbit (see Figure A-2)

Ω = longitude of ascending node

ι = inclination of orbit

v = spacecraft angle orbit from the equatorial plane

$\underline{R}^T = (0, 0, R)^T$, R - distance of spacecraft from the center of the earth

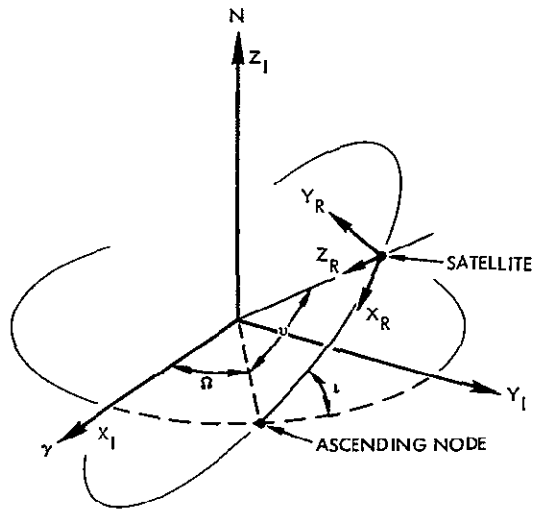

Figure A-2 Relationship Between ECI and OR Coordinate System

The transformation from the NO system to the TB system is

$$\underline{x}_B = S_1 \underline{x}_O \tag{A-5}$$

where

$$S_1 = \begin{bmatrix} \cos\theta \cos\psi & \cos\theta \sin\psi & -\sin\theta \\ \sin\phi \sin\theta \cos\psi - \cos\phi \sin\psi & \sin\phi \sin\theta \sin + \cos\phi \cos\psi & \sin\phi \cos\theta \\ \cos\phi \sin\theta \cos\psi + \sin\phi \sin\psi & \cos\phi \sin\theta \sin\psi - \sin\phi \cos\psi & \cos\phi \cos\theta \end{bmatrix} \tag{A-6}$$

Here the Euler angles are yaw (ψ) about the z axis, then pitch (θ) about the y axis and finally roll ϕ about the x axis as shown in Figure A-3

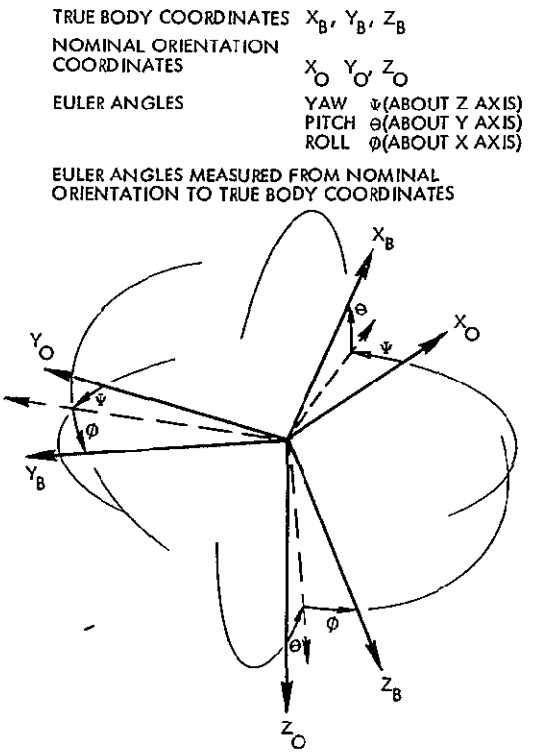

Figure A-3 Euler Angles Measured from Nominal Orientation to True Body Coordinates

The transformation T_3 from the OR system to the NO system

$$\underline{x}_O = T_3 \underline{x}_R \tag{A-7}$$

will now be derived From (4-11) we have

$$\tan \beta = \frac{\sqrt{B^2 - AC} \pm B}{A} \tag{A-8}$$

which is used to compute for the two roots of β, β_1 and β_2 For $\alpha = 0^o$ we compute from (A-8), a $\delta_{ROLL} \triangleq \delta_R$

$$\delta_R = \frac{1}{2}(\beta_2 - \beta_1) \tag{A-9}$$

For $\alpha = 90^{\circ}$ we compute from (A-8) a $\delta_{PITCH} \triangleq \delta_P$

$$\delta_P = \frac{1}{2}(\beta_2 - \beta_1) \tag{A-10}$$

Given δ_R and δ_P and the definition of the NO and OR system, the direction cosine matrix relating these coordinates system can now be derived Let $\underline{x}_o, \underline{y}_o, \underline{z}_o$ be the unit vectors in the NO system The components of $\underline{z}_o = (x_{z,R}, y_{z,R}, z_{z,R})^T$ in the OR system is solved by the following relationships (see Figure A-4)

$$x_{z,R} = \sin \delta_P$$

$$y_{z,R} = \sin \delta_R \tag{A-11}$$

$$z_{z,R} = 1 - x_{z,R}^2 - y_{z,R}^2$$

We now have

$$\underline{z}_o = (x_{z,R}, y_{z,R}, z_{z,R})^T \tag{A-12}$$

The components of $\underline{x}_o = (x_{x,R}, y_{x,R}, z_{y,R})^T$ and of $\underline{y}_o = (x_{y,R}, y_{y,R}, z_{y,R})^T$ are obtained by solving the following dot product equations respectively

$$\underline{z}_o \cdot \underline{x}_o = \begin{bmatrix} x_{z,R} \\ y_{z,R} \\ z_{z,R} \end{bmatrix} \begin{bmatrix} x_{x,R} \\ 0 \\ 1 - x_{x,R}^2 \end{bmatrix} = 0 \tag{A-13}$$

Figure A-4 $\underline{Z}_o$ Axis of the NO System and its Relationship to the OR System

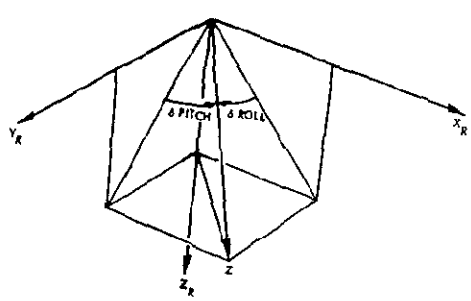

and

$$\underline{z}_o \quad \underline{y}_o = \begin{bmatrix} x_{z,R} \\ y_{z,R} \\ z_{z,R} \end{bmatrix} \begin{bmatrix} 0 \\ y_{y,R} \\ 1 - y^2_{y,R} \end{bmatrix} = 0 \qquad \text{(A-14)}$$

The equations are quadratic in the unknown $x_{x,R}$ and $y_{y,R}$ The positive roots are the required solutions The transformation is therefore

$$T_3 = \begin{bmatrix} x_{x,R} & 0 & 1 - x^2_{x,R} \\ 0 & y_{y,R} & 1 - y^2_{y,R} \\ x_{z,R} & y_{z,R} & z_{z,R} \end{bmatrix} \qquad \text{(A-15)}$$

In the development of the system equations we need to relate the body rates $\omega_{bx}, \omega_{by}, \omega_{bz}$ about the body x, y, z axes respectively to the Euler rates (ϕ, θ, ψ) with respect to the rotating NO system rotating at $\underline{\omega}_o$ To do this we successively apply the rotation matrix $S_1(\phi, \theta, \psi)$ given by (A-6) to each of the Eules rates as follows

$$\begin{bmatrix} \omega_{bx} \\ \omega_{by} \\ \omega_{bz} \end{bmatrix} = \begin{bmatrix} S_1(0,0,0) \end{bmatrix} \begin{bmatrix} \phi \\ 0 \\ 0 \end{bmatrix} + \begin{bmatrix} S_1(\phi,0,0) \end{bmatrix} \begin{bmatrix} 0 \\ \theta \\ 0 \end{bmatrix} + \begin{bmatrix} S_1(\phi,\theta,0) \end{bmatrix} \begin{bmatrix} 0 \\ 0 \\ \psi \end{bmatrix} \qquad \text{(A-16)}$$

or

$$\begin{bmatrix} \phi \\ \theta \\ \psi \end{bmatrix} = S_2(\phi, \theta) \begin{bmatrix} \omega_{bx} \\ \omega_{by} \\ \omega_{bz} \end{bmatrix}$$

where

$$S_2(\phi,\theta) = \begin{bmatrix} 1 & \tan\theta \sin\phi & \tan\theta \cos\phi \\ 0 & \cos\phi & -\sin\phi \\ 0 & \sin\phi/\cos\theta & \cos\phi/\cos\theta \end{bmatrix} \tag{A-17}$$

If we denote the transformation S_1, Equation (A-6) by

$$S_1(\phi,\theta,\psi) = S_1 \tag{A-18}$$

the transformation from the MC system to the EFC system is given by T_4

$$\underline{x}_F = T_4 \underline{x}_M \tag{A-19}$$

where

$$T_4^T = S_1(0^\circ, 11^\circ, -150^\circ) \tag{A-20}$$

Note that,

$$S_3 = S_2 S_1 \tag{A-21}$$

and the derivatives of S_2 and S_3 are given in terms of Euler angle rates as follows

$$S_2 = \begin{bmatrix} 0 & \dot\phi(\tan\theta \cos\phi) + \dot\theta(\sec^2\theta \sin\phi) & \dot\theta(\sec^2\theta \cos\phi) - \dot\phi(\tan\theta \sin\phi) \\ 0 & -\dot\phi \sin\phi & -\dot\phi \cos\phi \\ 0 & \dot\phi(\sec\theta\cos\phi) + \dot\theta(\tan\theta\sec\theta\sin\phi) & \dot\theta(\tan\theta\sec\theta\cos\phi - \dot\phi(\sec\theta\sin\phi) \end{bmatrix}$$

(A-22)

and

$$S_3 = \begin{bmatrix} \theta(\sin\theta\ \cos\psi) - \psi(\sec\theta\ \sin\psi) & \psi(\sec\theta\ \cos\psi) + \theta(\tan\theta\ \sec\theta) & 0 \\ -\psi\cos\psi & -\psi\sin\psi & 0 \\ \theta(\sec^2\theta\ \cos\psi) - \psi(\tan\theta\ \sin\psi) & \psi(\tan\theta\ \cos\psi) + \theta(\sec^2\theta\ \sin\psi) & 0 \end{bmatrix} \tag{A-23}$$

B ERTS Error Analysis
Figures of Merit

PRECEDING PAGE BLANK NOT FILMED.

APPENDIX B

ERTS ERROR ANALYSIS FIGURES OF MERIT

The absolute and relative error covariance matrices C_ξ and $C_{\Delta\xi}$ completely describe the error probability density functions for normally distributed error sources

$$p\,(\xi_x, \xi_y) = \frac{1}{2\pi \left| C_\xi \right|^{1/2}} \exp \left\{ -\frac{1}{2} \underline{\xi}^T C_\xi^{-1} \underline{\xi} \right\} \tag{B-1}$$

$$p\,(\Delta\xi_x, \Delta\xi_y) = \frac{1}{2\pi \left| C_{\Delta\xi} \right|^{1/2}} \exp \left\{ -\frac{1}{2} \underline{\Delta\xi}^T C_{\Delta\xi}^{-1} \underline{\Delta\xi} \right\} \tag{B-2}$$

Several "figures of merit" can be used to describe ERTS performance in terms of the covariance matrices C_ξ and $C_{\Delta\xi}$ The most common ones are

- One and three-sigma position error ellipses
- CEP
- Variance in the distance between two points on an ERTS picture

The first two figures of merit can be applied to both absolute and relative error (internal consistency), while the distance error variance is only applied to the internal consistency

ERROR ELLIPSE

The 1-sigma error ellipse is obtained from the equations

$$\underline{\xi}^T C_\xi^{-1} \underline{\xi} = 1 \tag{B-3}$$

or

$$\underline{\Delta\xi}^T C_\xi^{-1} \underline{\Delta\xi} = 1 \tag{B-4}$$

By substituting equations (B-3) and (B-4) in equations (B-1) and (B-2) it is obvious that the 1-sigma error ellipse is the locus of points with equal probability densities

$$p\,(\xi_x, \xi_y) = \frac{1}{2\pi \left| C_\xi \right|^{1/2}} e^{-1/2} \tag{B-5}$$

$$p\,(\Delta\xi_x, \Delta\xi_y) = \frac{1}{2\pi \left| C_{\Delta\xi} \right|^{1/2}} e^{-1/2} \tag{B-6}$$

The integrated probability density inside the 1-sigma error ellipse A is (in principal axis coordinates ξ_1 and ξ_2)

$$p_{1\sigma} = \iint_A d\xi_1\, d\xi_2\, \frac{1}{2\pi\sigma_1\sigma_2} \exp\left\{-\frac{1}{2}\left[\frac{\xi_1^2}{\sigma_1^2} + \frac{\xi_2^2}{\sigma_2^2}\right]\right\} \tag{B-7}$$

Equation (B-7) can be transformed to the integral over the unit circle A_1

$$p_{1\sigma} = \iint_{A_1} dw_1\, dw_2\, \frac{1}{2\pi} \exp\left\{-\frac{1}{2}\left[w_1^2 + w_2^2\right]\right\} \tag{B-8}$$

where

$$w_1 = \frac{\xi_1}{\sigma_1}, \quad w_2 = \frac{\xi_2}{\sigma_2}$$

or, in polar coordinates the 1-sigma error ellipse probability is

$$p_{1\sigma} = \int_0^1 \int_0^{2\pi} \frac{\rho}{2\pi} \exp\left[-\frac{1}{2}\rho^2\right] d\rho\, d\theta = 0\ 393468 \tag{B-9}$$

The 3-sigma error ellipse probability is, similarly

$$P_{3\sigma} = \int_0^3 \int_0^{2\pi} \frac{\rho}{2\pi} \exp\left[-\frac{1}{2}\rho^2\right] \rho d\theta = 0\ 988890 \qquad \text{(B-10)}$$

The numerical values (B-9) and (B-10) give the probability of finding an ERTS picture point within the 1-sigma and 3-sigma error ellipses respectively

DISTANCE BETWEEN TWO POINTS

Define two image points as follows

$$\text{Point 1} \quad (x_1 + \Delta x_1,\ y_1 + \Delta y_1) \qquad \text{(B-11)}$$

$$\text{Point 2} \quad (x_2 + \Delta x_2,\ y_2 + \Delta y_2)$$

the square of the distance between the points is given by

$$(S+\Delta S)^2 = \left[(x_1+\Delta x_1) - (x_2+\Delta x_2)\right]^2 + \left[(y_1+\Delta y_1) - (y_2+\Delta y_2)\right]^2 \qquad \text{(B-12)}$$

or, to first order in ΔS

$$S^2 + 2S\Delta S = \left(x_1-x_2\right)^2 + \left(y_1-y_2\right)^2 + 2(x_1-x_2)\Delta\xi_x + 2(y_1-y_2)\Delta\xi_y$$

where

$$\Delta\xi_x = \Delta x_1 - \Delta x_2 \qquad \text{(B-13)}$$

$$\Delta\xi_y = \Delta y_1 - \Delta y_2$$

thus

$$\Delta S = \frac{(x_1 - x_2)}{S} \Delta\xi_x + \frac{(y_1 - y_2)}{S} \Delta\xi_y \tag{B-14}$$

$$\Delta S = \underline{1}_S^T \underline{\Delta\xi}$$

where

$$\underline{1}_S = \mathrm{col}\left(\frac{x_1 - x_2}{S}, \frac{y_1 - y_2}{S}\right)$$

$$\underline{\Delta\xi} = \mathrm{col}\,(\Delta\xi_x, \Delta\xi_y)$$

the variance in the distance $\sigma_{\Delta S}^2$ is then

$$\sigma_{\Delta S}^2 = \langle \Delta S^2 \rangle = \underline{1}_S^T C_{\Delta\xi} \underline{1}_S \tag{B-15}$$

Equation (B-15) is a quadratic form (positive definite) in terms of the distance unit vector $\underline{1}_S$ It is obvious from (B-15) that the distance error variance lies between the maximum and minimum eigenvalues of $C_{\Delta\xi}$

$$\sigma_{min} \leq \sigma_{\Delta S} \leq \sigma_{max} \tag{B-16}$$

CEP

The CEP or circular probable error is defined as the radius of the circle around the correct image point for which there is a 50% probability of the erroneous point being within Thus, it is the value of R for which

$$0\ 500 = \frac{1}{2\pi\sigma_1\sigma_2} \int_0^R \int_0^{2\pi} \rho d\rho d\theta \exp\left\{-\frac{\rho^2}{2}\left[\frac{\cos^2\theta}{\sigma_1^2} + \frac{\sin^2\theta}{\sigma_2^2}\right\}\right. \tag{B-17}$$

An approximate solution to (B-17) which is accurate to better than 3% is

$$CEP = 0\ 589\ \left[\sigma_1 + \sigma_2\right] \tag{B-18}$$

This equation is accurate for the cases of interest in the ERTS error analysis

C Derivation of the Nominal Roll, Pitch Yaw Direction Cosines

PRECEDING PAGE BLANK NOT FILMED

APPENDIX C

DERIVATION OF THE NOMINAL ROLL, PITCH, YAW DIRECTION COSINES

Let the roll, pitch and yaw axes be denoted by $\underline{e}_x$, $\underline{e}_y$, $\underline{e}_z$ unit vectors respectively

$$\underline{e}_x = X_x \underline{i} + X_y \underline{j} + X_z \underline{k} \tag{C-1}$$

$$\underline{e}_y = Y_x \underline{i} + Y_y \underline{j} + Y_z \underline{k}$$

$$\underline{e}_z = Z_x \underline{i} + Z_y \underline{j} + Z_z \underline{k}$$

where

x, y, z = earth centered inertial (ECI) coordinates with x pointed in the direction of the vernal equinox

$\underline{i}$, $\underline{j}$, $\underline{k}$ = unit vectors along the ECI axes

The $\underline{e}_z$ (yaw) axis is directed downward along the local geodetic vertical of the ellipsoid representing the Earth. The $\underline{e}_x$ (roll) axis is oriented so that the orbital rate signal is sensed by the roll-yaw gyro Thus, $\underline{e}_x$ lies along the $\underline{e}_z$ vector with positive sense in the direction of flight Hence

$$\underline{e}_x = -\frac{\underline{e}_z}{|\underline{e}_z|} \tag{C-2}$$

or

$$X_x = -\frac{Z_x}{B}, \quad X_y = -\frac{Z_y}{B}, \quad X_z = -\frac{Z_z}{B} \tag{C-3}$$

with

$$B = \sqrt{Z_x^{\ 2} + Z_y^{\ 2} + Z_z^{\ 2}}$$

the $\underline{e}_y$ (pitch) axis is then

$$\underline{e}_y = \underline{e}_z \times \underline{e}_x \tag{C-4}$$

or, in terms of direction cosines

$$\begin{aligned} Y_x &= Z_y X_z - Z_z X_y \\ Y_y &= Z_z X_x - Z_x X_z \\ Y_z &= Z_x X_y - Z_y X_x \end{aligned} \tag{C-5}$$

The evaluation of the nine direction cosines of the attitude coordinate axes proceeds from the determination of the direction cosines of the local geodetic vertical The Earth's figure is defined by

$$S = x_e^{\ 2} + y_e^{\ 2} + \frac{a^2}{b^2} z_e^{\ 2} - a^2 = 0 \tag{C-6}$$

where x_e, y_e, and z_e are points on the Earth's surface in ECI coordinates, a is the equatorial radius, and b is the polar radius The attitude vector is

$$\underline{h} = \underline{r} - \underline{r}_s = h\,\underline{e}_s \tag{C-7}$$

where

$$\underline{r} = x\,\underline{i} + y\,\underline{j} + z\,\underline{k}, \text{ satellite position}$$

$$\underline{r}_s = x_s\,\underline{i} + y_s\underline{j} + z_s\underline{k}, \text{ sub-satellite position}$$

$$h = \text{scalar altitude}$$

$$\underline{e}_s = \frac{\nabla S}{|\nabla S|}, \text{ unit vector normal to Earth's surface}$$

the gradient of S at the sub-satellite point is

$$\nabla S = 2\left(x_s,\ y_x,\ \frac{a^2}{b^2} z_s\right) \tag{C-8}$$

If the scalar parameter, K, is denoted by

$$K = \frac{2h}{|\nabla S|} \tag{C-9}$$

then the satellite position and sub-satellite position are related as follows (from equations (C-7) - (C-9)

$$\begin{aligned} x &= (1+K)\,x_s \\ y &= (1+K)\,y_s \\ z &= (1+a^2/b^2\,K)\,z_s \end{aligned} \tag{C-10}$$

And since $\underline{r}_s$ satisfies equation (C-6).

$$S = \frac{x^2 + y^2}{(1+K)^2} + \frac{b^2}{a^2} \frac{z^2}{(b^2/a^2+K)^2} - a^2 = 0 \qquad \text{(C-11)}$$

the altitude vector $\underline{h}$ is then

$$\underline{h} = \frac{K\,x}{1+K}\,\underline{i} + \frac{K\,y}{1+K}\,\underline{j} + \frac{K\,q}{1+K}\,\underline{k} \qquad \text{(C-12)}$$

where

$$q = \left(\frac{1+K}{b^2/a^2+K}\right)z$$

The scalar altitude is

$$h = \frac{K}{1+K}A, \; A^2 = x^2 + y^2 + q^2 \qquad \text{(C-13)}$$

The scalar K is computed by iterating as follows The initial value of K is that for a circular earth b = a

$$K_o = \frac{\sqrt{x^2 + y^2 + z^2} - a}{a} \qquad \text{(C-14)}$$

Then

$$K_{n+1} = K_n + \Delta K_n \qquad \text{(C-15)}$$

and, from equation (C-11)

$$S_{n+1} = S_n + \left(\frac{dS}{dK}\right)_n \Delta K_n = 0$$

so that

$$\Delta K_n = -\frac{S_n}{\left(\frac{dS}{dK}\right)_n} \tag{C-16}$$

where

$$S_n = \frac{x^2 + y^2}{(1+K_n)2} + \frac{b^2}{a^2}\frac{z^2}{(b^2/a^2+K_n)^2} - a^2$$

$$\frac{dS_n}{dK_n} = -\frac{2(x^2 + y^2)}{(1+K_n)3} - 2\frac{b^2}{a^2}\frac{z^2}{(b^2/a^2+K_n)^3} \tag{C-17}$$

The direction cosines of the roll, pitch, and yaw unit vectors can now be evaluated The yaw axis $\underline{e}_z$ is along the normal to the Earth's surface Hence,

$$\underline{e}_z = -\underline{e}_s = -\frac{\underline{h}}{|\underline{h}|} \tag{C-18}$$

TRW
SYSTEMS GROUP
ONE SPACE PARK REDONDO BEACH CALIFORNIA

CODE IDENT 11982

TITLE

PROGRAM SPECIFICATION
FOR SYSTEM PERFORMANCE AND DESIGN
REQUIREMENTS
EARTH RESOURCES TECHNOLOGY SATELLITE PROGRAM

DATE 1 April 1970 NO D-13600

SUPERSEDING _____

PRELIMINARY

PREPARED BY _____

APPROVAL SIGNATURES

DATE	DATE
O L Brownlee	R C Turkoly
DATE	DATE
R L Kuehn	W W Royce
DATE	DATE
P W Woodson	C D Graves

D Calculation of Signal to Noise Ratios

APPENDIX D

CALCULATION OF SIGNAL TO NOISE RATIOS

Using Hughes data[1] on the radiance of agricultural targets (with 55° solar zenith angle) we can calculate similar signal to noise ratios Taking healthy oats and barley as an example, the radiance levels are

Crop	Band 1	Band 2	Band 3
Oats	0 402	0 275	0 350
Barley	0 396	0 407	0 447

Crop Radiance (mW $cm^{-2} ster^{-1}$)

Crop	Band 1	Band 2	Band 3
Oats/Barley	0 6 -4 dB	10 20dB	4 12dB

MSS S/N Ratio-Extended Crop Target

	Band 1	Band 2	Band 3	
S/N Ratio	-15 dB	9 dB	0 dB	Cross Track
	-18 dB	6 dB	-3 dB	Along Track

MSS S/N Ratio-200' Rows Crop Target

[1] "System Design Study Multi-Spectral Scanner (MSS)," Hughes Aircraft Company, Santa Barbara Research Center, 26 August 1969

PRECEDING PAGE BLANK NOT FILMED.

SPEC NO D-13600

TRW
SYSTEMS GROUP
ONE SPACE PARK REDONDO BEACH CALIFORNIA

AS OF 27 March 70
SUPERSEDING

SPECIFICATION CHANGE RECORD

SCN/REV	SCN/SPEC DATE	AUTHORIZATION		PRODUCTION EFFECTIVITY	PAGES AFFECTED
		ECP/CCN	OTHER		

SYSTEMS 1393 REV 11 67

(FILE DIRECTLY AFTER COVER SHEET)

PRECEDING PAGE BLANK NOT FILMED.

TABLE OF CONTENTS

			Page
1.	SCOPE		E-9
2	APPLICABLE DOCUMENTS		E-9
3.	REQUIREMENTS		E-12
	3.1	Performance	E-12
		3 1.1 Performance Characteristics	E-12
		3 1 2 System Definition	E-17
		3 1.3 Operability	E-27
	3.2	System Design and Construction Standards	E-33
		3 2.1 General Design and Construction Requirements	E-33
		3 2 2 Design Disciplines	E-36
	3.3	Performance Allocations	E-36
		3.3 1 Ground Data Handling System	E-36
		3.3 2 Earth Resources Technology Satellite System	E-39
		3 3 3 Data Collection System	E-46
		3.3.4 Launch Vehicle System	E-49
		3 3 5 Remote Tracking Stations System	E-50
		3 3 6 Users	E-53
4	PERFORMANCE ASSURANCE		E-54
	4.1	Phase I Program Test Requirements	E-54
		4.1 1 Engineering Test and Evaluation	E-54
		4 1 2 Qualification Testing	E-55
		4 1 3 Electrical and EMI Testing	E-55
		4.1 4 Reliability	E-55
		4 1 5 Acceptance Testing	E-55

			Page
	4.2	Phase II Program Test Requirements	E-55
		4 2.1 Integrated System Ground Tests	E-56
		4 2.2 Flight Test	E-56
		4 2 3 Failure Criteria	E-56
5	PREPARATION FOR DELIVERY		E-57
	5 1	Packaging	E-57
		5 1.1 Containers	E-57
		5 1 2 Special Instructions	E-57
	5 2	Marking	E-57
		5 2 1 Marking for Shipment	E-57
		5.2.2 Re-Inspection	E-57
6.	NOTES		E-58
	6 1	Definitions	E-58
	6 2	Abbreviations	E-58

LIST OF ILLUSTRATIONS

		Page
Figure 1	ERTS Program Top Flow Diagram	E-21
Figure 2	System Functional Schematic	E-22
Figure 3	System Specification Tree	E-23
Figure 4	Delta Shock Spectra Input Spacecraft Flight Acceptance	E-32
Figure 5	DCS Specification Tree	E-58
Figure 6	Payload Fairing Envelope	E-51
Figure 7	Spacecraft Attach Fitting	E-52

PRECEDING PAGE BLANK NOT FILMED

1 SCOPE

This specification establishes the performance, design, development and test requirements for the Earth Resources Technology Satellite Program

2 APPLICABLE DOCUMENTS

The following documents of the exact issue shown, form a part of this specification to the extent specified herein In the case of TRW Systems documents, the latest issue shall apply In case of conflict between documents referenced herein and the requirements of Sections 3, 4, and 5, the requirements of Sections 3, 4, and 5 shall apply

SPECIFICATIONS

Military

MIL-D-1000 01 March 1965	Drawings-Engineering and Associated Lists

TRW Systems Group

D-13353	Design Qualification Test, ERTS
D-13354	Environmental Acceptance Test, ERTS
D-13500	System Specification for Earth Resources Technology Satellites A & B
D-13503	Thor/Delta Launch Vehicle Interface
D-13505	ERTS Specification Government Furnished Parts List and Ground Support Equipment List
PR12-1	Identification and Marking
D-13700	ERTS Ground Data Handling System
D-13701	ERTS Personnel Subsystem
D-13750	ERTS-Operations Control Center Subsystem
D-13800	ERTS NASA Data Processing Facility

STANDARDS

Military

MIL-STD-100 01 March 1965	Engineering Drawing Practices
MIL-STD-129D 11 April 1969	Marking for Shipment and Storage
MIL-STD-143A 14 May 1963	Specifications and Standards, Order of Precedence for the Selection of
MIL-STD-803A-1 27 Jan 1964	Human Engineering Criteria for Aircraft, Missile, and Space Systems Ground Support Equipment
MIL-STD-1247A 20 Dec 1968	Marking, Functions, and Hazard Designations of Hose, Pipe, and Tube Lines, for Aircraft, Missile and Space Systems
MS-33586A 16 Dec 1958	Metal, Definition of Dissimilar

OTHER PUBLICATIONS

TRW Systems Group

	ERTS Configuration Management Plan
	ERTS Logistics Plan
	ERTS Maintainability Plan
	ERTS Quality Program Plan
	ERTS Reliability Program Plan
	ERTS Test Monitoring and Control Plan
PAR 700-53 11 November 1969	Procurement Product Assurance Requirements, Quality Systems Provisions, Project ERTS (Subcontracts)
PAR 700-54 27 November 1969	Subcontractor Reliability Requirements for ERTS
PAR 700-55 13 February 1970	Procurement, Performance Assurance Requirements, Quality, Reliability and Maintainability Provisions, ERTS Subcontractors (GDHS Equipment)

PAR-700-56 27 March 1970	Configuration Management Provisions for ERTS Major Subcontractors
PAR-700-61 27 March 1970	Procurement Performance Assurance Requirements, ERTS Subcontractors for GDHS Software

NASA

GMI 8040 1	Configuration Management Instruction
NHB 5300 4 (3A)	Requirements for Soldered Electrical Connections
NHB 5300 4 (1B) April 1969	Quality Program Provisions for Aeronautical and Space System Contractors
NPC 250-1 July 1963	Reliability Program Provisions for Spacecraft Contractors
GSFC PPL-10 July 1968	Preferred Parts List
S-320-G1 October 1969	General Acceptance Test Specification for Spacecraft and Components

3 REQUIREMENTS

3 1 Performance

3 1 1 Performance Characteristics

The Earth Resources Technology Satellite (ERTS) program shall consist of satellites, a Ground Data Handling System (GDHS) and a Data Collection System (DCS) The GDHS shall consist of an Operations Control Center (OCC) and the NASA Data Processing Facility (NDPF) The DCS shall consist of ground based collection platforms and transmitters for transmission of data to the satellite The DCS also includes receiver equipment located in the satellite

The satellites shall be launched into orbit by the Thor-Delta launch vehicle The program shall also include the ground support equipment necessary to support satellite functions The satellite shall consist of spacecraft structure (including launch vehicle adapter and payload mounts), communication and data handling (including antennas), electrical integration, active thermal control, orbit adjustment, stabilization and control, and solar array power supply subsystems and payload provisions

The program shall provide mission data necessary to satisfy the requirements of the Department of Agriculture, Department of Interior, Department of Navy, Department of Commerce and other users concerned with agriculture, forestry, geography, oceanography, hydrology, geology, and weather

3 1 1 1 Missions

The ERTS Program overall mission is to gather information about the natural and cultural resources of the earth and phenomena destroying or threatening these resources Specific missions shall include the following

3 1 1 1 1 Agricultural Applications

The ERTS program shall observe and acquire data for major agricultural applications which include

a) Species identification and measurement
b) Plant growth rate

3 1 1 1 1 (Continued)

c) Factors relating to stress on crops and forests
d) Assessment of crop vigor and health leading to yield predictions

3 1 1 1 2 Geological, Geographical, and Hydrological Applications

The ERTS Program shall observe and acquire data for major geological, geographic and hydrological applications which include

a) Improved classification of areas by geological or geomorphological characteristics such as surface composition, water runoff patterns, etc
b) More accurate monitoring of time-variant phenomena, such as population movements, transportaion flow, and environmental hazards to man (air pollution)
c) Measurements of specific hydrological parameters such as soil moisture, snow extent and depth, etc

3 1 1 1 3 Oceanographic and Hydrographic Applications

The ERTS program shall observe and acquire data for major oceanographic and hydrographic applications which include

a) Measurement of sea state
b) Location and tracking of major ocean currents
c) Mapping of sea-ice
d) Detection of specific phenomena of limited arial extent and varying locations, such as fish schools, oil slicks, Red Tide, etc
e) Shoreline analyses

3 1 1 2 Mission Support

To support the mission requirements the ERTS Program shall provide the following mission support functions

3 1 1 2 1 Data Handling

The ERTS Program shall be controlled by the Ground Data Handling System (GDHS) The GDHS shall convert the spaceborne sensor and relayed Data Collection System signals, in accordance with user requests, into interpretable data in a form that provides maximum utility to the system user

3 1 1 2 2 Payload

The payload of ERTS-A, and possibly ERTS-B shall consist of

a) Return Beam Vidicon Camera
b) Multi-Spectral Scanner
c) Data Collection Receiver
d) Wide Band Video Tape Recorder

3 1 1 2 3 Payload Weight and Volume

The satellite shall contain provisions for a payload of at least 450 lbs in a minimum volume of 13 cubit feet

3 1 1 2 4 Launch

The satellite shall be launched from the Western Test Range by a NASA Thor-Delta launch vehicle Launch and range support, facilities and services shall be provided during prelaunch and launch activities

3 1 1 2 5 Orbit

The satellite shall be placed into a 490 n mi circular, 99 degree inclination, sun synchronous orbit

3 1 1 2 6 Global Coverage

The measurements shall be global in coverage in less than three weeks, repetitive in observations at the same local time, with the resultant images having minimum distortion

3 1 1 2 7 Image Overlap

The image overlap and sidelap shall be such that continuous photographic coverage be produced in the presence of Satellite Attitude Excursions

3 1 1 2 8 On-Orbit Tracking

On-orbit tracking shall be provided by STADAN and Selected Ground Tracking Stations.

3 1 1 2 9 Command Control and Data Acquisition

The command and control, and data acquisition shall be performed by NASA STADAN/MSFN stations. The satellite shall be capable of transmitting PCM data and receiving commands from the ground stations for any satellite attitude

3 1 1 2 10 User Requirements

The data products required by the users for the various missions shall be as listed in Table I The data shall be transformed into user oriented media and stored in retrievable and reproducable form

3 1 1 2 11 Launch Vehicle Weight Capability

The launch vehicle shall be capable of launching a satellite weighing 1520 lbs into the specified orbit

3 1 1 2 12 Satellite Housekeeping Telemetry

The program shall be capable of acquiring satellite housekeeping telemetry data

3 1 1 2 13 Satellite Weight

The total satellite weight shall not exceed 1520 lbs (1480 lbs spacecraft and 40 lbs interface hardware)

3 1 1 2 14 Satellite Orientation

The satellite shall be 3 axis stabilized with one geometric axis coincident with the local vertical within 0 7 degree and the rate error not to exceed 0 04 degree per second

3 1 1 2 15 Command and Telemetry Software

The software shall contain a central file of active user sensor coverage requests, merge orbit data with this file to determine the predicted opportunities for observation by the sensors and schedule the payload events The software shall generate valid observatory commands based on the selected events and manual events These commands shall be checked for validity, safety and compatibility with the observatory

3 1 1 2 16 Housekeeping Data Storage

The GDHS software shall record all PCM health telemetry for storage in the NDPF, and shall be capable of generating trend data for off-line analysis

3 1 1 2 17 Command History

The GDHS software shall maintain a current history of all executed commands

TABLE I

ERTS PRODUCTS

Product Type	Product Form						
	Prints	Negatives	Positives	Digital Tape	Listings	Other	
RBV Bulk Imagery							
Black & White	✓	✓	✓				
Color Composite	✓						
MSS Bulk Imagery							
Black & White	✓	✓	✓				
Color Composite	✓						
RBV Precision Imagery							
Black & White	✓	✓	✓				
Color Composite	✓						
MSS Precision Imagery	✓	✓	✓				
Color Composite	✓						
Computer Readable Imagery							
RBV				✓			
MSS				✓			
Index/Abstract Data					✓		
Catalog				✓	✓		
DCS Data					✓		
Catalog				✓	✓		
Montage							
Sheets	✓						
Catalog	✓						
Spacecraft Performance				✓	✓	✓	Tapes, Listings, Plots as Required
Master Digital Data				✓	✓	✓	
SPECIAL USER REQUESTS	✓	✓	✓	✓	✓	✓	IMAGERY, DATA, TAPES LISTINGS, PLOTS AS REQUESTED

3 1 2 System Definition

3 1 2 1 System Engineering Documentation

The ERTS Program top flow diagram is shown in Figure 1 and the functional schematic diagram is shown in Figure 2

3 1 2 2 System List

The ERTS Program shall consist of the following systems

a) Ground Data Handling System
b) Earth Resources Technology Satellite System
c) Data Collection System
d) Launch Vehicle System
e) Remote Tracking Station System
f) Users

3 1 2 3 System Specification Tree

The system specification tree is shown in Figure 3

3 1 2 4 Government Furnished Equipment (GFE)

The system shall contain the following Government Furnished Equipment

Nomenclature	Part Number
1) Intercom Subsystem	TBD
2) Communications Panel Assembly	↑
3) Dial Exchange Phone System	
4) Teletype Terminal	
5) Teletype Punch	
6) MSS Status Monitor	
7) MSS Demultiplexer	
8) Console Power Supply	
9) Equipment Rack	
10) Matrix Monitor	
11) Payload Status Panel	
12) Spacecraft Status Panel	
13) RBV Tape Reproducer	
14) MSS Tape Reproducer	
15) RBV Tape Recorder	
16) Multi-Spectral Scanner	↓
17) Return Beam Vidicon Camera	TBD

18)	Yaw Gyro Assembly	201371-1
19)	Gyro Electronic Assembly	202163-1
20)	Horizon Scanner AC	A 0G0
21)	Horizon Scanner BD	A 0G0
22)	Sun Sensor	292384-1
23)	Sun Sensor	202744-1
24)	Sensor Electronic and Logic Assembly	200932-2
25)	Attitude Control Assembly	200833-1
26)	Drive Electronics Assembly	200934-1
27)	Rate Gyro Assembly	200935-2
28)	Inverter assembly	C 207450-2
29)	Control Switch Assembly	228576-3
30)	Array Drive Mechanism	202540-2
31)	Z Reaction Wheel	C218461-2
32)	Array Shaft Transducer	212075-1
33)	Pneumatic Tank	C-111928-1
34)	Valve	243553-1
35)	Pressure Switch	PT2-3003
36)	Regulator	PT2-3004
37)	High-Low Pressure Transducer	PT2-3000/01
38)	Battery Pack	323820-2
39)	Power Control Unit	232215-2
40)	Charge Control Assembly	204553-1
41)	Charge Control Assemlby	204553-2
42)	Converter Number 2	206566-1
43)	Converter Number 5	206569-1
44)	Converter Number 6	206569-2
45)	Converter Number 7	206805-1
46)	Converter Number 8	206805-2
47)	Converter Number 9	206570-1
48)	Command Receiver	217907-1
49)	137-154 MHz Diplexer Coupler	218264-2
50)	Digital Decoder	218303-1
51)	137-154 MHz Antenna	217530-1
52)	Special Purpose Telemetry Unit	202650-2

53)	Ten Watt Power Monitor	214252-2
54)	Analog Data Handling Assembly	201140-1
55)	Digital Data Handling Assembly	218486-1
56)	Low Frequency Timing Assemlby	218487-1
57)	Signal Conditioner	201738-1
58)	Digital Recorder Electronics	207463-2
59)	Digital Recorder Transport	207464-5
60)	Command Distribution Unit	201529-3
61)	RBV-BTE Target Collimators	TBD
62)	RBV-BTE Spacecraft Command Simulator	↑
63)	RBV-BTE Spacecraft Clock Simulator	
64)	RBV-BTE Power Supply System	
65)	RBV-BTE	
66)	RBV-BTE Quick Look Display System	
67)	RBV-BTE High Resolution Hard Copy Recorder	
68)	RBV-BTE Vidicon Thermal Controller Generator	
69)	RBV-BTE Vidicon Thermal Controller	
70)	RBV-BTE Linearity Checker	
71)	RBV-BTE Video Signal and Sync Processor	
72)	VTR-BTE Spacecraft Command Simulator	
73)	VTR-BTE Spacecraft Clock Simulator	
74)	VTR-BTE Power Supply System	
75)	VTR-BTE Telemetry Monitoring and Recording System	
76)	VTR-BTE Video Signal Simulator	
77)	VTR-BTE Downlink Simulator	
78)	VTR-BTE Signal Analyzer/ Monitor	
79)	VTR-BTE Standard Test Equipment	
80)	VTR-BTE Test Cables and Breakout Boxes	↓ TBD

81) MSS-BTE Precision Collimator
82) MSS-BTE Spacecraft Command Simulator
83) MSS-BTE Power Supply System
84) MSS-BTE Telemetry and Test Point Monitor
85) MSS-BTE Precision Oscilloscope
86) MSS-BTE Video Processor and Image Recorder (Single Channel Quick Look Capability Type)
87) Standard Test Equipment
88) Test Cable and Breakout Boxes
89) Spacecraft Structure (Kit)
90) Solar Array Drive Shaft
91) Louver Banks (+X, -X) (Kit)
92) Insulation (set)
93) Horizon Scanner Bracket
94) 137-154 MHz Antenna Support
95) Release System (Set)
96) Interstage and Separation (Kit)

TBD ↑ ↓ TBD

3 1 2 4 1 Ground Support Equipment

Government Furnished Equipment and Government Furnished Parts are as specified in TRW Systems Specification No D-13505

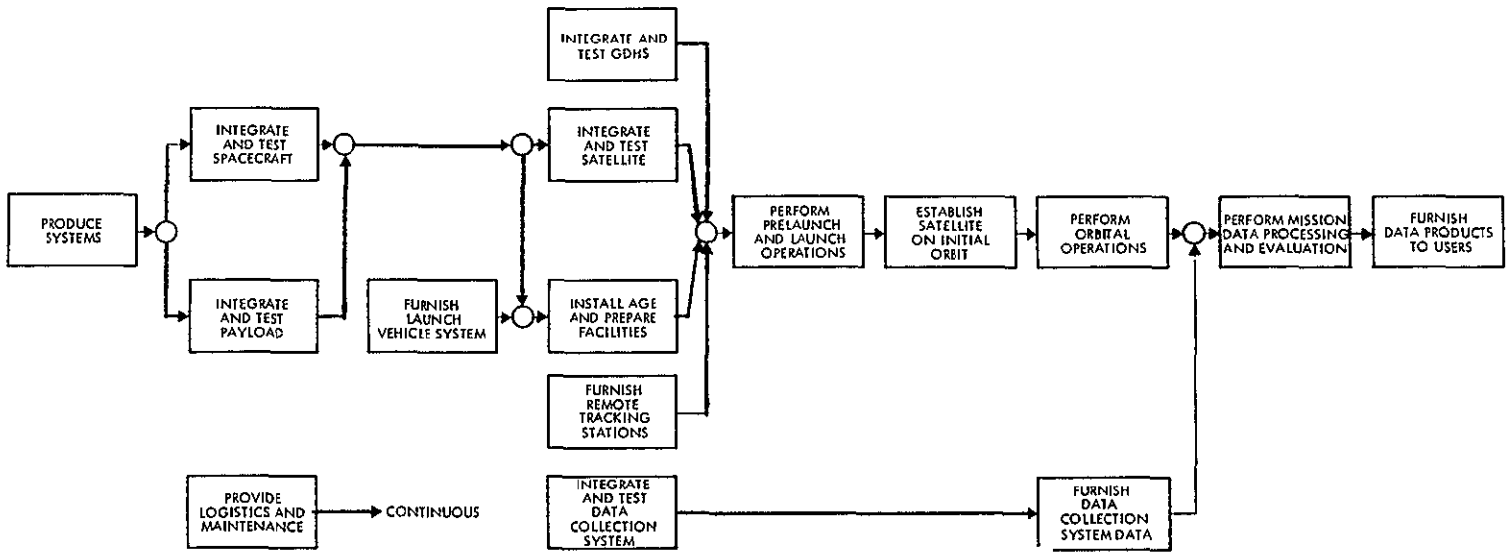

Figure 1 ERTS Program Top Flow Diagram

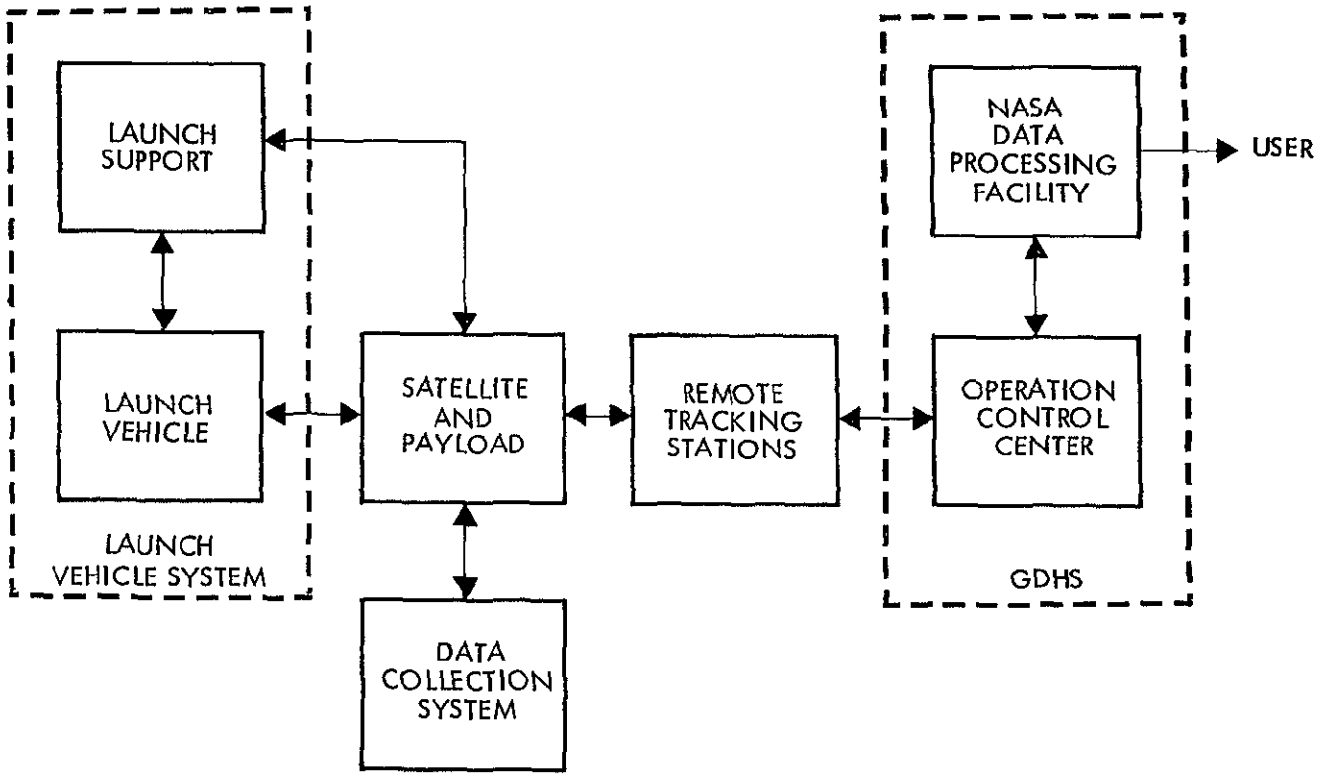

Figure 2 System Functional Schematic

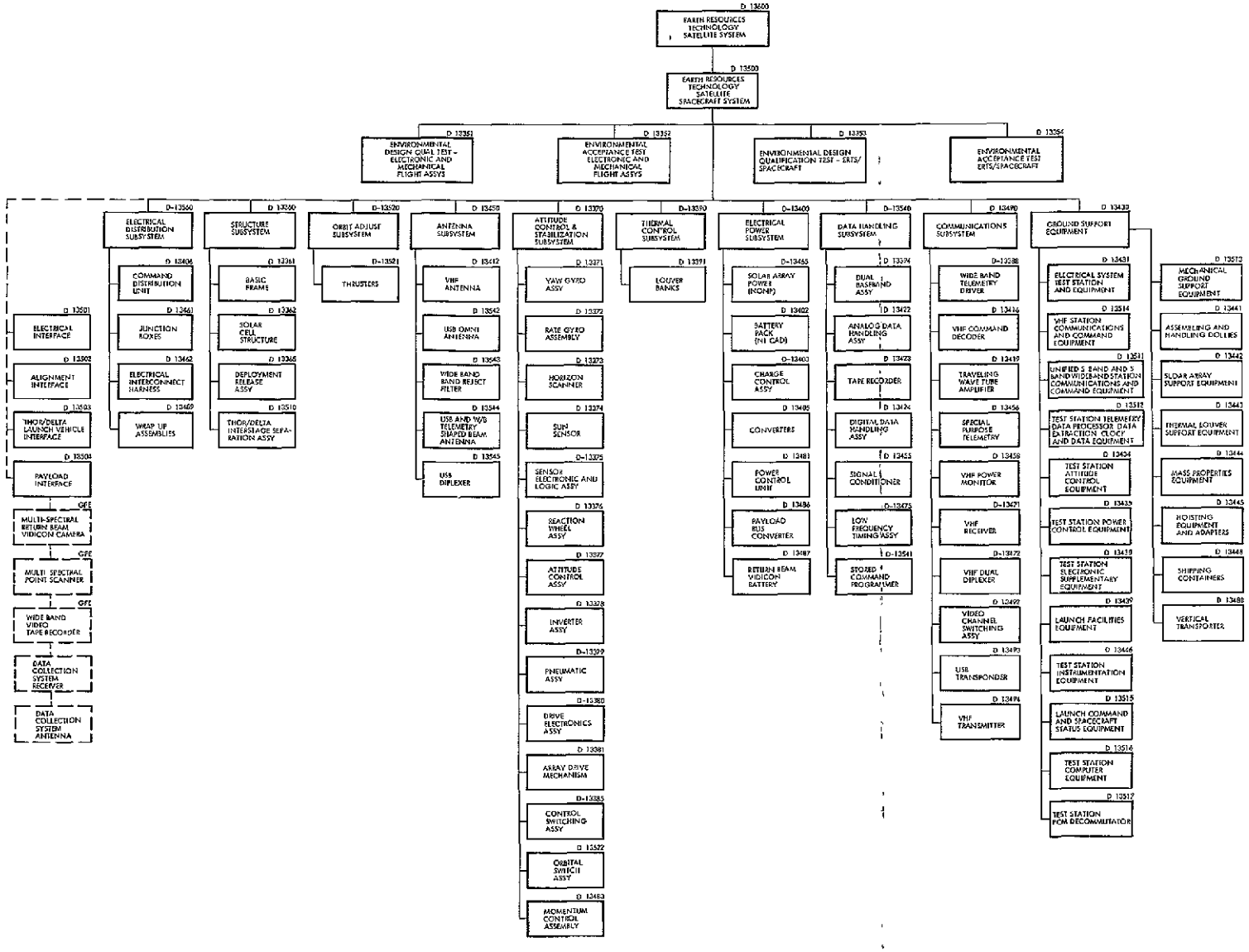

Figure 3 System Specification Tree

FOLDOUT FRAME

FOLDOUT FRAME

PRECEDING PAGE BLANK NOT FILMED

3 1 3 Operability

3 1 3 1 Reliability

As a design goal, the satellite shall have a minimum life time of one year in stabilized orbital flight The Operations Control Center shall be capable of fully supporting the satellites, following launch, on a 24 hour per day basis The NASA Data Processing Facility shall provide availability, in accordance with TRW Systems Document PAR 700-55, for processing observatory data for coverage Cases A or B

3 1 3 2 Maintainability

The ERTS Program elements shall be designed for maximum consideration of interchangeability, accessibility, and replaceability concepts The GDHS maintainability shall be in accordance with the contractor developed GDHS Maintainability Plan

3 1 3 3 Useful Life

The ERTS-A and B shall be designed for a minimum lifetime in orbit of one year The GDHS shall have a useful life of 10 years with routine maintenance

3 1 3 4 Environment

The satellite and ground support equipment shall be designed to withstand, without degradation of performance, the following ground, transporation and handling, storage, launch and ascent, and orbital environments The GDHS shall be capable of operating within a NASA furnished building

3 1 3 4 1 Ground Environments

a) Test Facility

Temperature	25°C ± 3°C
Relative Humidity	55% or less
Cleanness	Normal laboratory air conditioning

b) Launch Facility — In accordance with the requirements of Vandenberg Western Test Range

3 1 3 4 2 Transportation and Handling Environments

When packaged or otherwise prepared for shipment, the satellite and ground equipment shall withstand air, land, or sea transportation methods

3 1 3.4 3 Storage Environment

When packaged or otherwise prepared for storage, the satellite and ground equipment shall withstand the environments of paragraph 3 1 3 4.1

3 1 3 4 5 Launch and Ascent Environment

a) Temperature - On stand

The spacecraft shall be exposed to controlled temperature humidity and dust environment in an air-conditioned room The available environmental control for the spacecraft in the payload fairing shall be

1) Relative Humidity	10% to 50%
2) Conditioned Air	
Flow Rate	50 lbs/min
Temperature	10 to 15°C

b) Vibration

Thrust Direction

Frequency	Amplitude (Zero to Peak)	Sweep Octaves/Min
10 - 17 Hz	± 2 3 g	4 0
17 - 23 Hz	± 4 0 g	3 0
23 - 200 Hz	± 1 5 g	4 0

Lateral (Two axes orthogonal with thrust axis)

5 - 14 Hz	± 1 3 g	4 0
14 - 200 Hz	± 1 0 g	4 0

c) Acoustic Levels

The estimated acoustic spectra, inside and outside the aerodynamic shroud during flight are given in Table II

d) Loads

The following limit load factors are the maximum expected flight load factors expressed in gravity units (g)

1) Longitudinal (parallel to the thrust axis) aft minus 10 2g combined vectorially with 2 0g in either direction along any lateral axis (perpendicular to the thrust) The minus 10 2g aft load factor is composed of 6 2g from the vehicle "steady" thrust acceleration, plus 4 08g (vector) vibration occurring in the vehicle first longitudinal mode at 17 to 23 cps The 4 0g (vector) vibration is at the front end of the Delta assuming a rigid spacecraft at 17 to 23 cps If the spacecraft and adapter cannot be assumed rigid in this frequency band, the load factor must be increased to account for the additional load generated by dynamic amplification over the length of the spacecraft and spacecraft interstage adapter
2) Longitudinally forward 3 0g combined vectorially with 2 0g in either direction along any lateral axis

TABLE II

SPACECRAFT FLIGHT ACCEPTANCE
DELTA ACOUSTIC NOISE

Octave Band Center Frequency (Hz)	Sound Pressure Level (db, ref 0 0002)		Duration
	Exterior of Shroud	Interior of Shroud	
15 8	135	123	1 minute
31 5	136	123	
63	140	125	for
125	142	130	
250	145	133	complete
500	145	134	
1000	143	134	exposure
2000	140	131	
4000	136	127	
8000	131	121	
Overall	151	140	

e) Shock

The shock environment is specified in Figure 4

3 1 3 4 5 Orbital Conditions

The satellite shall be designed to withstand the following orbital conditions

a) Solar Radiation The intensity of solar radiation outside the atmosphere of the Earths mean distance from the sun shall be considered to have a mean intensity of 429 BTU/hr ft^2

b) Earth Albedo The ratio of the total luminous flux incident on the earth in all directions to the total flux incident on the earth in a beam of parallel light shall be considered to be 0 34

c) Earths Thermal Radiation The intensity of earth radiation outside the Earths atmosphere shall be considered to have a mean intensity of 68 BTU/hr-ft^2

d) Earths Shadow The satellites emergence from the Earth shadow shall be considered between 29 to 35 minutes from the time the satellite entered the shadow

3 1 3 5 Transportability

The ERTS satellite shall be designed to be transported by the ERTS transporter Each component of the GDHS shall be designed to be transported by common carrier with a minimum of protection Special handling or packaging techniques shall be used to assure that transportation methods do not impose design penalties

3 1 3 6 Human Performance

The design of all ERTS systems requiring man/machine interfaces shall use MIL-STD-803A, Part I, as a general guide

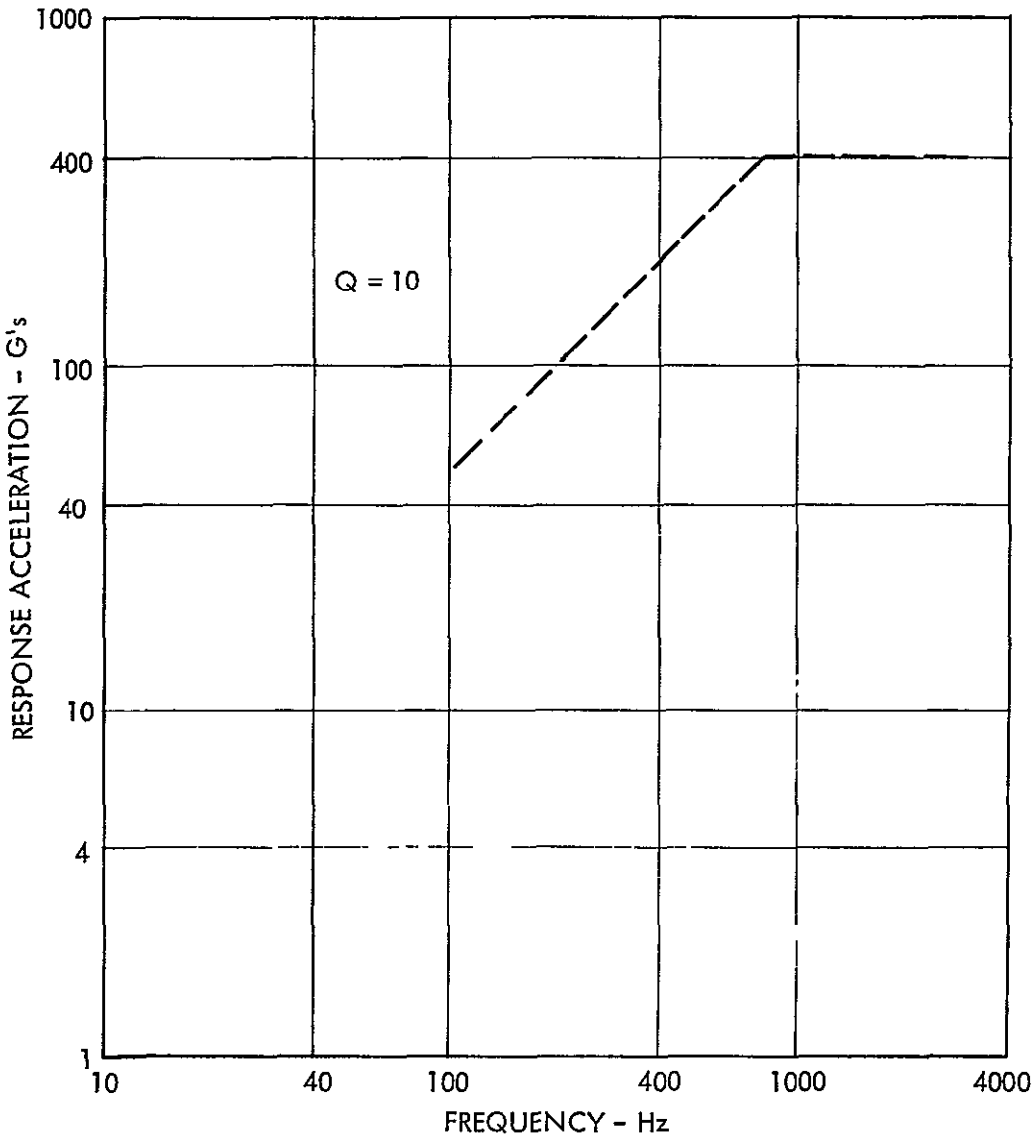

Figure 4 Delta Shock Spectra Input Spacecraft Flight Acceptance

3 1 3 7 Safety

3 1 3 7 1 Dangerous Materials and Components

Personnel functions within the hazardous area, following reaction control servicing and propulsion separation, or destruct system arming, shall be minimized

Design provisions and procedures for the safe handling, storage, and installation of propellants, explosives and exciter devices shall conform to the safety requirements as indicated on the applicable assembly and installation drawings

3 1 3 7 2 Noise and Vibration

The noise and vibration levels associated with the ERTS and its components in required combinations as specified in TRW Systems Specifications D-13353 and D-13354 shall be controlled under its operating conditions to levels of tolerance to personnel as specified in MIL-STD-803A, Part I

3 2 System Design and Construction Standards

3 2 1 General Design and Construction Requirements

3 2 1 1 Selection of Specifications and Standards

Selection of specifications and standards for identification, control, and procurement of parts, materials, and processes not specified herein shall be in accordance with the provisions of MIL-STD-143A

3 2 1 2 Materials, Parts, and Processes

Only materials, parts, and processes conforming to the applicable requirements of the GSFC Preferred Parts List PPL-10 and of Group I and V documents of MIL-STD-143A shall be considered standard and shall be used Engineering drawings and associated lists shall be in accordance with the provisions of MIL-D-1000 and MIL-STD-100

3 2 1 3 Standard and Qualified Parts

3 2 1 3 1 Electronic Parts

Electronic parts shall be as specified in the contractor's ERTS Reliability Program Plan

3 2 1 3 2 Screening Tests

Screening tests shall be as specified in the contractor's ERTS Reliability Program Plan

3 2 1 3 3 Derating

Derating shall be as specified in the contractor's ERTS Reliability Program Plan

3 2 1 4 Fungus and Moisture Resistance

Materials that are not nutrients for fungus shall be used whenever possible Where the use of fungus nutrients cannot be avoided, treating, packing, or other protective means shall be employed to ensure no degradation in system performance

3 2 1 5 Corrosion of Metal Parts

System parts, including spares, shall be protected against corrosion To avoid electrolytic corrosion, dissimilar metals, as defined in MS-33586A, shall not be used in direct contact Protective methods and materials for cleaning, surface treatment, and application of finishes and protective coating shall be accomplished in accordance with MIL-F-7179C, where applicable

3 2 1 6 Interchangeability and Replaceability

System designs shall meet the requirements of MIL-STD-100 for interchangeability and replaceability

3 2 1 7 Workmanship

3 2 1 7 1 Workmanship Standards

Workmanship shall conform to the requirements of the applicable process specifications relating to fabrication and assembly as invoked by the particular assembly drawing Critical steps of fabrication that are item-peculiar shall be detailed in drawing notes which shall include appropriate criteria of workmanship Workmanship relating to all other aspects of fabrication, general handling, and storage shall be deemed adequately covered by the quality control program

3 2 1 7 2 Personnel Certification

Personnel involved in assembly, soldering, welding, or other activity requiring special technical skills shall be certified as to their capability to perform such duties effectively as specified in the contractor's Quality Program Plan

3 2 1 8 Electromagnetic Interference

The satellites shall be designed to minimize or eliminate inductive or electromagnetic RF interference effects

3 2 1 9 Identification and Marking

3 2 1 9 1 Article Identification

System components and ground support equipment components shall be identified in accordance with PR 12-1

3 2 1 9 2 Pipelines

Fluid and gas tubing pipelines shall be identified and marked in accordance with MIL-STD-1247A, except for lines which do not have adequate space for such marking

3 2 1 9 3 Explosives

All propellant grains, ignitors, squibs, and ordnance charges shall be classified and marked in accordance with applicable TRW procedures in compliance with appropriate government requirements

3 2 1 10 Storage

The satellites and associated ground support equipment, with the exception of batteries, shall be designed to be stored for a period of one year without requiring major refurbishment, maintenance or retesting at the end of storage

3 2 2 Design Disciplines

3 2 2 1 Civil

Facility design shall be in accordance with joint industry conference standards and all other civil, architectural, and structural industry standards as applicable

3 3 Performance Allocations

3 3 1 Ground Data Handling System

The Ground Data Handling System shall consist of two major subsystems as described in TRW Systems specifications D-13750 and D-13800, the Operations Control Center (OCC) and the NASA Data Processing Facility (NDPF)

3 3 1 1 Allocated Performance and Design Requirements

3 3 1 1 1 Mission Data Handling

The Ground Data Handling System shall accept, record, process, and display PCM telemetry data and provide such data to users in compliance with the requirements of paragraphs 3 1 1 1 1, 3 1 1 1 2, 3 1 1 1 3, and 3 1 1 2 1

3 3 1 1 2 Command and Control

The GDHS shall generate, translocate and validate spacecraft commands in compliance with the requirements of paragraph 3 1 1 2 9

3 3 1 1 3 Satellite Housekeeping Telemetry

The GDHS shall accept and process spacecraft housekeeping telemetry data in compliance with the requirements of paragraph 3 1 1 2 12

3 3 1 1 4 Maintainability

The GDHS maintainability requirements shall be as specified in the contractor's GDHS Maintainability Plan

3 3 1 2 Peculiar Performance and Design Requirements

3 3 1 2 1 GDHS Software

The software requirements of paragraphs 3 1 1 2 15, 3 1 1 2 16, 3 1 1 2 17 and 3 1 1 2 18 shall apply in their entirety to the Ground Data Handling System

3 3 1 1 2 1 Command Generation

Command generation shall be provided to the appropriate STADAN & MSFN ground stations for translocation and uplink transmission to the satellite and payload

3 3 1 1 2 1 1 Command Modes

a Real-time command modes shall be provided as defined in TRW Systems Specification No D-13750

b Stored command modes shall be provided as defined in TRW Systems Specification No D-13750

3 3 1 1 2 2 Command Translocation

Commands shall be transmitted to the appropriate STADAN/MSFN ground station in a 600 bit message block via the NASCOM HSD lines by ADPE

3 3 1 1 2 3 Command Validation

Command validation shall be provided by

a Visual display prior to translocation

b ADPE comparison with the command library

c Automated MSFN error coding

3 3 1 2 2 Data Processing

The GDHS shall have the capability to automatically process data as requested by the user Data shall be transformed into user oriented media and retained for use by the various users as specified in paragraph 3 1 1 2 10

3 3 1 2 3 Unified Display Consoles

The GDHS shall have unified display consoles in both the OCC and the NDPF The displays shall be capable of interacting with either the OCC or the NDPF data bases

3 3 1 3 Functional Interfaces

3 3 1 3 1 Ground Data Handling System/Remote Tracking Stations System

The GDHS shall originate commands for spacecraft control and relay these commands to the remote tracking stations for transmission to the satellite The GDHS shall receive mission data and housekeeping telemetry from the remote tracking stations

3 3 1 3 2 GDHS/Users

The GDHS shall accept requests for data from the users and shall process and disseminate data in accordance with user requests as defined in TRW Systems Specification No D-13800

3 3 2 Earth Resources Technology Satellite System

The Earth Resources Technology Satellite (ERTS) System shall consist of spacecraft structure (including launch vehicle adapter and payload mounts), communication and data handling (including antennas), active thermal control, electrical integration, orbit adjustment, stabilization and control, and solar array power supply subsystems and payload experiment provisions The satellite system shall also include the necessary ground support equipment to support the satellite

3 3 2 1 Allocated Performance and Design Requirements

3 3 2 1 1 Primary Mission Requirements

The satellite system, in compliance with the requirements of paragraph 3 1 1 1 1, 3 1 1 1 2, and 3 1 1 1 3, shall acquire data through the utilization of the payload The payload data shall be managed by the Ground Data Handling Systems Operations Control Center and shall be processed by the NASA Data Processing Facility The data shall be subject to bulk and/or precision processing modes as defined in TRW Systems Specification No D-13800

3 3 2 1 2 Satellite Weight

The satellite weights, in compliance with the requirements of paragraph 3 1 1 2 11 and 3 1 1 2 13, for ERTS A shall be 1491 lbs , ERTS B shall be 1506 lbs

3 3 2 1 3 Payload

The satellite shall contain provisions for a payload as follows in compliance with the requirements of paragraph 3 1 1 2 2 and 3 1 1 2 3

Sensors

a) Return Beam Vidicon Camera
b) Multi-Spectral Scanner
c) Data Collection Equipment
d) Wide Band Video Tape Recorder

Weight

The satellite shall be capable of supporting a payload weight including harness and adapter structure of 475 pounds

Volume

13 cubic feet minimum

3 3 2 1 4 Orbit Injection

The satellite shall be capable of removing the launch vehicle injection errors in compliance with the requirements of paragraph 3 1 1 2 5 through an orbit adjust and Stabilization and Control function incorporating thrusters utilizing Krypton gas and reaction wheels as torque generators In plane and cross plane adjustment shall be provided yielding a capability of greater than 50 feet per second

3 3 2 1 5 Acquisition

The acquisition of the satellite reference axis shall be initiated at a predetermined time subsequent to separation from the launch vehicle and at any time when one or more reference axes are lost

3 3 2 1 5 1 Acquisition Sequence

After separation from the launch vehicle the acquisition of the sun, earth, and orbit plane shall occur in the following sequence

a) Sun Acquisition Sun acquisition in the sun-acquisition mode shall be achieved as early as possible, enabling the positive pitch axis of the satellite to be aligned to the sun

b) Earth Acquisition Earth acquisition in the earth-acquisition mode shall occur by rotation of the satellite about the pitch axis, for the necessary length of time in orbit, until the yaw axis of the observatory sufficiently intersects the earth at which time the earth trackers will lock-on the earth

c) Orbit Plane Acquisition Orbit plane acquisition shall occur on manual command In this mode, the pitch axis shall be rotated from sun pointing to a position where the X axis is in the orbit plane with the -X axis nominally aligned with the satellite orbital velocity This shall be accomplished by means of a gyro compass control mode

3 3 2 1 6 Satellite Housekeeping Telemetry

The satellite shall be capable of processing, storing and transmitting spacecraft and payload status information in recognition of the requirements of paragraph 3 1 1 2 12 The downlink bit error rate shall be no greater than 1×10^{-6} bps

The housekeeping telemetry bit rate shall be 1 Kbs and 32 Kbs

3 3 2 1 7 Communication and Command

The satellite shall provide a coherent S-band transponder for ranging and tracking by the MSFN stations, in compliance with the requirements of paragraphs 3 1 1 2 8 and 3 1 1 2 9 VHF equipment shall provide PCM data and a carrier for use by the STADAN network The satellite shall be capable of receiving, decoding and executing real time ground and stored commands The uplink error rate shall be no greater than 1×10^{-6} bps Mission data shall be transmitted over two S-band downlinks The MSS wideband data link shall have a bit rate of 15 mbs

3 3 2 1 8 Reliability

The spacecraft and payload shall have a design goal of one year, minimum, of stabilized orbital flight

3 3 2 1 9 Maintainability

The satellite and GSE shall be designed in accordance with the requirements of paragraph 3 1 3 2

3 3 2 1 10 Environments

The satellite shall withstand the environments and operate in orbit as specified in paragraph 3 1 3 4

3 3 2 2 Peculiar Performance and Design Requirements

3 3 2 2 1 Orbit Plane Orientation

The satellite shall be 3 axes stabilized and shall be aligned with the plane of the orbit within 0 7 degree during normal operation

3 3 2 2 2 Satellite Orientation Rate Errors

The satellite orientation rate errors shall not exceed those specified in paragraph 3 1 1 2 14

3 3 2 2 3 Global Coverage and Image Overlap

The requirements of paragraphs 3 1 1 2 6 and 3 1 1 2 7 shall apply in their entirety

3 3 2 2 4 Separation Velocity

The satellite separation equipment shall impart a velocity to the satellite relative to the final stage of the Thor-Delta of 4 2 ft/sec $\pm$ 10%

3 3 2 2 5 Electrical Power

Primary power for the satellite shall be supplied by an orientable array of solar cells mounted on two paddles The array shall be supplemented during periods of heavy load and eclipse by two rechargeable nickel-cadmium batteries In addition to the solar array and batteries the electrical power function shall include charge control devices, dc-dc converters, a payload converter and pulse power and standby batteries The power subsystem shall be capable of delivering a total of 30,000 watt-min of energy per orbit to the satellite and payload This capability shall be based on a 103 minute orbit with a 34 minute eclipse time at the end of a one year flight The satellite shall require 16,000 watt-min of energy per orbit, the remainder shall be available to the payload and permit 20 minute sensor operation per orbit

3 3 2 2 5 1 Power Profile

The power required from the bus shall vary in time and an arbitrary schedule of sensor operation to produce the power profile is shown in Table III

3 3 2 2 6 Satellite Ground Support Equipment

The satellite ground support equipment shall include equipment and instrumentation necessary for the verification and acceptance of the satellite for flight Equipment and instrumentation shall include capabilities for installing, aligning, and calibrating subsystems, and for verifying the electrical and functional integrity of components, subassemblies, and interrelated or cooperative end systems Equipment shall be provided to handle, service, and transport the spacecraft and satellite as well as to prevent malfunctions caused by dust, moisture, frost, airborne or applied chemicals, or other potentially degrading environmental factors

Table III Time History of Bus Current

Time	0-10	10-20	20-30	30-80	80-90	90-103
SUN/ECLIPSE	SUN				ECLIPSE 34 min	
Base Load, Amperes	5 29	5 29	5 29	5 29	5 29	5 29
Data Collection System	03	03	03	03	03	03
RBV, 155 W	--	5 65	5 65	--		--
MSS, 60W	--	2 15	2 15	--	--	--
W B Recorders, Z Record		--	6 0			
W B Recorders, Z P B		--	--	--	5 4	--
W B Transmitter, 72W		2 8	--	--	2 8	--
-24±1/2 V Conv Losses 15%		1 5	1 9		1 0	
TOTAL, Amperes	5 32	17 42	21 02	5 32	14 52	5 32

3 3 2 3 Functional Interface

3 3 2 3 1 ERTS System/Data Collection System

The satellite shall receive data from the data collection platforms when the satellite is within the line of sight of the platforms The satellite shall furnish power to operate the airborne DCS equipment and shall transmit DCS data to the remote tracking stations for transmission to the GDHS

3 3 2 3 2 ERTS System/Launch Vehicle System

Detailed interface requirements between the satellite and the launch vehicle shall be as specified in TRW Specification D-13503

3 3 2 3 2 1 Satellite/Launch Vehicle Adapter

The satellite to launch vehicle adapter shall be designed to align and attach to the fitting as described in paragraph 3 3 4 2 2

3 3 2 3 2 2 Volume Constraints

The satellite shall be designed to fit within the payload fairing envelope described in paragraph 3 3 4 2 1

3 3 2 3 2 3 Separation

The satellite separation signal and electrical power shall be furnished by the launch vehicle for separation from the launch vehicle

3 3 2 3 3 ERTS System/Remote Tracking Stations

The satellite shall be capable of receiving ground commands from the remote tracking stations The satellite shall transmit data from the airborne sensors and data collection platforms to the ground stations for retransmission to the GDHS

3 3 3 Data Collection System

The data collection system (Figure 5) shall consist of data collection platforms which include sensors on the ground to collect data and a transmitter capable of transmitting the data to the satellite and equipment on the satellite to receive and transmit DCS signals The system shall operate in a random mode to eliminate the need for timing signals and interrogation commands and shall allow for a finite number of message collisions

3 3 3 1 Allocated Performance and Design Requirements

3 3 3 1 1 Mission Data

The data collection system shall collect data in support of the primary ERTS missions in compliance with the requirements of paragraph 3 1 1 1 1, 3 1 1 1 2, and 3 1 1 1 3

3 3 3 1 2 Airborne Equipment

The DCS shall contain airborne receiving equipment in compliance with the requirements of paragraph 3 1 1 2 2 The DCS flight receiver shall be a double frequency conversion superhetrodyne design to operate on a frequency of 400 to 406 MHz with a noise figure limited to two db maximum

3 3 3 2 Peculiar Performance and Design Requirements

3 3 3 3 Functional Interfaces

3 3 3 3 1 Data Collection Platforms/satellite

The data collection platforms shall be capable of inputting data to the satellite DCS receiver on a 117 KHz bandwidth when the satellite is within the line of sight of the platforms

The data shall be converted to an IF frequency and routed to a subcarrier oscillator in the spacecraft The data collection airborne receiver equipment shall receive the necessary power to operate from the spacecraft

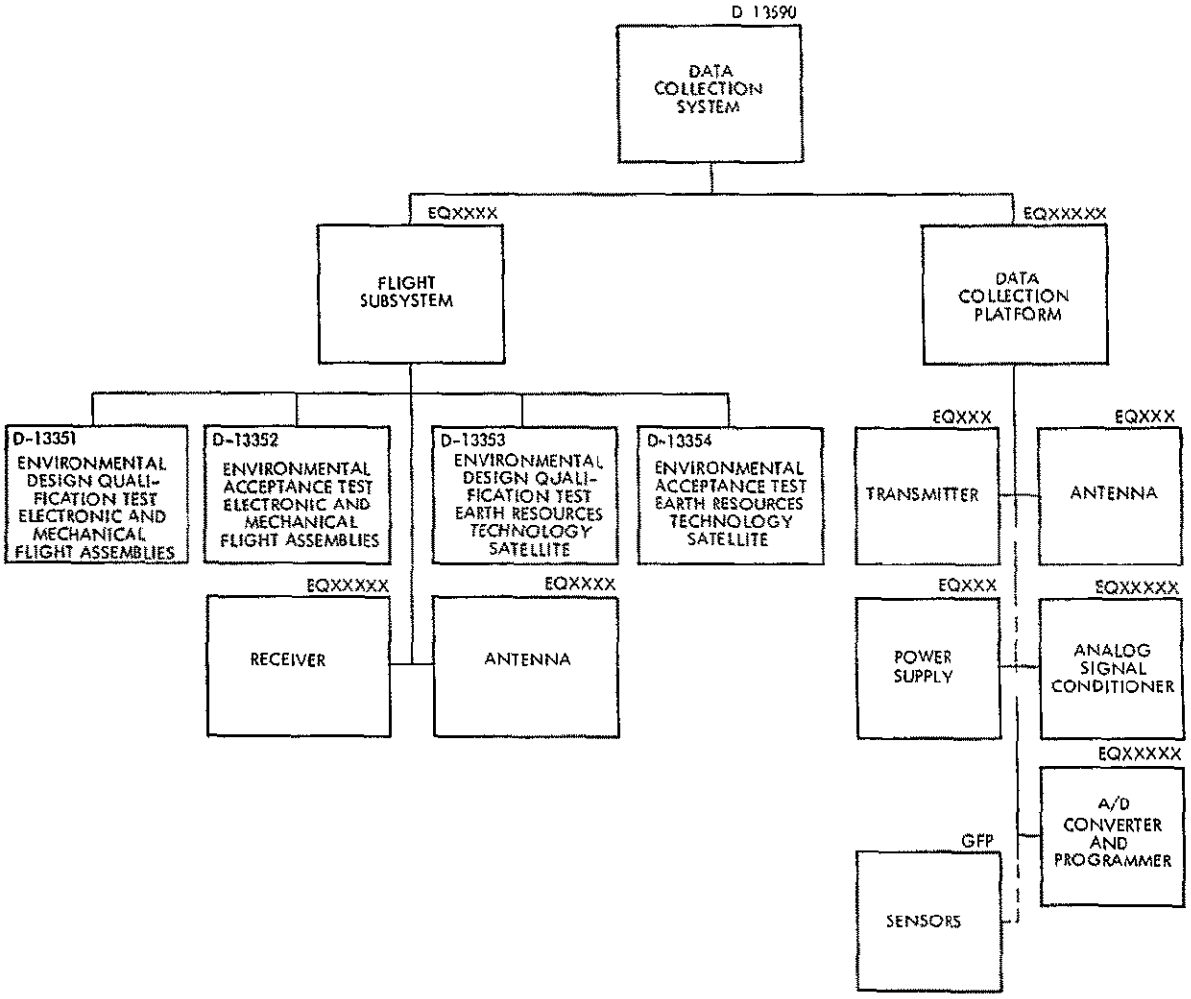

Figure 5 DCS Specification Tree

3 3 4 Launch Vehicle System

The launch vehicle system shall consist of a Thor-Delta launch vehicle, the launch pad, and other launch support facilities at the Western Test Range (WTR)

3 3 4 1 Allocated Performance and Design Requirements

3 3 4 1 1 Payload Capability

The launch vehicle payload capability shall be no less than 1520 lbs in compliance with the requirements of paragraph 3 1 1 2 3, 3 1 1 2 4, and 3 1 1 2 13

3 3 4 1 2 Orbit Injection Errors

The launch vehicle shall place the satellite in orbit within the following nominal parameters in compliance with the requirements of paragraph 3 1 1 2 5

a)	Inclination of orbit	99 08° ± 0 05°
b)	Equatorial Altitude	492 ± 1 0 nautical miles
c)	Right ascension of ascending node at vernal equinox	142 5 minus zero plus 7 5°
d)	Eccentricity	less than 0 006
e)	Eclipse duration	29 to 34 minutes
f)	Period	103 3 ± 0 3 minutes

3 3 4 1 3 Separation Rate Errors

The launch vehicle rate errors at satellite separation shall be limited to the following 3σ values

Pitch and Yaw	0 1 degree/sec
Roll	0 5 degree/sec

3 3 4 1 4 Ascent Loads

The launch vehicle shall support the satellite during lift-off, ascent, and insertion into orbit

3 3 4 2 Peculiar Performance and Design Requirements

The launch vehicle system shall provide the launch facilities and support functions required during all prelaunch and launch activities

3 3 4 2 1 Payload Fairing Envelope

The payload fairing envelope shall be as described in Figure 5

3 3 4 2 2 Alignment and Attachment

The launch vehicle shall provide alignment and attachment provisions for the satellite as shown in Figure 6

3 3 4 2 3 Satellite Separation

The launch vehicle system shall provide the signal and power required to initiate satellite separation when the orbit is achieved

3 3 4 3 Functional Interfaces

3 3 4 3 1 Launch Vehicle System/ERTS System

The detailed interfaces between the launch vehicle and the satellite shall be as specified in TRW Specification D-13503 The launch vehicle system shall provide facilities and equipment necessary for the operation of the satellite ground support equipment

3 3 5 Remote Tracking Stations System

The Remote Tracking Stations System shall consist of the Gilmore (Alaska), Corpus Christi (Texas), Rosman (North Carolina), and NTTF (GSFC/Maryland) stations dedicated to the ERTS program and other stations accessible through the NASCOM network for backup and launch and ascent support

3 3 5 1 Allocated Performance and Design Requirements

3 3 5 1 1 Orbit Determination

The ground stations shall track and acquire range and range rate data to permit precision orbit determination in compliance with the requirements of paragraph 3 1 1 2 5 and 3 1.1 2 8

3 3 5 1 2 Satellite Telemetry

The tracking stations shall acquire satellite housekeeping data in compliance with the requirements of paragraph 3 1 1 2 12

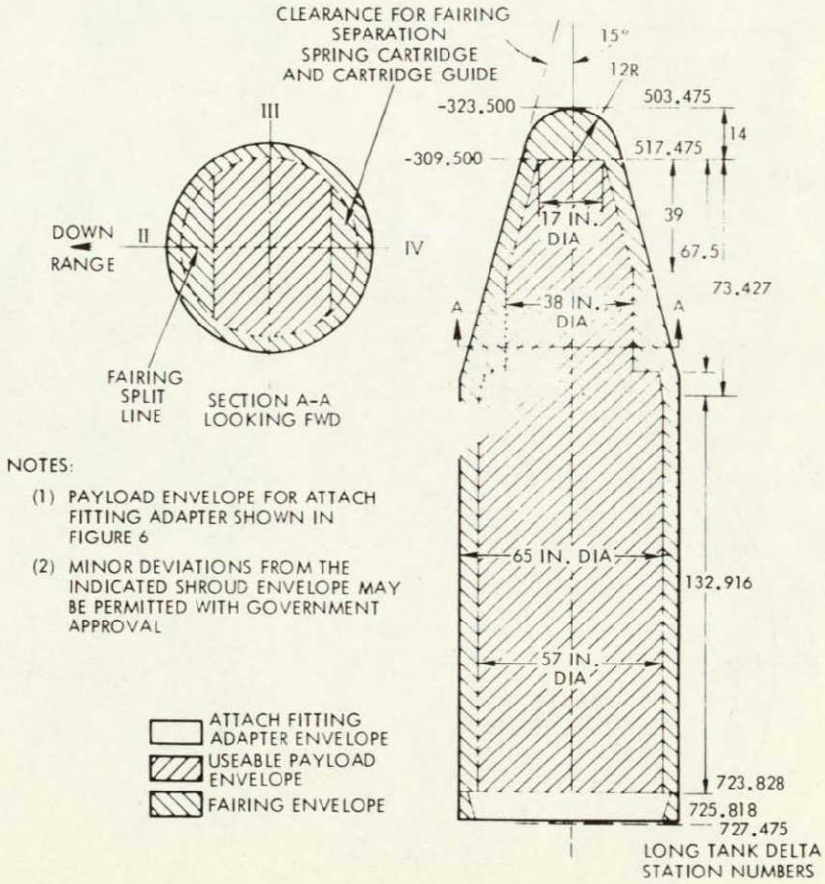

NOTES:

(1) PAYLOAD ENVELOPE FOR ATTACH FITTING ADAPTER SHOWN IN FIGURE 6

(2) MINOR DEVIATIONS FROM THE INDICATED SHROUD ENVELOPE MAY BE PERMITTED WITH GOVERNMENT APPROVAL

Figure 6. Payload Fairing Envelope

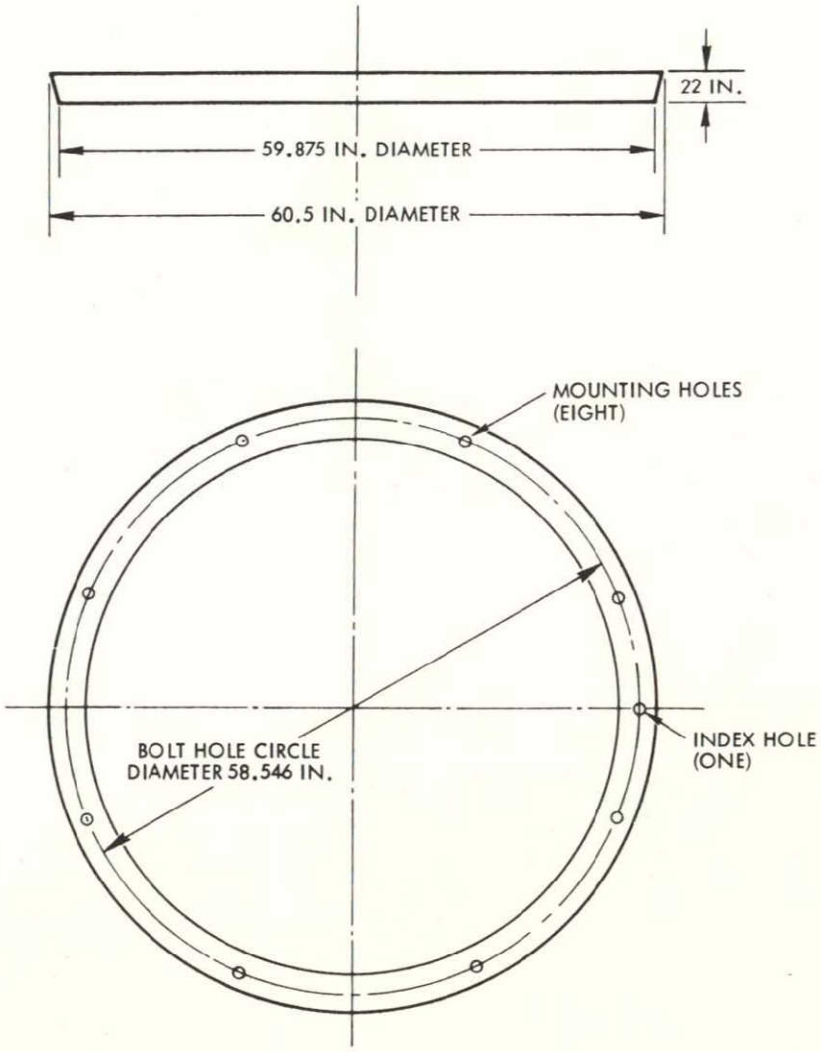

Figure 7. Spacecraft Attach Fitting

3 3 5 1 3 Satellite Command, Control and Data Acquisition

The ground stations shall transmit commands to the satellite and acquire mission data form the satellite in compliance with the requirements of paragraphs 3 1 1 1 1, 3 1 1 1 2, 3 1 1 1 3 and 3 1 1 2 9

3 3 5 2 Peculiar Performance and Design Requirements

3 3 5 2 1 Commanding and Control

The Remote Tracking Station shall transmit commands required to operate the satellite

3 3 5 2 2 Satellite Telemetry Data Receiving

The Remote Tracking Station shall be capable of receiving status and mission data telemetered from the satellite

3 3 5 3 Functional Interfaces

3 3 5 3 1 Remote Tracking Station System/GDHS

The Remote Tracking Stations shall receive commands originated in the GDHS for transmission to the satellite The remote tracking stations shall relay mission and housekeeping telemetry received from the satellite to the GDHS The availability of the long lines for transmission of data from remote tracking stations to the GDHS shall be at least 0 995

3 3 5 3 2 Remote Tracking Station System/ERTS System

The Remote Tracking Station shall transmit commands to the satellite and shall receive mission and housekeeping data from the satellite

3 3 6 Users

The users shall consist of the Department of Agriculture, Department of Interior, Department of Navy, Department of Commerce and other governmental and private agencies concerned with the earth's natural and cultural resources The users shall request data from the GDHS and furnish inputs to the GDHS for the format and types of data desired

4 PERFORMANCE ASSURANCE

The contractor shall develop a performance assurance program in compliance with the provisions of NASA document NPC-250-1, NHB 5300 4 (1B and 3A) as further defined by TRW documents Nos PAR 700-52, PAR 700-53, PAR 700-54, PAR 700-55, PAR 700-56, PAR 700-61 and the applicable TRW plans as shown in Section 2 The objectives of this program shall include

a Configuration Management in compliance with GMI 8040 1
b Verification of the total program performance
c Verification of individual system's performance
d Verification and accumulation of natural and cultural resource data for all missions
e Demonstration of ERTS System performance repeatability and overall program operability and reliability
f Isolation of failure modes and evaluation of resulting corrective action
g Verification of ground data handling and data collection system performance

Verification of performance, design, and construction of all program elements shall be accomplished by physical inspection, review of analytical data, demonstrations, tests, and reviews of test data Compliance with program requirements which cannot be validated by inspection, demonstration or test shall be validated by engineering analysis

The test program shall be made up of Phase I and Phase II tests as defined in Section 6

4 1 Phase I Program Test Requirements

4 1 1 Engineering Test and Evaluation

Integrated program tests shall be conducted on the developmental model systems in direct support of design and development activity Results of component, equipment, and subsystem tests performed on this and other programs shall be used to support the development test program

4 1 2 Qualification Testing

Formal qualification testing of the program elements shall be accomplished at the environment levels required to assure that the systems will comply with the requirements of paragraph 3 1 3 4 herein

Formal qualification testing of the ERTS satellite and the ground data handling system shall be accomplished at the worst probable combination of environmental levels specified in paragraph 3 1 3 4 Formal qualification testing of ground support equipment shall be accomplished at applicable environmental levels

4 1 3 Electrical and EMI Tests

Electrical and EMI tests shall be conducted to validate the performance of the program elements to satisfy the requirements of paragraph 3 2 1 8 when operating in a simulated system configuration Testing shall be accomplished by operating all electrical equipments in normal prelaunch and launch sequence except when more severe environments are required to establish operation with adequate safety margins

4 1 4 Reliability

Tests performed for the purpose of obtaining reliability and maintainability confidence shall be performed on components as approved by the procuring agency

4 1 5 Acceptance Testing

Formal acceptance testing of the program elements shall be accomplished at the environmental levels specified in the contractor's environmental test specifications, procedures and plans

4 2 Phase II Program Test Requirements

The Phase II test program shall validate the performance and operability of the system The validation shall be accomplished through the analysis of test data acquired from integrated system ground tests and flight tests

4 2 1 Integrated System Ground Tests

These tests shall validate the compatibility and performance of the integrated program airborne and ground equipment prior to, and for the purpose of, flight test initiation The tests to be performed shall include but not be limited to the following

a Compatibility verification of physical and functional interface between systems

b Verification of system performance in the presence of the EMI environment

4 2 2 Flight Test

The flight test program shall provide flight test data to verify that the performance requirements of the system have been satisfied The flight test data and analysis of the data shall validate the airborne equipment performance requirements of Section 3 of this specification

4 2 3 Failure Criteria

The inability of the flight test program to demonstrate (in accordance with the test capabilities available) the performance requirements of the program shall be defined as a system failure Individual system equipment failures which may cause system failure include but are not limited to the following

a Failure of the launch vehicle to insert the satellite into orbit

b Failure of the satellite to acquire data

c Failure to demonstrate system operability

d Failure of the remote tracking stations to support the satellite or failure to acquire satellite data

e Failure of the ground data handling system to acquire and process satellite data or to display information required by users

5 PREPARATION FOR DELIVERY

5 1 Packaging

Packaging of each item for delivery to the procuring agency shall be as specified below

5 1 1 Containers

Individual containers shall be so constructed as to allow removal of the article for inspection without destruction of the container or of the wrappers affixed to the article If paper wrapping is used on the article, acid free paper shall be used As an objective, the container shall provide equal protection, without use of special tools, to articles repackaged following inspection

5 1 2 Special Instructions

If the article requires special attention during receiving, inspection, installation and operation or if non-obvious characteristics require that special handling be used, the procuring agency shall be notified under separate cover and a removable instruction tag shall be attached Attachment shall be to the shipping container or to the article as appropriate

5 2 Marking

5 2 1 Marking for Shipment

Exterior shipping containers and non-carrier packages and separately shipped items shall be marked in accordance with MIL-STD-129D

5 2 2 Re-Inspection

Articles requiring periodic re-inspection shall be marked with the next inspection date

6 NOTES

6 1 Definitions

Phase I Program Test

Development test and evaluation of individual components, assemblies, and subsystems and in certain cases, the complete system, which is predominantly conducted by the contractor

Phase II Program Test

Testing and evaluation spanning the integration of configured items into a completed system in as near an operational configuration as is practicable, which is a joint contractor - NASA effort under NASA control

6 2 Abbreviations

BTE - Bench Test Equipment
ERTS - Earth Resources Technology Satellite
DCS - Data Collection System
GDHS - Ground Data Hnadling System
GSE - Ground Support Equipment
GSFC - Goddard Space Flight Center
MSFN - Manned Space Flight Network
MSS - Multi-Spectral-Spectrometer
MTBF - Mean Time Before Failure
MTTR - Mean Time To Repair
NDPF - NASA Data Processing Facility
OCC - Operations Control Center
RBV - Return Beam Vidicon
STADAN - Satellite Tracking and Data Acquisition Network
VHF - Very high frequency
WTR - Western Test Range